CHEMICAL THERMODYNAMICS VOLUME 10

CHEMICAL THERMODYNAMICS OF SOLID SOLUTIONS OF INTEREST IN NUCLEAR WASTE MANAGEMENT

A STATE-OF-THE-ART REPORT

AEN NEA

TDB Thermochemical Data Base Project

OECD

CHEMICAL THERMODYNAMICS OF SOLID SOLUTIONS OF INTEREST IN RADIOACTIVE WASTE MANAGEMENT

A STATE-OF-THE-ART REPORT

Jordi Bruno (Chair)
Enviros Spain SL,
Barcelona (Spain)

Dirk Bosbach
Forschungszentrum Karlsruhe
Institut für Nukleare Entsorgung (INE)
Karlsruhe, (Germany)

Dmitrii Kulik
Paul Scherrer Institut
Villigen (Switzerland)

Alexandra Navrotsky
University of California at Davis
Davis (California, USA)

Edited by

Federico J. Mompean (Series Editor and Project Co-ordinator)
Myriam Illemassène (Volume Editor) and Jane Perrone
OECD Nuclear Energy Agency, Data Bank
Issy-les-Moulineaux, (France)

ORGANISATION FOR ECONOMIC CO-OPERATION AND DEVELOPMENT

The OECD is a unique forum where the governments of 30 democracies work together to address the economic, social and environmental challenges of globalisation. The OECD is also at the forefront of efforts to understand and to help governments respond to new developments and concerns, such as corporate governance, the information economy and the challenges of an ageing population. The Organisation provides a setting where governments can compare policy experiences, seek answers to common problems, identify good practice and work to co-ordinate domestic and international policies.

The OECD member countries are: Australia, Austria, Belgium, Canada, the Czech Republic, Denmark, Finland, France, Germany, Greece, Hungary, Iceland, Ireland, Italy, Japan, Korea, Luxembourg, Mexico, the Netherlands, New Zealand, Norway, Poland, Portugal, the Slovak Republic, Spain, Sweden, Switzerland, Turkey, the United Kingdom and the United States. The Commission of the European Communities takes part in the work of the OECD.

OECD Publishing disseminates widely the results of the Organisation's statistics gathering and research on economic, social and environmental issues, as well as the conventions, guidelines and standards agreed by its members.

* * *

This work is published on the responsibility of the Secretary-General of the OECD. The opinions expressed and arguments employed herein do not necessarily reflect the official views of the Organisation or of the governments of its member countries.

NUCLEAR ENERGY AGENCY

The OECD Nuclear Energy Agency (NEA) was established on 1st February 1958 under the name of the OEEC European Nuclear Energy Agency. It received its present designation on 20th April 1972, when Japan became its first non-European full member. NEA membership today consists of 28 OECD member countries: Australia, Austria, Belgium, Canada, the Czech Republic, Denmark, Finland, France, Germany, Greece, Hungary, Iceland, Ireland, Italy, Japan, Luxembourg, Mexico, the Netherlands, Norway, Portugal, Republic of Korea, the Slovak Republic, Spain, Sweden, Switzerland, Turkey, the United Kingdom and the United States. The Commission of the European Communities also takes part in the work of the Agency.

The mission of the NEA is:

to assist its member countries in maintaining and further developing, through international co-operation, the scientific, technological and legal bases required for a safe, environmentally friendly and economical use of nuclear energy for peaceful purposes, as well as

to provide authoritative assessments and to forge common understandings on key issues, as input to government decisions on nuclear energy policy and to broader OECD policy analyses in areas such as energy and sustainable development.

Specific areas of competence of the NEA include safety and regulation of nuclear activities, radioactive waste management, radiological protection, nuclear science, economic and technical analyses of the nuclear fuel cycle, nuclear law and liability, and public information. The NEA Data Bank provides nuclear data and computer program services for participating countries.

In these and related tasks, the NEA works in close collaboration with the International Atomic Energy Agency in Vienna, with which it has a Co-operation Agreement, as well as with other international organisations in the nuclear field.

CHEMICAL THERMODYNAMICS

Vol. 1. Chemical Thermodynamics of Uranium, Wanner, H., Forest, I., OECD Nuclear Energy Agency Data Bank, Eds., North Holland Elsevier Science Publishers B. V., Amsterdam, The Netherlands, (1992).

Vol. 2. Chemical Thermodynamics of Americium, OECD Nuclear Energy Agency Data Bank, Ed., North Holland Elsevier Science Publishers B. V., Amsterdam, The Netherlands, (1995).

Vol. 3. Chemical Thermodynamics of Technetium, Sandino, M.C.A., Östhols, E., OECD Nuclear Energy Agency Data Bank, Eds., North Holland Elsevier Science Publishers B. V., Amsterdam, The Netherlands, (1999).

Vol. 4. Chemical Thermodynamics of Neptunium and Plutonium, OECD Nuclear Energy Agency Data Bank, Ed., North Holland Elsevier Science Publishers B. V., Amsterdam, The Netherlands, (2001).

Vol. 5. Update on the Chemical Thermodynamics of Uranium, Neptunium, Plutonium, Americium and Technetium, OECD Nuclear Energy Agency Data Bank, Ed., North Holland Elsevier Science Publishers B. V., Amsterdam, The Netherlands, (2003).

Vol. 6. Chemical Thermodynamics of Nickel, OECD Nuclear Energy Agency Data Bank, Ed., North Holland Elsevier Science Publishers B. V., Amsterdam, The Netherlands, (2005).

Vol. 7. Chemical Thermodynamics of Selenium, OECD Nuclear Energy Agency Data Bank, Ed., North Holland Elsevier Science Publishers B. V., Amsterdam, The Netherlands, (2005).

Vol. 8. Chemical Thermodynamics of Zirconium, OECD Nuclear Energy Agency Data Bank, Ed., North Holland Elsevier Science Publishers B. V., Amsterdam, The Netherlands, (2005).

Vol. 9. Chemical Thermodynamics of Complexes and Compounds of U, Np, Pu, Am, Tc, Zr, Ni and Se with Selected Organic Ligands, OECD Nuclear Energy Agency Data Bank, Ed., North Holland Elsevier Science Publishers B. V., Amsterdam, The Netherlands, (2005).

Preface

This is the tenth volume of the "Chemical Thermodynamics" series edited by the OECD Nuclear Energy Agency (NEA). Departing from the traditional scheme of reviewing the species and compounds of a particular element, this volume has been prepared as a state-of-the-art report on the chemical thermodynamics of aqueous-solid solution systems in the context of radioactive waste management, and more specifically oriented towards underground disposal. With a few exceptions, systems involving solid solutions have not been the subject of review in the preceding volumes of the series, started in the 1990s. Two factors justify the present interest in solid solutions within the NEA Chemical Thermodynamics Database (TDB) Project. First, in recent years, a significant number of species and stoichiometric compounds of several elements have been added (or updated) to the critically reviewed database. Second, powerful experimental techniques enabling the microscopic characterisation of systems are currently of widespread use, and advanced computational tools for both forward and inverse modelling of aqueous-solid solution equilibria have been developed. For this reason, the Management Board of the NEA TDB III Project decided to set up an Expert Team to prepare a state-of-the-art report that could constitute the basis for a more systematic effort in evaluating the thermodynamic properties of solid solutions as applicable to radioactive waste management. It is hoped that the present volume, resulting from the Expert Team's efforts, will contribute to the dissemination of the underlying thermodynamic formalism needed for modelling aqueous-solid solution systems, by linking it to experimental techniques that can provide information about structural details and to robust data analysis procedures. The report is based on literature published up to the end of 2006, as well as on material previously prepared for academic purposes by some of the Expert Team members. No attempt has been made to systematically review all the literature dealing with every aspect of solid solutions, although it is hoped that the literature cited will serve as a guide to the older seminal work, as well as a comprehensive view of recent research efforts.

The first meetings of the Expert Team took place in May 2004 at the Paul Scherrer Institute (PSI) and in September 2004 at the Karlsruhe Institute of Technology (FZK) Institute for Nuclear Waste Disposal (INE), at which the scope of the report was determined and the writing responsiblities were allotted to the members. Additional meetings were held in February 2005 at the OECD and at various conferences during 2006.

The team as a whole is responsible for the entire report, but various parts of the review have been the main responsibility of the individual members. Alexandra Navrot-

sky wrote Chapter II.1.1 on theory of solid solutions, with minor contributions from Dmitrii Kulik who also wrote Chapters II.1.2 and II.1.3 on methods and tools for thermodynamic description of aqueous-solid solution equilibria and retrieval of thermodynamic properties of solid solutions. Chapter II.2 on experimental and analytical aspects was mainly written by Dirk Bosbach. Chapter II.3, cases of specific interest in relevant systems, was a truly collective effort. The Ra/Ba example was prepared by Jordi Bruno with the assistance of Fidel Grandia. The cement C-S-H phases example was prepared by Dmitrii Kulik. The case for the incorporation of the actinide/lanthanide elements into calcite was written by Dirk Bosbach. The discussion about solid solutions in the nuclear cycle was prepared by Jordi Bruno with the assistance of Esther Cera. Finally, the extended summary in Part I (meant to present the relevant concepts in a condensed form without excessive mathematical and technical details) was written by the Chair with inputs from all team members.

At the NEA Data Bank, responsibility for the overall co-ordination of the Project was placed with Federico Mompean, with assistance from Myriam Illemassène and Jane Perrone.

Current knowledge of the thermodynamics of solid solutions as applied to deep geological disposal of radioactive waste may appear to be limited due to the scarcity of relevant thermodynamic data. Nevertheless, introduction of the solid solution formalism, which is more chemically plausible though requires more sophisticated experimental and modelling approaches than those needed for pure solid phases, is desirable since it is expected to provide a broader bridge between the thermodynamic and microscopic and mechanistic levels of description. Furthermore, because actinides are present in low concentrations in many solid phases, a solid solution approach is warranted to describe their partitioning in the environments of interest. Overall, the authors hope that readers will find this report useful.

Barcelona, January 2007 Jordi Bruno, Chair

Acknowledgements

For the preparation of this report, the authors have received financial support from the NEA TDB III Project. The following organisations take part in the Project:

ONDRAF/NIRAS, Belgium
OPG, Canada
RAWRA, Czech Republic
POSIVA, Finland
ANDRA, France
CEA, France
FZK, Germany
JAEA, Japan
ENRESA, Spain
SKB, Sweden
SKI, Sweden
HSK, Switzerland
Nagra, Switzerland
PSI, Switzerland
Nexia Solutions, UK
Nirex, UK
DoE, USA

The authors would like to express their sincere gratitude to the Peer Reviewers and the NEA TDB III participants for their numerous comments.

Jordi Bruno is particularly grateful to Fidel Grandia of Enviros Spain for his support throughout the preparation of the report. As Chairman, he feels indebted to the members of the Solid Solution Expert Team for their dedication and high-quality input to the report's specific chapters.

Dmitrii Kulik is thankful to Urs Berner, Enzo Curti, Michael Kersten, and Viktor Kurepin for years of stimulating discussions over years on various aspects of thermodynamics of aqueous-solid solution systems.

Project co-ordination was in the hands of Federico Mompean. The team is grateful for his continuous help and support in finalising it. The seemingly never-ending revisions of the original manuscript were managed by Myriam Illemassène and Jane Perrone. The authors wish to express their sincere gratitude to them.

The authors and editors are grateful to the following publishers for their permission to reproduce Figures I-1, I-2 and II-33 found in this volume:

Elsevier,

Mineralogical Society of America.

The full manuscript of this report has undergone a peer review by two independent reviewers:

Dr. Pierre Glynn, US Geological Survey, United States,

Dr. Erich Königsberger, Murdoch University, Australia.

Their contributions are gratefully acknowledged.

The peer reviewers have seen and approved the modifications made by the authors in response to their comments. The peer review comment records may be obtained on request from the OECD Nuclear Energy Agency.

Editor’s note

This is the tenth volume of the “Chemical Thermodynamics” series. Readers should note that it departs from the traditional scheme of reviewing the species and compounds of a particular element. It is intended to provide a state-of-the-art report on the chemical thermodynamics of aqueous-solid solution systems in the context of radioactive waste management.

No attempt has been made to systematically review the literature dealing with all aspects of solid solutions or to select data, although particular emphasis has been placed on the application of thermodynamic formalism to systems encountered in radio-active waste management which can be described as solid solutions.

How to contact the NEA TDB Project

Information on the NEA and the TDB Project, online access to selected data and computer programs, as well as many documents in electronic format are available at www.nea.fr.

To contact the TDB project co-ordinator and the authors of the review reports, to send comments on the TDB reviews, or to request further information, please send an e-mail to tdb@nea.fr. If this is not possible, write to:

TDB Project Co-ordinator
OECD Nuclear Energy Agency, Data Bank
Le Seine-St. Germain
12, boulevard des Îles
F-92130 Issy-les-Moulineaux
FRANCE

Contents

List of Figures

List of Tables

PART I: Extended summary

I.1 Introduction: scope, objectives and the audience of guidelines

I.1.1 Motivation

Aqueous-solid solution (Aq-SS) systems are ubiquitous both in natural and anthropogenic environments. In most nuclear waste repositories, solid solutions are intrinsic constituents of the various components of the repository system: from the waste source to the geosphere/biosphere interface.

Many components in UO_2 and MOX spent nuclear fuel are present as solid solutions of the UO_2 matrix, and their dissolution behaviour can be explained in the framework of Aq-SS, as we will illustrate in a later example in Chapter II.3. A similar situation has been described for the behaviour of trace components in the altered layer of vitrified nuclear wastes [2001GRA/MUL]. Cement, which is a central component in many designs and an unavoidable one in others, builds through its alteration an array of calcium silicate hydrate solid solution phases, commonly known as CSH. The corrosion of steel containers and cast iron inlets produces a variety of Fe(III)/Fe(II) oxyhydroxide solid phases which are able to incorporate trace components in their structures. While initially the trace metal interactions are mainly controlled by adsorption processes and described by surface complexation models [1990DZO/MOR] the evolution of these Fe(III) oxyhydroxide phases with time (ageing) and their interactions with contacting fluids may be described also in the context of Aq-SS systems. We will discuss in Section I.4 the evolution pathway of the various sorption processes and their influence upon the fate of trace metals in aqueous-solid systems.

Bentonite, which is one of the preferred backfill components in repository systems, contains both carbonates and sulphates as accessory minerals. The interaction of groundwater with the bentonite material produces the dissolution and reprecipitation of these carbonates and sulphates, mainly as calcite and gypsum. The behaviour of trace metals in these systems can be also modelled as an Aq-SS system. Besides, clay miner-

als montmorillonite and illite can also be treated as solid solutions, both with respect to cationic substitutions in the T-O-T layer and on particle edges, and regarding interlayer cation exchange.

The dissolution and precipitation of carbonates, sulphates and Fe(II)/Fe(III) oxyhidroxides is an ongoing process in many clay and granitic geosphere environments. Again, the solubility behaviour of the trace radionuclides in these environments cannot be decoupled from these main systems and their solubility behaviour is better approached by using the Aq-SS concept.

The thermodynamics of solid solutions/aqueous solutions are commonly used in metallurgy, ceramics and mineralogy, although the applicability of the concepts and methodologies to low temperature aqueous geochemical systems has been more limited. This is mainly due to the fact that solid diffusion is expected to be slow at low temperatures. However, as we will discuss later on, many solid phases show a remarkable structural flexibility to incorporate trace components even in situations when ionic size and charge are not the most favourable.

In this document, the specific emphasis is put on Aq-SS systems where partitioning of chemical elements of interest occurs between the solid solution and the aqueous electrolyte phases. Such systems are more complex than simpler systems involving solubility of stoichiometric solids or ion exchange. Only recently (since the 1980s), rigorous theoretical approaches have become available for Aq-SS systems (see Section II.1.2). All known features of Aq-SS behaviour show their fundamental property: the "dilution" of a minority (possibly hazardous) element in the host solid solution can greatly decrease its dissolved aqueous concentrations and, hence, mobility, compared with the case when the minority (hazardous) element forms its own "pure" solid phase. But it can also accumulate, for example, radionuclides beyond their assumed adsorption concentrations. This kind of radionuclide accumulation is then much more difficult to be mobilised when the geochemical conditions change.

Presently, the geochemical models used in the various stages of the safety assessment of a nuclear waste repository do not incorporate solid solutions in an explicit manner in the treatment of the solubility (and subsequent migration) of trace radionuclides, neither in the near nor in the far field of the repository system. While the solid solution concept is implicitly incorporated in the partition/distribution coefficients used to describe the overall radionuclide sorption process, only in the case of the solubility of Ra(II), the formation of Ra(II)/Ba(II) sulphate solid solutions has been taken into consideration [1999SKB]. The fact that solid solution formation is not considered as an acting process for radionuclide retardation has been justified in the grounds of a pessimistic consideration of the retardation capacity of the near field and the geosphere. But as already pointed out by Glynn [2003GLY], the formation of solid solutions may lead to radionuclide accumulation in certain parts of the system. These accumulations may

be later released when the geochemical conditions (redox, alkalinity…) change. In [2003GLY] this was exemplified by the oscillatory behaviour of Np and Pu pulses.

Except in some particular cases and certainly not in a systematic way, the thermodynamic properties of solid solutions have been also explicitly avoided in the previous review exercises performed within the various phases of the NEA TDB project ([1992GRE/FUG], [1995SIL/BID], [1999RAR/RAN], [2001LEM/FUG], [2003GUI/FAN], [2005OLI/NOL], [2005GAM/BUG], [2005BRO/CUR], [2005HUM/AND]). This was mainly due to the lack of agreed Guidelines concerning their treatment.

The Management Board of the OECD NEA TDB III Project felt in initiating an activity in the Programme of work of the Project leading to the preparation of scientific guidelines to assist in the evaluation and application of solid solution and Aq-SS systems in thermodynamic models.

I.1.2 Objectives

Hence, the objectives of this document are:

- To present state-of-the-art theoretical concepts and methods of solid solution thermodynamics from different scientific fields in order to propose methods to interpret and model experimental data for Aq-SS systems.
- To identify potential theoretical and experimental gaps that hinder the full applicability of Aq-SS systems in waste management.
- To provide guidance for the compilation and interpretation of solid solution thermodynamic data, both for experimenters and for reviewers within the NEA TDB Project.
- To present criteria and methods to model relevant Aq-SS systems.
- To present case studies which show the application of solid solution thermodynamics and Aq-SS systems in nuclear waste management-relevant uses and their potential application to the Performance Assessment of nuclear waste repositories.

I.1.3 Audience

The Guidelines contained in this document are in the first place directed to the various present and future expert review teams within the NEA TDB project in order to help them to use, interpret and incorporate aqueous-solid solution systems in their review work. In addition the Guidelines intend to target potential experimental groups in order to assist them to design experiments and interpret their solid solution experimental data in a way suitable to be incorporated in the current TDB efforts. The final outcome of these Guidelines should also be helpful to performance assessment modellers in order to stimulate them to incorporate such a relevant and ubiquitous concept for radionuclide

retention and, in turn, to provide a more scientifically robust description of the radionuclide migration in the various components of a repository system.

I.1.4 Scope

Since these Guidelines are mainly directed to the application of thermodynamic aqueous-solid solution models in the Performance Assessment of nuclear waste repositories, the emphasis will be placed on the solubility behaviour of radionuclide trace components incorporated into relevant host minerals (oxyhydroxides, carbonates, sulphates, sulphides, phosphates, clays) and anthropogenic materials (UO_2 solid solution and cements).

We limit our discussion to low temperature (t < 100 ºC) and atmospheric pressure systems and methods for temperature and pressure corrections (important for solid solutions considered in petrology and metallurgy) are largely left behind the scenes. This would in principle entail a number of kinetic restrictions to the solid solution formation process. However, consideration has to be given to phenomena such as the long residence times of water in the various parts of the repository system, the increased lithostatic and hydrostatic pressures in the geosphere and to the fact that, as we will document later in Section I.3, there is strong evidence of solid solution formation at low temperatures, particularly in soil systems where this process has been studied from the molecular point of view. However, specific methods of temperature and pressure corrections of thermodynamic properties (important for solid solutions considered in petrology and metallurgy) are largely left behind the scenes.

The elements to be considered will include those radionuclides for which there is fundamental evidence that their solubility behaviour is better rationalised in terms of Aq-SS systems. These are mainly actinides (U, Am, Cm), lanthanides (Eu) and some alkaline earth (Sr, Ra) and even more importantly some anionic fission products like selenate, and selenide that are known to substitute sulphate and sulphide in many mineral phases.

I.2 Definitions

These basic notions and definitions (mostly corresponding to IUPAC recommendations) are used and elaborated throughout the Guidelines. They are collected here to avoid misunderstandings or misinterpretations. Additional definitions will be provided in Section I.3 when describing the evolution between aqueous and solid solutions.

Phase is a homogeneous part of the (chemical) system such that temperature, pressure, and concentrations of the components are uniform within it. Different phases are separated by physical boundaries and can exist in solid, liquid, or gaseous aggregate states.

A **Mechanical mixture** can be viewed as a composition of two or more phases that are not chemically combined with each other and can be separated by mechanical means.

Miscibility is the ability of two or more substances to mix and form a single homogeneous phase called "solution".

Aqueous solution is a homogeneous mixture of one or more substances (the solutes) dissolved in another substance (the solvent - water). For example, a salt and a gas dissolved in water.

Solid solution is a homogeneous crystalline structure in which one or more types of atoms or molecules may be partly substituted for the original atoms and molecules without changing the structure, although the lattice parameters may vary.

Thermodynamically, the **composition** of a solid solution or an aqueous solution is expressed through concentrations of one or more chemical species (substances, components, end-members).

Composition of a **pure** (stoichiometric) **phase** can be described using one substance only, *i.e.*, it can appear in any system only having a definite constant (elemental) **stoichiometry** unequivocally related to structure. Examples are simple minerals like quartz SiO_2 or portlandite $Ca(OH)_2$.

Composition of a **solution** (multicomponent) **phase** needs two or more end-members for describing the whole range of it. Each **end-member** (species) must have a fixed elemental stoichiometry, but may have a variable concentration (*e.g.*, **mole fraction**) in the solution phase whose structure remains intact (with some minor change). Hence, the bulk elemental composition of a solution phase is variable. For example, the solid solution of Fe and Mn carbonate $(Fe,Mn)CO_3$ can be described as a homogeneous mixture $(1–x)FeCO_3 + xMnCO_3$ of two end-members $FeCO_3$ and $MnCO_3$ where x is the mole fraction of $MnCO_3$. In equilibrium with other phases present in the system, this mole fraction can take values from 0 (pure $FeCO_3$) to 1 (pure $MnCO_3$) depending on temperature, pressure and bulk elemental composition of the whole system.

Thermodynamically, an **ideal solution** is a solution where the enthalpy (heat) of solution is zero (see Section II.1.1). Any other solution is called **non-ideal**. The simplest regular non-ideal mixing model ignores non-configurational contributions to the entropy of mixing, assuming a zero excess entropy of mixing as a good first approximation.

In equilibrium between an ideal solution phase and an ideal gas, the partial (vapor) pressures of solution end-members are proportional to their mole fractions (**Raoult's law**). For simple ideal solid solutions, this law is often formulated in a different way: activities of end-members are equal to their mole fractions.

In real (solid) solutions, the thermodynamic **activities** of end-members differ from their mole fractions. To correct for that, the *activity coefficients* f_j defined through $a_j = f_j\, x_j$ are used (more in Chapter II.1). **Activity coefficients** are (often complicated) functions of the solution phase composition, usually defined such that the activity coef-

ficient of end-member equals 1 at its mole fraction $x = 1$ and approaches a constant at $x \to 0$. Various expressions for activity coefficients of solid solution end-members derived from the **excess** Gibbs energy of mixing G_{m}^{E} as function of phase composition, are considered in Section II.1.2.1.

Depending on the reference state convention used for the *j*-th component, the activity coefficient is denoted f_j (*symmetrical* convention used for gases, solid end-members and water solvent) or γ_j (*unsymmetrical* convention, used for solutes in aqueous electrolyte and solutes in dilute solid solutions). In literature, activity coefficients for solid end-members were sometimes denoted λ_j, which is not recommended by IUPAC and NEA TDB (f_j should be used instead).

The behaviour of a "trace" end-member ($x < 0.01$) is well approximated by **Henry's law**, originally stating that the mass of a gas dissolved in a definite volume of liquid is directly proportional to the partial pressure of the gas. This law is applicable to **dilute** components of all kinds of solutions (solid, aqueous, surface *etc*.). The coefficient of proportionality is called the Henry constant, k_H , and is related to a value of activity coefficient at infinite dilution.

Partition of a component (element) between two solution phases is usually characterised by a **distribution ratio** R_d (distribution coefficient) – a ratio of concentration of this component in one phase to that in another phase. This empirical value applies both to equilibrium and non-equilibrium situations. In the case of equilibrium, a ratio of concentrations of the same component M in two phases is called the **distribution constant** k_D. At low concentrations (*e.g*., for trace components), this constant defines the position of a (linear) uptake **isotherm** - a plot of concentration of M in solid solution *vs.* dissolved aqueous concentration of M.

Sometimes, for (B,C)L solutions, the **distribution coefficient** D is defined as the ratio of x_B/x_C (mole fractions of BL and CL) to $m_{B,aq}/m_{C,aq}$ (molalities of B and C, see Section II.1.2.1).

Solubility equilibrium in a strict sense describes the chemical equilibrium between the pure (solid) and the dissolved states of a compound. In the context of these Guidelines, "dissolved" is usually understood as dissolved in aqueous electrolyte. In the simplest case (*e.g*., dissolution of quartz at neutral pH), this is described by a reaction B(solid) $\rightleftharpoons$ B(aqueous) with **equilibrium constant** K_s . An ionic solid like ML dissolves to aqueous cations M^+ and anions L^- (or M^{2+}, L^{2-}, …), ML = $M^+ + L^-$. An equilibrium constant of such reaction is called the solubility product, $K_{s,0} = \{M^+\}\{L^-\}$ (braces denote ion activities). Other cases are described in Section II.1.2.1.

In a more general case (including equilibrium and non-equilibrium), the ion activity product $\{M^+\}\{L^-\}$ can be divided by the solubility product $K_{s,0}$ to obtain a **saturation index** SI. The case SI = 1 corresponds to equilibrium (saturation). If SI < 1 then

the aqueous solution is undersaturated to ML solid; if SI > 1, the aqueous phase is oversaturated.

Simple solubility relationships for a pure solid become more complex if the solid solution (*i.e.*, variable-composition solid) is dissolved. Such dependencies are usually represented using solubility products of pure end-members, *e.g.*, $K_{SP,BL}$, $K_{SP,CL}$, keeping in mind that their activities are no longer unity. There are two approaches – the **Lippmann functions** and diagrams, and the **unified theory** of solid solution solubility by Gamsjäger and Königsberger, both described in detail in Sections II.1.2.1 and II.1.2.2.

Theoretical approaches operate mainly with activities of dissolved components, while in experiments, the aqueous concentrations (molalities, molarities) are determined, often at high background electrolyte concentration (ionic strength). At such conditions, the activity of aqueous ion may be several times different from its measured concentration. This difference is accounted for by **aqueous activity coefficients** (see Section II.1.2.1) which must be considered in interpretation of almost any solubility data.

Further specific definitions about the various equilibrium status in Aq-SS systems, equilibrium, primary saturation, stoichiometric saturation and so on, are given in the following sections, where the theoretical grounds (fully developed in Part II, Section II.1) and the experimental techniques (detailed in Part II, Section II.2) are introduced.

I.3 From Aqueous to Solid Solutions

This section intends to demonstrate that there is a continuum between the processes that control the fate of trace components in the aqueous and solid phases.

From the process perspective we may describe the transfer and partitioning of chemical components between an aqueous phase and an adjacent solid phase under the general term of **Sorption.**

Mechanistically, sorption may occur through different mechanisms but the main ones from the perspective of this work are listed below.

Adsorption: the accumulation of the chemical component at the interface between the aqueous phase and an already existing solid phase without the development of a three-dimensional molecular arrangement. This is presently rationalised from a mechanistic point of view by using surface complexation models which integrate in the thermodynamic framework the electrostatic interactions and the chemical bonding between the adsorbed chemical species and the solid surface.

Absorption: the uptake through the diffusion of an (aqueous) chemical component into the whole volume of the existing (micro/nanoporous) solid phase (*e.g.*, in zeolites).

Precipitation: the transfer of an aqueous chemical component into the solid phase by growing a three dimensional molecular arrangement – the crystal structure. Precipitation may be initiated by a *homogeneous nucleation* forming a pure solid phase, or by a *heterogeneous nucleation* and growth into an already existing solid phase by inclusion or by precipitation onto an existing surface; the latter is known as **surface precipitation**.

Co-precipitation: the precipitation and crystal growth process, in which the minor component of interest forms a common (mixed-composition) structure with the major (host) component. This requires a certain oversaturation of aqueous solution with respect to pure major component, while most often an undersaturation with the pure minor component.

Recrystallisation: the process of rebuilding the crystal structure of the host solid solution in contact with the aqueous phase into the same type of structure, but possibly with different concentrations of minor components as a response to changes in composition, temperature and pressure in the system.

As previously defined a **solid solution** is a homogeneous crystalline structure in which one or more types of atoms or molecules may be partly substituted for the original atoms and molecules without changing the structure, although the lattice parameters may vary. The solid components are regularly ordered in a periodic three dimensional structure.

Adsorption, co-precipitation and surface precipitation are precursory mechanisms for the formation of solid solutions, although the regular molecular arrangement in a three dimensional structure requires additional processes like ion-diffusion into the solid and recrystallisation of the initial solid phase.

In the time scale, adsorption normally precedes the formation of surface precipitates and, therefore, there is certain continuity in the following process chain (arranged from short to long reaction times):

Aqueous complexation ⇒ Adsorption (surface complexation) ⇒ Absorption ⇒ Surface precipitation ⇒ Co-precipitation ⇒ Ion-diffusion ⇒ Solid Solution recrystallisation.

Figure I-1, extracted from Manceau *et al*. [2002MAN/MAR], gives an indication of the complexity and richness of the various sorption processes (governing the element partition between solid and aqueous phases) involved in natural systems.

Sorption is a key process in the retardation of radionuclides in the geosphere. As we can see, it involves a number of processes which are substantially different from the molecular point of view and occur in different time scales. A fundamental finding which is easily forgotten is that molecular processes have to be investigated at the molecular level. The macroscopic approximation (mass balance studies), although neces-

sary, it is never sufficient to distinguish between the various sorption processes, this was already pointed out by Sposito [1986SPO]. In addition, the incorrect identification of the sorption processes may lead to an inaccurate quantification of the process and consequently in their application to Performance Assessment as it has recently been illustrated by Glynn [2003GLY].

Figure I-1: Basic processes of absorbate molecules or atoms at mineral-water interface. a) physisorption; b) chemisorption; c) detachment; d) absorption or inclusion; e) occlusion; f) attachment; g) hetero-nucleation; h) organo-mineral complexation; i) complexation to bacterial exopolymer and to cell outer membrane (extracted from Manceau *et al*. [2002MAN/MAR]). Reprinted from [2002MAN/MAR], Copyright (2002), with permission from the Mineralogical Society of America.

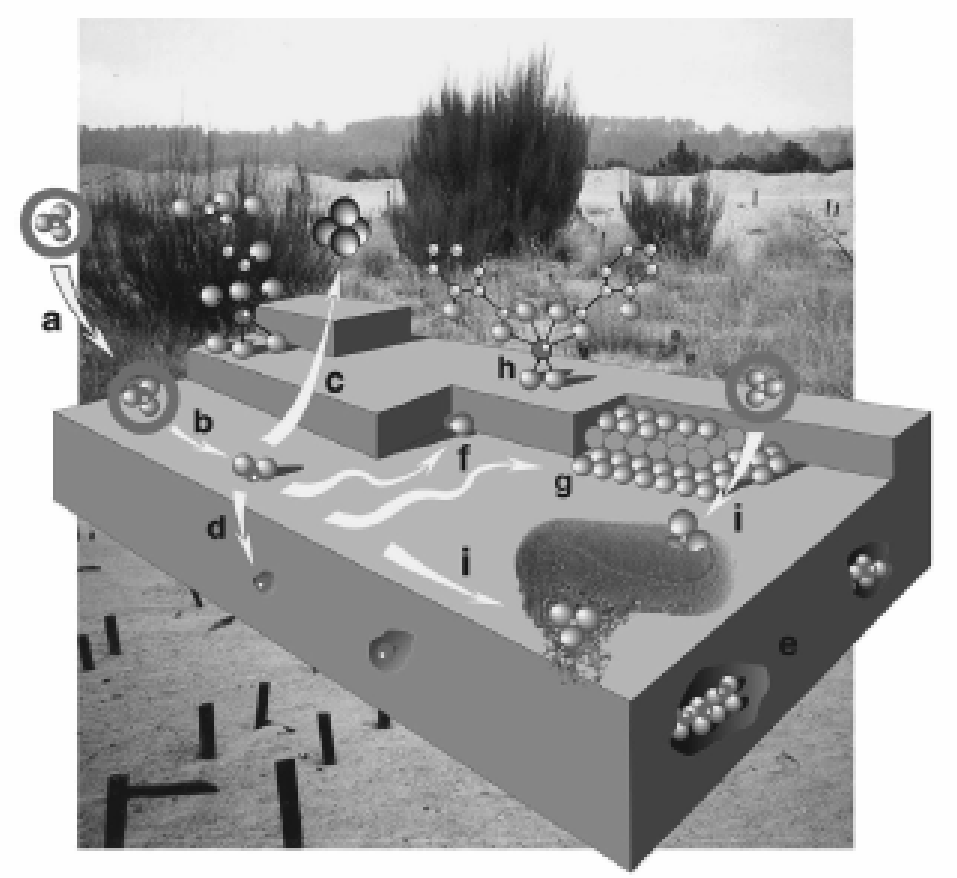

As we will discuss in Section II.2, the development and application of molecular and atomic spectroscopic techniques is key to the understanding and quantification of the Aqueous-Solid Solution processes and a prerequisite to their thermodynamic description.

It is interesting to point out in this context, that several spectroscopic techniques have been applied for discerning the various sorption processes as described in Part II, Chapter II.2, since the pioneering work of McBride in the use of Electron Spin Resonance (ESR) for discriminating the bonding environment of Mn^{2+} in carbonate phases [1982MCB]. The combination of ESR and solution chemical studies was used by Wersin *et al*. [1989WER/CHA] to describe the continuous transition between Mn^{2+} sorption and surface precipitation on siderite ($FeCO_3$(s)), as a function of the siderite surface coverage by Mn^{2+} The same process continuity has been found to describe the sorption products of Pb(II) onto the calcite surface investigated by Rouff *et al*. [2004ROU/ELZ] by a combination of batch tests and X-Ray absorption spectroscopy. Depending on the calcite surface coverage by Pb(II) the sorption mechanism changes from mononuclear inner sphere surface complexation to the surface precipitation of cerussite and hydrocerussite phases. The sorption continuity process is not only constrained to carbonates. The application of EXAFS spectroscopy and chemical solution methods to the investigation of the sorption of Zn(II) onto alumina oxides indicated the transition from Zn^{2+} bidentate complexes onto the alumina surface to the formation of Zn-hydrotalcite like nanophases as precursors of their co-precipitation [2000TRA/BRO].

A common thread in all these studies is that the transition between adsorption (surface complexation) and the formation of distinct trace component solid phases as surface precipitates occurs at trace metal surface coverage in the range 10^{-6} to 10^{-5} mol·m^{-2}.

The transition from the adsorbed layer or surface precipitate to solid solution is more difficult to ascertain, particularly at ambient temperatures, where ion diffusitivities in the solid phases are low, and where the recrystallisation and the epitaxial growth appear to be the only plausible mechanisms for the formation of solid solutions at low temperature.

There are some examples of low temperature solid solution formation *via* diffusion and recrystallisation, mainly for divalent carbonates. This is based on the fact that the diffusion coefficient of divalent cations in calcite is of the order of magnitude of 10^{-19} to 10^{-20} cm^2·s^{-1} [1964LAH/BOL], which gives depths of penetration of some 3 nm in two weeks [1992STI/HOC]. These authors presented a convincing case for the formation of $CdCO_3$/$CaCO_3$ solid solution formation through surface complexation of Cd^{2+} on the $CaCO_3$ surface followed by Cd^{2+} diffusion into the calcite lattice at ambient temperature. Similar mechanisms have been proposed to operate for other divalent cation calcium carbonate solid solution formation at low temperature. Low temperature diffu-

sion of cations into solid lattices is not only restricted to carbonates. In the soil science literature there are numerous examples of cation diffusion into Fe(III) oxyhydroxides, see for instance [1988BRU/GER] where they report evidence of the diffusion of Ni^{2+}, Zn^{2+} and Cd^{2+} into goethite.

While ferrites have been reported to be high temperature phases, Pérez-Perales and Umetsu [2002PER/UME] have investigated the formation of Zn(II) ferrites by a combination of solution chemistry diffraction and spectroscopic (XRD, EMPA, SEM) techniques. Their work indicates that crystalline Zn-ferrites are formed at low temperatures (25 ºC) when the appropriated redox, acidity and Zn/Fe ratios are satisfied.

Epitaxial growth and recrystallisation has been reported as solid solution formation mechanism for a number of aluminosilicate phases. The development of EXAFS spectroscopic techniques has been very useful in order to establish this mechanism for the solid solution formation at low temperature. As an example, we include in Figure I-2 the formation sequence of Zn/Mg phyllosilicate as monitored by EXAFS [2002MAN/MAR].

Figure I-2: Formation sequence of Zn/Mg phyllosilicate as monitored by EXAFS. Reprinted from [2002MAN/MAR], Copyright (2002), with permission from the Mineralogical Society of America.

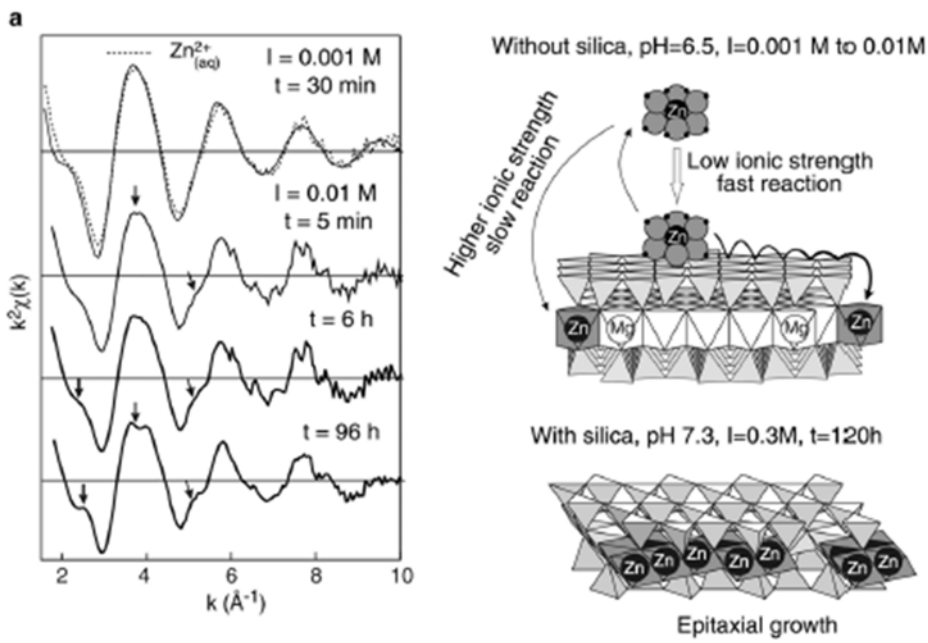

Another example of low temperature (5 - 15 ºC) rapid solution formation is encountered in the various phase transformations resulting from the sulphate attack on cement. Köhler *et al*. [2006KOH/HEI] report the effect of ettringite on thaumasite formation by studying pastes mixed using synthetic clinker phases, fly ash and nanosilica. The results indicate that thaumasite formation occurs through the heterogeneous nucleation of thaumasite on the surface of ettringite, due to the structural similarities of these minerals. This reaction is followed by further epitaxial growth of thaumasite from its components present in solution. Similar observations have been made by Blanco-Varela *et al*. [2003BLA/AGU].

It should be clear from the previous discussion that the transition of a trace component from being an aqueous solute to finally become a solid solute entails a number of complex processes which may occur sequentially and also in parallel. The thermodynamic description of the Aq-SS processes has to some extent acknowledged this complexity. Macroscopic determinations have to be complemented by proper molecular level spectroscopic analyses in order to gain the process understanding. This is further stressed in the discussion of the experimental methodologies for the determination of Aq-SS equilibria in Part II, Chapter II.2.

I.4 Basic Thermodynamics of Solid Solutions

This section intends to bring into this Part I the basic concepts related to the thermodynamic description of Aqueous Solution-Solid Solution systems. A more detailed account is given in Part II, Chapter II.1 of this document.

Consider the general reaction:

$$x_A A(s) + x_B B(s) \rightleftharpoons A(x_A)B(x_B)(s) \qquad (I.1)$$

where A(s) and B(s) are the end-members which mix to form a homogeneous solid solution of intermediate composition described with mole fractions, x_A, x_B (in a binary system, $x_A + x_B = 1$).

At atmospheric pressure and temperature T, the Gibbs energy per mole of an isostructural binary solid solution can be written as:

$$\Delta G_m\,(\text{solid solution}, T) = x_A\, G_m^o\,(A, T) + x_B\, G_m^o\,(B, T) + \Delta G_m\,(\text{mix}) \qquad (I.2)$$

where $\Delta G_m\,(\text{solid solution}, T)$ is the standard Gibbs energy of the solid solution, $G_m^o\,(A, T)$ and $G_m^o\,(B, T)$ are the standard Gibbs energies of the end-members A and B, and $\Delta G_m\,(\text{mix})$ is a Gibbs energy of mixing term. Note that throughout this section, the superscript zero refers to the standard state of pure component, $x = 1$.

The $\Delta G_m\,(\text{mix})$ term consists of an enthalpy and entropy terms:

$$\Delta G_m\,(\text{mix}) = \Delta H_m\,(\text{mix}) - T\,\Delta S_m\,(\text{mix}) \qquad (I.3)$$

The conceptualisation and quantification of the Gibbs energy of mixing is a fundamental issue in the determination and application of Aq-SS thermodynamics and it will be tackled in Parts 1 and 2 of this work both from the theoretical, the experimental and the modelling perspectives. In the following sections we will briefly discuss the nature of the contributors to the Gibbs energy of mixing in solid solution systems, this is the enthalpy and entropy of mixing. A more thorough discussion is found in Chapter II.1 of Part II.

I.4.1 The enthalpy of mixing

The enthalpy of mixing term contains the energetics of the interactions. Positive $\Delta H_{\mathrm{m}}^{\mathrm{o}}$ (mix) generally indicates clustering of like species and a tendency toward exsolution, while a negative $\Delta H_{\mathrm{m}}^{\mathrm{o}}$ (mix), generally suggests ordering of unlike species and a tendency toward formation of an intermediate compound. Both tendencies may occur simultaneously in the same system (see the examples of carbonates and feldspars in Chapter II.1 of Part II).

I.4.2 The entropy of mixing

There are three contributions to the entropy of mixing: (a) changes in the vibrational entropy term, (b) terms from changes in magnetic and electronic entropy, and (c) the configurational or statistical term arising from the occupancy of equivalent sites by different chemical species. The last is usually the most important. It arises through statistical mechanics and is fundamentally related to the greater randomness (or loss of information about which ion is on a particular site) in the solid solution compared to the pure end-member.

All substitutions must maintain electroneutrality (balance of formal charges) in the crystal. The substitutions may involve one or more sets of crystallographic sites (sublattices). They may involve ions of like charge, charge coupled substitutions on one sublattice or on several, or the creation or filling of vacant sites.

This structural complexity must be reflected in the thermodynamics of solid solution formation and its subsequent interaction with aqueous solutions. Thus, the crystal chemistry must be understood very well, and various analytical, structural and spectroscopic techniques applied to sample characterisation.

Although thermodynamics offer a macroscopic description, linking thermodynamic properties to the microscopic (atomistic or molecular level) features of the solids insures that the description is not simply and arbitrarily empirical. Such linkage is especially critical if one wishes to extrapolate properties to conditions of pressure, temperature, or composition outside the range where measurements have been made. This is clearly a very important condition when aiming to apply aqueous-solid solution thermodynamics to the performance assessment of nuclear waste repositories. The basic theoretical question is to relate the microscopic details of atomic interactions to site occu-

pancies and macroscopic thermodynamic parameters. The basic practical problem is to obtain useful expressions for the thermodynamic mixing properties of multicomponent solid solutions and to apply them to solid-aqueous phase systems. These practical models should be simple enough to be incorporated into computer codes describing phenomena such as the hydrothermal and geochemical evolution of a nuclear waste repository. They should be robust enough to withstand interpolation and some extrapolation.

I.4.3 Regular, subregular and generalised mixing models

The Gibbs energy of mixing —one of central themes in these Guidelines— can be theoretically analyzed in many ways, the most popular one suggested by Guggenheim (see Part II Chapitre II.1).

For a two-component system, the simplest formulation for ΔG_m^E (mix) (assuming zero excess entropy of mixing) is:

$$\Delta G_m^E(\text{mix}) = \Delta H_m(\text{mix}) = \text{R}T\,\alpha\, x_A x_B = W_H\, x_A x_B \qquad \text{(I.4)}$$

where α or W_H is the interaction parameter. For a large positive interaction parameter, the model reproduces a symmetric miscibility gap; negative interaction parameter means that the real solid solution is more stable than the ideal one. The end-member activity coefficients can be easily derived from equations like the one above. More complex expressions with even number of interaction parameters result in "asymmetric" mixing models, odd number of parameters —in "symmetric" models (more in Part II).

I.4.4 Dilute solid solutions

Dilute solid solutions represent a practically important case for incorporation of trace elements *Tr* (*e.g.*, radionuclides) into host mineral phases such as calcite, when the mole fraction of *Tr* does not exceed a percent. It can be shown that γ_{TrL} is approximately constant at trace mole fraction of *Tr*. Thus, at trace mole fraction, the analysis of non-ideal mixing becomes simple because the activity of dilute end-member can be well approximated using Henry's law. In recognition of this fact, a *dilute solid solutions formalism* has already been applied to solid solutions [1990BAL/PEL], [1992KON/GAM2].

I.4.5 On the relevance of non-ideality

Although the ideality treatment in some Aq-SS has been long controversial, there is a general consensus that two factors mainly control the degree of non-ideality [1975URU], [1996TES/PAN], [1999CUR]:

1/ similarity in size between host and substituting ions and
2/ similarity in crystal lattices.

As an example, Cd^{2+} incorporation to the calcite lattice can be treated as an ideal system since ionic radii of this ion is very similar to Ca^{2+} in calcite, and the crystal classes of pure phases (otavite, $CdCO_3$, and calcite) are the same. Tesoriero and Pankow

[1996TES/PAN] showed that the experimentally measured partition coefficient, D, between Cd^{2+} and calcite is close to that calculated if the system is treated as ideal. Conversely, for other cations such as Sr^{2+} and Ba^{2+}, whose sizes are significantly larger than Ca^{2+} and the solid phases (strontianite and witherite, respectively) belong to different crystallographic systems, the partition coefficients differ in more than two orders of magnitude, suggesting strong non-ideality.

The experience acquired from the study of cation incorporation in carbonate and sulphate phases has shown that most Aq-SS systems must be treated as non-ideal systems. This statement leads to a new question, to what extent the SS non-ideality is relevant? The answer depends on the objectives of the study and on the range of concentrations of interest. In the whole range, when all end-members are taken as major, the non-ideality may often cause the formation of intermediate phases due to ordering phenomena (*e.g.*, dolomite in $(Ca,Mg)CO_3$ system) and/or miscibility gaps due to exsolution. Inside of the miscibility gap, at least two solid solution phases with different fixed compositions coexist with the aqueous electrolyte, composition of which is also fixed. Any change in the bulk composition of the Aq-SS system will result upon equilibration only in changed masses of solid phases but in unchanged concentrations of all end-members and aqueous species. Outside the miscibility gaps, the solid solution non-ideality may result in a significant (several times) deviation of dissolved ion concentrations compared to the ideal case. At trace concentrations, the activity coefficients become (almost) constant and simply shift the uptake isotherm up or down, sometimes in 1-2 orders of magnitude if compared to the ideal isotherm for the same end-member.

The following question is also important: What is the right level of complexity of a non-ideal mixing model for the solid solution? The answer depends on the number of end-members and on the accuracy of experimental data used in regression of the interaction parameters of the mixing model. As discussed in Part II, Chapter II.3, the wet chemistry solubility data (K_d, compositions of coexisting aqueous and solid solution phases) usually are so scattered that only one regular interaction parameter (α in Eq. (I.4)) can be determined unequivocally in a binary SS system. In a ternary system, even in the regular model, three binary and one ternary interaction parameters must be determined, which requires a dramatically larger number of experiments which usually is very difficult to produce. On the other hand, the subregular (asymmetric) mixing models, better justified from theoretical viewpoint, can still be parameterised in some suitable Aq-SS systems using the results of galvanic cell measurements which are about 10 times more accurate than the solubility data. Any non-ideal mixing model is difficult to extend on a solid solution system containing more end-members because far more interaction parameters need to be determined.

I.4.6 Solid solution *versus* other uptake modes

Consider a multi-component solid with relatively insoluble end-members in a scenario with a high solid-to-aqueous ratio and short equilibration time. Under these conditions, such a solid may be treated as a pure phase because it is often observed that the dissolution of this solid is congruent during low-temperature reactions while no recrystallisation or precipitation of secondary phases occurs. Thorstenson and Plummer [1977THO/PLU] developed this idea and defined the concept of *stoichiometric saturation*, reviewed in these Guidelines.

In the second case, if the above conditions are not fulfilled, *i.e.*, the solid is able to recrystallise/reprecipitate adjusting its composition due to changes in the composition of the coexisting fluid, the thermodynamic equilibrium between solid solution and aqueous phases can be approached closely.

In the third case, upon the reaction progress, the initial solid solution dissolves until the point when the same solid solution of different composition starts precipitating. This scenario is called *primary saturation*, which is defined as the first ("snapshot" equilibrium) state reached during the congruent dissolution of a solid solution [1978GAR/WOL], [1983DEN/MIC], [1990GLY/REA].

As pointed out by [2000GLY], it is likely that in many natural Aq-SS systems, stoichiometric and primary saturation concepts do not fully explain the observed solubilities of solid solution, rather an intermediate behaviour is observed. An aqueous solution at primary saturation or at thermodynamic equilibrium with respect to a solid solution will be undersaturated with respect to all its pure end-member components.

The second and third cases of Aq-SS behaviour (formation of a new SS of different composition), as well as the co-precipitation of a minor component into a host mineral, may be difficult to discriminate from various sorption processes (adsorption, ion exchange, surface precipitation) on the basis of macroscopic partition data alone. Experiments in such systems often produce linear isotherms which tell nothing about the actual incorporation mechanisms. However, there are some practical criteria that help qualifying the process at least in some systems. A prerequisite for such criteria is that the specific surface of reactive solid is known.

(i) Kinetics and reversibility: adsorption and ion exchange (either on surface or in the interlayer) are relatively fast reactions; in comparison with chemisorption on mineral surfaces, the ion exchange is (almost) reversible. Experiments at high co-precipitation rates may result in weak partitioning of minor component into solid which does not correspond to Aq-SS equilibrium but rather to metastable adsorption states.

(ii) Balance and densities in the surface layer: In most cases, adsorption is limited to a surface monolayer. The maximum amount of metal adsorbed can be estimated from the amount of sorbent, its specific surface, and the site

density parameter. If the measured amount is significantly larger then lattice incorporation or surface co-precipitation processes are probably involved.

(iii) Measurement of the host mineral recrystallisation extent (*e.g.*, with radiotracers). In the case of adsorption or ion exchange, there should be (almost) no recrystallisation. If recrystallisation is significant and amounts to several surface layers (often the case for carbonates) then solid solution is a more likely mechanism than sorption.

(iv) Spectroscopic and microscopic studies, especially surface-sensitive, can support mechanistic interpretation of the macroscopic data either as surface-dependent uptake (adsorption, surface precipitation) or (layer) volume uptake (ion exchange, solid solution formation).

(v) Volume uptake mechanisms such as ion exchange in clays or zeolites can be modelled using either the solid solution concept or the (ad)sorption concept based on the capacity (surface site density) parameter. In this case, the (pore) surface- volume relationships must be known.

One must keep in mind that for most of the applications of interest in radioactive waste management, the radionuclides of concern will occur at rather small concentrations compared to the major components in the Aq-SS systems. In this context, the incorporation of radionuclide trace components into a host solid solution can be approached quasi-ideally, and the partition of trace radionuclides can be approximated by Henry's Law with conditional solubility products established as shown in Section II.1.1.4.1. Advantage of this simple approach is that no information about surfaces or pore volumes is needed, only the amount of reacted host mineral must be known.

I.4.7 Concepts and approximations in geochemical modelling of Aq-SS systems

As already mentioned in Section I.1.3, these Guidelines are intended to provide a scientific background for incorporating solid solution and Aq-SS concepts and data in the geochemical models used in performance assessment studies. To this end, two different approaches can be used depending of the existing data: the *forward* and *inverse modelling*.

Forward modelling consists of the prediction of concentrations (or activities) of chemical species in solution and of solid phases in a system under specific temperature and pressure conditions. In most codes, this type of models is based on the law of mass action (LMA) formalism. Most of the geochemical code packages used in PA related calculations are of this kind, *i.e.*, PhreeqC, EQ 3/6. Aq-SS systems can be treated in these codes to a limited extent (see Part II, Section II.1.2.3); solving Aq-SS equilibria with LMA codes is, in general, not a straightforward process because a single aqueous speciation calculation turns into a series of many runs controlled by non-rigorous test

procedures, without a theoretical guarantee of convergence to a unique solution. The only case which is easy to solve with LMA methods is the stoichiometric saturation state [1990GLY/REA] in which the solid solution is treated as a pure (fixed-composition) solid phase.

Inverse modelling is usually performed for determining some input parameters (*e.g.*, solubility products, initial system composition) provided that some output parameters (*e.g.*, dissolved concentrations, or mole fractions in equilibrium) are measurable and available. In the case of Aq-SS systems, inverse modelling may help to determine values of activity coefficients, interaction parameters, standard Gibbs energies and/or solubility constants of end-members. The available codes to perform extended inverse modelling calculations in Aq-SS systems include the GEMS-PSI package (see more in Part II, Section II.1.3).

I.4.7.1 Lippmann diagrams, a tool to visualise binary Aq-SS systems

Binary Aq-SS systems are, in fact, ternary systems in which two components are solid mixture end-members, and one component is the aqueous electrolyte solution. The latter is always in excess, therefore such systems are often called "pseudo-binary" or simply "binary" because they involve a binary solid mixture. In geochemistry and aquatic chemistry, the Lippmann phase diagram [1977LIP], [1980LIP], [1982LIP] became a popular tool for analysing pseudo-binary Aq-SS equilibria after papers by [1990GLY/REA], [1990GLY/REA2], enhanced with the MBSSAS code [1991GLY] for computing/plotting such diagrams, retrieving Margules parameters and equilibrium relations. This work has been extended and deepened by [1992KON/GAM], [2000GAM/KON], [2000PRI/FER]. A full description of the development and application of Lippmann diagrams is given in Part II, Section II.1.2.2.

Several illustrative examples of the theory and application of Aq-SS to trace elemental (radionuclide) solubility are developed in Part II.3.

I.4.8 Kinetic and thermodynamic approximations to Aq-SS in geochemical reactive transport modelling

Recently Lichtner and Carey [2006LIC/CAR] have presented a promising approach in order to link the kinetics and thermodynamics of solid solution formation into reactive transport modelling.

The method is applicable to problems involving advective, dispersive, and diffusive transport in a porous medium. The authors represent the continuously variable solid solution composition by a discrete set of stoichiometric solids that cover the composition range and they combine it with a kinetic formulation of the rates of reaction. In this way a spatial and temporal evolution of the solid solution concentration and composition is obtained. Lichtner and Carey [2006LIC/CAR] have demonstrated that equilibrium of an aqueous solution with a stoichiometric solid derived from a solid solution

corresponds to equilibrium of the solid solution itself if and only if equilibrium of the stoichiometric solid is stable. One advantage of this approach is that it is unnecessary to introduce any additional compositional variables to represent the solid solution. A major consequence of this kinetic discrete-composition solid solution representation is that modelling solid solutions is similar to modelling pure mineral phases with the exception of a weighting factor applied to reaction rates of stoichiometric solids corresponding to a common solid solution. With this approach, precipitation leads to a discrete zonation of the solid solution that approximates the continuous variation in composition expected for the actual solid solution. The approach is demonstrated for a hypothetical ideal and non-ideal binary solid solution $A_xB_{1-x}C$.

Recently, we have [2006AYO] implemented this Lichnter formalism in the Retraso reactive transport code with quite promising results.

I.5 Experimental and analytical aspects

Thermodynamics of solid solution-aqueous solution (Aq-SS) systems is relatively well established on theoretical side (see Chapter II.1) [2000GAM/KON], [2000GLY], [1990GLY/REA], [1980LIP] and advanced numerical methods have been developed to describe such systems quantitatively (see Chapter II.2). However, applying these concepts successfully to *real world* problems requires actual thermodynamic data as a baseline for geochemical modelling. Such thermodynamic data can be obtained either from laboratory experiments with synthetic compounds or from analysis of naturally occurring solid solution phases. Here, the focus will be on how to derive thermodynamic data from co-precipitation experiments using synthetic systems at relatively low (waste repository relevant) temperature $T < 373$ K. There will be some emphasis on high temperature synthesis as well as on samples from natural systems.

Characterising the aqueous solution and the solid phase on mineralogical and molecular levels is a prerequisite for deriving thermodynamic data. It is also crucial to prove that the Aq-SS system represents equilibrium conditions. Furthermore, synthesising solid solution phases from aqueous solution involve various potential pitfalls which need to be identified before one starts to interpret experimentally obtained data in terms of Aq-SS thermodynamics. Therefore, the intention of Chapter II.2 is to provide a critical overview of analytical techniques which are typically used to characterise the aqueous solution and the solid solution phase and how one obtains raw data usable for the thermodynamic description of such a system.

First of all, synthesis procedures, as well as some fundamental aspects of co-precipitation experiments in aqueous solution, will be discussed. Special emphasis will be on actinides and fission products in the trace level concentration range.

I.5.1 Synthesis procedures

Probably the most common way to synthesise solid solution phases is by simple ***batch type*** experiments where the host solid phase (major component) is supersaturated. This is done by mixing two different components to produce the solid phase and a trace component to co-precipitate. Normally, these kinds of experiments produce chemical zonation and logarithmic distribution laws (Doerner-Hoskins). Potential experimental approaches to minimise these effects are explain in full detail in Section II.2.1.1.1, they include ***batch-type constant composition methods***, and ***counter-diffusion experiments*** [1997PRI/FER], [1993PRI/PUT]. Many of the drawbacks involved in the above-mentioned techniques can be overcome by performing co-precipitation experiment in a ***mixed flow reactor.*** With respect to experimental studies on Aq-SS systems, it seems crucial that one understands the involved reaction mechanisms that occur throughout an experiment on a molecular level. In particular, when working under low (room)-temperature conditions in aqueous systems, kinetic effects, the formation of precursor phases and the metastability effects have to be critically taken into account before using experimental results for determining thermodynamic data. The synthesis procedure will ultimately depend on the final objective of the solid solution to be investigated.

I.5.2 Characterization of the solid solution

As we have repeatedly pointed out, the characterisation and determination of the resulting solid phase at molecular or even atomic level is a fundamental prerequisite for the establishment of the appropriated sorption mechanism and consequently for the determination of the thermodynamic properties of the Aq-SS.

The following table gives a brief account of the presently existing techniques to characterise solid solutions. This is at present a very dynamic research and more and better techniques are becoming available these days.

Table I-1: Overview of some selected analytical techniques to obtain key information of solid solution phases.

Mineralogical composition	***Phase identification, element concentrations, compositional homogeneity***
ICP-AES/MS (Inductively Coupled Plasma−Atomic Emission Spectrometer/Mass Spectrometer)	ICP-AES/MS provides element concentrations down to the ultra trace concentration range.
SEM (Scanning Electron Microscopy), TEM (Transmission Electron Microscopy), EM (Electron Microprobe)	SEM, TEM, EM can provide spatially resolved chemical analysis.
XRD (X-ray Diffraction)	XRD allows identification of solid phases (based on known crystal structures).
Speciation	***Characterisation of redox state and identification of molecular species***
XAS (X-ray Absorption Spectroscopy) XANES (X-ray Absorption Near Edge Structure)	The XANES region in a X-ray absorption spectrum provides information about the redox state (valence shift) in the sense of fingerprinting.
TRLFS (Time Resolved Laser Fluorescence Spectroscopy)	TRLFS provides information about the coordination sphere of certain radionuclides. Fluorescence energy and associated life time can be analysed independently. Changes in the peak maxima of the emission spectra indicate a change in the chemical environment or ligand field. Changes in the life time indicate the presence of quenchers such as H_2O or OH^- molecules in the 1st coordination sphere.
Structure	***Lattice constants and associated long-range order (LRO) and short-range order (SRO) phenomena***
XRD (X-ray Diffraction)	Characterisation of long-range order phenomena (*e.g.*, lattice constants, superstructures) and site occupancies based on powder or single crystal measurements.
XAFS (X-ray Absorption Fine Structure) EXAFS (Extended X-ray Absorption Fine Structure)	XAFS spectroscopy provides information about SRO phenomena. The XANES region contains information about coordination geometry and orientation. The EXAFS region provides information about bond lengths, coordination numbers and type of coordinating atoms (EXAFS equation).
NMR (Nuclear Magnetic Resonance)	NMR spectroscopy provides information about local coordination environment of a nuclide, based on differences between allowed spin states of atomic nuclei.
Thermodynamics	***Thermodynamic mixing properties (e.g., entropy, enthalpy, heat capaciy)***
Calorimetry	Measurement of heat capacities and heats of phase transitions (thermophysical measurements) and measurement of heats of reaction (thermochemical measurements).
Electrochemical measurements	The electrochemical potential between well defined aqueous-solid solution systems can provide directly thermodynamic data on solid solution-aqueous solution equlibria.

I.5.3 Solubility measurements in aqueous solutions

The natural way to experimentally characterise Aq-SS equilibria is by means of solubility measurements. In contrast to solubility studies of pure compounds, the solubility measurements in Aq-SS systems potentially involve a number of experimental complexities that have to be fully assessed prior to the data interpretation. In Section II.2.2, three solubility concepts for Aq-SS systems are introduced and discussed for a simple binary (B,C)A system —*e.g.*, (Ba,Sr)SO_4, Barite-Celestite:

(1) Thermodynamic equilibrium,

(2) Primary saturation and

(3) Stoichiometric saturation.

The graphical interpretation of Aq-SS solubility experiments in quasi-binary systems (two solid end-members and the aqueous phase) can be done by applying Lippmann diagrams based on the total solubility product ΣΠ [1990GLY/REA].

The main difficulty arising from direct solubility measurements of Aq-SS systems concerns the evolution and the determination of the resulting solid solution phase(s) which may form as a result of putting in contact an initial solid solution phase with an aqueous solution. Upon the incongruent dissolution of the initial solid solution phase, secondary phases may form. In this context, much care has to be taken in order to ensure that the solid solution under study has been properly characterised, otherwise the resulting thermodynamic data can be wrong. Various spectroscopic techniques available for the characterisation of solid solutions are described in the following section and more extensively in Chapter II.2.

Additionally, once the resulting solid solution phase is well characterised the required precautions have to be put in place when dealing with the measurement and determination of the resulting aqueous solution. In this respect we submit the reader to the appropriated Guidelines of the NEA TDB project concerning solubility determinations and ionic strength corrections [1999NEA].

I.5.4 Partition/distribution experiments

Partition experiments are a specific variation of solubility measurements in Aq-SS systems, which have been largely used in the past and form the basis for the initial description of homogeneous and heterogeneous (logarithmic) distribution laws as a means to quantify sorption/uptake of trace components. In this case, the emphasis of the experimental determination resides on the trace component concentration in the solid and in the aqueous phases, because the distribution coefficient is usually defined as the ratio of both.

Two different experimental setups were used. (1) *Co-precipitation uptake:* the trace component is co-precipitated with a certain host solid (*i.e.*, calcite), and the distribution of the trace component between the solid and the aqueous phase is monitored as

a function of time and initial trace component addition in the system. (2) *Recrystallization uptake*, when a spike of the trace component is introduced into an already equilibrated Aq-SS system, and the distribution of the trace component is monitored as a function of time and aqueous trace element concentration.

Most past experiments of either type (1) or (2) were not supported by the appropriate spectroscopic characterisation of the resulting solid phases and, therefore, no conclusive data on the incorporation mechanisms can be derived from the partition experiments alone. There are, however, notable exceptions, where the distribution data is complemented with proper spectroscopic characterisation of the trace component bonding environment in the solid phase [1989WER/CHA]. In this case, the distribution data can be used to derive the thermodynamic properties of solid solution end-members.

More detail on the development and shortcomings of distribution experiments is given in Chapter II.2.

I.5.5 Direct measurements of thermodynamic and mixing properties of solids in Aq-SS systems

I.5.5.1 Retrieval of excess Gibbs energy from electrochemical measurements

The difference between the chemical potentials of pure solid and its solid solution with another end-member in (metastable) equilibrium with aqueous solutions of the same ionic strength and with the same atmospheres can be determined using emf measurements in two or three interconnected electrochemical cells ([1990KON/GAM], [1994ROC/CAS], [1998MCB/ROC]). Such experiments yield results that are much more precise than any results of "classic" solubility measurements (Section II.2.2), which has been demonstrated for the $(Mn,Co)CO_3$-aqueous system by Königsberger and Gamsjäger [1990KON/GAM] and for the $(Ca,Cd)CO_3$-aqueous system by Rock *et al.* [1994ROC/CAS] and McBeath *et al.* [1998MCB/ROC]. The latter paper also contains a detailed description of the experimental setup with measured, intermediate and final calculated data, as well as a discussion of the advantages of the direct electrochemical methods compared to solubility measurements. They are thoroughly discussed in the appropriated section of Chapter II.2.

I.5.5.2 Calorimetry

Calorimetry, the measurement of heat effects, is a fundamental tool of experimental thermodynamics. It provides data on heat capacities, entropies, and enthalpies and is thus complementary to solubility and other equilibrium measurements that provide Gibbs energies. Calorimetric data is being extensively used in the derivation and validation of thermodynamic data and cycles through out the NEA TDB project. Guidelines [1999PUI/RAR] contain information about how to use calorimetric data in general.

Here, we will emphasize the use of calorimetric data to derive thermodynamic properties of Aq-SS.

Broadly speaking, calorimetry can be divided into two categories: the measurement of heat capacities and heats of phase transition within a material of constant composition and the measurement of heats of reaction. Sometimes the first category is called “thermophysical” and the second “thermochemical” measurement.

Cryogenic adiabatic calorimetry [1972ROB/HEM2] is the most accurate method for measuring low temperature heat capacities but it requires several grams of sample. In general, the instruments are custom built and the work is performed in a small number of specialised laboratories. It is capable of determining heat capacities with an accuracy of 0.1 - 0.5% and standard entropies with an accuracy of 0.5 - 1%.

Differential scanning calorimetry (DSC) [1992BOE/CAL], [1982STE/WEI] provides heat capacity measurements from about 100 to 1700 K, with accuracy ranging from about 1% near room temperature to 3 - 5% at the highest temperatures [2005MOR/NAV]. Many commercial instruments are available for the range 100 to 1000 K, and several for higher temperatures. Differential thermal analysis to 2773 K can provide enthalpies of phase transitions with an accuracy of about 5 - 10% at the higher temperatures [2005NAV/BEN]. Drop calorimetry (sample of 10 - 100 g) dropped from a high temperature furnace into a room temperature calorimeter provides the heat content ($H_T - H_{298}$), differentiation of which gives the heat capacity [1982STE/WEI]. Accuracy is 0.5 - 1% in the best cases.

Despite the apparent maturity of the field of heat capacity measurement, the available data for end-member and solid solution phases relevant to nuclear materials are surprisingly incomplete. Many of the older data, used to calculate standard entropies of common materials, in fact rely on extrapolations from 50 K to absolute zero and also suffer from sample characterisation inadequate by modern standards. There are still relatively few studies of solid solutions, and researchers in this field are encouraged to use calorimetry to establish the basic thermodynamic properties of solid solution phases.

To obtain the heat of formation of a material, a chemical reaction must take place in a calorimeter which relates that phase to products of known thermodynamic properties. That reaction may be direct, as in reaction calorimetry of a metal to a sulphide [1988BRY/KLE] or indirect, involving a process in which reactants and products are each converted to the same final state, and a thermodynamic cycle is written to relate their enthalpies. This final state often involves the dissolution of the solids in an appropriate solvent, which can range from water or aqueous acid [1972ROB/HEM2] to a molten oxide at high temperature [1977NAV], [1997NAV]. Because many of the solids relevant to nuclear materials are not readily soluble (in terms of both solubility limits and kinetics of dissolution) in aqueous solvents near room temperature, the latter

route, high temperature oxide melt solution calorimetry, has proven very useful [1977NAV], [1997NAV].

I.6 Testing the Aq-SS concepts and methods in nuclear waste management relevant systems

One of the main objectives of this work is to determine to which extent the current status of the thermodynamics of Aq-SS can be integrated in the models and sub-models used in the Performance Assessment of nuclear waste repositories. To this end we have compiled a number of test cases that are fully developed in Chapter II.3. What follows is a summary of the cases and their main findings.

I.6.1 Radium and its incorporation into the barite solid solution family: environmental implications

I.6.1.1 The radium-barite relationship in natural and anthropogenic environments

Perhaps, the co-precipitation between radium isotopes and barite precipitates is one of the best known examples. Dozens of studies on several scientific disciplines have established a link between the concentration of radium and the precipitation of barite, since the work of Doerner and Hoskins in 1925 [1925DOE/HOS], from which the theory of growth as incremental layers was defined (*Doerner-Hoskins logarithm distribution law*, Doerner and Hoskins, 1925). Radium is divalent and has an ionic radius (1.43 Å) quite similar to the Ba^{2+} one (1.36 Å), so that it is expected to be well accommodated in the barite lattice.

The role of barite as solubility-controlling phase of radium has been proposed in natural and in *anthropogenic* environments. Radium-bearing barite is present in uranium mill tailings [1987NIR]. Uranium is concentrated from ore minerals by leaching with acid sulphuric. Due to its relative low mobility during leaching conditions, radium is accumulated in the fine fraction of the waste, which is eventually stored in mill tailings. From these tailings, radium may be released to the soil, resulting in a serious concern due to its high radioactivity. The mobility of radium after storage have recently been evaluated by Martin and Akber [1999MAR/AKB] and Martin *et al.* [2003MAR/CRU]; Martin and Akber [1999MAR/AKB] used the relative concentrations of radium isotopes to evaluate the absorption/desorption of radionuclides and secondary mineral formation in groundwater systems close to uranium mine tailings. Their data indicated that almost all ^{226}Ra was removed by the formation of barite solid solution. On the other hand, Martin *et al.* [2003MAR/CRU] concluded that dissolution of a solid $(Ba,Ra)SO_4$ solid solution controls the aqueous concentration of radium and barium in waste porewater, confirming previous data by Snodgrass and Hileman [1985SNO/HIL].

I.6.1.2 Numerical modelling involving (Ba,Ra)SO_4 solid solutions

As already indicated in the previous section, the seminal work of Doerner and Hoskins on this system ([1925DOE/HOS]) was crucial to establish the basic principals of solid solution precipitation from aqueous solution and the development of the logarithmic distribution law. This is based on the experimentally proven assumption that the [Ra(II)]/[Ba(II)] ratio in the surface layer is proportional to their ratio in aqueous solution. As the composition of the aqueous phase changes with time as a result of the changes in the elemental composition, so does the composition of the crystal surface, leading to the so-called logarithmic distribution law (see details in Chapter II.3).

More recently, Langmuir and Riese [1985LAN/RIE] used empirical distribution coefficient data to derive Gibbs energies and enthalpies of solid solution of Ra(II) into various alkaline earth sulphate and carbonate minerals and established some interesting trends in the stability of these solid solution phases. According to this study, the distribution of Ra(II) into these minerals decreased in the following order: anhydrite > celestite > anglesite > barite > aragonite > calcite > strontianite > whiterite > cerussite.

In a recent work, Zhu [2004ZHU2] implemented the thermodynamic and kinetic data of the (Ba,Ra)SO_4 solid solution system in reactive transport codes (EQMOD, [1992YEH], and PHREEQC, [1999PAR/APP]) and compared the data obtained when considering pure phases and solid solutions. The approach by Zhu, included aqueous speciation and complexation, thermodynamic properties of solid and aqueous solutions and precipitation and dissolution kinetics. The obtained results clearly showed that Ra^{2+} concentrations in water differ several orders of magnitude whether equilibrium with a solid solution is considered or not. In one of these models, an oil-field brine was simulated to cool down from 100 to 25 ºC over five days. The numerical outcome showed a quick precipitation of a (Ba,Ra)SO_4 solid solution, implying a significant decrease of radium in solution. During the precipitation process, the solution was undersaturated with respect with pure $RaSO_{4(cr)}$.

Berner and Curti [2002BER/CUR] used the GEM approach (see Section II.1.2.4) to calculate the retention of radium in a nuclear waste repository hosted by the Opalinus Clay. Their results showed that the solubility limit in the clay porewater considering the "conventional" approach, *i.e.*, the total concentration of dissolved radium being controlled by the least soluble pure phase ($RaSO_{4(c)}$), was 4.8×10^{-8} M. In contrast, the co-precipitation of radium into ideal solid solution with barite lowered the solubility limit to 8.2×10^{-12} M. The solubility limit for Ra was even lower, 7×10^{-13} M, when a more complex Aq-SS system involving gypsum, barite and celestite $SrSO_4$ solid solutions was considered. When both barium sulphate and carbonate were present in the system, Ra^{2+} was almost exclusively partitioned into barite due to much higher solubility of witherite (Ba carbonate).

The consequences of the $RaSO_4$(s)-$BaSO_4$(s) solid solution formation for reactive transport modelling of Ra(II) in clay environments are further explored in some calculations performed in Section II.3.1.2.

I.6.1.3 Conclusions

Formation of $RaSO_4$(s)-$BaSO_4$(s) solid solution is well documented in both natural and anthropogenic environments. The Aq-SS equilibria have been largely investigated in well controlled laboratory systems and there are both macroscopic and spectroscopic investigations of the resulting solid solution formation. Both direct and inverse modelling techniques have been used to describe its behaviour and coupling of this Aq-SS to reactive transport codes has been successfully done. The outcome of it is that the predicted Ra(II) solubilities are substantially lower than the ones predicted by using the individual solubility of $RaSO_4$(s). In this context, it constitutes a clear case for the application of Aq-SS thermodynamics for PA.

The results from the (Ba,Ra)SO_4 Aq-SS system strongly support the idea that the knowledge of Aq-SS systems is essential when evaluating the behaviour of radionuclides in PA. Conventional numerical models failed in reproducing environmental data because most codes still use pure phases as solubility-controlling components

I.6.2 Cement phases – Solubility of calcium silicate hydrates (C-S-H)

I.6.2.1 Relevance of cement phases in radioactive waste management

Ordinary Portland Cement (OPC) is the most widespread matrix material currently considered in disposal of low-to-intermediate level nuclear (and non-nuclear) waste ([1992BER], [1992REA], [1997GLA]).

Ca. 60% of hydrated OPC consist of the *calcium silicate hydrate* phase (C-S-H in cement chemistry notation, where CaO is denoted as C, SiO_2 as S, and H_2O as H) of variable composition expressed with the C/S (Ca/Si molar) ratio, usually in the range $0.8 < C/S < 1.7$. The structure and stability of C-S-H has been the subject of a long debate because C-S-H is a major binder in the hydrated cement paste, and because it can immobilise many hazardous elements. The C-S-H structure is flexible enough to accommodate variable fractions of calcium and to provide exchange sites for various cations (Na, K, Cs, Sr, Al, Zn, …) and, consequently, to bind additional metals and radionuclides in their structures.

I.6.2.2 Thermodynamic modelling of C-S-H and its limitations

In principle, if the end-member properties are known, thermodynamic modelling can calculate stable phase assemblages and the resulting metal partitioning between phases as a function of physicochemical conditions and bulk composition of the system. How-

ever, the $CaO\text{-}SiO_2\text{-}H_2O$ system poses special problems to thermodynamic modelling when C-S-H phases are involved. The C-S-H "gel" is, in fact, a less-polymerised metastable precursor of crystalline tobermorite or jennite, and it tends to convert into a more polymerised form with time or at elevated temperatures. C-S-H phases have significant and variable specific surface area (up to 200 $m^2 \cdot g^{-1}$ or more) which makes them quite reactive, prone to incongruent dissolution with preferential release of Ca upon acidification or carbonation of the system, or even upon decreasing solid/water (S/W) ratio, which leads to precipitation of more silica-rich secondary (but again metastable) C-S-H phases. This kind of incongruent, non-stoichiometric dissolution behaviour, typical for Aq-SS equilibria, must be duly addressed in any experimental work or physico-chemical modelling related to cement-water interactions.

Kulik and Kersten [2001KUL/KER] have identified two alternative ways to perform the thermodynamic modeling of partial-equilibrium Aq-SS systems such as $C\text{-}S\text{-}H\text{–}H_2O$.

(i) By assuming end-member stoichiometries derived from stable mineral analogs such as tobermorite, jennite, or portlandite, and eventually include non-ideal behavior into solid solutions formed by these end-members, if this is needed for fitting experimental solubility data.

(ii) By seeking for such C-S-H end-member stoichiometries and their standard molar Gibbs energy G^{o}_{m} (298.15 K) values that would make possible to apply the ideal solid solution approach.

However, the need for a further extension to describe trace metal or radionuclide (*i.e.*, multi-component) C-S-H systems makes the first approach (i) not possible in practice due to the necessity to introduce many more (semi-empirical) interaction parameters with little hope to collect enough experimental data for finding parameter values with reasonable precision. For those reasons, the second approach (ii) based on optimisation of end-member stoichiometries to fit experimental data appears to be the only practically feasible opportunity [2001KUL/KER][2006LOT/WIN].

These authors have shown that the behaviour of C-S-H Aq-SS system can be reduced to ideal by the appropriated scaling of the end-member stoichiometries.

I.6.2.3 Geochemical modelling of C-S-H systems of interest in radioactive waste management

The validity of this approach has been tested by applying the GEMS-PSI code and database to the C-S-H solubility data derived in the experiments by [1965GRE/CHA], which, in principle, fulfil the necessary requirements for Aq-SS solubility data. The result of this validity test in terms of reproducing the dissolved Ca and Si concentrations, as well as the pH data, are quite encouraging and cover the full $0 < C/S < 1.7$ compositional range (more in Section II.3.2.)

The C-S-H ideal solid solution model has been further extended [2002KUL/KER] to incorporate a trace metal end-member for the case of Zn, where limited solubility data are available [1999JOH/KER]. The limitations on available thermodynamic data for Zn-Ca silicates and Zn-C-S-H end-member phases has been overcome by using dual-thermodynamic calculations (see Section II.1.3.2) in order to estimate the appropriated end-member stoichiometries and their associated thermodynamic properties.

I.6.2.4 Conclusions

The examples developed in Section II.3.2 show the potential of multicomponent ideal solid solutions to model the Aq-SS C-S-H system and the incorporation of cations in the ill-defined gel structures. Future work is going to be devoted to extend the applicability of this approach to increase amount of experimental data being reported for the sorption of Na, K, Al, Sr and Cs in these systems.

I.6.3 Structural incorporation of trivalent actinides/lanthanides into Calcite

I.6.3.1 The relevance of calcite for radioactive waste management

Calcite is a ubiquitous mineral phase in most geological environments, and it is particularly abundant in clay rocks like the ones forming the Opalinous clay in Switzerland (up to 11% content) [1998BRA/BAE] and in the Bure argillite [2001AND]. It is also a key secondary phase in cementitious materials. Consequently, radionuclide sorption processes in calcite comprise an important component of the migration models used in performance assessment of nuclear waste repositories.

In this particular context, we will be interested to investigate the co-precipitation/solid solution formation processes related to the interaction of actinides and lanthanides with the calcite structure.

Co-precipitation of various trace metals with calcite has been extensively studied through the years. The review work performed by Curti [1999CUR] constitutes a good compilation of the main studies up to 1998, although much information has been generated since then. As pointed out in [2000GLY], there is a substantial amount of thermodynamic data for divalent metal incorporation into calcite. In addition, sorption studies of U(VI), Th(IV), Np(V), Pu(V)/Pu(VI) and Cm(III) on calcite have been reported [1992CAR/BRU], [2005MAR/STU], [1982SHA/MOR], [2002STU/FAN2] and [2005ZAV/ROB].

The main focus of this test case will be on experimental studies of the structural incorporation of trivalent f-elements, primarily Pu(III), Am(III) and Cm(III).

I.6.3.2 Macroscopic information related to the sorption of f-elements into calcite

There is a substantial amount of experimental information concerning the partition of lanthanides and trivalent actinides in the calcite/aqueous solution system. The lanthanide most extensively studied has been Eu(III). The macroscopic information has been mainly rationalised in terms of distribution coefficients indicating the following general patterns:

1. Experiments by Lakshtanov and Stipp [2004LAK/STI] at pH about 6 indicate that the partition of Eu(III) is not much affected by the precipitation rate. A similar observation (in seawater at pH about 8) was made by Zhong and Mucci [1995ZHO/MUC].
2. Distribution coefficients derived in [1995ZHO/MUC] indicate a positive dependence with the total lanthanide concentration in aqueous solution. For Eu(III), the partition coefficient $k_D = (x_{Me} \cdot [Ca]) / (x_{Ca} \cdot [Me])$ ranged from 200 at dissolved concentration [Eu(III)] = 10 nM to k_D = 1400 at [Eu(III)] = 170 nM. The distribution coefficients reported in [2004LAK/STI] are $k_D = (770 \pm 290)$ in the [Eu(III)] range from 0.1 to 6.9 nM.
3. Zhong and Mucci [1995ZHO/MUC] observed a correlation between the lanthanide content in calcite with the [Na^+] in the artificial seawater they used in their experiments. This was not observed by Lakstanov and Stipp [2004LAK/STI].
4. The reaction mechanism proposed in [1995ZHO/MUC] implied the following substitution reaction at the solid phase: $2Ca^{2+} \rightleftharpoons Na^+ + Eu^{3+}$.
5. The proposed mechanism in [2004LAK/STI] implied the combined reaction substitution $3Ca^{2+} \rightleftharpoons 2Eu^{3+} + vac_{calcite}$ (vacancy site in the calcite structure), together with the substitution reaction $2Ca^{2+} \rightleftharpoons Eu(OH)_2^+$

I.6.3.3 Spectroscopic information on the incorporation of f-elements into the calcite structure

This can be summarised as follows:

1. EXAFS studies by Elzinga *et al.* [2002ELZ/REE] indicate that the investigated lanthanides occupy a Ca site within the calcite structure. For Dy and Yb they observed the expected 6-fold coordination, while Nd and Sm appear to be 7-fold coordinated and with longer Nd-O and Sm-O distances than expected by the sum of the respective ionic radii. A similar observation is made for the Nd(III) calcite system in EXAFS by Whiters *et al.* [2003WHI/PEA], and their near IR studies brought them to suggest the incorporation of $NdOH^+$ into the calcite structure.

2. The TRLFS studies by Marques-Fernandes *et al*. [2005MAR/STU] indicated that Cm(III) is truly incorporated into the structure and that two incorporated species may be distinguished. The spectroscopic data is consistent with substitution reactions previously discussed.

I.6.3.4 Thermodynamic modelling of the Eu(III)/calcite system

Curti *et al.* [2005CUR/KUL] have recently performed a thermodynamic modelling of the Eu(III)/calcite Aq-SS system . The data used was a combination of batch type sorption experiments at high pH = 13 and the data from [1995ZHO/MUC] and [2004LAK/STI].

It was not possible to fit all the data to a simple quasi-binary Aq-SS system with the end-members $CaCO_3$ and Eu_2CO_3 or $EuNa(CO_3)_2$. However, the results from the DualTh GEM modelling (see Section II.1.3.2 for more details) indicated a good fit by assuming the following three end-members EuO(OH), $EuH(CO_3)_2$ and $CaCO_3$. This would indicate the incorporation of two different Eu species in the calcite lattice, one involving the substitution of $2Ca^{2+}$ by Eu^{3+} and H^+, and another, the incorporation of the Eu(III)-hydroxo moiety. This implies a significant relaxation of the calcite structure with a Eu^{3+} 9-fold coordinated. The modelling results have not been directly verified by spectroscopy although they are consistent with recent TRFLS observations.

I.6.3.5 Conclusions

There is a large body of macroscopic chemical data regarding the sorption of lanthanide and trivalent actinide elements into calcite. The spectroscopic data so far available would indicate that trivalent lanthanides and actinides are incorporated into the calcite structure and in two different forms. However, there is no consensus about the precise substitution mechanisms involved. The inverse thermodynamic modelling done by using the dual-thermodynamic approach indicates that a consistent Aq-SS model can be derived for this system which accounts for most of the Eu(III)/calcite partition data published in the literature.

I.6.4 Solid solutions in the nuclear fuel cycle

I.6.4.1 The applicability of Aq-SS thermodynamics to spent nuclear fuel

The nuclear fuel cycle constitutes one of the areas where the applicability of Aq-SS thermodynamics becomes most relevant. Most of the components involved from cradle (mineral phases in uranium ore deposits) to grave (spent nuclear fuel and other immobilising matrices) can be considered as solid solutions.

There has been a large amount of research effort directed to characterise and amount and location of the various radionuclides in the UO_2 spent fuel matrix. This has led to the application of Aq-SS concepts and models to interpret the various processes

governing the dissolution behaviour of the various radionuclides from the spent fuel matrix.

I.6.4.2 Main results from the characterisation of UO_2 spent nuclear fuel

The key observations regarding the evolution of the occurrence and location of radionuclides from the large amount of information collected so far (for details, see Section II.3), are as follows:

Processes occurring when irradiation increases [1988KLE3]:

1. Increase in the relative concentration of fission products.
2. Changes (decrease) in the oxygen to metal ratio and the oxygen chemical potential.
3. Existence of radial variations in the fission product concentrations due to thermal gradients.
4. Decay of β-active fission products.

The resulting fission products can be classified in the following groups according to the nature of the phases where they are hosted in the spent fuel matrix:

1. Fission gases (Kr, Xe, Br, I);
2. Metallic phases (Mo, Tc, Ru, Rh, Pd, Ag, Cd, In, Sn, Sb, Te);
3. Oxide phases (Rb, Cs, Ba, Zr, Nb, Mo and Te) and
4. Solid solutions in the fuel matrix (Actinides, Lanthanides, Sr, Zr and Nb).

I.6.4.3 Application of Aq-SS thermodynamics to spent fuel dissolution data

The stoichiometric saturation concept as postulated by Thorstenson and Plummer [1977THO/PLU] and defined by [1990GLY] has been applied to some of the dissolution data of those fission products that have been identified to be present as solid solution in the UO_2 matrix. The stoichiometric saturation approach is well suited to be applied to the spent fuel system as it explains the behaviour of Aq-SS that are not in true equilibrium.

The general dissolution mechanism is as follows: by assuming that the minor radionuclides are dissolving congruently with the UO_2 matrix the radionuclide concentration in solution can be related to the uranium concentration in solution by the molar fraction of the radionuclide in the spent fuel solid solution.

This approach has been applied to a number of carefully performed spent fuel dissolution studies [1999BRU/CER] and [2003BRU/CER]. The details of the thermodynamic modelling are given in Section II.3. What follows is a summary of the main findings:

For Sr(II) the observed aqueous concentrations can be reproduced for all those spent fuel experiments which are sufficiently away from saturation, in the Sr concentration range $1 \cdot 10^{-9}$ to $1 \cdot 10^{-7}$ mol·dm^{-3}.

For Np, the observed aqueous concentrations can be reproduced for the data collected away from saturation, in the Np concentration range $1 \cdot 10^{-9}$ to $1 \cdot 10^{-8}$ mol·dm^{-3}. At higher concentrations the saturation with respect to $Np(OH)_4(s)$ was apparent.

For Pu a similar behaviour was observed in the concentration range $1 \cdot 10^{-9}$ to $1 \cdot 10^{-8}$ mol·dm^{-3}.

For the lanthanides, Eu(III), Sm(III), Gd(III) and La(III) the observed aqueous concentrations could be explained by the stoichiometric saturation model in the concentration range $1 \cdot 10^{-10}$ to $1 \cdot 10^{-7}$ mol·dm^{-3}.

I.6.4.4 Conclusions

The combination of a substantial solid characterization effort together with the dissolution data properly conducted has enabled the application of the stoichiometric saturation approach to model the Aq-SS behaviour of a number of radionuclides that are known to be present in solid solution in the spent fuel matrix.

I.7 Report conclusions

The main conclusions arising from this contribution are the following:

1. Aqueous-Solid Solution (Aq-SS) systems are ubiquitous in nature and therefore intrinsic to the understanding and quantification of radionuclide containment and retardation processes represented in Performance Assessments for geological repositories.
2. The partition behaviour of trace elements in general and radionuclides in particular is the result of a number of uptake (sorption) processes that range from adsorption and ion exchange to structural incorporation and solid solution formation. Molecular spectroscopic methods have to be used to properly qualify and understand these processes quantified in macroscopic partition experiments.
3. Thermodynamics of Aq-SS systems is an established discipline and most of the conceptual framework is solidly built. However, there is a lack of fundamental thermodynamic data that prevents its use in a more consistent way. Experimental programmes should be launched to deal with some priority elements.
4. For most of the Aq-SS systems of interest in the PA of repository systems, the solid radionuclide end-member is present in minor to trace amounts and, therefore, assuming its ideal solid solution behaviour is a reasonable first approximation.

5. There are a number of geochemical modelling codes that can handle solid solutions either in indirect (*i.e.*, PhreeqC, EQ3/6) or direct (*i.e.*, GEMS-PSI, ChemApp, HCh) way. Inverse modelling techniques like the dual-thermodynamic GEM approach have proven to be quite powerful to estimate end-member stoichiometries and to approximate non-ideal Aq-SS systems like the cement C-S-H phases with ideal solid solution models.

6. There are a number of well established macroscopic wet chemical methods which can be useful in determining some of macroscopic properties of Aq-SS systems. Calorimetric data is always very useful to close the appropriated thermodynamic cycles in Aq-SS. However, due to the atomistic nature of the solid solution incorporation, there is a need to complement macroscopic thermodynamic data with a detailed molecular characterisation. The current development of molecular simulation and atomic spectroscopic techniques will certainly bring more grounds under the determination of feasible Aq-SS models.

7. The applicability of Aq-SS thermodynamic models has already been explored for a number of systems of interest in the Performance Assessment of Nuclear Waste repositories, including the Ra(II)- Ba(II) sulphate system, the solubility of C-S-H phases, the uptake of trivalent lanthanides and actinides in calcite, and the dissolution behaviour of minor radionuclides present in solid solution in the UO_2 fuel matrix. In all cases, the combination of macroscopic chemical information with molecular spectroscopy methods has led development of chemically plausible Aq-SS thermodynamic models that agreed satisfactorily with the experimental observations.

PART II: Theory, experimental aspects and cases for study

II.1 Theoretical aspects of solid solutions and their solubility

II.1.1 Theory of solid solutions

II.1.1.1 Introduction

The complexity and richness of natural minerals and multicomponent ceramics (like UO_2 spent nuclear fuel) arise not only from the large number of phases and crystal structures, but also from the variety of solid solutions, complex elemental substitutions, order-disorder relations, and exsolution phenomena one encounters. Indeed, a pure mineral of end-member composition is the exception rather than the rule. Elemental substitutions in minerals may be classified in terms of the crystallographic sites on which they occur and the formal charges of the chemical elements (ions) which participate.

For instance, most common rock-forming silicates can be said to have a general formula $A_aM_mT_tO_oY_y$, where the capital letters refer to types of sites and the lower case to their multiplicity per formula unit. "A" represents large 8-12 coordinated cations (alkalis, alkaline earth elements, sometimes lanthanides or other "incompatible" elements). "M" represents smaller divalent or trivalent cations in approximately octahedral coordination. These include Mg^{2+}, Fe^{2+}, Fe^{3+}, Cr^{3+}, Al^{3+} and other transition metals. "T" represents smaller ions in tetrahedral coordination, chiefly Si^{4+} and Al^{3+}, sometimes B^{3+}, Be^{2+}, and P^{5+}, as well as smaller to trace amounts of Fe^{3+}, Ga^{3+}, and Ge^{4+}. "O" represents oxygen, and "Y" various substituting anions, chiefly F^- and OH^-.

Carbonates, sulphates, halides, and sulphides follow their own crystal chemical patterns and ionic substitutions. Lanthanides and actinides sometimes form their own phases but often substitute at trace levels in more common minerals.

The UO_2 based nuclear fuel is itself a complex solid solution, as are the ferrous alloys surrounding it. Vitrified borosilicate waste forms contain both glassy and crystalline solid solution phases.

Within each classification above, there may be several crystallographically distinct sites, *e.g.*, the M_1 and M_2 sites of olivine, the many M sites of amphiboles, micas and clay minerals, or the several T sites in feldspars, clays, and zeolites. The substitution of atoms or ions in a solid solution may proceed in a number of different ways (Table II-1).

Table II-1: Charge-coupled substitutions in minerals.

Substitution	Examples
Same charge	
$Mg_T^{2+} = Fe_M^{2+}$	Pyroxene, olivine
$Al_T^{3+} = Fe_T^{3+}$	Mica, clay, epidote, feldspar, tourmaline
$Al_M^{3+} = Fe_M^{3+}$	Mica, clay, amphibole, garnet, spinel, pyroxene
$Al_T^{3+} = B_T^{3+}$	Feldspar, tourmaline, borosilicate glass
$Si_T^{4+} = Ge_T^{4+}$	Olivine, garnet, spinel, pyroxene, feldspar
$Na^+ = K^+$ or other alkali	Feldspar, mica, clay, zeolite
Different charges	
$Si_T^{4+} + Na_A^+ = Al_T^{3+} + Ca_A^{2+}$	Plagioclase substitution: feldspar, pyroxene, amphibole, mica, clay, zeolite
$Si_T^{4+} = Na_A^+$ (or other alkali) $+ Al_T^{3+}$	Silica stuffing substitution: amphibole, mica, clay, silica minerals, zeolite, glass
$Ca_M^{2+} + Si_T^{4+} = Al_M^{3+} + Al_T^{3+}$	Pyroxene, amphibole, mica, clay
$Si_T^{4+} + Si_T^{4+} = Al_M^{3+} + Al_T^{3+}$	Pyroxene, amphibole, mica, clay
$3\,Fe_M^{2+} = vacancy_M + 2\,Fe_M^{3+}$	Defects in olivine, spinel,amphibole, mica, clay
$Si_T^{4+} = 4\,H_T^+$	Hydrogarnet

All substitutions must maintain electroneutrality (balance of formal charges) in the crystal. The substitutions may involve one or more sets of crystallographic sites (sublattices). They may involve ions of like charge, charge-coupled substitutions on one sublattice or on several, or the creation or filling of vacant sites.

This structural complexity must be reflected in the thermodynamics of solid solution formation and its subsequent interaction with aqueous solutions. Thus, the crystal chemistry must be understood very well, and various analytical, structural and spectroscopic techniques applied to phase characterisation.

Although thermodynamics offer a macroscopic description, linking thermodynamic properties to the microscopic (atomistic or molecular level) features of the solids insures that the description is not simply and arbitrarily empirical. Such linkage is especially critical if one wishes to extrapolate properties to conditions of pressure, temperature, or composition outside the range where measurements have been made. This is clearly a very important condition when aiming to apply Aq-SS thermodynamics to the performance assessment of nuclear waste repositories. The basic theoretical question is to relate the microscopic details of atomic interactions to site occupancies and macroscopic thermodynamic parameters. The basic practical problem is to obtain useful ex-

pressions for the thermodynamic mixing properties of multicomponent solid solutions and to apply them to solid-aqueous phase systems. These practical models should be simple enough to be incorporated into computer codes describing phenomena such as the hydrothermal and geochemical evolution of a nuclear waste repository. They should be robust enough to withstand interpolation and some extrapolation in pressure-temperature-composition (p, T, x) space, even in the hands, heads, and computers of those who are neither crystallographers nor thermodynamicists.

At first glance, the theoretical and practical goals appear almost contradictory. The main part of this review will deal with how one tries to serve both taskmasters. The formalism and examples presented are meant to emphasise three points.

1. Any expression one writes for a Gibbs energy of mixing, an activity, or an activity coefficient has buried in it some assumptions about the mixing process on an atomic scale. Therefore, one must make sure that those assumptions are reasonable.
2. Equations, whose form is constrained by theoretical considerations and whose parameters are physically reasonable, are more reliably extrapolated than arbitrary polynomials fit to data in a small p, T, x range.
3. Models which simultaneously include constraints imposed by phase equilibria, calorimetry, and crystal chemistry are more reliable than those based on any one source alone.

The goal of this section is to summarise some of the needed thermodynamic formalism and to link it to the structural complexity of the solid solutions encountered in the interaction of nuclear waste with aqueous solutions. For additional details of thermodynamic formulations and of crystal chemistry, a number of textbooks, monographs, and reviews are recommended [1967GUG], [1987CAP/BRO], [1987NAV], [1990ERI/HAC], [1994GHI], [1994NAV], [1995GAS], [1997OTT], [1998NAV], [2000OTT/BOE], [2000OTT/BOE2], [2001GAN], [2001GEI].

II.1.1.2 Thermodynamic formalism

Consider the general reaction

$$x_A A + x_B B \rightleftharpoons A(x_A)B(x_B) \qquad \text{(II.1)}$$

where A and B are end-members of a solid solution series which mix to form an intermediate phase of mole fraction, x_A, x_B, where, in a binary system, $x_A + x_B = 1$. If both end-members have the same crystal structure, a continuous Gibbs energy curve can be drawn to represent the substitution (see Figure II-1a,b). However, if the space group of the structure of one end-member is a subgroup of that of the other, complex Gibbs energy relations may lead to higher-order phase transitions. If the two structures are not so related, then each represents a different Gibbs energy surface (see Figure II-1c). That being the case, complete miscibility cannot occur, but common tangents to the two

Gibbs energy curves (or appropriate generalisations to many dimensions) define the mutual solubility curves.

Figure II-1: Schematic Gibbs energy of mixing curves for solid solutions: (a) end-members have same structure, and there is complete miscibility, (b) end-members have the same structure but there is immiscibility at the given temperature, (c) end-members have different structures.

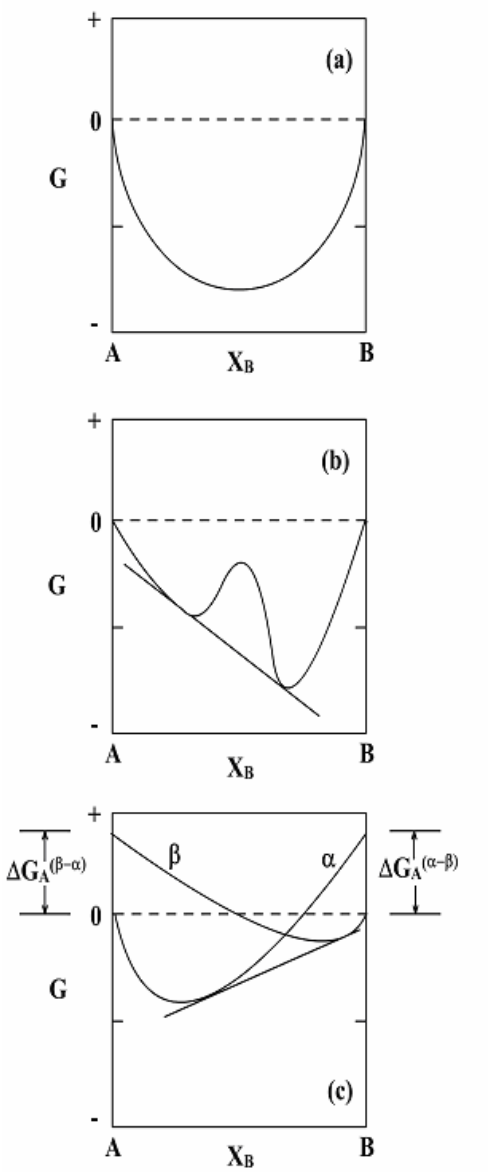

At atmospheric pressure and temperature T, the Gibbs energy per mole of an isostructural binary solid solution can be written as:

$$\Delta G\,(\text{solid solution}, T) = x_{\text{A}}\, G^{\text{o}}\,(\text{A}, T) + x_{\text{B}}\, G^{\text{o}}\,(\text{B}, T) + \Delta G\,(\text{mix}) \qquad \text{(II.2)}$$

where ΔG (solid solution, T) is the molar Gibbs energy of the solid solution, G^{o} (A, T) and G^{o} (B, T) are the standard Gibbs energies of the pure end-members A and B, and $\Delta G\,(\text{mix})$ is a Gibbs energy of mixing term. Note that throughout this section, the superscript zero refers to an atmospheric pressure pure substance standard state.

The $\Delta G\,(\text{mix})$ term consists of an enthalpy and entropy term:

$$\Delta G\,(\text{mix}) = \Delta H\,(\text{mix}) - T\Delta S(\text{mix}) \qquad \text{(II.3)}$$

The enthalpy of mixing term contains the energetics of the interactions; a positive $\Delta H\,(\text{mix})$ generally indicates clustering of like species and a tendency toward exsolution, while a negative $\Delta H\,(\text{mix})$ generally suggests ordering of unlike species and a tendency toward formation of an intermediate compound. Both tendencies may occur simultaneously in the same system (see the examples of carbonates and feldspars below).

The Gibbs energy in Eq. (II.2) can be written in terms of chemical potentials of components A and B:

$$G\,(\text{solid solution}, T) = x_{\text{A}}\ \mu^{\text{o}}\,(\text{A}, T) + x_{\text{B}}\,\mu^{\text{o}}\,(\text{B}, T) + x_{\text{A}}\Delta\mu(\text{A}) + x_{\text{B}}\Delta\mu(\text{B}) \qquad \text{(II.4)}$$

The μ^{o} (A, T) and μ^{o} (B, T) terms are the standard chemical potentials of pure A and B (identical to the G^{o} (A, T) and G^{o} (B, T) terms in Eq. (II.2)). The $\Delta\mu$ terms represent partial molar Gibbs energies of mixing. Therefore:

$$\Delta G\,(\text{mix}) = x_{\text{A}}\Delta\mu\,(\text{A},T) + x_{\text{B}}\Delta\mu\,(\text{B},T) \qquad \text{(II.5)}$$

The thermodynamic activity is defined as:

$$\text{R}T \ln a_{\text{A}} = \Delta\mu\,(\text{A}) \text{ and } \text{R}T \ln a_{\text{B}} = \Delta\mu\,(\text{B}) \qquad \text{(II.6)}$$

where R is the universal gas constant (8.31451 $\text{J}\cdot\text{K}^{-1}\cdot\text{mol}^{-1}$). The changes in chemical potentials on mixing can be related to partial molar enthalpies and entropies of mixing:

$$\begin{aligned} \Delta\mu\,(\text{A}, T) &= \Delta\bar{h}\,(\text{A}, T) - T\Delta\bar{s}\,(\text{A}, T), \\ \Delta\mu\,(\text{B}, T) &= \Delta\bar{h}\,(\text{B}, T) - T\Delta\bar{s}\,(\text{B}, T). \end{aligned} \qquad \text{(II.7)}$$

The two chemical potentials (and other partial molar quantities) are not independent of each other but are related by the Gibbs-Duhem equation, a form of which is:

$$\text{x}_{\text{A}}\left(\frac{\partial\,\Delta\mu_{\text{A}}}{\partial\,\text{x}_{\text{A}}}\right) + \text{x}_{\text{B}}\left(\frac{\partial\,\Delta\mu_{\text{B}}}{\partial\,\text{x}_{\text{B}}}\right) = 0 \qquad \text{(II.8)}$$

Pressure affects the above equations through the volume term, since

$$\left(\frac{\partial G}{\partial p}\right)_T = V, \left(\frac{\partial \Delta G(\text{mix})}{\partial p}\right)_T = \Delta V_{\text{mix}}, \left(\frac{\partial \Delta \mu_A}{\partial p}\right)_T = \overline{\Delta v}_A \qquad \text{(II.9)}$$

The enthalpy of mixing at p and T is related to the enthalpy of mixing at standard pressure of 1 atm (1.013 bar), or 1 bar since 1980, and T by a pressure-volume term, with ΔV_{mix}, Δv_A dependent, in general, on p and T:

$$\Delta H(\text{mix}) = \Delta H^{(1)}(\text{mix}) + \int_1^p \Delta V_{\text{mix}} dp \qquad \text{(II.10)}$$

The partial molar enthalpy of mixing of component A is:

$$\Delta \bar{h}(\text{A}) + \int_1^p \Delta \bar{V}_A dp \qquad \text{(II.11)}$$

The effect of pressure is minor in considering the equilibrium between solid solutions and aqueous phases under normal conditions but, may become significant at the upper p–T range of hydrothermal systems. The above equations can all be generalised to multicomponent systems.

II.1.1.3 The entropy of mixing

There are three contributions to the entropy of mixing: (a) changes in the vibrational entropy term, (b) terms from changes in magnetic and electronic entropy, and (c) the configurational or statistical term arising from the occupancy of equivalent sites by different chemical species. The last is usually the most important. It arises through statistical mechanics and is fundamentally related to the greater randomness (or loss of information about which ion is on a particular site) in the solid solution compared to the pure end-member.

If Eq. (II.1) represents the random mixing of a total of one mole of species over a total of one mole of sites, then (and only then) the entropy of mixing is given by:

$$\Delta S(\text{mix}) = -\text{R}\,[x_A \ln x_A + x_B \ln x_B] \qquad \text{(II.12)}$$

and

$$\Delta \bar{s}(\text{A}) = -\text{R} \ln x_A\,,\ \Delta \bar{s}(\text{B}) = -\text{R} \ln x_B \qquad \text{(II.13)}$$

If, furthermore, the enthalpy of mixing is zero, then the simple ideal solution results, with

$$\Delta G(\text{mix}) = \text{R}T\,[x_A \ln x_A + x_B \ln x_B] \qquad \text{(II.14)}$$

$$\Delta \mu(\text{A}) = \text{R}T \ln x_A\,,\ \Delta \mu(\text{B}) = \text{R}T \ln x_B \qquad \text{(II.15)}$$

$$a_A = x_A\,,\ a_B = x_B. \qquad \text{(II.16)}$$

Equation (II.16) is familiar as Raoult's Law, often used as a first approximation when little information is available. Note that this formulation predicates the mixing of one mole of species per formula unit of solid solution. Thus it is directly applicable to the following systems relevant to nuclear waste: $BaSO_4$-$RaSO_4$ solid solutions, $FeCr_2O_4$-$NiCr_2O_4$ spinel solid solutions if one assumes Ni and Fe mix on tetrahedral sites only, and UO_2-PuO_2 solid solutions if one neglects variation in oxygen content. In each of the cases above, ideality would mean activity equal to mole fraction.

More complex expressions, even for "*statistically* ideal mixing" (in the sense of a random distribution of species with no preferred energetics) arise when stoichiometry dictates several species per formula unit. A relevant example to visualise such statistically ideal entropies is the spinel solid solution $FeAl_2O_4$-$FeCr_2O_4$ in which there are two moles of (Al + Cr) per mole of $Fe(Al,Cr)_2O_4$. Assuming that this spinel solid solution has a normal cation distribution (no trivalent ions on tetrahedral sites), one can formulate the entropy of mixing in either of two ways:

One can redefine the formula unit as $Fe_{0.5}(Al,Cr)O_2$. Then, for ideal mixing,

$$a_{Fe_{0.5}AlO_2} = x_A, \text{ where } A = Fe_{0.5}AlO_2 \text{ and}$$
$$a_{Fe_{0.5}CrO_2} = x_B, \text{ where } B = Fe_{0.5}CrO_2. \qquad \text{(II.17)}$$

The second procedure for calculating entropies of mixing and activities is to leave the formula units as conventionally written. Then, for the random mixing of $x_A(FeCr_2O_4)$ and $x_B(FeAl_2O_4)$

$$\Delta S\,(\text{mix}) = -2R[x_A \ln x_A + x_B \ln x_B] \qquad \text{(II.18)}$$

with the factor of two arising because entropy is an extensive parameter, and two moles of ions are being mixed instead of one. If ΔH (mix) = 0, then

$$\Delta\mu_{FeCr_2O_4} = -2RT \ln x_A,\ \Delta\mu_{FeAl_2O_4} = -2RT \ln x_B \qquad \text{(II.19)}$$

and

$$a_{FeCr_2O_4} = x_A^2,\ \ a_{FeAl_2O_4} = x_B^2 \qquad \text{(II.20)}$$

The statistically ideal solid solution is a convenient and an appropriate first approximation for application to element distribution equilibria. For example, the distribution of Al and Cr between spinel and corundum phases can be written as:

$$Fe_{0.5}AlO_2(sp) + CrO_{1.5}(cor) \rightleftharpoons Fe_{0.5}CrO_2(sp) + AlO_{1.5}(cor) \qquad \text{(II.21)}$$

$$K_D = a_{Fe_{0.5}CrO_2} \cdot a_{AlO_{1.5}} \ / \ a_{Fe_{0.5}AlO_2} \cdot a_{CrO_{1.5}} \qquad \text{(II.22)}$$

Then, $-RT\cdot\ln K_D$ is the standard Gibbs energy change of Reaction (II.21), given as:

$$\begin{aligned}\Delta_r G\ (\text{II.21}) &= -RT \ln K_D \\ &= \Delta_f G^o\,(Fe_{0.5}CrO_2) + \Delta_f G^o\,(AlO_{1.5}) - \Delta_f G^o\,(Fe_{0.5}AlO_2) \\ &\quad - \Delta_f G^o\,(CrO_{1.5}) \qquad \text{(II.23)}\end{aligned}$$

or

$$\begin{aligned}\Delta_r G\ (\text{II.21}) &= -1/2\ \mathrm{R}T \ln K_D \\ &= 1/2\ \Delta_f G^o\ (FeCr_2O_4) + 1/2\ \Delta_f G^o\ (Al_2O_3) \\ &\quad - 1/2\ \Delta_f G^o\ (FeAl_2O_4) - 1/2\ \Delta_f G^o\ (Cr_2O_3) \qquad \text{(II.24)}\end{aligned}$$

where the $\Delta_f G^o$ terms are appropriate Gibbs energy of formation terms, all taken with respect to elements or to oxides. The factors of "1/2" appear because Eq. (II.21) is written involving one mole of exchangeable species per formula unit. In this particular case, if one takes the Gibbs energies of formation relative to the oxides (with $\Delta_f G^o\ (Al_2O_3)$ and $\Delta_f G^o\ (Cr_2O_3)$ both zero), then the value of $\Delta_r G^o$ (II.21) is determined by the difference in Gibbs energy of formation from oxides of the two spinel end-members.

If mixing in the corundum phase is also statistically ideal, then

$$a_{AlO_{1.5}} = x_A', \text{ where A} = AlO_{1.5} \text{ and } a_{CrO_{1.5}} = x_B', \text{ where B} = CrO_{1.5} \qquad \text{(II.25)}$$

$$\begin{aligned}K_D &= (x_A'\ x_B) / (x_A\ x_B') \\ &= [Cr/(Cr+Al))_{spinel}][Al/(Cr+Al)_{corundum}]/[(Cr/Cr+Al)_{corundum}][Al/(Cr+Al)_{spinel}]\end{aligned} \qquad \text{(II.26)}$$

When dealing with partition of elements between solid solution phases and aqueous solution, the statistically ideal solid is still an important approximation, but the activity-composition relations in the aqueous phase must be considered separately within the formalisms appropriate to the particular temperature and ionic strength. Some examples are given in Chapter II.3.

Although not directly encountered in nuclear waste disposal, garnets provide a clearcut example of the substitution of ions on different sublattices. The general formula $A_3M_2T_3O_{12}$ allows separate substitution on three distinct sets of sites, the large 8–coordinated "A" sites hosting larger divalent cations, the octahedral "M" sites holding smaller mainly trivalent ions, and the tetrahedral "T" sites harboring small highly charged cations (mainly Si). Thus, if one considers $Mg_3Al_2Si_3O_{12}$-$Fe_3Al_2Si_3O_{12}$ garnet solid solutions, with Mg and Fe mixing ideally in 8–fold sites, the activity-composition relationship can be written either as:

$$a_{Mg_3Al_2Si_3O_{12}} = x_A^3\ ,\ a_{Fe_3Al_2Si_3O_{12}} = x_B^3 \qquad \text{(II.27)}$$

or as:

$$a_{MgAl_{2/3}SiO_4} = x_A,\ a_{FeAl_{2/3}SiO_4} = x_B \qquad \text{(II.28)}$$

In the garnet series $Mg_3Al_2Si_3O_{12}$-$Mg_3Cr_2Si_3O_{12}$, ideal mixing of Al and Cr on octahedral sites means that:

$$a_{Mg_3Al_2Si_3O_{12}} = x_A^2\ ,\ a_{Fe_3Cr_2Si_3O_{12}} = x_B^2 \qquad \text{(II.29)}$$

or

$$a_{Mg_{1.5}AlSi_{1.5}O_6} = x_A,\ a_{Mg_{1.5}CrSi_{1.5}O_6} = x_B \qquad \text{(II.30)}$$

Finally for garnets $Mg_3Al_2Si_3O_{12}$-$Mg_3Al_2Ge_3O_{12}$ with ideal mixing of Si and Ge on tetrahedral sites,

$$a_{Mg_3Al_2Si_3O_{12}} = x_A^3 \ , \ a_{Mg_3Al_2Ge_3O_{12}} = x_B^3 \tag{II.31}$$

or

$$a_{MgAl_{2/3}SiO_4} = x_A, \ a_{MgAl_{2/3}SiO_4} = x_B \tag{II.32}$$

These concepts of *statistically* ideal solution can be extended to involve simultaneous mixing of ions on several sets of sites. *Statistically* ideal is different from and more general than ideal in the Raoultian sense, in that in the former the number of moles of sites per mole of solid solution can be different from one, but in both cases, mixing over the relevant sites is random. If no heterovalent substitutions occur, and each species can be unambiguously assigned to a given sublattice, this extension is quite straightforward. Consider for example, a natural garnet containing Mg^{2+}, Fe^{2+}, Ca^{2+}, Fe^{3+}, Mn^{2+}, Fe^{3+}, Cr^{3+}, Al^{3+}, and Si^{4+} as major constituent. Its formula may be written as $(Mg,Fe^{2+},Ca,Mn^{2+})_3(Al,Cr,Fe^{3+})_2Si_3O_{12}$. The activity of pyrope $Mg_3Al_2Si_3O_{12}$ in such a complex garnet may then be estimated as:

$$a_{Mg_3Al_2Si_3O_{12}} = x^3 \, (x')^2 \tag{II.33}$$

where x is the fraction of 8–fold sites occupied by Mg, x = Mg/(Mg+Fe^{2+}+Ca^{3+}+Mn^{2+}) and x' is the mole fraction of octahedral sites occupied by Al, x' = Al/(Al+Cr+Fe^{3+}).

For multicomponent solid solutions, there is not always a unique way of picking end-member components. Thus a spinel $(Fe^{2+},Ni)(Cr,Fe^{3+})_2O_4$ may be written as a solid solution between Fe_3O_4 and $NiCr_2O_4$ or between $FeCr_2O_4$ and $NiFe_2O_4$. Since the reciprocal reaction:

$$Fe_3O_4 + NiCr_2O_4 \rightleftharpoons NiFe_2O_4 + FeCr_2O_4 \tag{II.34}$$

does not in general have a zero change in Gibbs energy, a "reciprocal term" must often be incorporated in the thermodynamic formulation [1978WOO/NIC], [1983PEL/LIN].

For clays, zeolites, and other complex phases relevant to the interaction of nuclear materials with the environment, a similar approach, delineating specific substitutions on different crystallographic sites, can be taken. The important inference is that, even if each of these sublattices has random mixing and there is no heat of mixing, the solid solution does not necessarily obey Raoult's law, simply because the numbers of species being mixed must be counted correctly. The clinoptilolite zeolites, occurring in the tuffs at Yucca Mountain [2003BIS/VAN], are an example. Their idealised formula is often given as $(Na,K)_6Al_6Si_{30}O_{72}{\cdot}20H_2O$. This formula reflects the contents of a crystallographic unit cell and allows for the charge balanced substitution Si = (Na or K) + Al. Then, taking the pure Na and K end-members as components, and assuming statistically ideal mixing of Na and K, the activity expression is:

$$a_{Na_6Al_6Si_{30}O_{72}\cdot 20H_2O} = (x_{Na_6Al_6Si_{30}O_{72}\cdot 20H_2O})^6 \tag{II.35}$$

or

$$a_{NaAlSi_5O_{12}\cdot 3.67H_2O} = (x_{NaAlSi_5O_{12}\cdot 3.67H_2O}) \quad \text{(II.36)}$$

Analogous expressions would hold for the cesium component present at low concentrations from the exchange of Cs from the waste with Na and K in the zeolite.

However, in the above formalism, several important simplifying assumptions were made: (1) that the Al/Si ratio is constant, (2) that there is no change in the degree of short-range order of Al and Si on tetrahedral sites, and (3) that the water content is constant. None of these assumptions is strictly true. Probably, most important is the issue of water content and its effect on the dehydration equilibria that may become important in a repository because of the heat generated by radioactivity.

This discussion has given specific examples rather than general formulas involving "the *j*–th species on the *i*–th sublattice". This loss of generality is purposeful; one is better off tailoring a thermodynamic model to a specific crystal chemical situation. The entropy model then needs not be needlessly cumbersome, yet it must count all the important contributions to the entropy of mixing. In applications to silicate melts, similar statistical counting of site occupancies for framework and nonframework cations has been termed the "two-lattice" model ([1980WEI/HON], [1981HON/HEN], [1982HEN/NAV]). When end-member compositions also contain configurational disorder, additional care must be taken to correctly compute the entropy of mixing (see below).

II.1.1.4 Regular, subregular and generalised mixing models

A starting point for thermodynamic models is the useful but inherently contradictory assumption that, though the heats of mixing are not zero, the configurational entropies of mixing are those of random solid solution. The molar excess Gibbs energy of mixing is then (in all cases, regular solution or not):

$$\Delta G^E(\text{mix}) = \Delta H(\text{mix}) - T\Delta S^E(\text{mix}) \quad \text{(II.37)}$$

The excess entropy of mixing $\Delta S^E(\text{mix})$ arises from two sources. First, it is the non configurational (vibrational, magnetic, electronic) contribution to the entropy of mixing. This may be positive or negative. Second, it is the correction to the configurational entropy arising from deviation from a random distribution of ions. Whether this deviation arises from ordering or from clustering, it diminishes the configurational entropy from its maximum (random) value.

Both the excess enthalpy and the excess entropy reflect changes in chemical bonding (*e.g.*, strengths of metal-oxygen bonds and lattice vibrations) and changes in order-disorder and/or clustering of like atoms (affecting energetics and configurational entropy). Both clustering of like atoms (positive enthalpy of mixing) and ordering among unlike atoms (negative enthalpy of mixing) tend to decrease the configurational entropy and thus diminish the entropy of mixing. The excess vibrational entropy may be

either positive, indicating looser bonding, which is common when atoms of different sizes are mixed, or negative, indicating tighter bonding, which sometimes accompanies ordering. The overall effect on Gibbs energy of mixing is thus a combination of enthalpic and entropic factors and these often, though not always, act in opposite directions. For a two-component system, the simplest formulation for $\Delta G_{\mathrm{m}}^{E}(\mathrm{mix})$ is:

$$\Delta G_{\mathrm{m}}^{E}(\mathrm{mix}) = \Delta H_{\mathrm{m}}(\mathrm{mix}) = \mathrm{R}\,T\,\alpha x_{\mathrm{A}} x_{\mathrm{B}} = W_{\mathrm{H}}\,x_{\mathrm{A}} x_{\mathrm{B}} \qquad \text{(II.38)}$$

where $\Delta S_{\mathrm{m}}^{E}(\mathrm{mix})$ is assumed to be zero, and α or W_{H} is the enthalpy interaction parameter. If this parameter is independent of temperature then Eq. (II.38) represents the "strictly regular" solution. For a positive interaction parameter, the Gibbs energy of mixing and activity composition relations at different temperatures are shown in Figure II-2. Increasingly positive deviations from ideality lead to immiscibility, see below.

The formalism can be generalised to more complex behaviour in several essentially equivalent ways. Deviations from ideal behaviour are described in geochemistry mainly using the Guggenheim [1952GUG], or the Redlich-Kister, and the Margules (in Thompson and Waldbaum notation, [1967THO]) models ([1991GLY], [1993AND/CRE], [1994NOR/MUN], [2000GLY]). For a binary system, the Guggenheim model is based on a power-series expression for the excess molar Gibbs energy of mixing $G_{\mathrm{m}}^{E}(\mathrm{mix})$, which reduces to zero when either x_1 or x_2 approaches unity:

$$G_{\mathrm{m}}^{E}(\mathrm{mix}) = \mathrm{R}T(x_1 \ln f_1 + x_2 \ln f_2) = \mathrm{R}Tx_1x_2 \sum_r \alpha_r (x_1 - x_2)^r \qquad \text{(II.39)}$$

where the coefficients α_r are called *interaction parameters* (dimensionless in Redlich-Kister, or expressed in RT units in Guggenheim models). Activity coefficients can be obtained by the partial differentiation of $G_{\mathrm{m}}^{E}(\mathrm{mix})$ over the mole fraction x_1 or x_2:

$$\ln f_1 = x_2^2\left(\alpha_0 + \alpha_1\left(3x_1 - x_2\right) + \alpha_2\left(x_1 - x_2\right)\left(5x_1 - x_2\right) + \ldots\right) \qquad \text{(II.40)}$$

$$\ln f_2 = x_1^2\left(\alpha_0 - \alpha_1\left(3x_2 - x_1\right) + \alpha_2\left(x_2 - x_1\right)\left(5x_2 - x_1\right) + \ldots\right) \qquad \text{(II.41)}$$

Two parameters α_0 and α_1 (*subregular* model), or even a single parameter α_0 (*regular* model), are usually sufficient in binary systems. Some low-temperature binary systems may require more parameters [2000PRI/FER]. The subregular model is equivalent to the asymmetric Margules model in the Thompson-Waldbaum notation:

$$G_{\mathrm{m}}^{E}(\mathrm{mix}) = \mathrm{R}T(x_1 \ln f_1 + x_2 \ln f_2) = x_1x_2(W_{12}x_2 + W_{21}x_1) \qquad \text{(II.42)}$$

where the parameters are related to those used in the Redlich-Kister model as:

$$W_{12} = \mathrm{R}T\left(\alpha_0 - \alpha_1\right);\; W_{21} = \mathrm{R}T\left(\alpha_0 + \alpha_1\right) \qquad \text{(II.43)}$$

and, in general, depend on temperature and pressure. In the Thompson-Waldbaum model, the activity coefficients of end-members are expressed as:

$$\mathrm{R}T \ln f_1 = \left(2W_{21} - W_{12}\right)x_2^2 + 2\left(W_{12} - W_{21}\right)x_2^3 \qquad \text{(II.44)}$$

$$\mathrm{R}T \ln f_2 = \left(2W_{12} - W_{21}\right)x_1^2 + 2\left(W_{21} - W_{12}\right)x_1^3 \qquad \text{(II.45)}$$

Figure II-2: Gibbs energy of mixing, solvus, and activity-composition relations for a regular solution with an interaction parameter of 16.6 kJ·mol^{-1} (W_H/(RT) = 2.0 at 1000 K).

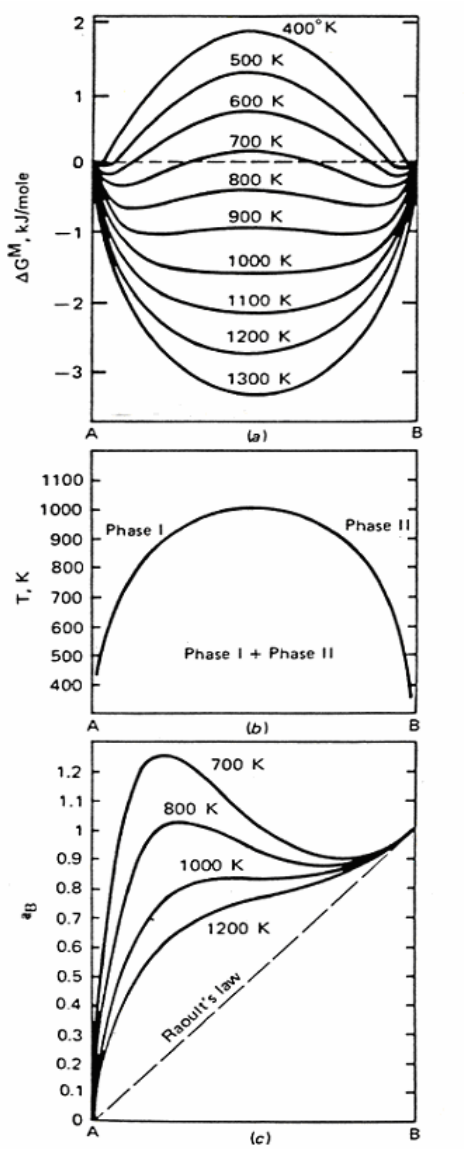

In the symmetric Margules model, $W_{12} = W_{21} = W_H$ and $W_H = RT\alpha_0$, *i.e.*, both Redlich-Kister and Margules models reduce to expressions of the same type. However, the Redlich-Kister model may be preferable for two reasons. (i) It is easier to extend if more terms in Eq. (II.39) need to be considered. (ii) It seems to be better suited for multi-component non-ideal solid mixtures than the Margules or Thompson-Waldbaum model, (*cf.* [1998HIL]).

Equations for activity coefficients in ternary and higher-order systems become very cumbersome [1989HEL/WOO] because of the need to account not only for binary, but also for ternary, quaternary, and possibly higher interactions. Even for the simplest, regular (symmetric) mixing, one interaction parameter is needed for a binary mixture; three binary and one ternary parameter are needed for the ternary mixture, and so on. The problem of retrieval of values of higher-order parameters from experimental data quickly becomes intractable. Even for binary systems, there are few cases in which the data are accurate enough to allow for the unique determination of four parameters in the temperature dependent subregular model. In general it is probably better to use the smallest number of parameters, consistent with any obvious asymmetry or temperature dependence, rather than to simply fit a generalised model.

Immiscibility occurs when positive W_H terms outweigh the configurational entropy contribution. For the strictly regular solution, the miscibility gap closes at a temperature (critical point or consolute temperature) $T = \alpha/2R = W_H/2R$, see Figure II-2. In other cases the miscibility gaps are asymmetric. The conditions for equilibrium between two phases (α and β) are the simultaneous equalities of chemical potential or activities:

$$\mu(\text{A, phase } \alpha) = \mu(\text{A, phase } \beta) \qquad \text{(II.46)}$$

and

$$\mu(\text{B, phase } \alpha) = \mu(\text{B, phase } \beta) \qquad \text{(II.47)}$$

This is equivalent to:

$$a(\text{A, phase } \alpha) = a(\text{A, phase } \beta) \qquad \text{(II.48)}$$

and

$$a(\text{B, phase } \alpha) = a(\text{B, phase } \beta) \qquad \text{(II.49)}$$

In general, such coexisting compositions need to be found by a numerical process, rather than by a closed-form algebraic solution (see Section II.1.2).

Figure II-3 shows the Gibbs energy of mixing at a temperature below the critical point. Two regions of instability of the solid solution can be distinguished.

Figure II-3: Gibbs energy of mixing for a system showing immiscibility at the temperature of interest. The points α and β, defining a common tangent to ΔG_{mix}, are the two coexisting compositions on the binodal or solvus. The two points of inflection, labeled S, define the spinodal. Within the spinodal region, any fluctuation in composition lowers the Gibbs energy (a line joining them falls below the curve), while between the spinodal and binodal, a small fluctuation in composition raises the Gibbs energy (line above curve), though exsolution to α and β lowers it.

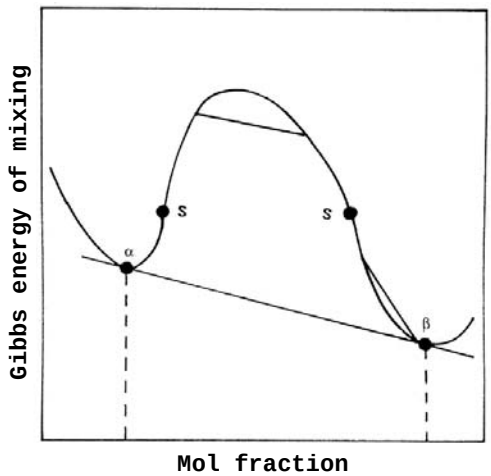

Figure II-4: Representation of solvus (binodal), spinodal, and coherent spinodal (taking interfacial energy or strain into account) in a binary system.

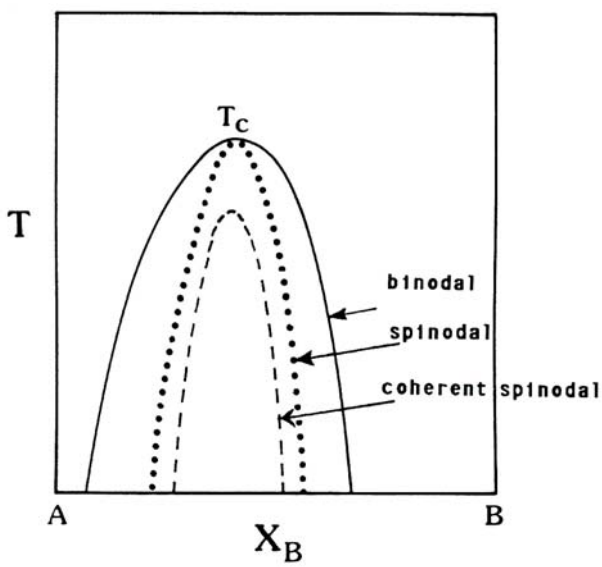

Within the miscibility gap or binodal (solid curve on Figure II-4), the Gibbs energy of the system can be lowered by the formation of two phases defined by the common tangent, as shown. However, a small fluctuation in composition raises the Gibbs energy in the region between the solid and dotted curves. Within a narrower region defined by the dotted curve, called the spinodal, which connects the points of inflection on the Gibbs energy curves at various temperatures, even an infinitesimal fluctuation in composition lowers the Gibbs energy. Within the spinodal region, there is thus no barrier to phase separation; spontaneous fluctuations in composition can grow and lead to phase separation. Distinctive textures of spinodal decomposition, representing the dominance of certain length scales of fluctuations, can result. From the point of view of the persistence of metastable solid solution phases, the decomposition kinetics are expected to be faster within the spinodal region than in the region between the spinodal and the binodal.The initial phase separation produces interfaces between the growing phases of different compositions. If these interfaces maintain crystallographic continuity (are coherent), and the two phases have different lattice parameters, then a destabilizing strain is developed, which acts to thermodynamically retard exsolution. Thus, the "coherent spinodal" lies at lower temperature than the spinodal itself.

II.1.1.4.1 Dilute solid solutions

Dilute solid solutions represent a practically important case for incorporation of trace elements *Tr* (*e.g.*, radionuclides) into host mineral phases such as calcite, when the mole fraction of *Tr* does not exceed a percent. When a (Tr,M)L mixture model based on the symmetric convention is used, then the host end-member mole fraction x_M and its activity coefficient f_{ML} can be approximated as unity, the *Tr* activity coefficient f_{TrL} is constant, and the distribution coefficient D_{Tr} becomes:

$$D_{Tr} = \frac{x_{Tr} \cdot m_{M^+}}{x_M \cdot m_{Tr^+}} = \frac{K_{S,ML} \cdot f_{ML} \cdot \gamma_{Tr^+}}{K_{S,TrL} \cdot f_{TrL} \cdot \gamma_{M^+}} \approx x_{Tr} \frac{m_{M^+}}{m_{Tr^+}} \qquad \text{(II.50)}$$

where $K_{S,ML}$ and $K_{S,TrL}$ are the pure end-member solubility products (for reactions $ML \rightleftharpoons M^+ + L^-$; $TrL \rightleftharpoons Tr^+ + L^-$).

At constant ionic strength, the molality of M^+, as well as the ratio of aqueous activity coefficients ($\gamma_{Tr^+} / \gamma_{M^+}$), are also constants, so D_{Tr} is almost constant, and the *uptake isotherm* – the dependence of trace ion mole fraction x_{Tr} on its dissolved molality – is linear:

$$x_{Tr} \approx k_{D,Tr} \cdot m_{Tr} \quad \text{where} \quad k_{D,Tr} = \frac{D_{Tr}}{m_{M^+}} = \frac{K_{S,ML} \cdot \gamma_{j^+}}{K_{S,TrL}\ \gamma_{TrL}\ \gamma_{M^+}\ m_{M^+}} \qquad \text{(II.51)}$$

where $k_{D,Tr}$ is a partition constant.

It can be shown that γ_{TrL} is approximately constant at trace mole fraction of *Tr*. Thus, at trace mole fraction, the analysis of non-ideal mixing becomes simple and the

activity of dilute end-member can be well approximated using Henry's law. Hence, the infinite dilution reference state would be convenient for dilute solid "solutes". In recognition of this fact, a *dilute solid solutions formalism* has already been applied to solid solutions [1990BAL/PEL], [1992KON/GAM2]. Consider a binary solid solution made of a "solvent" A and a "solute" B end-members. The molar Gibbs energy of this solution is:

$$G_m = (1-x)G_A^o + xG_{x,B}^{(\infty)} + \mathrm{R}T\left[(1-x)\ln(1-x) + x\ln x\right] + \mathrm{R}T\left[x\ln\gamma_{x,B}^{\infty} + \frac{\varepsilon'}{2}x^2 + \frac{\varepsilon''}{2}x^3 + \frac{\varepsilon'''}{2}x^4 + \ldots\right] \quad \text{(II.52)}$$

where x is the mole fraction of the solute; $\gamma_{x,B}^{(\infty)}$ is the activity coefficient of solute at infinite dilution ($x \to 0$) and $\varepsilon', \varepsilon'', \varepsilon'''$ are the first, second, third order interaction coefficients. The last term in the above equation corresponds to the excess Gibbs energy of the dilute solid solution. The following equations for activity coefficients are valid not only at infinite dilution, but also at the finite mole fraction of the solute:

$$\ln\gamma_A = -\frac{\varepsilon'}{2}x^2 - \frac{\varepsilon''}{2}x^3 - \frac{\varepsilon'''}{2}x^4 - \ldots \quad \text{(II.53)}$$

$$\ln\gamma_{x,B} = \ln\gamma_B^{(\infty)} + \ln\gamma_A + \varepsilon' x + \varepsilon'' x^2 + \varepsilon'' x^3 + \ldots \quad \text{(II.54)}$$

To apply these equations in the entire composition range, certain constraints for the parameters must be satisfied. For instance, if only the first-order parameter is retained ($\varepsilon'' = \varepsilon''' = \ldots = 0$), the relationship $\ln\gamma_B^{(\infty)} = -\varepsilon'/2$ reduces the dilute formalism to the regular solution model [1992KON/GAM2].

In the "Unified Interaction Parameter Formalism" [1990BAL/PEL], the dilute formalism with only the first-order interaction parameters ε_{jk} has been extended onto a system including one solid solvent (with index 0) and N solutes, leading to the following equations for activity coefficients:

$$\ln\gamma_0 = -\frac{1}{2}\sum_{j=1}^{N}\sum_{k=1}^{N}\varepsilon_{jk}x_j x_k \quad \text{(II.55)}$$

$$\ln\gamma_{x,j} = \ln\gamma_j^{(\infty)} + \ln\gamma_0 + \sum_{k=1}^{N}\varepsilon_{jk}x_k \quad \text{(II.56)}$$

It is usually assumed that the interaction coefficients are symmetric, *i.e.*, $\varepsilon_{jk} = \varepsilon_{kj}$. The unified formalism can be further extended to any number of solute end-members and it is valid at arbitrary compositions. Compared to classic models like Redlich-Kister or Thompson-Waldbaum, the "unified dilute approach" has two advantages. First, the non-ideal interactions are clearly attributed: the solvent "feels" only a weighted average of interactions with all solutes. This term becomes negligible when their mole fractions together do not exceed approximately 0.01. Each solute interacts

with all others in the same way as the solvent (through γ_0) plus specific interactions with all solutes expressed *via* interaction coefficients. In a very dilute solid solution, the activity coefficients of "trace" solutes become constants equal to $\gamma_B^{(\infty)}$ that, in fact, reflect an interaction of a solute entity with the solvent only. Second, the unified formalism is much easier to extend on multi-component systems than the classic ones. For those reasons, the dilute solid solution approach is appropriate for application to trace radionuclide incorporation into host mineral phases.

II.1.1.5 Phases with different structures

Partial solid solution can also exist among end-members of different structure. Consider two substances, A with structure "α" and B with structure "β". Writing formula units corresponding to one mole of ions being mixed, one has:

$$\mu(A,\alpha) = \mu^o(A,\alpha) + RT \ln a(A,\alpha) \quad \text{(II.57)}$$

$$\mu(A,\beta) = \mu^o(A,\alpha) + \Delta\mu(A, \alpha\rightarrow\beta) + RT \ln a(A,\beta) \quad \text{(II.58)}$$

$$\mu(B,\alpha) = \mu^o(B,\beta) + \Delta\mu(B, \beta\rightarrow\alpha) + RT \ln a(B,\alpha) \quad \text{(II.59)}$$

$$\mu(B,\beta) = \mu^o(B,\beta) + RT \ln a(B,\beta) \quad \text{(II.60)}$$

where $\mu^o(A,\alpha)$ is the Gibbs energy per mole of pure A in structure "α", $\Delta\mu^o(A(\alpha\rightarrow\beta))$ is the Gibbs energy change for the transformation of A from structure "α" to structure "β". a(A, α) refers to the activity of A in structure "α" (unity for pure A) and a(A,β) refers to the activity of A in structure "β" (also unity for pure A, with structure "β" taken as standard state). Analogous definitions hold for the terms in component B. Pure A in structure "β" can be real phase at some p and T or a physically unrealizable "cryptomodification" or "fictive phase" unstable at all p and T. The limiting solubilities are given by equating chemical potentials:

$$\mu(A,\alpha) = \mu(A,\beta) \quad \text{(II.61)}$$

$$\mu(B,\alpha) = \mu(B,\beta). \quad \text{(II.62)}$$

It is important to remember that if the structures are different (and cannot be related by order-disorder phenomena), the Gibbs energy curve for each phase is distinct, rather than being part of a single Gibbs energy curve. The miscibility will persist until it intersects melting (a eutectic) or other phase transformation occurs. This type of limited terminal solid solution is not a solvus.

This case of non-isostructural end-members is potentially important for the description of solid solution uptake of trace/minor amounts of actinides and fission products into common host minerals such as carbonates, sulphates or silicates. A suitable and simple formulation for such complex mixing has been suggested long ago in metallurgy by Darken [1967DAR], [1967DAR2], and 20 years later introduced in mineralogy and petrology by Powell [1987POW] as "Darken's quadratic formalism"

(DQF). This approach has already been used for multicomponent solid solutions of amphiboles [1992WIL/POW], micas [1993VAN/HOL], plagioclase feldspar [1992HOL/POW], and ternary garnet [1996GUI/POW]. A brief description of DQF presented below follows the discussions by Powell [1987POW], Will [1998WIL], and Ganguly [2001GAN], restricted to binary systems for clarity reasons; the DQF approach, however, can be applied equally well to ternary and higher systems.

DQF simply states that over composition ranges adjacent to end-members, a complex solid solution can be approximated by a simple model such as the regular or even the ideal solution. In these *simple* composition intervals, the DQF can model a severely asymmetric solution by assuming a *simple* solution which extends from the *real* end-member A with Gibbs energy $G^{\circ}_{A} = \mu^{o}(A)$ to a *fictive* end-member B with Gibbs energy $G^{*}_{B} = \mu^{*}(B)$, as shown on Figure II-5.

Figure II-5: Schematic representation of excess Gibbs energy in DQF for a binary solid solution AB showing a simple composition range where the regular mixing model is applicable (from www.esc.cam.ac.uk/astaff/holland/ds5/plagioclases/plag.html)

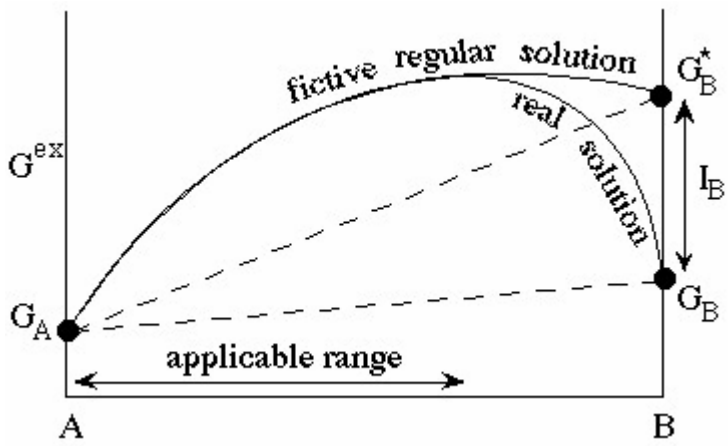

Darken [1967DAR] has made a plausible suggestion that, in general, one mixing model cannot be applied satisfactorily over the entire compositional range in a given real system. Instead, as he demonstrated for several metal systems, a simple mixing model might work well over the simple regions, whereas complex relationships apply for the range in between. The simple mixing model applied to *simple* regions is commonly the regular model Eq. (II.38) (the ideal mixing obviously being a special case of it). The name "quadratic formalism" results from the form of the binary regular model (Eq. (II.38)) and its activity coefficient (Eq. (II.63)), which are proportional to the square of the mole fraction x. Darken has pointed out that, if the activity coefficient f_A of

a major component (component A) obeys a regular solution model with the interaction parameter W_{AB}

$$\mathrm{R}T \ln f_A = W_{AB} x_B^2 \tag{II.63}$$

then the Gibbs-Duhem relation

$$x_A \cdot d(\ln f_A) + x_B \cdot d(\ln f_B) = 0 \tag{II.64}$$

only requires that the activity coefficient f_B of the minor component (B) obeys the relation

$$RT \ln f_B = W_{AB} x_A^2 + I_B \tag{II.65}$$

where I_B is an integration constant, and $x_A = 1 - x_B$. Thus, in the simple region A where the mole fraction x_B of the end-member B is minor, the excess Gibbs energy is given by

$$\Delta G^E = W_{AB}\, x_A x_B + I_B x_B \tag{II.66}$$

The DQF equations (II.65) and (II.66) lead to the following expression for the molar Gibbs energy of solid solution in the simple region A:

$$G_{mix} = x_A G_A^{\mathrm{o}} + x_B \left(G_B^{\mathrm{o}} + I_B \right) + \Delta G_{mix} = x_A G_A^{\mathrm{o}} + x_B G_B^{*} + \Delta G_{mix} \tag{II.67}$$

where

$$\Delta G_{mix} = -TS_{ideal} + \Delta G^E = RT \left(x_A \ln x_A + x_B \ln x_B \right) + W_{AB} x_A x_B \tag{II.68}$$

The last two equations explain why a solid solution obeying DQF in the terminal region A may be viewed as a regular solution between the *real* end-member A and a *fictive* end-member whose molar Gibbs energy, G_B^*, is given by that of the real end-member B (G_B^{o}) plus the value of Darken's integration constant, I_B. In general, the I_B parameter is temperature dependent and composition independent, while the W_{AB} parameter is usually taken temperature- and composition independent. Furthermore, in a simple region adjacent to the pure end-member B, assuming a regular mixing with (now) minor component A,

$$\mathrm{R}T \ln f_B = W_{BA} x_A^2 \tag{II.69}$$

and, from Eq. (II.64),

$$\mathrm{R}T \ln f_A = W_{BA} x_B^2 + I_A \tag{II.70}$$

where $I_A = G_A^* - G_A^o$. Note that there is no correlation between the two simple (terminal) regions in a binary system. In other words, regular fitting parameters W_{AB} and W_{BA} are not necessarily equal, and there is no way to predict one from another. The same applies to the DQF fitting parameters I_B and I_A and, correspondingly, to the Gibbs energies of fictive end-members G_B^* and G_A^*.

In some cases, the fictive end-members may correspond to pure solids that can be observed, for instance, if there is a phase transformation from structure α of end-

member A to structure β of end-member B, as in the calcite $CaCO_3$-strontianite $SrCO_3$ system. The pure calcite has a rhombohedral structure ($R\bar{3}c$ space group), whereas the pure strontianite has an orthorhombic structure (*Pmcn* space group). Therefore, in the calcite simple region, we expect the fictive minor $SrCO_3$ end-member having a rhombohedral structure. Such pure phase does not exist, although its standard molar Gibbs energy can be estimated from linear Gibbs energy correlations such as suggested in [1984SVE]. In the strontianite simple region, a fictive minor $CaCO_3$ end-member should have an orthorhombic structure. Such pure phase exists in nature – a mineral aragonite, the standard molar properties of which (including G°) can be found in chemical thermodynamic databases. Note that in this strongly non-ideal system, the transitional region between rhombohedral and orthorhombic simple regions is hidden behind a miscibility gap.

The microscopic rationale for DQF can be traced back to the "nearest neighbour model" (also referred to as the Ising model) from which the regular mixing model can be derived [1998WIL]. In this context, the energy of a system is calculated as the sum of contributions from the interaction energies of the next nearest neighbour atomic pairs, ε_{ij}. The properties of mixing depend only on the characteristic potentials, $\Delta\varepsilon_{ij} = 2\varepsilon_{ij} - \varepsilon_{ii} - \varepsilon_{jj}$ for $i,j = 1,2,\ldots, n$; $i \neq j$. For a binary solid solution AB,

$$\Delta\varepsilon_{AB} = 2\varepsilon_{AB} - \varepsilon_{AA} - \varepsilon_{BB}, \tag{II.71}$$

and the enthalpy of mixing is given by:

$$\Delta H_{AB}^{mix} = \frac{1}{2} Nz\Delta\varepsilon_{AB} x_A x_B = W_{AB} x_A x_B \tag{II.72}$$

where z is the next nearest shell coordination number, and N is the total number of A and B atoms. It follows from Eq. (II.72) that interaction parameters W_{ij} are proportional to $\Delta\varepsilon_{ij}$. In the regular mixing model, $\Delta\varepsilon_{ij}$ and W_{ij} are independent of composition x_A, x_B,…, whereas in the subregular model, $\Delta\varepsilon_{ij}$ and W_{ij} are linear functions of composition (or non-linear in more complex mixing models). Equation (II.71) also implies that $\Delta\varepsilon_{ij}$, ε_{ij}, ε_{ii} and ε_{jj} have the same composition dependence, *i.e.*, if the regular model is valid then they are all composition independent, or linearly depend on x_j in the subregular model. In the latter case, the atomic environment of each site, the factor controlling ε_{ij}, also changes linearly with composition.

Since the energetic environment of a site is controlled by the dominant neighbours (*e.g.*, in an AB solution $A_{90}B_{10}$, the site environment is obviously dominated by A atoms), it is more likely that $\Delta\varepsilon_{ij}$ are composition-independent in the vicinity of end-members forming simple regions, and that $\Delta\varepsilon_{ij}$ vary only between the simple regions. This is the underlying idea of DQF, with simple regions being regular mixtures between real and fictive end-members, and transitional ranges occurring between the simple regions. In multicomponent solutions, it may happen that $\Delta\varepsilon_{ij}$ are not composition-dependent in simple regions that include several end-members. Thus, DQF may be

used for complex systems as a simple way of approximating the complex mixing behaviour in a significant composition range, which would otherwise be intractable for conventional thermodynamics at all.

In applying DQF to treat the activity-composition data, one has to take care about the data quality. Since even a binary system is divided into three segments —two simple (terminal) regions and one complex (central) region— there is a greater flexibility in fitting the data, which permits a better formal fit of the poor quality data by DQF than by a subregular or a more complex model. For Aq-SS systems, this kind of analysis can and should be combined with Lippmann diagrams or general Aq-SS solubility theory (see Chapters II.1 and II.2).

Volume-composition experimental data are usually more precise than the calorimetrically determined enthalpy-composition data or solubility data. Therefore, applying DQF concepts to volumetric data, one can get a better idea about the location of simple and complex regions on phase composition diagrams. More about this subject can be found in [1987POW], [1998WIL].

II.1.1.6 Order-disorder phenomena

II.1.1.6.1 General comments

Ordering phenomena complicate the thermodynamic behaviour of solid solutions in several ways:

1. If the order-disorder process is slow, several series of solid solutions, each having a differing degree of order can be prepared or observed in nature. Then the thermodynamics of mixing other species (*e.g.*, Na, K or Na, Ca in feldspars) will depend on the degree of order in the aluminosilicate framework [1985CAR/MCC], [1977HOV/WAL].

2. The extent of ordering depends on temperature in a complex fashion. The kinetics of ordering is generally slower for Si - Al than for non-framework cations. Extrapolation of measured properties to temperatures higher or lower than that of measurement is far more risky than in "simple" systems. The enthalpy and entropy of mixing will then depend strongly on temperature because the degree of order is temperature dependent. The calculated entropies of mixing can be quite asymmetric, *e.g.*, for the mixing of a normal and an inverse spinel ([1984ONE/NAV]). This results in significantly asymmetric Gibbs energies of mixing, not because one invokes Margules parameters and asymmetric enthalpies and non configurational entropies of mixing, but because the configurational entropy term itself departs from symmetrical behaviour and does not resemble $-n\,\mathrm{R}\,[x\,\ln x + (1-x)\,\ln(1-x)]$ in form. At low temperature, this asymmetry is pronounced and, for example, a solvus between a largely normal and a largely inverse spinel develops [1984ONE/NAV]. Again, such asymmetry can arise from the form of the entropy

of mixing and not from strongly asymmetric energies. Thermodynamic models that specifically include order-disorder, and are tailored for each particular system, must be developed.

3. The observed degree of ordering is often kinetically controlled. At low temperatures, changes in the degree of order are hindered, thus both ordering and disordering occur slowly, and many metastable states are preserved. At intermediate temperatures, equilibrium is attained and that state can be quenched to ambient conditions. At high temperature, equilibrium is attained, but it may be impossible to quench the full extent of disorder back to ambient conditions. The effect of pressure on the rates of order-disorder reactions has only begun to be explored. Thus, the interpretation of experimental observations must be made with both thermodynamics and kinetics in mind. Specifically, the extent to which order-disorder contributes to experimentally measured heat capacities poses a complex problem.

4. Related to the kinetics, precipitation of solids from aqueous solution at low temperature can produce metastable disordered phases. Examples are high magnesium calcites rather than dolomite [1987NAV/CAP], or very disordered spinels [1998MCH/NAV]. Heating such materials may lead, first, to an increase in the state of order as kinetic barriers are overcome, followed by a decrease in ordering as a normal equilibrium effect. Further complications in such materials prepared at low temperature may be small particle size and adsorbed water, both of which may affect the thermodynamics.

5. A strong tendency to ordering is manifested in significant negative heats of mixing and sometimes leads to an intermediate compound formation (*e.g.*, dolomite, omphacitic pyroxenes, *etc*.). Both the heat and entropy of mixing in such systems may depend strongly on the degree of order, and therefore on temperature. In addition, destabilising energetic effects from mixing of ions in the disordered state may be present at the same time as the stabilising effect of ordering, leading to complex interplay between ordering and exsolution.

6. Order-disorder reactions often involve a change in the symmetry of the structure. Such changes may be ordinary first-order phase transitions, or they may be higher-order phase transitions leading to some unconventional phase diagram topologies. The lattice parameter can vary rather nonlinearly with composition, especially at low temperature and when the end-members have different cation distributions. A sigmoid variation of the lattice parameter with composition is commonly seen in solid solutions between a normal and an inverse spinel (*e.g.*, $FeCr_2O_4$-Fe_3O_4) [1984ONE/NAV].

II.1.1.6.2 An example: carbonates with calcite and dolomite structures

The calcite and dolomite crystal structures commonly occur in nature for divalent metal carbonate minerals (usually $CaCO_3$ and $CaMg(CO_3)_2$). The major crystal-chemical dif-

ference between the calcite and dolomite structures is that calcite contains only one distinct metal layer while dolomite has two. The chemical difference between these layers results in two geometrically non-equivalent cation sites. Furthermore, a continuous range of structures between the ordered dolomite and disordered calcite is possible because the space group of dolomite is a subgroup of that of calcite. Indeed, some natural dolomites are reported to have disordered structural states [1984REE] while synthetically disordered samples may be obtained by annealing ordered material at high temperature. However, the high temperatures involved and possible problems in quenching the disordered phase make detailed study of the order-disorder transition in $CaMg(CO_3)_2$ difficult.

The system $CdCO_3$-$MgCO_3$ is analogous to the $CaCO_3$-$MgCO_3$ system in that similar ordered and disordered phases exist. Because chemical homogenisation of distinct Cd and Mg layers proceeds within an experimentally accessible range of pressure and temperature (p_{CO_2} 1 - 10 kbar and 600 to 850 ºC), samples can be prepared which, on quenching, possess greatly different states of order. Phase diagrams for both the $CaCO_3$-$MgCO_3$ and the $CdCO_3$-$MgCO_3$ systems are shown in Figure II-6. Calorimetric studies [1987NAV/CAP], [1987CAP/BUR] provide data on the dependence of long range order parameter and of enthalpy of mixing on quench temperature.

Figure II-6: Phase diagrams for the $CdCO_3$-$MgCO_3$ and $CaCO_3$-$MgCO_3$ systems, consistent with [1972GOL], [1961GOL/HEA]. The terms calcite and dolomite refer to the two structure types (disordered and ordered, respectively) rather than to specific compositions.

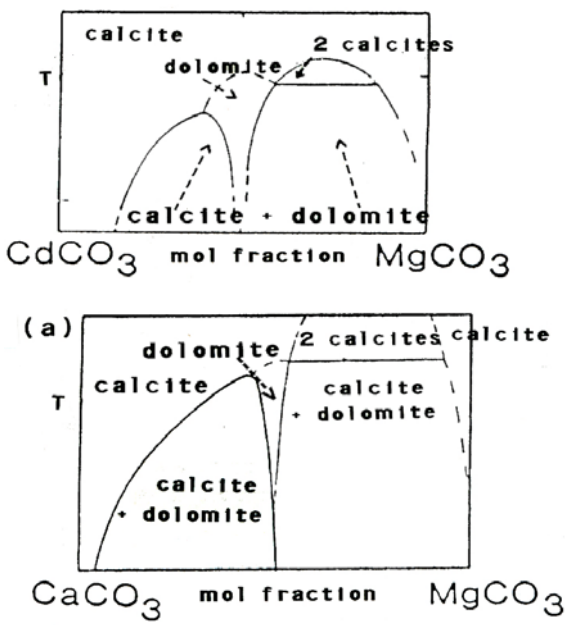

The Cd, Mg disordering reaction is convergent [1969THO], *i.e.*, alternate cation layers are crystallographically distinct only when the cations are ordered. The simplest model (see [1987CAP/BUR]) which can be applied to the order-disorder reaction is of the Bragg-Williams type, in which the long range order parameter, s, is related to one energy parameter, W, by the equation (at the stoichiometric dolomite composition):

$$s = \tanh(-W_s/2R) \qquad \text{(II.73)}$$

W_s is negative and its absolute value reflects the energy of ordering per mole $CdMg(CO_3)_2$. The enthalpy of mixing (formation of $CdMg(CO_3)_2$ from $CdCO_3$ and $MgCO_3$) is then:

$$\Delta H\,(\text{mix}) = W_s\,[0.5 - 0.25(1 - s2)] \qquad \text{(II.74)}$$

The critical temperature at which s becomes zero is given by $T_c = -W_s/2R$. It is about 830 ºC for $CdMg(CO_3)_2$ and about 1150 ºC for $CaMg(CO_3)_2$ [1961GOL/HEA], [1972GOL].

A striking feature of both systems is that the ordered dolomite phase has a negative enthalpy of mixing from the end-member carbonates, while the disordered phase at dolomite composition has a positive enthalpy of mixing. This cannot be accounted for by a simple Bragg-Williams model because its one parameter, W_s, must be negative for ordering to take place at low temperatures. Thus, even the disordered phase would show a negative heat of mixing.

To include positive heats of mixing in the disordered phase, one can apply a generalised Bragg-Williams, or generalised point approximation (PA), see discussion by Capobianco *et al.* [1987CAP/BUR] and Burton [1987BUR]. In such a model, there are two distinct interactions: (1) an attractive (interlayer) interaction promoting unlike pair formation (parameterised as W_{ier}) and (2) a repulsive (intralayer) interaction promoting segregation (parameterised as W_{ira}).

The Gibbs energy of mixing (formation of $(Cd_{1-x}Mg_x)_2(CO_3)_2$ from $CdCO_3$ and $MgCO_3$) is given by, per formula unit containing two carbonates:

$$\Delta G_m(\text{mix}) = W_{ier}[x - x^2(1 - s^2)] + W_{ira}[x - x^2(1 + s^2)] + RT \sum_i \sum_j x_{ij} \ln x_{ij} \qquad \text{(II.75)}$$

where x_{ij} is the cation site occupancy of the "j–th"atom on the "i–th" sublattice.

Thus for $i = \alpha$ (layer preferred by Mg), β (layer preferred by Cd) and j = Mg, Cd,

$$x_{\alpha,Mg} = x + xs,$$
$$x_{\alpha,Cd} = 1 - x - xs,$$
$$x_{\beta,Mg} = x - xs, \text{ and}$$
$$x_{\beta,Cd} = 1 - x + sx.$$

Here x is the mole fraction of $MgCO_3$ and s, as before, is the long range order parameter. As in the original Bragg-Williams model, the equilibrium value of s is found by minimising $\Delta G_m(\text{mix})$ with respect to variations in s, and the critical temperature for disordering is obtained by setting the second derivative of $\Delta G_m(\text{mix})$ to zero for $s = 0$. For $W_{ier} < 0$ and $W_{ira} > 0$, intersite ordering decreases $\Delta H_m(\text{mix})$ while intrasite mixing increases it, and at low temperature the ordered phase is stable. Above T_c, $s = 0$, so that $\Delta H_m(\text{mix})$, given by $(W_{ier} + W_{ira})(x - x^2)$ is positive for $W_{ira} > |W_{ier}|$. W_{ier} and or W_{ira} may depend on composition, leading to asymmetry in solution properties.

A model based on the tetrahedral approximation (TA) in the cluster variation method (CVM) also can be applied [1987BUR]. The CVM approach includes the effects of short range order (which the point or Bragg-Williams approximations neglect) by considering the possible arrangements of clusters of atoms (tetrahedral of cations in this case). The calculated equilibrium proportions of the chemically distinct tetrahedra are constrained by the total solution composition and the energetic interactions between the atoms of the tetrahedron. These calculated proportions then provide information on both long-range and short-range order. Because of short-range order, the configurational entropy in the CVM calculations is generally smaller than in the previous models.

Calculations using both the PA and TA models correctly predict the topology and qualitatively fit the observed phase boundaries in both the $CaCO_3$-$MgCO_3$ and $CdCO_3$-$MgCO_3$ systems [1987BUR], [1987CAP/BUR]. Such models account qualitatively for positive heats of mixing in the disordered phases. However, quantitative fit to the structural and thermochemical data in $CdCO_3$-$MgCO_3$ is poor. This failure may be related to several factors. First, the carbonate group may undergo shifts of position and small deviations from a planar configuration as a result of Cd,Mg ordering. Such involvement of CO_3 groups might give the transition more cooperative character and compress it, as observed, into a smaller temperature interval. Second, the compositional asymmetry of inter- and intra-layer interactions may be more complex than considered in the above models. Third, differences in lattice vibrations between ordered and disordered phases may result in excess heat capacities, excess entropies, and temperature dependent enthalpies not considered in simple models.

Nevertheless, it is important to note the essential features of a model that can qualitatively explain the variation of long-range-order with temperature, the enthalpy of mixing, and the topology of the phase diagram. Such a model must incorporate three main features: a negative (stabilising) interaction for ordering of cations between layers, a positive (destabilising) interaction for the mixing of cations within a layer, and a compositional asymmetry for at least one parameter. These features lead to strong temperature dependence of the order parameters and of the enthalpy and entropy of mixing. Empirical models based on a Margules formulation simply cannot build in the appropriate temperature dependence and cannot account for the phase diagram topology.

The $CaMg(CO_3)_2$-$CaFe(CO_3)_2$ system (dolomite-ankerite) shows a generally decreasing degree of order as iron substitutes for magnesium. Calorimetric studies have been performed on samples of various degrees of disorder [1996CHA/NAV], [1999NAV/DOO]. The samples studied fell on the trends: those with extensive order, those with almost complete disorder, and an intermediate group. Analysing these three groups separately allowed an estimate of the enthalpy of complete disordering to be (33 ± 6) kJ·mol^{-1} for dolomite and (18 ± 5) kJ·mol^{-1} for ankerite. Highly ordered samples have negative enthalpies of formation from end-members ($CaCO_3$, $MgCO_3$, $FeCO_3$), but highly disordered ones have positive enthalpies. Varying degrees of order and metastability in the low temperature aqueous environment will clearly complicate any attempt to describe the thermodynamics of this system.

To summarise, choosing an appropriate thermodynamic model for dealing with a solid solution is an essential first step in modelling solid solution-aqueous phase interactions. Because of the variety of stoichiometries, charge-balanced ionic substitutions, and order-disorder phenomena encountered, "one size does not fit all". Rather, the model chosen must be appropriate to the crystal chemistry of the solid solution phase.

II.1.2 Methods and tools for thermodynamic description of aqueous-solid solution (Aq-SS) equilibria

Calculation of equilibrium speciation in a thermodynamic system involving two or more multi-component phases in the mass balance is not trivial and requires application of computer-aided numerical algorithms. Aqueous-solid solution systems (that often include also gas mixture and several single-component solids) belong to this category. In plain words, mathematical problems arise because the equilibrium compositions of coexisting non-stoichiometric phases depend on each other and at the same time – on bulk composition of the whole system, temperature, and pressure. These dependencies are usually non-linear and may be dramatic if strongly non-ideal solutions are involved. Methods for solving such systems have been intensively developed since 1970es [1973ERI/ROS], [1974BRO/SKI], [1977PEL/BAL], [1981KAR], [1987WOO], [1989ERI/THO], [1992GLY/PAR], [1994GHI], [1997KAR/CHU], [2000GLY], [2001GAN], [2001PEL].

The most advanced algorithms based on Gibbs energy minimisation are available as computer codes such as ChemSage/FactSage ([1990ERI/HAC], [2002BAL/CHA]), GEM-Selektor [2001KAR/CHU], or Hch [1992BOR/SHV] (see Section II.1.2.4 below).

Results of any computer-aided model cannot be better than its input data, normally available from internally consistent compilations such as NEA TDB series [1992GRE/FUG], [1995SIL/BID], [1999RAR/RAN], [2001LEM/FUG], [2003GUI/FAN], [2005GAM/BUG], [2005OLI/NOL], [2005BRO/CUR], [2005HUM/AND]. The input thermodynamic data include the formula stoichiometry and standard molar thermody-

namic properties (Gibbs energy G_m^o, volume V_m^o) of each component in each phase, corrected from reference (p_r, T_r), to pressure p and temperature T of interest. Such corrections require knowledge of other standard molar properties at (p_r, T_r) (entropy S_m^o or enthalpy H_m^o), as well as coefficients describing how the molar heat capacity at constant pressure $C_{p,m}$ depends on temperature, and how the molar volume depends on T and p.

Alternatively, thermodynamic properties (of gases, liquids and aqueous species) can be raised to (p, T) of interest using formulae and coefficients derived from the respective equations of state. Various methods of (p, T) corrections will not be considered further in this contribution because they are well known and available in literature [1994NOR/MUN]. The required subroutines are built into many computer codes for modeling phase equilibria (FactSage, GEMS-PSI) or chemical reactions (SUPCRT92). Many code packages include databases of chemical thermodynamic input data. Specialised databases were compiled for applications related to (nuclear) waste management at low to moderate temperatures and pressures, in which equilibrium constants at (p_r, T_r) are given instead of G_m^o values [1990NOR/PLU], [2002HUM/BER]. Internal consistency of thermodynamic data is maintained within a given data base, but the data taken from different data bases are not mutually consistent.

Another kind of input data for modelling chemical equilibria in aqueous-solid solution (Aq-SS) systems describes the non-ideality of mixing between components (end-members) in the aqueous electrolyte and in solid solution phases. Almost any model for aqueous electrolyte produces individual activity coefficients of ions and complexes as function of the ionic strength I – a measure of the "concentration of charge" in aqueous solution. The ion association models based on the Debye-Hückel equation (*cf.* [1993MOR/HER], [1997LAN]) can be used with reasonable accuracy up to I_m = 0.1 - 0.7 m effective ionic strength. The ion-interaction SIT (Brønsted-Scatchard-Guggenheim) model [1997GRE/PLY2] can be used up to I_m = 2 - 3 m. The most complex Pitzer model is applicable to mixed electrolytes of any ionic strength with accuracy of a few percent [1991PIT], although it requires a large number of interaction parameters, often difficult to determine or to extrapolate beyond intervals of experimental data. Each of these families of aqueous electrolyte models requires a different set of aqueous complexes. In ion interaction models, only "strong" complexes are included, while ion association models require many weak complexes and "ion pairs" with respective thermodynamic properties (more in [1997GRE/PLY2], [1997PUI/RAR]). Please, note that aqueous data for minor and trace elements at ionic strengths greater than 4 m are rather limited.

As already shown in Section II.1.1, non-ideality of solid solutions is usually described on the basis of the power-series extension of excess Gibbs energy of mixing [1967GUG] as function of mole fractions of end-members. Depending on the number of power-series terms considered, several popular models can be obtained (Redlich-Kister (Guggenheim), Margules, Thompson-Waldbaum, Wilson, Bale-Pelton), formulated

either for binary or for multi-component mixing. Some of these models will be considered below in detail, with special emphasis on estimation of their parameters from experimental data.

II.1.2.1 Definitions and basic thermodynamics relations

In this section, some definitions, thermodynamic concepts and relations are put together that are necessary for understanding methods described in the following sections with emphasis on Aq-SS equilibria. By no means is this "theoretical minimum" complete or exhaustive —for this, the reader is addressed to source textbooks [1967GUG], [1993AND/CRE], IUPAC publications [2003GAM/KON], [2003LOR], [2003LOR/COH] and references therein. The mixing models for solid solutions have been summarised in Section II.1.1.4.

Thermodynamic methods are applied to a *system* – the object of interest. The system is made up of the *independent components* or the minimum number of composition variables (*stoichiometry units*) required to define a system of interest. A *heterogeneous* system contains a number of *phases*; a phase is a homogeneous part of the system such that all intensive variables (temperature T, pressure p, composition, *etc*.) are uniform within it. Different phases are separated by physical boundaries and can exist in solid, liquid or gaseous aggregate states.

Any phase that contains more than one *end-member component* is called *mixture* or *solution*. IUPAC recommends a distinction between mixtures and solutions following [1967GUG], although these terms are still used loosely in the literature. A *mixture* [1997MCN/WIL] describes a homogeneous gaseous, liquid or solid phase containing more than one substance intimately mixed at molecular level, where the substances (end-members) are all trated in the same way. A solution [1997MCN/WIL] describes a homogeneous liquid or solid phase containing more than one substance, where for convenience one of the substances is called *solvent*, and may itself be a mixture. This is treated differently than the other substances called *solutes*. If the sum of mole fractions of solutes is much less than unity, the solution is called *dilute* (see [2003LOR/COH], p.20). Thermodynamic treatments of mixtures and solutions differ in important ways set by the definitions of the standard and reference states of an end-member, a solvent, and a solute. However, the above distinction between *mixture* and *solution* is arbitrary and is frequently not followed. For instance, homogeneous solid mixtures in the above sense are usually called *solid solutions* in the geological literature.

The general solubility equilibrium is that of a component B in phase α in equilibrium with the same component in phase β: B(phase α) = B(phase β), when chemical potentials on both sides of this reaction are equal:

$$\mu_B^{(\alpha)}\left(p,T,x_1^{\alpha},...,x_C^{\alpha}\right)=\mu_B^{(\beta)}\left(p,T,x_1^{\beta},...,x_C^{\beta}\right) \tag{II.76}$$

where x_i^{α}, x_i^{β} are the mole fractions of other components in the system. Introducing the analytical expressions for the chemical potentials, one obtains [2003LOR/COH]

$$\Delta_{sln}G_m^o(p,T)=\mu_B^{o(\beta)}-\mu_B^{o(\alpha)}=-RT\ln\frac{a_B^{(\beta)}}{a_B^{(\alpha)}} \tag{II.77}$$

where the standard chemical potentials μ_B^o must be compatible with the definitions of activities a_B^o of substance B for a chosen composition scale; $\Delta_{sln}G_m^o$ is the standard Gibbs energy of solution, and R is the gas constant. In most cases (with some exceptions), Eq. (II.77) enables calculation of solubility equilibria, if the activities in both phases can be expressed through amounts or concentrations of the components. Activities will be denoted by a_i if the i-component is in the solid solution phase, while it will be denoted {i} if it is present in the aqueous phase.

The standard chemical potentials and activities of the components in the solid mixtures (solid solutions), non-electrolyte liquid mixtures, and in the gas phase, are usually expressed using the *symmetric* convention, meaning that each component is treated in the same way and in mole fraction (rational) scale. The standard chemical potentials and activities of solutes in aqueous electrolyte and sometimes in the solid solution are expressed using the *unsymmetric* convention because they are treated differently from those of a selected component called *solvent*.

The *standard state* of a *j*-th solid (liquid) end-member and of any solvent is usually a pure substance ($x_j = 1$) at the temperature of interest and standard pressure p^o (1 bar = 10^5 Pa, before 1980 - 1 atm = 1.013 bar), *i.e.*

$$\mu_j^o(T)=\mu_j^*(p^o,T) \tag{II.78}$$

The *relative activity* (for a component B in a real mixture at T and p of interest) in this case is defined as:

$$RT\ln a_B=RT\ln\left(f_B x_B\right)=\mu_B-\mu_B^o-\int_{p^o}^{p}V_B\,dp \tag{II.79}$$

where x_B is the *mole fraction* of B in the mixture, and f_B is the *activity coefficient* referenced to Raoult's mixing law (for liquids and solids, the last term with the molar volume V_B in Eq. (II.79) is rather small and is in practice usually combined with μ_B^o). The activity a_B and the activity coefficient in Eq. (II.79) are defined relative to the *reference state* of an *ideal* or *perfect* mixture:

$$\mu_B^{id}=\mu_B^o+RT\ln x_B \tag{II.80}$$

using the mole fraction concentration scale. For solid and liquid mixtures, the above definitions apply to each end-member and, thus, correspond to the symmetric convention. The chemical potential of a component can be written as:

$$\mu_{\mathrm{B}} = \mu_{\mathrm{B}}^{(\mathrm{o})} + \mu_{\mathrm{B}}^{\mathrm{id}} + \mu_{\mathrm{B}}^{E} \tag{II.81}$$

where $\mu_{\mathrm{B}}^{(\mathrm{o})} = \mu_{\mathrm{B}}^{\mathrm{o}} + \int_{p^{\mathrm{o}}}^{p} V_{\mathrm{B}} dp$,

and $\mu_{\mathrm{B}}^{E} = \mathrm{R}T \ln f_{\mathrm{B}}$

is the *excess* chemical potential. For the whole symmetric mixture phase α, the components of its integral Gibbs energy G_α at p,T and system composition of interest are defined as:

$$G_{\alpha} = G_{\alpha}^{(\mathrm{o})} + G_{\alpha}^{\mathrm{id}} + G_{\alpha}^{E} \tag{II.82}$$

where

$$G_{\alpha} = \sum_{j}^{c} \mu_j n_j \tag{II.83}$$

$$G_{\alpha}^{(\mathrm{o})} = \sum_{j}^{c} \mu_j^{(\mathrm{o})} n_j \tag{II.84}$$

$$G_{\alpha}^{\mathrm{id}} = \mathrm{R}T \sum_{j}^{c} n_j \ln x_j \tag{II.85}$$

$$G_{\alpha}^{E} = \mathrm{R}T \sum_{j}^{c} n_j \ln f_j \tag{II.86}$$

and c is the index of the last mixture end-member. From the excess Gibbs energy G_{α}^{E}, the partial molar excess Gibbs energy $\bar{G}_k^E$ of a selected k-th component can be found by partial differentiation:

$$\left(\frac{\partial G_{\alpha}^{E}}{\partial n_k} \right)_{T,p,n_j,j\neq k} = \bar{G}_k^E \tag{II.87}$$

Relationships such as (II.82) to (II.86) play a central role in thermodynamic analysis of mixtures (solutions), where models actually differ in the functional representation of the molar and partial excess Gibbs energies, as discussed below.

For solutes (*e.g.*, aqueous electrolyte species), the pure-component standard state (Eq. (II.78)) and the Raoultian reference state (Eq. (II.80)) are not convenient, and the standard state is usually chosen together with the reference state of *infinite dilution* of the solute (*i.e.*, unsymmetrical convention). There are alternative choices for the composition variable (relative content).

II.1.2.1.1 Mole fraction scale

The activity coefficient of solute B referenced to Henry's law and on the mole fraction scale $\gamma_{x,\mathrm{B}}$, is defined through:

$$\mu_{\mathrm{B}}(p,T) = \mu_{x,\mathrm{B}}^{(\infty)}(p,T) + \mathrm{R}T \ln\left(\gamma_{x,\mathrm{B}} x_{\mathrm{B}}\right) \tag{II.88}$$

where the standard chemical potential (a function of temperature and pressure) is defined as:

$$\mu_{x,\mathrm{B}}^{(\infty)}(p,T) = \lim_{x_A \to 1}[\mu_{\mathrm{B}}(p,T) - \mathrm{R}T\ln x_{\mathrm{B}}] \text{ and } \lim_{x_{\mathrm{A}} \to 1}\gamma_{x,\mathrm{B}} = 1 \text{ with all } x_S \to 0$$

[2003LOR/COH]. The limit with all $x_S \to 0$ means that, in a multi-component system, the mole fraction of each solute approaches zero. For the solvent, the activity coefficient and the standard chemical potential are still defined by the symmetrical convention (Eqs. (II.79) and (II.78)). The relation between symmetrical and unsymmetrical definitions of the activity coefficient of solute component B is:

$$\ln\gamma_{x,\mathrm{B}} = \ln f_{\mathrm{B}} - \ln f_{\mathrm{B}}^{\infty} \tag{II.89}$$

where f_{B}^{∞} is the limiting value of f_{B} at $x_{\mathrm{B}} \to 0$.

II.1.2.1.2 Molality scale

The aqueous phase is almost always sufficiently dilute to consider the *molality* (mol·kg^{-1}) a convenient composition variable (the molarity mol·dm^{-3} scale is temperature/pressure dependent and hence not practical in thermodynamic models). Molality of a solute B is defined as:

$$m_{\mathrm{B}} = n_{\mathrm{B}}\left(\sum_s n_s M_s\right)^{-1} \tag{II.90}$$

where n_{B} is the amount of B, n_s is the amount and M_s is the molar mass of s-th solvent component, and the summation occurs over all components of the (mixed) solvent. Usually the solvent is only water (indexed w) and Eq. (II.90) takes the form:

$$m_{\mathrm{B}} = \frac{n_{\mathrm{B}}}{n_w M_w} \tag{II.91}$$

where $M_w \approx 0.0180153$ kg·mol^{-1}. The standard state for the aqueous solute is a hypothetical one molal solution ($m^{\mathrm{o}} = 1$ mol·kg^{-1}) at standard pressure p_r and temperature T of interest, chosen to exist in the reference state of infinite dilution:

$$\mu_{\mathrm{B}}(p,T) = \mu_{\mathrm{B}}^{\infty}(p,T) + \mathrm{R}T\ln\left(\gamma_{\mathrm{B}}\, m_{\mathrm{B}}/m^{\mathrm{o}}\right) \tag{II.92}$$

The activity coefficient γ_{B} is taken relative to Henry's law on the molality scale, and the standard chemical potential is defined as:

$$\mu_{\mathrm{B}}^{\infty}(p,T) = \lim_{m \to 0}[\mu_{\mathrm{B}}(p,T) - \mathrm{R}T\ln\left(m_{\mathrm{B}}/m^{\mathrm{o}}\right)],$$

which means that $\lim_{m \to 0}\gamma_{\mathrm{B}} = 1$.

The chemical potential is independent of the choice of standard and reference state and of the concentration scale. Thus, for an (aqueous) species B, one can write [1997THO]:

$$\mu_{\mathrm{B}} = \mu_{\mathrm{B}}^{\mathrm{o}} + \mathrm{R}T\ln\left(x_{\mathrm{B}} f_{\mathrm{B}}\right) = \mu_{x,\mathrm{B}}^{(\infty)} + \mathrm{R}T\ln\left(x_{\mathrm{B}}\gamma_{x,\mathrm{B}}\right) = \mu_{\mathrm{B}}^{\infty} + \mathrm{R}T\ln\left(m_{\mathrm{B}}\gamma_{\mathrm{B}}\right) \tag{II.93}$$

From Eq. (II.93), the conversions between values of standard chemical potentials can be obtained:

$$\mu_{\mathrm{B}}^{\mathrm{o}} - \mu_{x,\mathrm{B}}^{(\infty)} = -\mathrm{R}T \ln f_{\mathrm{B}}^{\infty} \tag{II.94}$$

$$\mu_{\mathrm{B}}^{\mathrm{o}} - \mu_{\mathrm{B}}^{\infty} = -\mathrm{R}T \ln\left(M_w f_{\mathrm{B}}^{\infty}\right) \tag{II.95}$$

$$\mu_{x,\mathrm{B}}^{(\infty)} - \mu_{\mathrm{B}}^{\infty} = -\mathrm{R}T \ln M_w \approx 4.016534\mathrm{R}T \tag{II.96}$$

II.1.2.1.3 Aqueous activity coefficients

From the above consideration, it is clear that the composition of each coexisting phase is related to its Gibbs energy through standard molar chemical potentials, concentrations and activity coefficients of all its components (end-members). The activity coefficient —a function of phase composition and other physical variables— as such, is a non-thermodynamic function reflecting a deviation from the reference (*ideal*) dependence of activity on concentration. Activity coefficients of dissolved salts or ions in the aqueous electrolyte are significant even at relatively low ionic strength because of the long-range electrostatic interactions between ions. Therefore, neglecting aqueous activity coefficients will cause significant errors in interpreting stability of solid solutions using measured composition of the coexisting aqueous phase; such errors can be very large in concentrated aqueous electrolytes. For those reasons, a topic of aqueous activity coefficient models is important; for details, the reader is addressed to literature [1970ROB/STO], [1993MOR/HER], [1997GRE/PLY2] and references therein. Only a few basic formulae will be provided below.

In thermodynamics of aqueous solutions, either individual activity coefficients of aqueous ions, or mean activity coefficients of salts (electrolytes) are considered. The most important parameter in relation to aqueous activity coefficients is called *ionic strength*, defined as:

$$I_{\mathrm{m}} = \frac{1}{2}\sum_j m_j Z_j^{\,2} \tag{II.97}$$

where the summation goes over all ionic substances (indexed with j) having molality m_j and charge Z_j. For a solution containing a single salt B (of molality m_{B}) completely ionised into ions with charges Z_+, Z_-, Eq. (II.97) turns into:

$$I_{\mathrm{m}} = \frac{1}{2}\left|Z_+ Z_-\right| \nu_{\mathrm{B}} m_{\mathrm{B}} \tag{II.98}$$

where $\nu_{\mathrm{B}} = \nu_+ + \nu_-$ is a sum of stoichiometric coefficients of ions in the salt.

The classic Debye-Hückel theory [1970ROB/STO] assumes a purely Coulombic interaction of ions of constant size $\dot{a}$ in a strongly dissociated dilute aqueous electrolyte. This theory leads to the *Debye-Hückel equation* for the mean activity coefficient $\gamma_{x,\pm}$ of an electrolyte dissociating into cations of charge Z_1 and anions of charge Z_2 ([1970ROB/STO] p. 229):

$$\log_{10}\gamma_{x,\pm} = -\frac{A_{DH}\left|Z_1 Z_2\right| I^{0.5}}{1 + B_{DH}\dot{a} I^{0.5}} \qquad \text{(II.99)}$$

The ion size parameter $\dot{a}$ is set at a value chosen from an interval 3.5 to 5 Å, and the parameters A_{DH} and B_{DH} are calculated as:

$$A_{DH} \approx 1.82493\cdot 10^6 \cdot \frac{\rho^{0.5}}{(\varepsilon T)^{1.5}}; \qquad B_{DH} \approx 50.29 \cdot \left(\frac{\rho}{\varepsilon T}\right)^{0.5} \qquad \text{(II.100)}$$

in units of ($\text{mol}^{-0.5}\cdot\text{l}^{0.5}\cdot\text{K}^{1.5}$) and ($\text{Å}^{-1}\cdot\text{mol}^{-0.5}\cdot\text{l}^{0.5}\cdot\text{K}^{0.5}$), respectively, where ρ is the density ($\text{g}\cdot\text{cm}^{-3}$) and ε is the dielectric constant of water-solvent (at p, T of interest). At 25 ºC and 1 bar, $\rho = 0.9971$, ε = 78.453, thus $A_{DH} = 0.5092$ and $B_{DH} = 0.3283$ (p. 128 in [1997LAN]). At pressures below 100 bar and temperatures below 100 ºC, ρ_w and ε can be found from the empirical functions:

$$\rho(t) = 1 - \frac{(t-3.9863)^2\cdot(t+288.9414)}{508929.2(t+68.12963)} + 0.011445\exp\left(-\frac{374.3}{t}\right) \qquad \text{(II.101)}$$

$$\varepsilon(T) = 2727.586 + 0.6224107\cdot T - 466.9151\cdot\ln T - 52000.87\cdot T^{-1} \qquad \text{(II.102)}$$

where $t = T - 273.15$ (T is expressed in Kelvin) [1990NOR/PLU], [1997LAN]. The density of liquid water in this region changes very little with pressure. More pronounced is the compositional dependence of density of aqueous solution which, strictly speaking, should be used in Eqs. (II.100) and (II.116) in place of ρ. In a concentrated aqueous solution, the account of its density in the calculation of A_{DH} can change the $\log_{10}\gamma_x$ value by a few percent.

The mean activity coefficient $\gamma_\pm$ of a dissolved salt $M_{\nu+}L_{\nu-}$ is an experimentally measurable quantity, related to individual ionic activity coefficients as:

$$\gamma_\pm = \left(\gamma_+^{\nu+}\cdot\gamma_-^{\nu-}\right)^{\frac{1}{\nu}} \qquad \text{(II.103)}$$

where $\nu = \nu_+ + \nu_-$. For instance, in Na_2SO_4 electrolyte, $\gamma_{\pm,Na_2SO_4} = (\gamma^2_{Na^+}\cdot\gamma_{SO_4^{2-}})^{1/3}$. For an individual i-th ion of charge Z_i, the Debye-Hückel equation has the form:

$$\log_{10}\gamma_{x,i} = -\frac{A_{DH} Z_i^2 I^{0.5}}{1 + B_{DH}\dot{a}\ I^{0.5}} \qquad \text{(II.104)}$$

In calculations of aqueous speciation, aqueous activity coefficients are taken in molal (or molar) concentration scale according to:

$$\mu_i = \bar{G}_i^o + \mathrm{R}T\ln m_i + \mathrm{R}T\ln\gamma_i \qquad \text{(II.105)}$$

or $a_i = m_i\gamma_i$, where $\bar{G}_i^o$ is the standard partial molal Gibbs energy and γ_i is the molal activity coefficient of i-th ionic species [1997LAN], [1999PAR/APP]. However, Eqs. (II.99) and (II.104) refer to the mole fraction scale, although the ionic strength I is calculated in the molality scale. Conversions in both directions occur as follows:

$$\gamma_i = \gamma_{x,i} x_w \text{ or } \gamma_\pm = \gamma_{x,\pm} x_w \tag{II.106}$$

$$\gamma_{x,i} = \gamma_i \left(1 + M_w \sum_j^s m_i \right) \text{ or } \gamma_{x,\pm} = \gamma_\pm \left(1 + M_w \nu m \right) \tag{II.107}$$

where m is the molality of electrolyte $M_{\nu+}L_{\nu-}$ with $\nu = \nu_+ + \nu_-$. From Eq. (II.106), it can be seen that the common practice of taking $\gamma_{x,i}$ (Eq. (II.104)) as the molal activity coefficient γ_i is justified only for dilute solutions where the mole fraction of the solvent x_w is very close to 1. But in a concentrated aqueous electrolyte of, say, 10 m of total solutes, $x_w \approx 0.85$ and the error in γ_i will be about 15%. Equation (II.106) holds also when part or all dissolved salts remain undissociated.

Equations (II.99) or (II.104) are usually referred to as *extended* Debye-Hückel model and are assumed to be valid at $I \leq 0.1$ m for monovalent, $I \leq 0.01$ m for divalent, and $I \leq 0.001$ m for trivalent aqueous ions. Some improvement can be achieved by introducing an individual ion size parameter $\dot{a}_i$ into Eq. (II.104):

$$\log_{10} \gamma_{x,i} = \frac{-A_{DH} Z_i^2 I^{0.5}}{1 + B_{DH} \dot{a}_i I^{0.5}} \tag{II.108}$$

According to Kielland [1937KIE], the values of $\dot{a}_i$ for inorganic ions range from 2.5 to 4.5 Å for monovalent (except Li^+ and H^+), 4 to 8 Å for divalent, 4 to 9 Å for trivalent, and 5 to 11 Å for tetravalent ions. Many of these values were tabulated [1937KIE], [1997LAN]. The ion size parameter $\dot{a}_i$ is thought to be a function of ion hydration, roughly proportional to the ratio of ionic radius to charge.

The experimental mean activity coefficients [1970ROB/STO], as well as individual ion activity coefficients [1997LAN] generally decrease with increasing ionic strength to minima around one to several mol·kg^{-1} and increase at higher ionic strength. However, Eqs. (II.104) or (II.108) predict values that decrease continuously, and are insufficient for a correct description of ionic activity in concentrated aqueous electrolytes (with $I_m > 0.1$ to 0.5 m). Hence, various semi-empirical extensions has been proposed and widely used for extending the applicability of the aqueous ion association model to *ca*. 0.3 - 0.5 m ionic strength (see [1981HEL/KIR]) and overviews in [1990MIL], [1997GRE/PLY2], [1997LAN]. One of the most popular variants, in fact proposed by Hückel in 1925, is called *Truesdell-Jones* equation, merely an extension of Eq. (II.108) with an additional term b_i:

$$\log_{10} \gamma_{x,i} = \frac{-A_{DH} Z_i^2 I^{0.5}}{1 + B_{DH} \dot{a}_i I^{0.5}} + b_i I \tag{II.109}$$

The empirical values of b_i and $\dot{a}_i$, fitted simultaneously to individual activity coefficients of *ca*. 17 inorganic cations and 7 anions obtained from the mean salt data, can be found in [1974TRU/JON], [1990PAR] and in [1997LAN]. These values apply up to $I_m = 2$ m mainly to chloride solutions for cations and to potassium solutions for

anions and have been used in SOLMINEQ.88 and PHREEQE computer speciation codes. A similar form of Debye-Huckel equation, but with a common ion size parameter $\dot{a}_i = 3.72$ and a common third parameter b_γ of value depending on selected background electrolyte has been proposed by [1981HEL/KIR] and used in their HKF EoS (equation of state) for aqueous electrolytes and fluids valid in a wide range of temperatures and pressures, and implemented in the SUPCRT92 reaction calculation code and database [1992JOH/OEL]. At low *p, T* and in NaCl background electrolyte, this variant of Eq. (II.109) works reasonably well up to $I_m = 0.5 - 1.0$ m.

Another variant used almost in any chemical speciation code is called *Davies* equation:

$$\log_{10} \gamma_{x,i} = -A_{DH} Z_i^2 \left(\frac{I_m^{0.5}}{1 + I_m^{0.5}} - 0.3 I_m \right) \qquad \text{(II.110)}$$

The add-on term $-0.3 I_m$ ($-0.24 I_m$ in the MINTEQA2 code) accounts for effects such as decrease of the dielectric constant of water and increase of ion pairing upon the increase in dissolved ion concentrations [1958HAR/OWE]. The Davies equation is believed good at $0.01 < I_m < 0.3$ m; it takes into account only charges of the ions but not their individual chemical characteristics. In order to account for those, the concept of ion pairing needs to be introduced, where deviations between measured mean activity coefficients and those calculated using equations such as (II.125) are assumed to occur due to the formation of weak complexes such as $Na^+ + Cl^- \rightleftharpoons NaCl(aq)$ described by equilibrium constants. However, it is generally agreed that such *ion association* aqueous models can be used in dilute aqueous electrolytes only [1984HAR/MOL], [1997GRE/PLY2].

For strongly non-ideal concentrated or mixed-solvent electrolytes, other models were developed that account for specific interactions between cations, anions and neutral aqueous species. These *specific ion interaction* models use a Debye-Hückel term describing long-range electrostatic forces, and specific interaction terms that account for short-range molecular interactions, usually in the form of a virial series expansion in powers of the molality of electrolyte(s). These models use "single-ion" activity coefficients and allow the equations describing the activity coefficients in simple electrolytes be extended to multi-component solution systems. Out of many, three model approaches are worth of mentioning: the Brønsted-Guggenheim-Scatchard (SIT) [1997GRE/PLY2]; the Pitzer model [1991PIT], [2004CHR/MOL]; and the new Extended UNIQUAC model [1997THO], [2005THO]. Details can be found in the cited references; we only provide a brief general summary below.

II.1.2.1.3.1 SIT model

SIT model is recommended to use for ionic strength corrections throughout NEA TDB projects [1992GRE/FUG], [1997GRE/PLY2] and it is also recommended by IUPAC [2003PET/PUI]. Shortcomings of the SIT model, as discussed in [1997GRE/PLY2],

[2002FAN], [2002SPA], consist mainly in its limited temperature and pressure applicability range. At present, the SIT coefficients are available for ambient conditions only; some SIT enthalpy parameters that permit application to higher temperatures have been given in [1997GRE/PLY2]. Although SIT is widely used in correction of complexation constants to zero ionic strength, its usage in forward modelling of aqueous equilibria is still restricted to simple systems. The SIT model is not valid for high ionic strength (above 3 m) and has to be improved at lower ionic strength for high-charge ions.

II.1.2.1.3.2 Pitzer model

Theoretical basis of the Pitzer ion interaction model (suggested in 1973) has been discussed in many publications *cf.* [1991PIT] and references therein. [1984HAR/MOL] showed that this approach could be extended to construct accurate models of solubility in complex brines that have been successfully applied to natural fluids at ambient temperatures, supported by a specially written Gibbs energy minimisation code [1987HAR/GRE]. Later on, this model has been extended to a broad temperature range (0 to 250 ºC) [1989GRE/MOL], [2004CHR/MOL]. The Pitzer model has been also used in marine chemistry [1998MIL/PIE] and in research related to nuclear waste disposal [2002FAN]. The Pitzer model is capable to describe data from high ionic strength systems (above 1 m) practically with experimental accuracy, also in complex systems. However, generally accepted shortcomings of Pitzer approach are that relatively large amount of precise experimental data is needed for parameterisation; there is a redundancy (correlation) among parameters which are difficult in physical interpretation and cannot be extrapolated beyond the experimental range. Pitzer model parameters do not have a fundamental temperature or pressure dependence [2002KON].

II.1.2.1.3.3 Extended UNIQUAC model

In this approach, Nikolaisen *et al.* [1993NIK/RAS] and Thomsen [1997THO], [2005THO] combined a Debye-Hückel term with the UNIQUAC local composition model [1975ABR/PRA]. The model uses only the mole fraction scale. Water is considered as the only solvent; ions, non-electrolytes including alcohols, and dissolved gases are considered as solutes. This rather new model has been successfully applied to predict solid-liquid equilibria in several systems involving a heavy metal cation (Mn^{2+}, Fe^{2+}, Co^{2+}, Ni^{2+}, Cu^{2+}, or Zn^{2+}) and a number of anions [2002ILI/THO]. The model parameters were found to be generally valid in the temperature range from the cryohydratic (a eutectic composition at which the electrolyte solution has the lowest freezing temperature) point to the boiling point of the respective solutions. In another work [2005VIL/THO], [2006VIL/THO], pressure parameters were added to the Extended UNIQUAC model, which has then been used for correlation and prediction of solid-liquid equilibrium of scaling minerals (sulphates and carbonates) at temperatures up to 300 ºC and pressures up to 1000 bar. This model is able to represent binary, ternary and quaternary solubility data within the experimental accuracy in the temperature range from – 20 to 300 ºC, and the pressure range from 1 to 1000 bar. It seems that, if com-

bined with a Gibbs energy minimisation solver and the appropriate solid solution models, the Extended UNIQUAC model will have a serious potential to compete with Pitzer and SIT approaches in the future development of Aq-SS models, including those related to radiochemistry and nuclear waste geochemistry.

II.1.2.1.4 Gas mixtures and gas solubility

Many Aq-SS systems of interest exist at equilibrium with the air or another gas mixture. As many gases dissolve in water (*e.g.*, CO_2, O_2), the composition of gas phase may have a strong influence on that of the aqueous solution and the solubility of solids. For clarity and completeness, some basic equations for gases, gas phase and gas solubility are provided below (more *cf.* [1993AND/CRE], [2003LOR/COH]).

An ideal gas phase consisting of gases B, C, … with mole fractions y_B, y_C, … under general pressure p and temperature T obeys the ideal gas law $pV_m = RT$, where V_m is the volume per 1 mole of the gas mixture. The stability of a gas component in ideal gas is defined by its partial pressure $p_B = p \cdot y_B$. In a real gas, the deviations from ideal behavior are described in terms of the fugacity, f_B, and the fugacity coefficient $\phi_B = f_B/p_B$, defined *via* the chemical potential μ_B as:

$$\mu_B(T,p) - \mu_B^o(T) = RT\ln\frac{f_B}{p^o} = RT\ln\frac{\phi_B p_B}{p^o} = RT\ln(y_B\phi_B) + RT\ln\frac{p}{p^o} \qquad \text{(II.111)}$$

Fugacity has dimensions of pressure. The standard chemical potential of gas B is defined at standard pressure p^o and referenced to zero pressure when ϕ_B is unity (ideal gas):

$$\mu_B^o(T) = \lim_{p\to 0}\left[\mu_B(T,p) - RT\ln\frac{y_B p}{p^o}\right] \qquad \text{(II.112)}$$

From Eqs. (II.111) and (II.112) it is seen that the relative activity of a gas B is $a_B = f_B / p^o$. At low pressures, $pV_m \approx RT$ and the gas phase can (at first approximation) be treated as an ideal mixture of ideal gases where $a_B \approx p_B / p^o$. However, at moderate pressures (> 10 bar) at room temperature, even pure gases do not show ideal behaviour and need to be characterised by *fugacity* or *fugacity coefficient* and pressure through the difference between the real V_B and the ideal RT/p volumes:

$$RT\ln\phi_B = \int_0^p \left(V_B - \frac{RT}{p}\right)dp \qquad \text{(II.113)}$$

For real gases and gas mixtures (fluids), the fugacity has a complex dependence on temperature, pressure and composition, usually expressed with help of an equation of state with virial coefficients, or from critical parameters using the theory of corresponding states (*cf.* [1993AND/CRE], [1994NOR/MUN]).

Equilibrium solubility of a gas component B in the aqueous electrolyte according to the reaction B(gas) ⇌ B(aq) can be defined at constant *p, T* using Eqs. (II.76), (II.77), (II.111) and (II.93):

$$\Delta_{\text{sln}} G^{\text{o}}_{\text{m}}(T,p) = \mu^{\infty}_{\text{B},aq}(T,p) - \mu^{o}_{\text{B},g}(T) = -\text{R}T\left(\ln\frac{\gamma_{\text{B}} m_{\text{B}}}{m^{o}} - \ln\frac{\phi_{\text{B}} p_{\text{B}}}{p^{o}}\right) \qquad \text{(II.114)}$$

The right-hand side of Eq. (II.114) defines a standard-state Henry constant $K^{\infty}_{\text{H,B}}$ for gas B in water

$$K^{\infty}_{\text{H,B}} = \frac{\gamma_{\text{B}} m_{\text{B}}}{m^{o}} \frac{p^{o}}{\phi_{\text{B}} p_{\text{B}}} = \frac{m_{\text{B}}}{p_{\text{B}}} \frac{\gamma_{\text{B}} p^{o}}{\phi_{\text{B}} m^{o}} = k^{(m)}_{H,\text{B}} \frac{\gamma_{\text{B}} p^{o}}{\phi_{\text{B}} m^{o}} \qquad \text{(II.115)}$$

where $k^{(m)}_{H,\text{B}} = m_{\text{B}} / p_{\text{B}}$ (in mol·kg^{-1}·bar^{-1}) is the experimentally measurable Henry constant for a gas B in water [2003FER/ALV]. The activity coefficients of dissolved gases in aqueous electrolyte can be estimated using the Sechenov equation [1958HAR/OWE], which for the molal scale can be written as:

$$\ln\gamma_{\text{B}} = \ln\frac{m^{\infty}_{\text{B}}}{m_{\text{B}}} = k^{(m)}_{S,\text{B}} I_{\text{m}} \qquad \text{(II.116),}$$

where m^{∞}_{B} denotes the pure solvent, and $k^{(m)}_{S,\text{B}}$ is the experimentally measured Sechenov coefficient [2003LOR]. This equation is valid to high ionic strength and is often used in aqueous speciation calculations in the form

$$\log_{10}\gamma_{\text{B}} = k^{*}_{S,\text{B}} I_{\text{m}} \qquad \text{(II.117)}$$

which in fact, is the same as the Hückel Eq. (II.109) for uncharged species (at $Z_j = 0$).

The coefficients k^{*}_{S} are generally found to be in the range from 0.02 to 0.23 at 25 ºC ([1997LAN] p.144); hence, Eq. (II.117) reflects a "*salting-out*" behaviour of molecular species. There were suggestions to apply a common salting-out coefficient k^{*}_{S} = 0.1 to all neutral aqueous species other than the dissolved gases, as done in the MINTEQA2 speciation code. Among those species, some (like H_4SiO_2 or SiO_2) are important because they define solubility of the respective solid (like amorphous SiO_2 or quartz) in a wide range of conditions. The salting-out effect can be neglected in relatively dilute aqueous solutions of $I_{\text{m}} < 0.3$ because even at $k^{*}_{S} = 0.2$, $\gamma_B < 1.15$ in this case.

II.1.2.1.5 Solid solubility

Solid solubility in aqueous electrolytes is a central topic in thermodynamics of Aq-SS systems. It has been explored by Lippmann [1977LIP], [1980LIP] improved and extended by Glynn and Reardon [1990GLY/REA], [1992GLY/REA], Königsberger and Gamsjäger [1992KON/GAM], and recently reviewed in [2003GAM/KON].

Equilibrium solubility of a stoichiometric solid B that does not undergo dissociation (*e.g.*, quartz SiO_2) according to the reaction B(solid) $\rightleftharpoons$ B(aq) can be defined at constant *p, T* using Eqs. (II.76), (II.77), (II.79), (II.81) and (II.92) as:

$$\Delta_{\mathrm{sln}} G^{\mathrm{o}}_{\mathrm{m}}(p,T) = \mu_B^{\infty(aq)} - \mu_B^{(\mathrm{o},solid)} = -\mathrm{R}T \ln \frac{a_B^{(aq)}}{a_B^{(solid)}} = -\mathrm{R}T \ln K \tag{II.118}$$

where $K = \dfrac{\gamma_B m_B}{m^{\mathrm{o}}}$ is the equilibrium constant. Note that for the pure B(solid), both mole fraction and activity coefficient are unity and $f_B x_B = 1$. In a more general case, when a pure hydrated solid dissociates upon dissolution according to the reaction:

$$\mathrm{M}_{\nu_{\mathrm{M}}}\mathrm{L}_{\nu_{\mathrm{L}}} \cdot \nu_{\mathrm{w}}\mathrm{H_2O(s)} \rightleftharpoons \nu_{\mathrm{M}}\mathrm{M}^{Z_{\mathrm{M}}+} + \nu_{\mathrm{L}}\mathrm{L}^{Z_{\mathrm{L}}-} + \nu_{\mathrm{w}}\mathrm{H_2O} \tag{II.119}$$

one obtains instead of Eq. (II.118):

$$\begin{aligned} \Delta_{\mathrm{sln}} G^{\mathrm{o}}_{\mathrm{m}}(T,p) &= \nu_{\mathrm{M}}\mu_M^{\infty} + \nu_{\mathrm{L}}\mu_L^{\infty} + \nu_{\mathrm{w}}\mu^{(\mathrm{o})}_{\mathrm{H_2O}} - \mu^{(\mathrm{o})}_{\mathrm{MLH}} \\ &= -\mathrm{R}T \ln \frac{a_M^{\nu_M} a_L^{\nu_L} a_{H_2O}^{\nu_w}}{a_{MLH}^{(solid)}} = -\mathrm{R}T \ln K_{S,MLH} \end{aligned} \tag{II.120}$$

where the subscript *M* denotes the aqueous cation $\mathrm{M}^{Z_{\mathrm{M}}+}$, the subscript *L* denotes the anion $\mathrm{L}^{Z_{\mathrm{L}}-}$, and the subscript *MLH* denotes the stoichiometric solid. $K_{\mathrm{s},0}$ is the equilibrium constant called *solubility product:*

$$K_{s,MLH} = \frac{\gamma_M^{\nu_M}\ m_M^{\nu_M}\ \gamma_L^{\nu_L} m_L^{\nu_L}\ f_{\mathrm{H_2O}}^{\nu_w} x_{\mathrm{H_2O}}^{\nu_w}}{(m^{\mathrm{o}})^{\nu_M}\,(m^{\mathrm{o}})^{\nu_L}\, f_{MLH}\, x_{MLH}} \tag{II.121}$$

Because m° = 1 mol·kg^{-1}, $f_{MLH}\, x_{MLH}$ = 1, and in dilute electrolytes both the mole fraction and the activity coefficient of water are close to unity, the solubility product is usually simplified to:

$$K_{s,MLH} \approx a_M^{\nu_M} a_L^{\nu_L} = \gamma_M^{\nu_M} m_M^{\nu_M}\ \gamma_L^{\nu_L} m_L^{\nu_L} \tag{II.122}$$

However, for soluble ionic solids or concentrated background electrolytes, the activity of water $a_{H_2O}^{\nu_w}$ cannot be neglected (it can be calculated together with ionic activity coefficients *e.g.*, using one of specific ion interaction models).

At arbitrary (non-equilibrium) conditions, the reaction quotient *Q* can be used for describing the composition of aqueous electrolyte in relation with the reaction (II.119):

$$Q_{S,MLH} = a_M^{\nu_M} a_L^{\nu_L} = \gamma_M^{\nu_M} m_M^{\nu_M} \gamma_L^{\nu_L} m_L^{\nu_L} \tag{II.123}$$

From the known aqueous speciation, Q and the *saturation index* Ω_S can be obtained:

$$\Omega_{S,MLH} = \log_{10} \frac{Q_{S,MLH}}{K_{S,MLH}} = 0.4343\left(\ln Q_{S,MLH} - \ln K_{S,MLH}\right) \qquad \text{(II.124)}$$

cf. [1997LAN]. The saturation index, Ω_S, can be calculated either when the MLH solid is included into the mass balance or not included; both calculations are routinely done in speciation computer codes. At equilibrium, Ω_S is (numerically) zero; negative values of saturation index reflect an under-saturation, while positive values reflect an over-saturation of the aqueous phase with respect to the pure MLH solid, thus defining a respective tendency to dissolution or precipitation.

It is important to realise that Reaction (II.119) refers to aqueous ions whose concentrations can be very different from the measured total dissolved concentrations of the respective elements. Therefore, an aqueous complexation model stays behind the scenes and must be accounted for.

Equations (II.119) to (II.124) form the basis for the analysis of equilibrium solubility of pure stoichiometric solids; indeed, many sparingly soluble minerals can be safely treated in this way. However, these equations are difficult to use for analysing equilibria between the solid mixture and aqueous electrolyte (*i.e.*, Aq-SS equilibria) because composition of the solid phase and the stoichiometry coefficients in the Reaction (II.119), as well as the solubility product (II.121) are no longer constant and, in general, depend on the compositions of both coexisting phases.

Hence, a more general and flexible concept is needed. For ionic solids with different cations and common anion (or with different anions and common cation), such a concept – the unified theory of solid solution solubility – has been suggested in [1992KON/GAM] and [2003GAM/KON].

II.1.2.1.6 Unified theory of ionic solid solution solubilities

For an ionic solid solution $B_{1-x}C_xL$ (or xCL·(1–x)BL) in aquatic medium, a general transformation reaction can be written:

$$\begin{aligned} n\mathrm{B}_{1-x_0}\mathrm{C}_{x_0}\mathrm{L}(s) \rightarrow{}& (n-\xi)\mathrm{B}_{1-x}\mathrm{C}_x\mathrm{L}(s) \\ &+\left[n(1-x_0)-(n-\xi)(1-x)\right]\mathrm{B}^+_{aq}+\left[nx_0-(n-\xi)x\right]\mathrm{C}^+_{aq}+\xi\mathrm{L}^-_{aq} \end{aligned} \qquad \text{(II.125)}$$

where ξ is the reaction extent variable. The total Gibbs energy function G of this system is:

$$\begin{aligned} G_{x,\xi} ={}& (n-\xi)\left[(1-x)\mu^{(s)}_{BL}+x\mu^{(s)}_{CL}\right]+ \\ &+\left[n(1-x_0)-(n-\xi)(1-x)\right]\mu^{(aq)}_{B^+}+\left[nx_0-(n-\xi)x\right]\mu^{(aq)}_{C^+}+\xi\mu^{(aq)}_{L^-}+n_w\mu_{H_2O} \end{aligned} \qquad \text{(II.126)}$$

The general equilibrium condition at fixed T and p is the minimum of total Gibbs energy function, *i.e.*

$$dG = \left(\frac{\partial G}{\partial \xi}\right)_x d\xi + \left(\frac{\partial G}{\partial x}\right)_\xi dx = 0 \qquad \text{(II.127)}$$

where $\left(\frac{\partial G}{\partial \xi}\right)_x = \left[(1-x)\mu_{B^+}^{(aq)} + x\mu_{C^+}^{(aq)} + \mu_{L^-}^{(aq)}\right] - \left[(1-x)\mu_{BL}^{(s)} + x\mu_{CL}^{(s)}\right]$ (II.128)

and $\left(\frac{\partial G}{\partial x}\right)_\xi = (1-\xi)\left[\mu_{CL}^{(s)} - \mu_{BL}^{(s)} - \left(\mu_{C^+}^{(aq)} - \mu_{B^+}^{(aq)}\right)\right]$ (II.129)

Denoting $\mu_{BL}^{(aq)} = \mu_{B^+}^{(aq)} + \mu_{L^+}^{(aq)}$, $\mu_{CL}^{(aq)} = \mu_{C^+}^{(aq)} + \mu_{L^+}^{(aq)}$, as well as

$$\Delta_{sol}\mu_{BL} = \mu_{BL}^{(aq)} - \mu_{BL}^{(s)}\ ,\ \Delta_{sol}\mu_{CL} = \mu_{CL}^{(aq)} - \mu_{CL}^{(s)}\ , \qquad \text{(II.130)}$$

Eq. (II.127) can also be rewritten as:

$$\left[(1-x)\Delta_{sol}\mu_{BL} + x\Delta_{sol}\mu_{CL}\right]d\xi + \left[(1-\xi)\left(\Delta_{sol}\mu_{BL} - \Delta_{sol}\mu_{CL}\right)\right]dx = 0 \qquad \text{(II.131)}$$

Conditions (II.127) or (II.131) can be satisfied in three different ways.

- ***Equilibrium***.

  If both ξ and x are allowed to vary ($d\xi \neq 0$ and $dx \neq 0$) then $\left(\frac{\partial G}{\partial \xi}\right)_x = 0$ and $\left(\frac{\partial G}{\partial x}\right)_\xi = 0$. As seen from Eq. (II.131), this is only possible if $\Delta_{sol}\mu_{BL} = 0$ (or $\mu_{BL}^{(aq)} = \mu_{BL}^{(s)}$) and $\Delta_{sol}\mu_{CL} = 0$ (or $\mu_{CL}^{(aq)} = \mu_{CL}^{(s)}$), *i.e.*, when chemical potentials of all end-members are the same in the solid and the aqueous phase. This can be easily extended to any number of end-members and corresponds, in fact, to the general equation of solubility equilibrium (II.76) and (II.120).

- ***Stoichiometric saturation***.

  If the composition of solid phase remains fixed ($dx = 0$) because of kinetic restrictions upon the progress of dissolution ($d\xi \neq 0$) then the rightmost term on l.h.s. of Eq. (II.131) vanishes. This state of minimum *stoichiometric saturation* is characterised by a condition $(1-x)\Delta_{sol}\mu_{BL} + x\Delta_{sol}\mu_{CL} = 0$ which, using Eqs. (II.130), can be written as:

  $$(1-x)\mu_{BL}^{(aq)} + x\mu_{CL}^{(aq)} = (1-x)\mu_{BL}^{(s)} + x\mu_{CL}^{(s)} \qquad \text{(II.132)}$$

  i.e., equal integral molar Gibbs energies of the $B_{1-x}C_xL$ mixture in aqueous and solid phases:

  $$G_{m,BCL}^{(aq)} = G_{m,BCL}^{(s)} \qquad \text{(II.133)}$$

  Eq. (II.133) manifests the "Equal-G" principle [1992KON/GAM].

▪ ***Partition.***

Setting the r.h.s. term Eq. (II.129) to zero $\mu_{CL}^{(s)} - \mu_{BL}^{(s)} = \mu_{C^+}^{(aq)} - \mu_{B^+}^{(aq)}$ and substituting full expressions for chemical potentials (Eqs. (II.78), (II.92)) leads to a *distribution coefficient D*:

$$D = \frac{x \quad m_{B^+}}{(1-x)\, m_{C^+}} = \frac{K_{S,BL}\, f_{BL}\ \gamma_{C^+}}{K_{S,CL}\, f_{CL}\ \gamma_{B^+}} \tag{II.134}$$

The condition $\left(\frac{\partial G}{\partial \xi}\right)_x = 0$ (see also Eq. (II.127)), with the appropriate definitions of activities and standard chemical potentials, results in a solubility product of the binary mixture $B_{1-x}C_xL$:

$$\left(a_{B+}^{(aq)} a_{L-}^{(aq)}\right)^{1-x} \cdot \left(a_{C+}^{(aq)} a_{L-}^{(aq)}\right)^{x} = \left(K_{S,BL} a_{BL}^{(s)}\right)^{1-x} \left(K_{S,CL} a_{CL}^{(s)}\right)^{x} = K_{S,BCL}^{(x)} \tag{II.135}$$

The above equation links the activities of dissolved ions with that of solid mixture end-members; it holds for both the cases of equilibrium and stoichiometric saturation.

II.1.2.1.7 *Multicomponent* ionic Aq-SS system (following [2003GAM/KON])

Consider the dissolution reaction of an ionic solid solution $A_{x_A} B_{x_B} C_{x_C} \ldots L$ in n_w moles H_2O, where $x_A = 1 - \sum_j x_j$, j = B, C, … The reaction extent variable is now defined by:

$$d\xi = -\sum_j dn_j^{(solid)} \tag{II.136}$$

Equation (II.127) holds also in this case, but the partial derivatives of Gibbs energy take the form:

$$\left(\frac{\partial G}{\partial \xi}\right)_x = \left[\sum_j x_j \mu_{j^+}^{(aq)} + x_A \mu_{A^+}^{(aq)} + \mu_{L^-}^{(aq)}\right] - \left[\sum_j x_j \mu_{jL}^{(s)} + x_A \mu_{AL}^{(s)}\right] \tag{II.137}$$

$$\left(\frac{\partial G}{\partial x}\right)_\xi = (1-\xi)\left[\sum_j \mu_{jL}^{(s)} - \mu_{AL}^{(s)} - \left(\sum_j \mu_{j^+}^{(aq)} - \mu_{A^+}^{(aq)}\right)\right] \tag{II.138}$$

Taking into consideration Eqs. (II.130), the condition of equilibrium (II.131) becomes:

$$dG = \left[x_A \Delta_{sol}\mu_{AL} + \sum_j x_j \Delta_{sol}\mu_{jL}\right] d\xi + (1-\xi)\sum_j \left(\Delta_{sol}\mu_{AL} - \Delta_{sol}\mu_{jL}\right) dx_j = 0 \tag{II.139}$$

At equilibrium, $\Delta_{sol}\mu_{AL} = 0$ and $\Delta_{sol}\mu_{jL} = 0$ for any end-member, which with the usual definition of activities and solubility products (Eq. (II.121) and (II.122)) is equivalent to:

$$K_{S,jL} \cdot f_{jL} x_{jL} = \gamma_{j+} m_{j+} \gamma_{L-} m_{L-} \quad \text{or} \quad K_{S,jL} \cdot a_{jL}^{(s)} = a_{j+}^{(aq)} a_{L-}^{(aq)} \tag{II.140}$$

where $K_{S,jL}$ is the standard solubility constant of j-th end-member (including the first one, AL).

At minimum stoichiometric saturation (dx_j =0 for all end-members), the criterion of equal integral molar Gibbs energies of the (A,B,C,…)L mixture in aqueous and solid phases holds:

$$G_{m,BCL}^{(aq)} = G_{m,BCL}^{(s)} \quad \text{or} \quad \sum_j x_j \mu_{jL}^{(aq)} = \sum_j x_j \mu_{jL}^{(s)} \tag{II.141}$$

where summation includes the AL end-member. This results in the following mass action law:

$$\prod_j \left(a_{j+}^{(aq)} a_{L-}^{(aq)} \right)^{x_j} = \prod_j \left(K_{S,jL} a_{jL}^{(s)} \right)^{x_j} = K_{S,ML}^{(x)} \tag{II.142}$$

where M encompasses all cations A, B, … . This mass action law also holds in the equilibrium state together with equations (II.140).

From Eq. (II.142), the molar Gibbs energy of mixing at known composition x = $\{x_1, x_2, \ldots, x_j, \ldots\}$ follows immediately [2000GAM/KON], [2003GAM/KON] :

$$\frac{G_{m,x}(\text{mix})}{\mathrm{R}T} = \ln K_{S,ML}^{(x)} - \sum_j \left(x_j \ln K_{S,jL} \right) \tag{II.143}$$

In the case of thermodynamic equilibrium between $n(M)$ component solid mixture and the aqueous solution, the Gibbs energy of mixing (II.143) must be consistent with $n(M) - 1$ distribution coefficients between the j-th component (B,C, …) and the component A:

$$D_{jA} = \frac{x_j \; m_{A^+}}{x_A \; m_{j^+}} = \frac{K_{S,AL} \; f_{AL} \; \gamma_{j^+}}{K_{S,jL} \; f_{jL} \; \gamma_{A^+}} \tag{II.144}$$

Distribution coefficients are experimentally measurable quantities. They can be interpreted (see Section II.1.3) in terms of either a solubility product $K_{S,AL}$ or activity coefficient f_{AL} in the solid mixture, provided that the aqueous ion activity coefficients are known. For cations of similar charge, the ratio of aqueous activity coefficients is often assumed to be unity. Activity coefficients of solid solution end-members have been considered in detail in Section II.1.1.4 because they are closely related to crystal structures, energetics, and order-disorder effects.

II.1.2.2 Lippmann diagrams, a tool to visualise binary Aq-SS systems

Binary Aq-SS systems are, in fact, ternary systems in which two components are solid mixture end-members, and one component is the aqueous electrolyte solution. The latter is always in excess, therefore such systems are often called “pseudo-binary” or simply “binary” because they involve a binary solid mixture. In geochemistry and aquatic

chemistry, the Lippmann phase diagram [1977LIP], [1980LIP], [1982LIP] became a popular tool for analysing pseudo-binary Aq-SS equilibria after papers by [1990GLY/REA], [1990GLY/REA2], enhanced with the MBSSAS code [1991GLY] for computing/plotting such diagrams, retrieving Margules parameters and equilibrium relations. This work has been extended and deepened by [1992KON/GAM], [2000GAM/KON], [2000PRI/FER], and others.

The equilibrium between the aqueous electrolyte and a mixed ionic solid (B,C)L can be expressed by two law of mass action (LMA) equations:

$$\{B^+\}\{L^-\} = K_{BL}a_{BL} = K_{BL}x_{BL}f_{BL} \tag{II.145}$$

$$\{C^+\}\{L^-\} = K_{CL}a_{CL} = K_{CL}x_{CL}f_{CL} \tag{II.146}$$

where $\{L^-\},\{B^+\},\{C^+\}$ are the aqueous activities of L^-, B^+,C^+ (or L^{2-}, B^{2+}, C^{2+}); K_{BL} and K_{CL} are the solubility products of pure BL and CL end-members with (symmetric convention) activities a_{BL}, a_{CL}, mole fractions x_{BL}, x_{CL}, and activity coefficients f_{BL}, f_{CL}, respectively. Using the Lippmann's *total solubility product* ΣΠ defined as:

$$\Sigma\Pi = \{L^-\}\left(\{B^+\}+\{C^+\}\right) \tag{II.147}$$

the equilibrium ΣΠ value can be alternatively expressed as:

$$\Sigma\Pi_{eq} = K_{BL}x_{BL}f_{BL} + K_{CL}x_{CL}f_{CL} \tag{II.148}$$

Eq. (II.148) defines the so-called *solidus* curve.

The molar excess Gibbs energy of mixing G_m^E at stoichiometric saturation can be found as:

$$G_{\mathrm{m}}^E = \mathrm{R}T\left(x_{\mathrm{BL}}\ln f_{\mathrm{BL}} + x_{\mathrm{CL}}\ln f_{\mathrm{CL}}\right) = \mathrm{R}T\left(\ln\Sigma\Pi - x_{\mathrm{BL}}\ln K_{\mathrm{BL}} - x_{\mathrm{CL}}\ln K_{\mathrm{CL}}\right) \tag{II.149}$$

[1985GAM], [1990KON/GAM2].

The Lippmann *solutus* curve equation is (*e.g.*, [1990GLY]):

$$\Sigma\Pi_{eq} = 1\Big/\left(\frac{x_{B,aq}}{K_{BL}f_{BL}} + \frac{x_{C,aq}}{K_{CL}f_{CL}}\right) \tag{II.150}$$

where the *aqueous activity fractions* of B and C are defined as

$$x_{B,aq} = \frac{\{B^+\}}{\{B^+\}+\{C^+\}};\ x_{C,aq} = \frac{\{C^+\}}{\{B^+\}+\{C^+\}} \tag{II.151}$$

The solidus and solutus curves drawn on a Lippmann diagram with the common ordinate $\Sigma\Pi_{eq}$ and two superimposed abscissas x_{CL} and $x_{C,aq}$ (note that $x_{BL} = 1 - x_{CL}$ and $x_{B,aq} = 1 - x_{C,aq}$) define a series of possible equilibrium states for a pseudo-binary Aq-SS system (in fact, a ternary system with the H_2O component in great excess). It is inherently assumed that activity-concentration relations in the aqueous phase are set by the appropriate aqueous speciation model (*i.e.*, activity coefficients of B^+ and C^+ are

known). Other useful curves that can be drawn on Lippmann diagrams include [1990KON/GAM2], [1991GLY]: the "equal-G" EGC or *minimum stoichiometric saturation* curve for the solid $B_{1-x}C_xL$

$$\Sigma\Pi_{EGC} = K_{CL}^{x} K_{BL}^{1-x} \cdot \frac{a_{CL}^{x} a_{BL}^{1-x}}{x_{CL}^{x} x_{BL}^{1-x}} \tag{II.152}$$

or $$\log_{10} \Sigma\Pi_{EGC} = x \log_{10} K_{CL} + (1-x) \log_{10} K_{BL} + \frac{1}{\ln 10} \cdot \frac{G^E}{RT} \tag{II.153}$$

where $x_{CL} = x_{C,Aq}$ (this curve can be drawn for the entire solid-solution range regardless of the miscibility gap); and the *distribution coefficient* curve defined by

$$D = \frac{x_{BL} / x_{CL}}{\{B^+\} / \{C^+\}} = \frac{K_{CL} f_{CL}}{K_{BL} f_{BL}} \tag{II.154}$$

(compare with Eq. (II.144)) which depends on the composition of the solid in the case of non-ideal mixing. By equating Eqs. (II.148) and (II.150) using Eq. (II.154), one can obtain:

$$(1-D)(1-x_{C,aq}) x_{CL} + \left(1 - \frac{1}{D}\right)(1-x_{CL}) x_{C,aq} = 0 \tag{II.155}$$

By solving it algebraically, the solid mole fraction x_{CL} can be found from the aqueous fraction $x_{C,aq}$:

$$x_{C,aq} = \left(1 + \frac{1-x_{CL}}{D \cdot x_{CL}}\right)^{-1} \tag{II.156}$$

A solution of Eq. (II.155) for the solid mole fraction at equilibrium x_{CL} may be more useful:

$$x_{CL} = \left(1 + D \frac{1-x_{C,aq}}{x_{C,aq}}\right)^{-1} \tag{II.157}.$$

If $x_{C,aq}$ and x_{CL} are known from equilibrium experiments then solving Eq. (II.155) for D yields

$$D = \frac{(x_{CL} - 1) x_{C,aq}}{x_{CL} (x_{C,aq} - 1)} \tag{II.158}$$

Then, using Eq. (II.154), either the activity coefficient or the solubility product of one solid solution end-member can be found. For instance, in the case of regular mixing, the Margules interaction parameter W_G can be directly retrieved even from a single experiment:

$$W_G = \frac{RT\left(\ln D + \ln K_{BA} - \ln K_{CA}\right)}{\left(1-\chi_{CA}\right)^2 - \chi_{CA}^2} \qquad \text{(II.159)}$$

Lippmann functions and diagrams also help determining the positions of binodal and spinodal miscibility gaps, and to find critical, peritectic, "eutectic" and alyotropic points [1991GLY].

II.1.2.2.1 Example of the use of Lippmann diagrams

For Aq-SS systems, construction and visual analysis of Lippmann diagrams help much in understanding qualitatively thermodynamic and kinetic solubility behaviour of the binary solid mixture. Here, a $Co_{1-x}Mn_xCO_3$-H_2O system will be considered using data and results of [1985GAM], [1990KON/GAM]. Rhombohedral carbonates of transitional metals together with calcite and magnesite form many solid solutions, with some systems showing a complete miscibility if cationic radii are similar. Gamsjäger [1985GAM] presented the apparent solubility constants $\log_{10} {}^*K_{p,s,0}$ (II.160) for carbonates of Mn, Fe, Co, Ni, Cu and Zn, measured in 1.0 *m* $NaClO_4$ solutions at 50 ºC. These solubility constants refer to the reaction:

$$MCO_3 + 2H^+ \rightleftharpoons M^{2+} + CO_2(g) + H_2O \qquad \text{(II.160)}$$

where M stays for one of the cations. One of the binary series, $CoCO_3$-$MnCO_3$, was selected for synthesising a series of homogeneous solid mixtures, to carry out conclusive solubility measurements, and to estimate the excess Gibbs energies of mixing as well as the interaction parameters.

The conventional solubility method by pH variation resulted in minimum stoichiometric saturation states, from which using equations similar to (II.149), the values of molar excess Gibbs energy G_m^E were estimated and found to be consistent with the regular Guggenheim model, $G_m^E = RT\alpha \cdot x(1-x)$ with $\alpha = (1.1 \pm 0.4)$ [1985GAM] or $RT\alpha = (3.4 \pm 1.6)$ kJ·mol^{-1} ($\alpha = (1.27 \pm 0.6)$) [2000GAM/KON], favourably compared to $RT\alpha = 2.6$ kJ·mol^{-1} predicted from cation-anion distances using the Lippmann approach. Subsequent measurements with galvanic cells [1990KON/GAM] for the same system at 50 ºC yielded far more precise values of G_m^E which could be fitted to a subregular Guggenheim expression $G_m^E = x(1-x)\left[A_0 + A_1(2x+1)\right]$ with interaction parameters $A_0 = (3.61 \pm 0.11)$ kJ·mol^{-1} and $A_1 = -(0.61 \pm 0.21)$ kJ·mol^{-1} [2000GAM/KON]. This asymmetric mixing is more realistic and consistent with the general rule [1975URU] that the substitution of a smaller ion (Co^{2+}) for a larger one (Mn^{2+}) is energetically easier than the opposite substitution.

Let us construct the Lippmann diagram for the $Co_{1-x}Mn_xCO_3$-H_2O system using for both end-members the thermodynamic solubility products $K_{s,0}$ for the reaction:

$$MCO_3(s) \rightleftharpoons M^{2+} + CO_3^{2-} \qquad \text{(II.161)}$$

To calculate $K^{\circ}_{s,0}$ (II.161) that refer to zero ionic strength, values of ${}^{*}K_{p,s,0}$ (II.160) must first be converted to $I_m = 0$, which requires knowledge of aqueous activity coefficients of M^{2+} and H^+ at $I = 1$ m $NaClO_4$ at 50 ºC. Using the IUPAC SIT program [2003PET/PUI], one calculates with the SIT model $\log_{10}\gamma_{H^+} = -(0.714 \pm 0.03)$ (SIT parameter, $\varepsilon(H^+, ClO_4^-) = (0.14 \pm 0.02)$ kg·mol^{-1}) and $\log_{10}\gamma_{Co^{2+}} = -(0.514 \pm 0.03)$ (SIT parameter $\varepsilon(Co^{2+}, ClO_4^-) = (0.34 \pm 0.03)$ kg·mol^{-1}). As the SIT parameter for Mn^{2+} in perchlorate medium is not available, the activity coefficient of Mn^{2+} can be taken equal to that of Co^{2+}. From the LMA expressions for ${}^{*}K_{p,s,0}$ (II.160) and ${}^{*}K^{\circ}_{s,0}$ (II.160) it follows that $\log_{10}{}^{*}K_{s,0} = \log_{10}{}^{*}K^{\circ}_{s,0} + \log_{10}\gamma_{M^{2+}} - 2\log_{10}\gamma_{H^+}$ or, taking the above values into account, $\log_{10}{}^{*}K_{s,0} = \log_{10}{}^{*}K^{\circ}_{s,0} + 0.914$ for both cations of interest.

$K_{s,0}$ (II.161) and ${}^{*}K_{p,s,0}$ (II.160) are connected *via* the LMA expression of the reaction:

$$CO_3^{2-} + 2H^+ \rightleftharpoons CO_2(g) + H_2O(l) \qquad \text{(II.162)}$$

with the equilibrium constant $\log_{10} K$ (II.162) = 18.155 at 50 ºC, 1 bar (calculated using the Nagra-PSI data base [2002HUM/BER] and GEMS-PSI code). $K_{s,0}$ for a pure MCO_3 carbonate is found from $\log_{10} K^{\circ}_{s,0}$ (II.161) = $\log_{10}{}^{*}K^{\circ}_{s,0}$ (II.160) – $\log_{10} K$ (II.162). Results of these calculations are given in Table II-2.

Table II-2: Solubility products of spherocobaltite $CoCO_3$ and rhodochrosite $MnCO_3$ at 50 ºC.

Pure solid	$\log_{10}{}^{*}K_{s,0}$ [a]	$\log_{10}{}^{*}K^{\circ}_{s,0}$	$\log_{10} K^{\circ}_{s,0}$
$CoCO_3$	(7.19 ± 0.04)	8.104	– 10.05
$MnCO_3$	(7.36 ± 0.06)	8.274	– 9.88

a: Data from [1985GAM].

Now, the Lippmann functions for the solidus (Eq. (II.148)), solutus (Eq. (II.150)), and the EGC curve (Eq. (II.152)) can be computed using the two-parameter Guggenheim expressions for end-member activity coefficients (Eqs. (II.40), (II.41)) and plotted on the phase diagram (Figure II-7). Calculations can be done with commercial software (*e.g.*, MatLab) or with the MBSSAS program [1991GLY].

Figure II-7: Lippmann diagram of the $CoCO_3$-$MnCO_3$-H_2O system constructed using $K_{s,0}$ values from Table II-2, and subregular interaction parameters A_0 = 3.61 and A_1= – 0.61 (in kJ·mol^{-1} from [1990KON/GAM], [2000GAM/KON]). EGC is the minimum stoichiometric saturation curve.

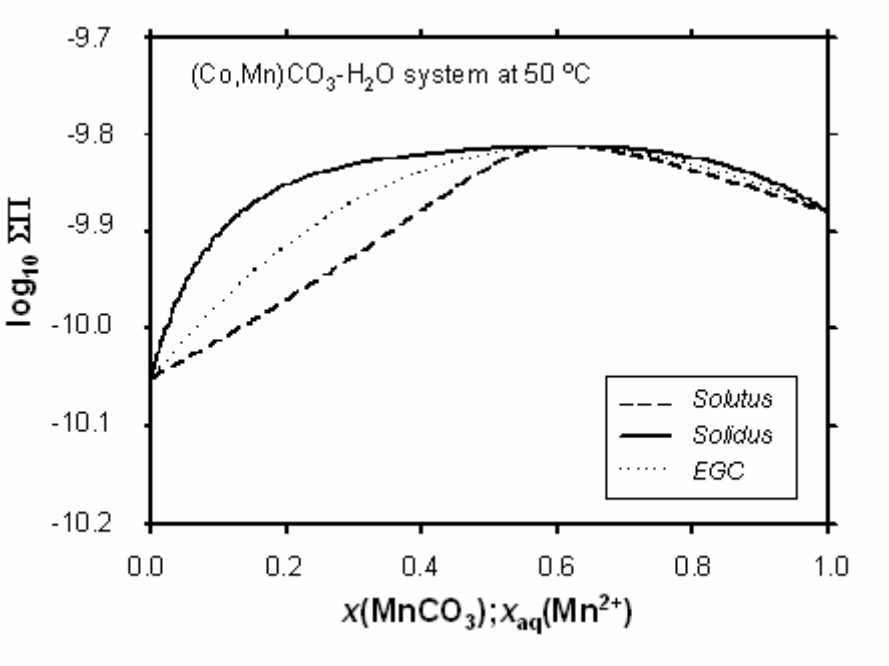

The shape of diagram in Figure II-7 is identical to that of Figure 3 in [1990KON/GAM] plotted in the $\ln\Sigma^* K_{pso}$ scale with experimental points. The Lippmann diagram on Figure II-7 shows that the two end-members are miscible over the whole interval of Mn mole fractions. Because solubility products of end-members are similar, the partition of Co into solid phase is weak, especially at x(Mn) > 0.5, and there is no partition at all at x(Mn) ≈ 0.61 (the *alyotropic point*).

The Mn partitioning between aqueous and solid solution phases can be better seen on the x-x diagram (sometimes called *Roozeboom diagram* [1991GLY]) shown on Figure II-8. Compared to the equilibrium partition in the case of ideal mixing, non-ideality leads to the inflected, more complicated shape of the curve.

Figure II-8: Equilibrium *x*-*x* partition diagram for the same model as shown on Figure II-7. Diamond shows the alyotropic point at *x*(Mn) = 0.61. Equilibrium for the ideal mixing is shown as dashed line.

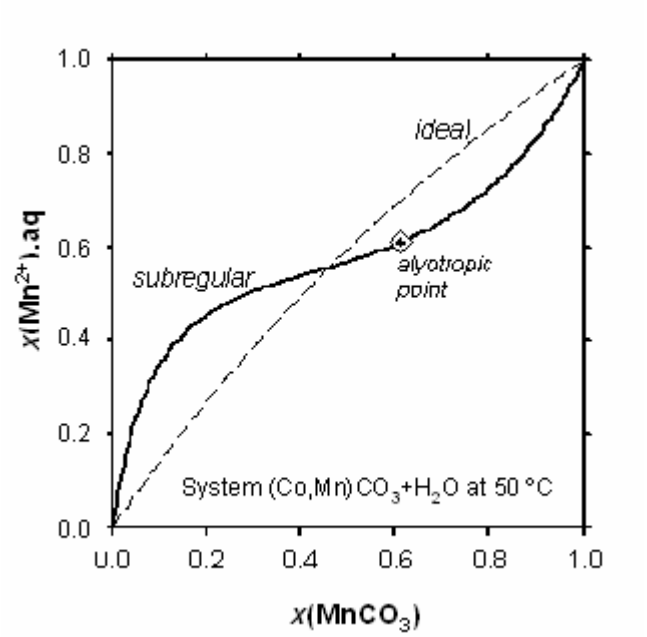

Many Aq-SS systems exhibit a higher non-ideality of mixing at low temperatures. One of the classic examples is the aragonite $CaCO_3$-strontianite $SrCO_3$ system [1987PLU/BUS], [1990GLY/REA], the Lippmann diagram of which is shown in Figure II-9 and the *x*-*x* diagram on Figure II-10.

In the system (Ca,Sr)CO_3-H_2O, the end-member solubility products differ more than in the system (Co,Mn)CO_3-H2O, and the non-ideality of mixing is also more pronounced. Consequences of this are the miscibility gap B1-B2 and the "eutectic" point on the solutus curve (Figure II-9). Strontium is partitioned towards the "Ca-strontianite" phase (at the B2 composition, *ca*. 8 times more than in the aqueous solution). Compared to the ideal mixing, non-ideality makes the partitioning stronger at relatively higher *x*($SrCO_3$) and weaker at low *x*($SrCO_3$) in the solid (Figure II-10).

Figure II-9: Lippmann diagram of the $CaCO_3$-$SrCO_3$-H_2O system at 25 ºC constructed using $\log_{10} K_{s,0} = -8.34$ for aragonite, $\log_{10} K_{s,0} = -9.27$ for strontianite, and Redlich-Kister subregular interaction parameters α_0 = 3.43 and $\alpha_1 = -1.82$ [1990GLY/REA]. EGC is the minimum stoichiometric saturation curve; E is the "eutectic" point on the solutus. A dashed horizontal line from this point crosses the solidus at two mole fractions B1 and B2 that mark compositions of two solid phases coexisting in equilibrium inside of the miscibility gap B1-B2. Part of the solidus curve between B1 and B2 is metastable.

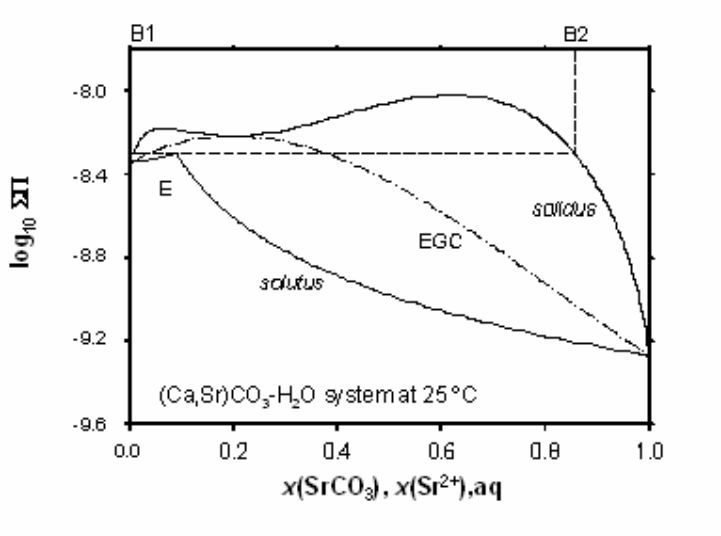

Figure II-10: Equilibrium *x*-*x* (partition) diagram for the same system and model as shown on Figure II-9. Horizontal part of the dense curve corresponds to the miscibility gap which does not appear in the case of ideal mixing shown for comparison as a dashed line.

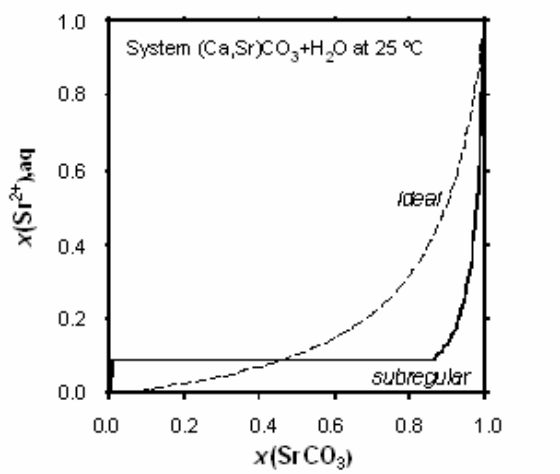

The system celestite-barite (Figure II-11 and Figure II-12) is characterised by about 2000 times different end-member solubilities but symmetric non-ideality [2000PRI/FER] with a theoretical miscibility limited only to 2% at ambient temperatures. This breadth of the miscibility gap is consistent with the regular mixing parameter $\alpha_0 \approx 4.0$; the corresponding Lippmann diagram (Figure II-11) looks very similar to that of Figure 2 in [2000PRI/FER] based on a more complex excess Gibbs energy expression with Redlich-Kister parameters α_0, α_2 and α_4. However, as seen on the *x*-*x* diagram (Figure II-12), the non-ideality plays no significant role in the partitioning of Ba which is almost completely concentrated in the solid phase even at its aqueous mole fraction of 1%. From this example, it is seen that the distribution of Ba is much more affected by a huge difference in solubility products of end-members than by the positive excess Gibbs energy of mixing.

Figure II-11: Lippmann diagram of the $SrSO_4$-$BaSO_4$-H_2O system at 25 ºC constructed using $\log_{10} K_{s,0} = -6.63$ for celestite, $\log_{10} K_{s,0} = -9.98$ for barite, binodal mole fractions of barite 0.021 and 0.979 [2000PRI/FER], and regular interaction parameter $\alpha_0 = 4.01$ ($\alpha_1 = 0$) determined from binodal compositions using the MBSSAS program [1991GLY]. EGC is the minimal stoichiometric saturation curve; dashed horizontal line from the peritectic point crosses the solidus at points B1 and B2 that mark the binodal compositions of two phases coexisting within the miscibility gap. Due to a large difference in end-member solubility products, the solutus curves for ideal or non-ideal cases are almost the same.

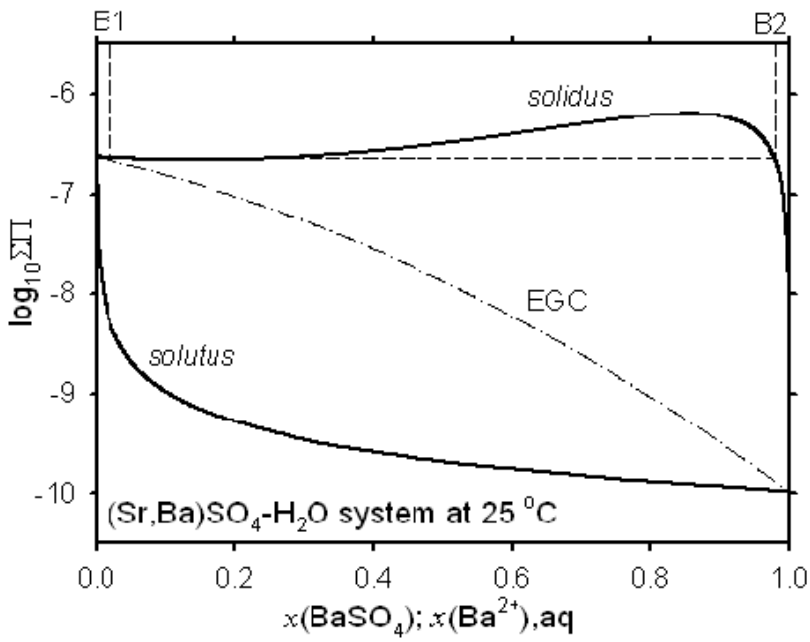

Figure II-12: The *x*-*x* (partition) diagram for the same system as shown on Figure II-11. The thick curve covers the lines for both non-ideal and ideal cases and indicates an extremely strong partition of Ba into the solid phase(s).

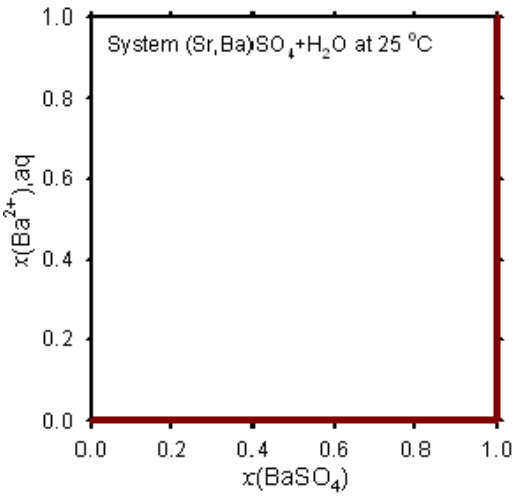

To summarise, the Lippmann diagram is a useful tool to represent equilibria between a binary solid solution and the aqueous electrolyte. Its main limitation lies in that it was developed for aquatic quasi-binary ionic systems such as common-ligand (B,C)L or common-cation C(A,L), and become intractable for ternary or higher-order systems, or for the solids of complex stoichiometry. Lippmann functions use ionic activities and activity fractions and, thus, depend specifically on the chosen aqueous speciation and activity coefficient model, if the diagram is used for fitting experimental Aq-SS partition data. On the other hand, if the goal is just to construct the Lippmann diagram from known interaction parameters and end-member solubility products, then the aqueous speciation model and aqueous activity coefficients play no role.

II.1.2.3 Law of mass action (LMA) method for computing equilibrium speciation

The generic *forward chemical modeling problem* consists in finding the concentrations (or amounts) and activities of chemical species in aqueous and other phases present in a complex chemical system in a complete equilibrium defined by temperature *T*, pressure *p*, and the system bulk composition. In practice, calculations for solving such problems range from trivial to enormously complex, depending on the number of species, phases, and stoichiometry units. The complexity further increases when several pure and solution phases involving redox sensitive components are included in the mass balance; a typical case is the Aq-SS system with a gas mixture phase. Such problems are usually solved with the help of a sophisticated program based on the reaction - law of mass ac-

tion (LMA) formalism and the Newton-Raphson numerical method, supported with tools such as calculation of Lippmann functions and saturation indexes.

A good introduction into modern LMA chemical speciation numerical methods can be found in several textbooks [1970VAN/STO], [1993AND/CRE], [1994NOR/MUN], [1996BET] and in the manuals of speciation codes such as MINEQL [1986WES/ZAC] or PHREEQC [1999PAR/APP]. Below in this section, a brief overview of the setup of LMA speciation calculations is provided following mainly [1996BET]. Finally, its shortcomings in solving Aq-SS equilibria are discussed together with some improved approaches.

Consider an arbitrary (aquatic) system of $n(B)$ components belonging to the *basis* set B, sufficient for specifying the bulk composition of the system and for expressing all chemical species of interest. It is convenient to subdivide the list of basis species into sub-lists (subsets) for water B_w, aqueous B_{aq}, minerals B_{mi}, and gases B_g of known fugacity, so that $B = \{B_w, B_{aq}, B_{mi}, B_g\}$ is a set of $n(B)$ indexes made of one index B_w for water, $n(B_{aq})$ indexes for aqueous master species, $n(B_{mi})$ indexes for minerals, and $n(B_g)$ indexes for gases. Any remaining species of interest - the *product species* A_j belonging to the set $Q = \{Q_{aq}, Q_{mi}, Q_g\}$ - can be expressed *via* the reaction:

$$A_j = \nu_{wj} B_w + \sum_{i \in B_{aq}} \nu_{ij} B_i + \sum_{k \in B_{mi}} \nu_{kj} B_k + \sum_{m \in B_g} \nu_{mj} B_m, \quad j \in Q \tag{II.163}$$

where ν_{wj}, ν_{ij}, ν_{kj}, ν_{mj} are the reaction species stoichiometry coefficients. In practice, the set B usually includes aqueous ions and water, while aqueous complexes are treated as product species. The mole balance equations for the basis entities are:

$$n_w^{(T)} = n_w + m_w \left(M_w^{-1} + \sum_{j \in Q} \nu_{wj} m_j \right) \tag{II.164}$$

$$n_i^{(T)} = m_w \left(m_i + \sum_{j \in Q} \nu_{ij} m_j \right), \quad i \in B_{aq} \tag{II.165}$$

$$n_k^{(T)} = n_k + m_w \sum_{j \in Q} \nu_{kj} m_j, \quad k \in B_{mi} \tag{II.166}$$

$$n_m^{(T)} = m_w \sum_{j \in Q} \nu_{mj} m_j, \quad m \in B_g \tag{II.167}$$

Here, m_w is the mass (kg) and M_w is the molar mass (mol·kg^{-1}) of water-solvent, and m_j is the molality of j-th product (aqueous) species. When the basis components are not charge-balanced (neutral), an additional equation – the electroneutrality condition – is required:

$$0 = \sum_{i \in B_{aq}} m_i Z_i + \sum_{j \in Q} m_j Z_j \tag{II.168}$$

If some product species are expressed using the electron *e-* basis species, then the electron balance condition must also be introduced. At equilibrium, m_j can be found from equilibrium constants K_j and activity coefficients γ_j through the LMA expressions for Reactions (II.163):

$$m_j = \frac{1}{K_j \gamma_j}\left[a_w^{\nu_{wj}} \cdot \prod_{i \in B_{aq}} \left(\gamma_i m_i\right)^{\nu_{ij}} \cdot \prod_{k \in B_{mi}} a_k^{\nu_{kj}} \cdot \prod_{m \in B_g} f_m^{\nu_{mj}} \right], \quad j \in Q \qquad \text{(II.169)}$$

where f_m stands for the m-th gas fugacity; a_k is the activity of k-th solid (assumed to be unity), and the activity of water a_w and activity coefficients of aqueous species γ_j, γ_i are found by iteration using the Davies, Debye-Hückel, or other appropriate equations (see Section II.1.2.1). Equation (II.169) can then be substituted for m_j into all $n(B) + 1$ balance (Eqs. (II.164)-(II.168)), thus making them non-linear. The system of balance equations can be solved in the computer for the unknowns n_w, m_i, m_j, and n_k using the Newton-Raphson or similar numerical algorithm that iteratively minimises the mass balance residuals. To do that, the analytical derivatives of all balance equations are needed.

Thus, the input data of the LMA speciation calculation includes the amounts of water, aqueous, and other basis components ($n_w^{(T)}$, $n_i^{(T)}$, $n_k^{(T)}$), fugacities of gases f_m, optionally redox state (pe), as well as the reaction stoichiometry coefficients and equilibrium constants K_j for the product species. It is a useful practice to represent the LMA input data in the "Tableau" form [1993MOR/HER]. In principle, the selection of basis components is arbitrary and depends on the purposes of modelling. There is a mathematical transformation from one to another set of basis components, which involves also the conversion of reactions for product species and recalculation of their equilibrium constants [1996BET].

The equilibrium solubility of a stoichiometric (pure) mineral phase in a given amount of aqueous electrolyte is readily calculated using the LMA method outlined above, if this mineral is surely stable (*e.g.*, given at input in a sufficiently large amount). However, this implies that the list of minerals existing at equilibrium with the given aqueous solution must be known in advance to be included into the mass balance. In other words, a single LMA calculation does not predict the assemblage of minerals which is stable in a given Aq-SS system. To circumvent the difficulty, many LMA programs can calculate the saturation index SI (Eq. (II.124)) over the whole list of stoichiometrically feasible pure mineral phases with known solubility products but not included into the mass balance. This makes it possible to see which minerals are under-saturated (SI < 0) and super-saturated (SI > 0); for any mineral present in equilibrium, SI = 0 (within a small numerical error).

To find an equilibrium assemblage, a semi-empirical "swap procedure" as described by ([1996BET], section 5.4) or similar is used in many LMA codes. This procedure (Figure II-13) gives reasonable results in solving a wide range of problems, although it is not mathematically guaranteed to arrive at the correct equilibrium state. It performs a LMA equilibrium speciation calculation and then first checks for under-saturated minerals in the mass balance which have negative amounts n_k (Eq. (II.166)). If any found, the one with the most negative n_k is removed from the basis set, and the speciation problem is solved again. Once there are no under-saturated minerals left, the

procedure checks for supersaturated minerals with SI > 0. The one with the largest SI is then swapped into the basis, and the LMA problem is solved again. Precipitating a new mineral, however, may make another dissolved, so now the process goes back to checking for under-saturated minerals. The procedure stops when all under-saturated minerals are removed from the basis set and no more supersaturated minerals can be found.

Calculations get much more complicated if solid solution phases must be considered in LMA speciation models because the activities of end-members are no more unity, thus, the end-member cannot be treated as a basis mineral in (Eq. (II.166)).

For this reason, the Geochemists Workbench GWB [1996BET] is one of LMA codes that do not handle solid solutions at all. Other codes (*e.g.*, PHREEQC), however, do it, at least in relatively simple Aq-SS systems, by treating minerals and gases as the product species rather than the basis (master) components.

Figure II-13: Flow chart of the "swap procedure" for finding an equilibrium assemblage of pure (stoichiometric) mineral phases in aquatic systems (modified after [1996BET]).

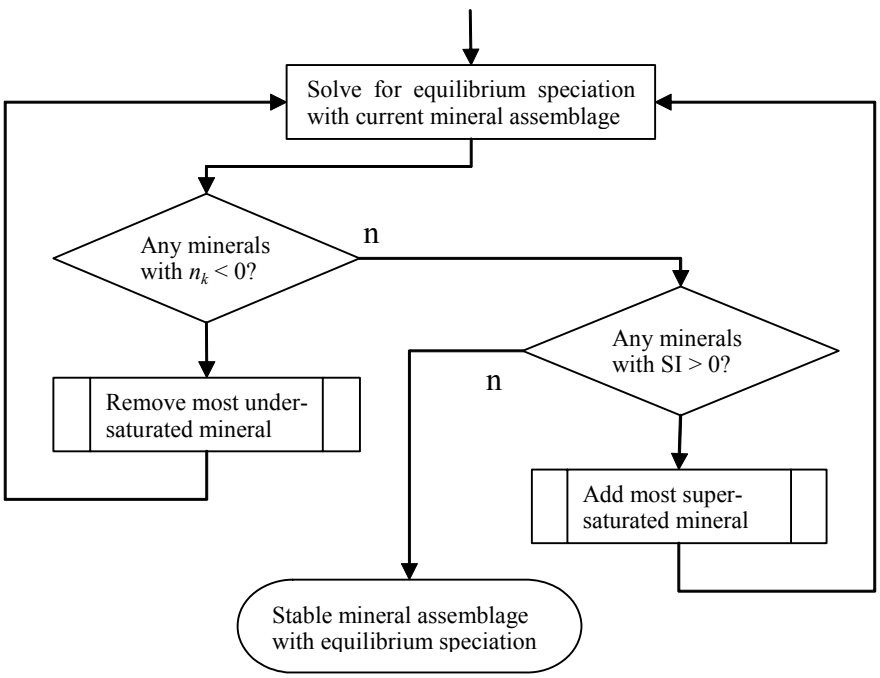

As described by [1982REE2], the set of equations to be solved for molalities and amounts with the Newton-Raphson technique includes $n(N)$ mole balance equations for "component" or "master" species out of the set N (usually aqueous ions, water and SiO_2), and $n(\Phi)$ mass action equations for "phases", *i.e.*, saturated minerals and gases of the set Φ. The bulk composition of the system is set in terms of amounts of component species only, subject to $n(N)$ balance equations:

$$n_i^{(T)} = m_w\left(m_i + \sum_{j\in Q} \nu_{ij} m_j\right) + \sum_{k\in\Phi} \nu_{ik} n_k,\ i \in N \tag{II.170}$$

where Q is now a set of the product aqueous species with molalities m_j substituted by the LMA equations written in terms of master species only:

$$m_j = \frac{1}{K_j \gamma_j} \cdot \prod_{i\in N} \left(\gamma_i m_i\right)^{\nu_{ij}},\ j \in Q \tag{II.171}$$

and n_k is the amount of pure mineral or gas, stability of which is described by a LMA equation:

$$K_k = \frac{1}{a_k} \cdot \prod_{i\in N} \left(\gamma_i m_i\right)^{\nu_{ik}},\ k \in \Phi \tag{II.172}$$

where K_k is the equilibrium constant (*e.g.*, solubility product), and a_k is the activity of k–th mineral or fugacity of a k-th gas. For a pure mineral or a gas at standard pressure (1 bar), $a_k = 1$.

Under the given total fluid pressure p_f, for a gas mixture component indexed with g, Eq. (II.172) takes the form:

$$p_f K_g = \frac{1}{\phi_g y_g} \cdot \prod_{i\in N} \left(\gamma_i m_i\right)^{\nu_{ig}},\ g \in \Phi_g,\ \Phi_g \in \Phi,\ y_g = \frac{n_g}{\sum\limits_{g\in\Phi_g} n_g} \tag{II.173}$$

where ϕ_g is the fugacity coefficient (Eq. (II.173)), and y_g is the mole fraction of g-th gas component belonging to a subset Φ_g of gaseous species. With this form of the mass action equation, the gas mixture can be treated in the LMA technique in the same way as the solid solution [1982REE2].

For a k-th solid solution end-member, the LMA equation takes the form:

$$K_k = \frac{1}{f_k x_k} \cdot \prod_{i\in N} \left(\gamma_i m_i\right)^{\nu_{ik}},\ k \in \Phi_{ss},\ \Phi_{ss} \in \Phi,\ x_k = \frac{n_k}{\sum\limits_{k\in\Phi_{ss}} n_k} \tag{II.174}$$

where Φ_{ss} is a subset of solid solution end-members, x_k is the mole fraction, and f_k is the activity coefficient of k-th end-member. In the case of ideal Raoultian solid mixture, $f_k = 1$; otherwise, it must be computed using an appropriate mixing model as function of end-member mole fractions and interaction parameters (see Section II.1.1.4). This is usually done between the iterations of Newton-Raphson algorithm together with calculation of the ionic strength and aqueous activity coefficients. The analytical derivatives

of all equations like (II.170) to (II.174), as well as those for activity coefficients, are needed [1999PAR/APP].

In principle, the described LMA method can handle multiple mixture phases which can exist in equilibrium with the aqueous phase (and pure substance phases), subject to the limitations of the Gibbs phase rule [1967GUG]:

$$n(F) = n(N) - n(\Phi) + 2 \tag{II.175}$$

where $n(F)$ is the number of degrees of freedom, $n(N)$ is the number of independent components (in the present case, the number of mass balance equations), and $n(\Phi)$ is the number of phases. At fixed temperature and pressure, Eq. (II.175) takes the form:

$$n(\Phi) = n(N) - n(F) \tag{II.176}$$

In the PHREEQC code [1999PAR/APP], an ideal solid solution may contain two or more end-members, but a non-ideal solid mixture is limited to two end-members treated using the Guggenheim expressions (Eq. (II.39)) truncated to the first two terms with the known interaction parameters α_0 and α_1. In general, the strong non-ideality introduced by the aqueous activity coefficients in concentrated solutions, as well as by the solid activity coefficients, may cause bad convergence or failure in the LMA-based speciation algorithms; this trouble even forced some researchers to switch from LMA to GEM methods (J.Weare, personal communication, 1998). However, the problem has been avoided to some extent by inventing smart numerical procedures for picking up the initial guesses of n_k and m_i values.

As stated in [1982REE2], the real challenge lies in the selection of mineral phases, especially solid solutions, to be included into the mass balance through Eqs. (II.170) with boundary conditions (II.174). Selection of pure phases is normally done upon checking the saturation indexes SI over the whole list of minerals in the process of solving the LMA speciation task many times in a semi-empirical procedure such as described above (Figure II-7). But selection of a *solid solution* in this way is considerably complicated by the fact that *pure end-members may be under-saturated while their solid solution is super-saturated*. There is no easy way to check this because to do it, the end-member mole fractions x_k (and end-member activity coefficients f_k if the mixture is non-ideal) must be known. However, the amount and composition of the solid solution depends on that of the coexisting aqueous electrolyte, and both amounts are initially unknown. To work around this limitation of the LMA method, some more or less successful semi-empirical procedures have been suggested [1982REE2], [1993BOE/EMR]. According to Reed [1982REE2], the saturation of aqueous phase of known composition with respect to a solid solution or a gas mixture of unknown composition can be tested as follows:

(a) Assume that the aqueous phase is exactly saturated with a solid solution φ having end-member mole fractions $x_k^{(\varphi)}$ and activities $a_k^{(\varphi)}$.

(b) Calculate expected values of end-member activities using the rearranged:

$$\text{Eq. (II.172):}\quad a_k^{(\varphi)} = \frac{1}{K_k}\prod_{i\in N}\left(\gamma_i m_i\right)^{\nu_{ik}},\quad k \in \varphi\,.$$

Notice that the product in this equation is an equivalent to the dissolution reaction quotient Q_s(II.123), thus $Q_{s,k} = \prod_{i\in N}\left(\gamma_i m_i\right)^{\nu_{ik}}$ and $a_k^{(\varphi)} = \dfrac{Q_{s,k}}{K_k}$.

(c) Calculate the expected mole fractions of end-members as $x_k^{(\varphi)} = a_k^{(\varphi)} \big/ f_k^{(\varphi)}$, where the activity coefficient $f_k^{(\varphi)}$ is taken unity for the ideal mixture, or obtained from guess $x_k^{(\varphi)}$ values using the appropriate mixing model with known interaction parameters.

(d) Calculate the expected sum of mole fractions in the mixed phase $\Sigma_\varphi = \sum_k x_k^{(\varphi)}$. Check: if $\Sigma_\varphi > 1$ then the solid solution or gas is super-saturated; if $\Sigma_\varphi < 1$ then it is under-saturated.

If the solid solution or gas is super-saturated, all of its end-members are included into LMA balance (Eqs. (II.170) to (II.174)), and the speciation calculation is repeated to improve on the m_i, m_j and n_k sought-for values and on the $x_k^{(\varphi)}$ approximations. Then, the Reed' test procedure (a) – (d) is repeated together with the follow-up LMA speciation runs, until the mole fractions $x_k^{(\varphi)}$ do not change anymore. If the whole mixed phase becomes under-saturated (*e.g.*, due to inclusion of other minerals along the process) then all end-members of the phase φ must be removed from the LMA setup. A possible flow chart of LMA calculation of the Aq-SS equilibrium is shown in Figure II-14.

At the beginning of the LMA Aq-SS system modelling sequence, the problematic point in the Reed's procedure lies in the step (a), where mole fractions $x_k^{(\varphi)}$ or activities $a_k^{(\varphi)}$ of the potential solid solution end-members are initially guessed, based on the approximated molalities m_i or activities a_i of aqueous ions.

Figure II-14: Flow chart of the extended LMA procedure for finding an equilibrium assemblage of pure mineral phases together with a solid solution or a gas mixture in the aquatic system.

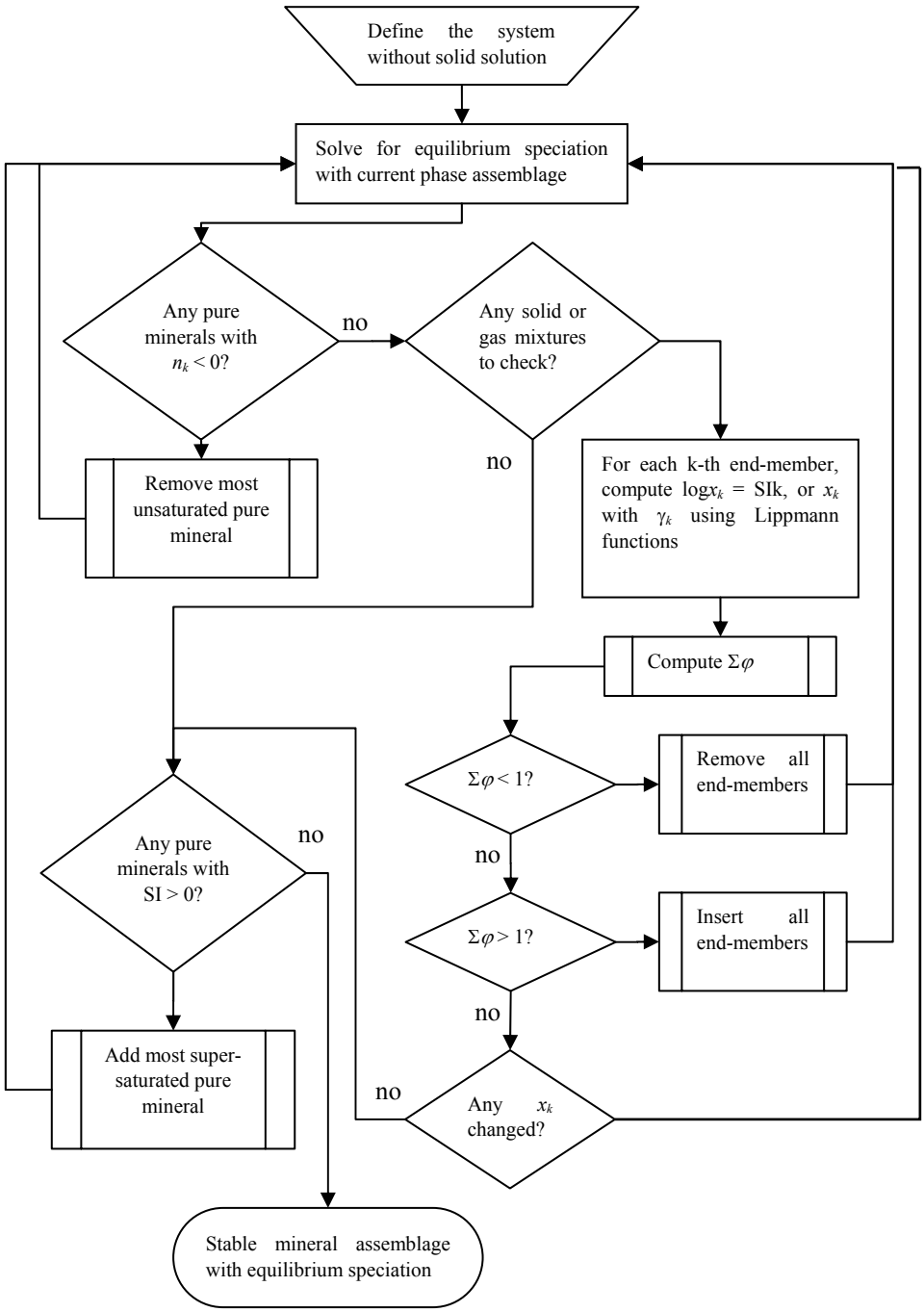

A simple way to avoid problems would be to guess mole fractions $x_k^{(\varphi)}$ in the solid as equal to ionic molality fractions:

$$x_{k,aq}^{(\varphi)} = \frac{m_{i,k}^{(\varphi)}}{\sum_k m_{i,k}^{(\varphi)}}$$

or to ionic activity fractions (see Eqs. (II.151)). However, if the solubility products of end-members are different, equilibrium mole fractions in solid solution can be very different from ionic activity fractions in the aqueous phase due to the partitioning effects. Therefore, another possibility is to estimate the activity $a_k^{(\varphi)}$ of each end-member from the current saturation index (Eq. (II.124)) of this end-member taken as pure substance. For a multi-component ideal solid solution, this directly yields the guess mole fraction values $x_k^{(\varphi)} = a_k^{(\varphi)}$, but there is no easy way to get $x_k^{(\varphi)}$ values from activities in the cases of non-Raoultian or non-ideal mixture.

For the above reasons, the use of Lippmann diagrams (Section II.1.2.2) and MBSSAS code [1991GLY] appears to be the only theoretically sound method for estimating activities or mole fractions of solid solution end-members in equilibrium with the aqueous solution in the context of LMA approach to Aq-SS systems, at least when only binary solid solutions are involved. For multi-component solid mixtures, the unified theory of solid solution solubilities [2003GAM/KON] (Eqs. (II.136) to (II.144)) can, in principle, be applied. In some cases, the answers about the Aq-SS equilibrium (with a binary solid solution) can be read out from the Lippmann diagram, and no mass-balance LMA speciation calculation is necessary at all.

Solving the Aq-SS equilibria with LMA codes is, in general, an inefficient and awkward process because a single aqueous speciation calculation turns into a series of many runs controlled by non-rigorous test procedures such as described above, without a theoretical guarantee of convergence to a unique solution. The only case which is easy to solve with LMA methods is the stoichiometric saturation state [1990GLY/REA], when the solid mixture is effectively "frozen" and behaves as a pure solid of known stoichiometry (*i.e.*, with fixed mole fractions x_k of end-members). This solid can be directly included into the LMA setup as a "pure phase" with the mixture solubility product $K^{(x)}$ obtained from Eqs. (II.135) or (II.142), if the end-member solubility products and non-ideal interaction parameters are known.

II.1.2.4 Gibbs energy minimisation (GEM) method

In GEM setup, the total mole amounts of chemical elements n_i and (zero) charge n_Z comprise the input bulk composition of the chemical system expressed using $n(N)$ *independent components* (IC). All $n(L)$ stoichiometrically feasible chemical species or *dependent components* (DC) belonging to a set L are taken into the mass balance through their chemical formulae and mole amounts n_j, $j \in L$. A dependent component belongs to a single- or multi-component aqueous, gaseous, fluid, liquid, solid, or sorption phase. Stability of j-th chemical species (DC) at temperature T and pressure p of interest is

defined by its input standard molar Gibbs energy function g_j°. Activities and concentrations of dependent components are treated separately in each phase (through subsets of indexes L_α, $\alpha \in \Phi$), taking into account appropriate standard and reference states, concentration scales, and mixing models. Conversely, GEM algorithms can solve complex Aq-SS equilibria in one GEM run, in a straightforward way, without any supporting tools such as Lippmann functions and semi-empirical iterative procedures required in LMA Aq-SS speciation models. The applicability of GEM is limited only by the knowledge of standard-state molar properties of end-members and the non-ideal interaction parameters for each phase.

The GEM method has been applied for solving highly non-ideal water-salt equilibria [1987HAR/GRE]. It is available in several computer codes such as ChemSage ([1989ERI/THO], [1990ERI/HAC] http://gttserv.lth.rwth-aachen.de/~sp/tt/chemsage/); FactSage http://www.factsage.com/ [2002BAL/CHA]; Gibbs/HCh [1992BOR/SHV] http://www.ga.gov.au/rural/projects/HCh.jsp; Selektor-C [2001KAR/CHU]; GEM-Selektor [2003KUL/DMY], [2004KUL/BER2]). In the following description, mainly the variant of GEM known as *convex programming approach* [1997KAR/CHU], [2001KAR/CHU], [2004KUL/BER2] will be considered, recast into a different notation adjusted to NEA TDB and IUPAC-recommended symbols. The convex programming GEM algorithm computes simultaneously the *primal* (amounts of dependent components) and the *dual* (chemical potentials of independent components) results from which other thermodynamic quantities and criteria of equilibrium can be obtained.

GEM forward modeling means here a calculation of (unknown) equilibrium phase assemblage and speciation in the system defined by *p, T,* bulk composition, thermodynamic data for dependent components, and, optionally, parameters of mixing in multicomponent phases. Solving this problem is equivalent to finding a vector of mole amounts of dependent components $n^{(x)} = \{n^{(x)}_j,\ j \in L\}$ (vector x in [1997KAR/CHU]) such that:

$$G(n^{(x)}) \Rightarrow \min \qquad \text{subject to} \qquad \mathrm{A}n^{(x)} = n^{(b)} \tag{II.177}$$

where $n^{(b)} = \{n^{(b)}_i,\ i \in N\}$ is the input vector of amounts of independent components belonging to the set N; $\mathrm{A} = \{a_{ij},\ i \in N,\ j \in L\}$ is a matrix made of the formula stoichiometry coefficients of dependent components; and $G(n^{(x)})$ is a total Gibbs energy function of the system:

$$G(n^{(x)}) = \sum_j n_j^{(x)} \upsilon_j, \quad j \in L \tag{II.178}$$

In Eq. (II.178), υ_j is the normalised chemical potential of j–th dependent component, which can be written in a simplified dimensionless form as

$$\upsilon_j = \frac{g_j^\circ}{\mathrm{R}T} + \ln C_j + \ln \gamma_j + \Xi, \quad j \in L \tag{II.179}$$

where g_j^o is the standard molar Gibbs energy function at temperature T (K) of interest (pressure dependence is omitted here for simplicity); R = 8.3145 J·K^{-1}·mol^{-1} is the universal gas constant; $C_j = f(n^{(x)}_j)$ is the concentration that depends on the choice of standard concentration scale. C_j equals the mole fraction $x_j = n_j^{(x)} / \sum_j n_j^{(x)}$, $j \in L_\alpha$ for components of α–th gas or condensed mixture phases, and for the water-solvent; C_j equals the molality m_j for aqueous electrolyte species, and unity for the pure multi-component phases. The activity coefficient γ_j of j–th dependent component in its respective phase is taken in the chosen standard concentration scale and reference state (unity in a Raoultian ideal mixture or for the single-component pure phase). The term Ξ for conversion into the rational scale depends on the chosen standard state:

$\Xi = \ln p$ for the gas phase components;
$\Xi = 1 - x_w$ for the aqueous species
(x_w is the mole fraction of water in aqueous phase);
$\Xi = 2 - x_w - 1/x_w$ for the water-solvent;
$\Xi = 0$ for the (solid) mixture end-members and pure-substance phases.

Activity coefficients γ_j, as functions of the respective phase composition, should be calculated between the GEM iterations according to the model of non-ideal mixing chosen for each phase.

The *Interior Points Method* (IPM) non-linear GEM algorithm finds simultaneously two vectors – the *primal* $\hat{n}^{(x)}$ and the *dual* u solutions of the problem (1) – using the *Karpov-Kuhn-Tucker* necessary and sufficient conditions of equilibrium [1997KAR/CHU]:

$$\begin{aligned} &\upsilon - \mathrm{A}^T u \geq 0; \\ &\mathrm{A}\hat{n}^{(x)} = n^{(b)};\ \hat{n}^{(x)} \geq 0; \\ &\hat{n}^{(x)} \left(\upsilon - \mathrm{A}^T u \right) = 0 \end{aligned} \qquad \text{(II.180)}$$

where ^{T} is the transpose operator. The first condition in Eq. (II.180), rewritten with indices,

$$\frac{g_j^{\mathrm{o}}}{\mathrm{R}T} + \ln C_j + \ln \gamma_j + \Xi - \sum_i \mathrm{a}_{ij} u_i \geq 0, \quad j \in L, \quad i \in N \qquad \text{(II.181)}$$

implies that for any j–th species present at some *equilibrium* concentration C_j in its phase, the *primal* chemical potential υ_j numerically equals the *dual* chemical potential

$$\eta_j = \sum_i \mathrm{a}_{ij} u_i, \ j \in L, \ i \in N \qquad \text{(II.182)}$$

From the duality theorem that leads to conditions (II.180) it also follows that, at equilibrium, the total Gibbs energy of the system is $G\left(\hat{n}^{(x)}\right) = G(u)$, where $G\left(\hat{n}^{(x)}\right)$ is given by Eq. (II.178) and

$$G(u) = \sum_i \hat{n}_i^{(b)} u_i, \; i \in N \qquad \text{(II.183)}$$

As seen from Eq. (II.178), the partial derivative of $G\left(\hat{n}^{(x)}\right)$ by $\hat{n}_j^{(x)}$ is the (primal) chemical potential υ_j. From (II.183) it can be seen that u_i is the partial derivative of $G(u)$ by $n_i^{(b)}$. Hence, the GEM dual solution u_j values (Lagrange multipliers) are *chemical potentials of independent components* at the equilibrium state of interest because $n_i^{(b)}$ is the mole amount of *i*–th independent component in the system, and u_i has the same value in all coexisting phases.

The last Kuhn-Tucker condition of *orthogonality* in Eq. (II.180) zeroes off the molar amounts of unstable species and phases. Conditions (II.180) have also been extended for the case when the sought-for molar quantities $\hat{n}_j^{(x)}$ of some metastable species are constrained from below and/or above to model "partial equilibrium" states [2001KAR/CHU]. GEM calculations are implemented in the GEM-Selektor v.2–PSI code [2004KUL/BER2] with a built-in Nagra/PSI chemical thermodynamic data base [2002HUM/BER], both available for download at: http://les.web.psi.ch/Software/GEMS-PSI.

II.1.2.4.1 GEM IPM algorithm

In the GEM IPM algorithm described in detail in [1997KAR/CHU], as in other numerical methods (Section II.1.2.3), finding a feasible initial approximation (FIA) of the $n^{(x)}$ vector is critically important for the efficient convergence to the global minimum of the $G\left(n^{(x)}\right)$ function. There is even a higher demand to the quality of FIA because, in fact, the algorithm minimises the total Gibbs energy and not the mass balance residuals, as the Newton-Raphson algorithm does in the LMA technique. The mass balance precision of IPM is, in fact, inherited from that of the initial approximation vector [2002CHU/KAR]. In the GEM-Selektor code, a special strategy is used for getting the result with good mass balance accuracy at all circumstances, as shown on the flow-chart (Figure II-13) briefly commented below.

An automatic FIA must be used in all cases when the stable phase assemblage or the redox state is going to be different from the previously computed equilibrium state, or the latter is not available. If so then the generic non-linear GEM problem is truncated into a supplementary, linear minimisation sub-problem by cutting off all the activity terms in chemical potential expressions for all species. In other words, each dependent component is treated as a pure substance "phase". The sub-problem is solved using a simplex linear programming procedure which returns $n(N)$ or less non-zero values $n_j^{(y)}$ for species with very small mass-balance residuals ($\varsigma < 10^{-12}$ mol).

After that, the original non-linear minimisation problem (with all the activity terms for species in solution phases) is restored. The initial values of $n_j^{(x)}$ are set equal to simplex-calculated amounts $n_j^{(y)}$ if $n_j^{(y)} > 0$, or to a small constant ($\varepsilon_2 = 10^{-6}$ mol) if $n_j^{(y)} = 0$. This fill-out procedure ensures that no relevant phases and species will be lost from the final GEM result. At the same time, this operation worsens the mass balance residuals.

The calculation proceeds with the *FIA Domain Entry 1* procedure which iteratively adjusts some initial $n_j^{(x)}$ values in such a way that any mass balance residual ς_i does not exceed a small prescribed value ε_2 (10^{-7} mol or less). After this is done, the main GEM IPM descent procedure iteratively adjusts both primal and dual solution vectors trying to decrease the total Gibbs energy function of the system. Activity coefficients are recalculated between IPM iterations. After each *r*–th iteration, the IPM convergence criterion *CD* is calculated:

$$CD = \sqrt{\sum_{j\in L_S} n_j^{(x,r)2} \left(\sum_{i\in N} a_{ij} u_i^{(r)} - \upsilon_j^{(r)} \right)^2} \qquad \text{(II.184)}$$

Calculations are finished when $CD \le \varepsilon_1$ where ε_1 is a small number about 10^{-5}.

Next, the *Select–2* procedure is executed. For each α–th phase, the f_j values for its components and then the f_α value for the whole phase are calculated:

$$f_\alpha = \sum_{j\in l_\alpha} f_j \quad \text{where} \quad f_j = \exp\left(-\upsilon_j + \ln n_j^{(x)} + \eta_j\right) - n_j^{(x)}, \quad j \in L_S, \; \eta_j = \sum_{i\in N} a_{ij} u_i \qquad \text{(II.185)}$$

Here, l_α is a subset of dependent components belonging to α–th phase, and L_S is a set of all components except those eliminated (zeroed off) from stable multicomponent phases.

For a single-component phase ($n_j^{(x)} = 1$), $f_\alpha = f_j$. For any multi-component phase,

$$f_\alpha = \sum_{j\in l_\alpha} \left[\exp\left(-\upsilon_j + \ln n_j^{(x)} + \eta_j\right) \right] - 1, \quad j \in L_S \qquad \text{(II.186)}$$

This f_α value is used in a Karpov phase stability criterion [1981KAR] to decide whether a phase must be present or absent from the equilibrium assemblage:

if $f_\alpha = 0$ (numerically, if $-\varepsilon_3 \le f_\alpha \le \varepsilon_3$) then $\sum_{j\in l_\alpha} n_j^{(x)} \ge 0$ (phase exists); (II.187)

if $f_\alpha \le 0$ (numerically, if $f_\alpha < -\varepsilon_3$) then $\sum_{j\in l_\alpha} n_j^{(x)} = 0$ (phase is absent) (II.188)

where $\varepsilon_3 = 0.01$ is the criterion threshold. All phases (also those eliminated during the IPM descent) are checked in the *Selekt–2* procedure using the above criteria to prevent any uncertainty in the detection of the equilibrium phase assemblage. If there is a "contradictory" phase which is present in the mass balance, but the criterion (II.188) suggests that it is unstable, then this phase is removed by setting $n_j^{(x)} = 0$ for all its components. If the phase has been eliminated, but the criterion (II.187) shows that it must be present, the phase will be inserted by setting $n_j^{(x)} = \varepsilon_2$ for all its components. If either of these situations has happened then the control goes back to the *FIA Domain Entry* procedure, and the whole GEM IPM calculation is repeated. Persistence of one these situations points to a serious inconsistency in input thermodynamic data or DC stoichiometries.

Hence, the *Selekt–2* procedure provides diagnostics of the quality of GEM-solved equilibrium speciation. Provided that internally consistent thermodynamic data is used, the GEM algorithm always yields a correct equilibrium phase assemblage and speciation, regardless of how many solution phases were included into the system definition.

The "standard" GEM IPM algorithm outlined above converges with mass balance residuals of *ca*. 10^{-7} – 10^{-9} mol – an accuracy much worse than in the Newton-Raphson method, although quite sufficient for most chemical systems. However, in many applications, the input total amounts of some chemical elements are below $\varepsilon_2 = 10^{-6}$ mol, for instance, in many systems involving trace metals or radionuclides. In such cases, the mass balance residuals may exceed 1000 % for trace elements, which is unacceptable. As shown on Figure II-15, if any input trace amounts of independent components were detected, the control goes to the second stage of the GEM IPM algorithm aimed at reducing mass balance deviations and improving the accuracy of the result.

The idea of this improvement [2002CHU/KAR] follows the property of the *FIA Domain Entry* algorithm to converge with very small balance residuals when the FIA lies very close to the minimum total Gibbs energy point (*i.e.*, the standard GEM IPM solution is taken as the FIA). The *FIA Domain Entry 2* procedure assigns the very strict balance residual thresholds separately for each input element of the bulk composition to ensure residuals with $|\varsigma_i| < 10^{-12}$ for major elements and $|\varsigma_i| < 10^{-17}$ mol for other elements and charge. Then, as usual, the control goes to the Main IPM Descent procedure (which now does at most a few iterations), followed by the *Modified Selekt-2* procedure. The individual balance precision thresholds are checked again in the *Residuals Check* procedure; if necessary, the whole Stage 2 loop is repeated (up to 14 times) until the GEM result with excellent accuracy is obtained. In rare cases, the required precision cannot be reached, most probably due to hidden inconsistencies in the input thermodynamic data.

Figure II-15: Simplified flow chart of the two-stage enhanced-precision GEM IPM algorithm (modified from [2002CHU/KAR]).

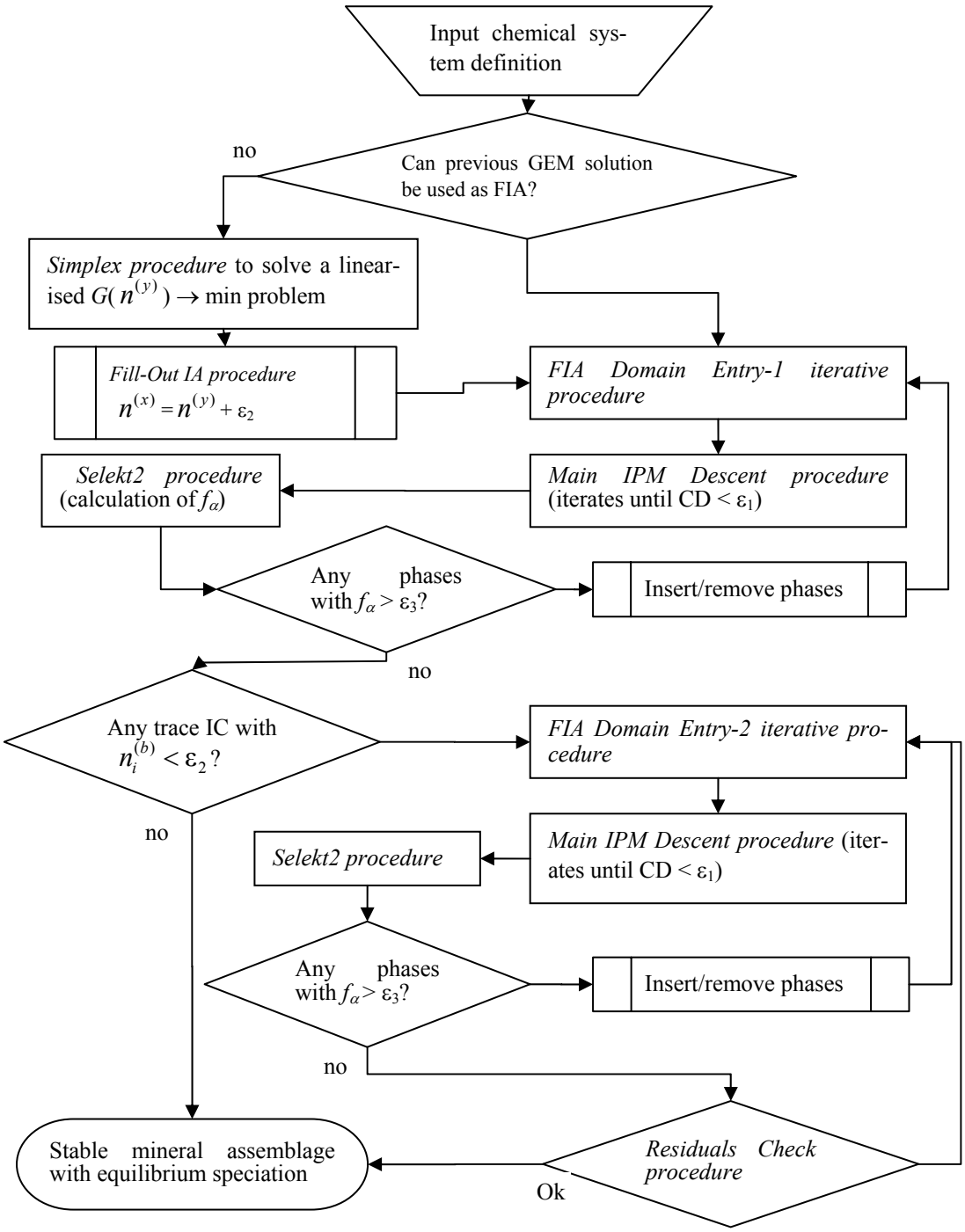

II.1.2.4.2 GEM dual-thermodynamic calculations in forward modelling

For any species in any phase present in equilibrium, the first Karpov-Kuhn-Tucker condition (II.180) can be combined with Eqs. (II.179) and (II.110) into a generic *dual thermodynamic equation* $\eta_j = \upsilon_j$ or in the extended form

$$\sum_i \mathrm{a}_{ij} u_i = \frac{g^{\circ}_{j,T}}{\mathrm{R}T} + \ln C_j + \ln \gamma_j + \Xi \qquad \text{(II.189)}$$

In the forward speciation modelling, aimed at computing concentrations and activity coefficients of species in phases, the equations derived from Eq. (II.189) are internally used (in GEM-Selektor code) to calculate: (i) activities of gaseous, aqueous, solid-solution and sorption species, (ii) activity functions such as pH, pe, Eh; and (iii) saturation indices of single-component condensed phases. The activity of *j*–th dependent is understood here as a *relative activity* $a_j = r_j \gamma_j$ from the IUPAC definition of chemical potential:

$$\mu_j = \mu^{\circ}_j + \mathrm{R}T \ln a_j = \mu^{\circ}_j + \mathrm{R}T \ln r_j + \mathrm{R}T \ln \gamma_j \qquad \text{(II.190)}$$

where r_j stands for a *relative content*. Comparison with Eq. (II.190) shows that r_j is related to concentration as $\ln r_j = \ln C_j + \Xi$. According to Eqs. (II.189) and (II.190), the DualTh equation for calculation of activity of any component in any multi-component phase at equilibrium is:

$$\ln a_j = \sum_i \mathrm{a}_{ij} u_i - \frac{g^{\circ}_j}{\mathrm{R}T}, \quad j \in L, \quad i \in N \qquad \text{(II.191)}$$

Compare this with the traditional calculation of activities: $\ln a_j = \ln C_j + \Xi + \ln \gamma_j$. As both C_j and γ_j are functions of the primal solution $\hat{n}^{(x)}$ vector, thus computed activities are subject to numerical limitations. For instance, neither GEM nor LMA algorithms need to consider amounts below 10^{-18} to 10^{-20}; smaller values are usually automatically zeroed off for convergence reasons. For "zeroed-off" species, Eq. (II.191) is *the only* way to compute activities, also applicable to stoichiometrically feasible minor species not even included into the mass balance, for instance, to the "aqueous electron" e_{aq} – a hypothetical species used in the definition of pe – a measure of redox potential. For the e_{aq} species (formula charge $Z = -1$ and $g^o = 0$ by convention), Eq. (II.191) takes the form $\ln a_e = -1 \cdot u_{\mathrm{Charge}}$. By defining $\mathrm{pe} = -\log_{10} a_e$,

$$\mathrm{pe} = -\frac{1}{\ln 10}\left(-u_{\mathrm{Charge}}\right) \qquad \text{(II.192)}$$

Using the fundamental relation $\mathrm{pe} \cdot \mathrm{R}T \cdot \ln 10 = \mathrm{F} \cdot \mathrm{Eh}$ ($\mathrm{F} = 96485$ C·mol^{-1} is the Faraday's constant), pe can be converted into Eh (in Volts):

$$\mathrm{Eh} = \frac{\mathrm{R}T}{\mathrm{F}} \cdot T \cdot u_{\mathrm{Charge}} \qquad \text{(II.193)}$$

In a similar way, pH can be calculated for any aquatic system, even if the H^+ species is not explicitly included:

$$\mathrm{pH} = -\frac{1}{\ln 10}\left(u_{\mathrm{H}} + u_{\mathrm{Charge}}\right) \tag{II.194}$$

This equation, consistent with the electrochemical convention $g°(H^+) = 0$ at any T and p, does not require the activity coefficient of H^+ ion. This is an important advantage because of difficulties related to estimation of the ion-size or interaction parameters for the H^+ species.

Another useful case is the calculation of fugacity f_j of a gaseous component, *e.g.*, O_2 or CO_2. Now, the relative activity can be defined as $\mu_j - \mu_j^{\circ} = \mathrm{R}T \ln a_j = \mathrm{R}T\left(\ln f_j - \ln f^{\circ}\right)$ [1993AND/CRE]. Because the standard-state fugacity $f^{\circ} = 1$ bar for any gaseous component, its activity a_j (dimensionless) is numerically equal to the fugacity f_j (in bars). Hence, Eq. (II.191) can be used for computing a gas fugacity value directly, even if the gas mixture is not present in positive amount at equilibrium, or even has not been included into the system definition. For example, the fugacity of ideal methane (CH_4) gas at t = 25 ºC in any system containing C and H can be found using the DualTh equation,

$$\log_{10} f_{\mathrm{CH_4},g} = \frac{1}{\ln 10}\left[u_{\mathrm{C}} + 4u_{\mathrm{H}} - \left(-20.44\right)\right]$$

where – 20.44 is the normalised (*i.e.*, divided by RT = 2479 J·mol^{-1}) standard molar Gibbs energy of methane gas at 25 ºC.

There are two cases of application of the dual-thermodynamic activity equation to solid phases. If the solid solution phase is present at equilibrium in a positive amount then Eq. (II.191) directly yields the activity of any its end-member. For instance, for the strontianite ($SrCO_3$) end-member in any solid solution at 25 ºC and 1 bar,

$$\log_{10} a_{\mathrm{Stront.},s} = \frac{1}{\ln 10}\left[u_{\mathrm{Sr}} + u_{\mathrm{C}} + 3u_{\mathrm{O}} - \left(-461.77\right)\right].$$

For a single-component (pure substance) phase, Eq. (II.191) yields instead the numerical value of the saturation index SI:

$$\Omega_{S,j} = \frac{1}{\ln 10}\left(\sum_i \mathrm{a}_{ij} u_i - \frac{g_j^{\circ}}{\mathrm{R}T}\right), \quad j \in L, \quad i \in N \tag{II.195}$$

To prove this statement, compare the definition of SI (Eq. (II.124)) with the definition of the dissolution reaction quotient for the BL ionic solid:

$$10^{\Omega_{S,BL}} = \frac{Q_{S,BL}}{K_{S,BL}} = \frac{\left(a_{B+} a_{L-}\right)}{K_{S,BL}} \tag{II.196}$$

Activities of aqueous ions are valid regardless of whether the pure solid is stable (present in positive amount in the mass balance) or not, and can always be found using Eq. (II.196):

$$\ln Q_{S,BL} = \left[u_{\mathrm{B}} + u_{\mathrm{Charge}} - \frac{g^{\circ}_{B+}}{\mathrm{R}T} \right] + \left[u_{\mathrm{L}} - u_{\mathrm{Charge}} - \frac{g^{\circ}_{L-}}{\mathrm{R}T} \right] = u_{\mathrm{B}} + u_{\mathrm{L}} - \frac{\left(g^{\circ}_{B+} + g^{o}_{L-} \right)}{\mathrm{R}T}$$

The solubility product $K_{S,BL}$ is defined as $\ln K_{S,BL} = -\left(g^{\circ}_{B+} + g^{\circ}_{L-} \right) \Big/ \left(\mathrm{R}T \right) + g^{\circ}_{s,BL} \Big/ \left(\mathrm{R}T \right)$. By substituting it and the above equation into Eq. (II.196), one obtains

$$\Omega_{\mathrm{S,BL}} = \frac{1}{\ln 10} \ln \left(Q_{S,BL} \Big/ K_{S,BL} \right) = \frac{1}{\ln 10} \left(u_B + u_L - g^{\circ}_{s,BL} \Big/ \mathrm{R}T \right),$$

the rightmost part of which has *exactly* the same form as Eq. (II.195), which is the proof (it can easily be repeated for any pure solid dissolution reaction). For example, the SI of barite ($BaSO_4$) as a pure phase at 25 ºC can be calculated as:

$$\Omega_{\mathrm{S,Barite}} = 1 \Big/ \ln 10 \left[u_{\mathrm{Ba}} + u_{\mathrm{S}} + 4u_{\mathrm{O}} - \left(-549.48 \right) \right]$$

In the above examples, the g° values were taken from the GEMS-PSI version of the Nagra-PSI database [2002HUM/BER].

For a pure phase at equilibrium, SI is (numerically) zero. In the GEM IPM algorithm, negative values of SI are always computed for unstable single-component solid phases eliminated from the mass balance; positive values can be obtained only for solids with the amount $n_j^{(x)}$ kinetically constrained from above (*cf.* [2001KAR/CHU]). Equation (II.195) applies also to stoichiometrically feasible single-component solids not included into the mass balance. Note that the DualTh Eq. (II.195) involves neither reactions nor ion activity and solubility products, as it would be required if the classic definition of SI (Eq. (II.124)) had been used.

II.1.2.4.3 Multiple solid solutions and miscibility gaps

The GEM method based on dual thermodynamics has a rigorous theoretical basis – the Karpov-Kuhn-Tucker necessary and sufficient conditions of minimum of the total Gibbs energy function and, hence, of chemical equilibrium speciation in a *multisystem*. The latter is understood [1997KAR/CHU] as a heterogeneous chemical system that can include simultaneously aqueous electrolyte, gas mixture, many mixtures with two or more end-members, and any number of stoichiometrically feasible pure substance phases. All multi-component phases may be non-ideal, and the total number of phases initially included in the mass balance may far exceed the number of phases predicted by the Gibbs' phase rule. A unique solution corresponding to the global minimum of total Gibbs energy function is ensured when all phases are ideal or moderately non-ideal. The GEM IPM algorithm can also find correct equilibrium speciation in highly non-ideal systems where the *miscibility gaps* (see Section II.1.1.4) are possible in some mixtures, although an adequate chemical system definition and a special automatic initial approximation are needed in such cases.

If the system bulk composition is such that the mixture is likely to exsolve into two phases, but only one such phase is included into the system definition, then an incorrect (metastable) solution of the equilibrium problem is *guaranteed* because the phase composition will be located in the two-phase region. Therefore, if a binary mixture has a miscibility gap, then the mixture must be thermodynamically represented by *two* binary solid solution phases. If a ternary mixture has a miscibility gap along one binary, then two ternary phases need to be included; and so on.

Two cases are now possible. (1) If the equilibrium composition of the mixture falls outside the miscibility gap then both solution phases will have the same composition (mole fractions of end-members) but different amounts, or one phase will disappear. (2) When the whole mixture composition falls into a miscibility gap, the GEM result may still be incorrect if both phases get the same composition after the automatic FIA. To avoid this, the following automatic FIA procedure must be used.

Suppose there is a binary mixture (*e.g.*, barite $BaSO_4$ and celestite $SrSO_4$) known to have a miscibility gap at low temperatures (see Figure II-9). Accordingly, two definitions of solid solution phases need to be inserted into the GEM model: "Ba–Celestite" and "Sr–Barite". Thermodynamic data for the end-members and the mixing models are identical. The only difference is that in the first phase definition, the $SrSO_4$ end-member must be marked as "major" and $BaSO_4$ as "junior", and in the second phase $SrSO_4$ end-member is marked as "junior" and $BaSO_4$ as "major". These declarations are used only to obtain a special automatic initial approximation before entering the main GEM IPM algorithm.

On entering the simplex procedure (see Figure II-7), large positive increments to standard g^o values (17 to 20 $kJ \cdot mol^{-1}$) will be assigned to all "junior" end-members in order to make them relatively unstable with respect to "major" end-members. As a result, both solid solution phases will enter the main GEM IPM iteration process having rather different compositions with "junior" end-members having very small mole fractions (at this point, the g^o increments are removed). In the final GEM result, the two phases will coexist with different (binodal) compositions if the whole mixture composition falls into the miscibility gap.

Note that there is still no way to reproduce spinodal compositions in GEM forward calculations, other than simulating them with a "less non-ideal" mixing model.

II.1.3 Methods of retrieval of stoichiometry, stability of solid solutions end-members, and parameters of non-ideal mixing (inverse modelling)

Inverse thermodynamic modelling can be performed when part of the output speciation vector or some functions of it are independently known (experimental fugacities, bulk compositions, concentrations of ions *etc*.), but part of the input data ($n^{(b)}$, T, p, g^{o}, parameters of mixing) are missing. The goal is to obtain (or refine) values of unknown or uncertain input parameters. At earlier times, the recognition of inverse problems has led to development of speciation codes such as FITEQL [1996HER/WES] using the least-squares algorithms. A pitfall of inverse modelling consists in that the results usually depend on the model assumptions [1970GRE]; many inverse problems are also ill-posed in mathematical sense.

The present contribution is focused on three specific cases related to Aq-SS systems:

1. Finding unknown activity coefficients f_j and/or interaction parameters of the non-ideal mixing model at known end-member stoichiometry and its solubility constant K_s or standard molar Gibbs energy G^{o}_{m};
2. Determination of unknown standard Gibbs energies G^{o}_{m} or solubility constants K_s of end-members using the known mole fractions and parameters of the mixing model;
3. Finding stoichiometry of a minor/trace end-member together with its apparent molar Gibbs energy G^{*}_{m} or solubility product K^{*}_{s} when neither G^{o}_{m} nor f_j are known separately.

The following text is tightly connected to both the theoretical Section II.1.2 and phenomenological Section II.1.1 and Chapter II.2. We will concentrate on a few methods that have been successfully used in all three variants or some of them in interpreting experimental data for low-temperature Aq-SS systems. Many of these retrieval methods use concentrations of the "salt" or ionic components of interest in coexisting aqueous and solid solution phases either in equilibrium (proximity to it must be demonstrated in co-precipitation or recrystallisation experiments) or at the minimum stoichiometric saturation (in the dissolution experiments). The electrochemical methods based on "chemical potentiometry" allow for a direct estimation of end-member chemical potentials and can be much more precise than any solubility methods.

II.1.3.1 The "activity ratios" technique

McCoy and Wallace [1956MCC/WAL] evaluated enthalpies and entropies of mixing in KCl–KBr solid solutions at 25 ºC from known solubilities of the pure salts and the solid solutions in water and measured activity coefficients in the saturated aqueous ternary systems. These authors have shown that the difference of chemical potential of KCl

(component 1) in the solid solution and in the pure solid is $\left(\mu_1 - \mu_1^{\circ}\right) = \mathrm{R}T\left(\ln a_1'' - \ln a_1'\right)$, where a_1'' is the activity of KCl in the aqueous phase saturated with solid solution ($a_1'' = a_{\mathrm{K}^+}'' \cdot a_{\mathrm{Cl}^-}''$), and a_1' is the activity of KCl in the aqueous phase saturated with pure KCl at the same temperature ($a_1' = a_{\mathrm{K}^+}' \cdot a_{\mathrm{Cl}^-}'$). In the same manner for KBr (component 2), $\left(\mu_2 - \mu_2^{\circ}\right) = \mathrm{R}T\left(\ln a_2'' - \ln a_2'\right)$. The molar Gibbs energy of mixing in the solid solution phase, $G_{\mathrm{m}}(\mathrm{mix}) = G_{\mathrm{m}}(SS) - G_{\mathrm{m}}^{\circ}$, now becomes (see also Eqs. 1 and 7 in [1996CHR]):

$$G_{\mathrm{m}}(\mathrm{mix}) = G_{\mathrm{m}}(SS) - \left(x_1\mu_1^{\circ} + x_2\mu_2^{\circ}\right) = \mathrm{R}T\left(x_1 \ln a_1 + x_2 \ln a_2\right) \qquad \text{(II.197)}$$

or

$$G_{\mathrm{m}}(\mathrm{mix}) = \mathrm{R}T\left[x_1\left(\ln a_1'' - \ln a_1'\right) + x_2\left(\ln a_2'' - \ln a_2'\right)\right] \qquad \text{(II.198)}$$

where x_1, x_2 are the mole fractions and a_1, a_2 are the activities of solid end-members. Eliminating $G_{\mathrm{m}}(\mathrm{mix})$ by combining Eqs. (II.197) and (II.198), one can find either the standard chemical potential μ_j° of one solid solution end-member, or the excess Gibbs energy of mixing G_{m}^E and then the interaction parameter(s), if mole fractions of end-members in solid solution x_j, dissolved molalities m_j, and molal mean aqueous activity coefficients $\gamma_j^{(aq)}$ of the components are known. For instance, in the case of a simple solid solution like K(Cl,Br), the molar excess Gibbs energy $G_{\mathrm{m}}^E = G_{\mathrm{m}}(\mathrm{mix}) - G_{\mathrm{m}}(\mathrm{id}) = \mathrm{R}T\left(x_1 \ln f_1 + x_2 \ln f_2\right)$ can be found as:

$$G_{\mathrm{m}}^E = \mathrm{R}T\left[x_1\left(\ln a_1'' - \ln a_1'\right) + x_2\left(\ln a_2'' - \ln a_2'\right)\right] - \mathrm{R}T\left(x_1 \ln x_1 + x_2 \ln x_2\right) \qquad \text{(II.199)}$$

Expressing activities in this equation through molalities ($m_1^2 = m_{\mathrm{K}^+} m_{\mathrm{Cl}^-}$) and mean activity coefficients ($\gamma_1^2 = \gamma_{\mathrm{K}^+}\gamma_{\mathrm{Cl}^-}$) of KCl (component 1) and KBr (component 2),

$$G_{\mathrm{m}}^E = \mathrm{R}T\left(x_1 \ln \frac{m_1'' m'' \gamma_1''^2}{m_1'^2 \gamma_1'^2} + x_2 \ln \frac{m_2'' m'' \gamma_2''^2}{m_2'^2 \gamma_2'^2}\right) - \mathrm{R}T\left(x_1 \ln x_1 + x_2 \ln x_2\right) \qquad \text{(II.200)}$$

where $m'' = m_1'' + m_2''$ is the total molality (also molality of the common cation K^+) in the ternary system. The interaction parameters can be obtained from the appropriate functional expression for G_{m}^E (Eq. (II.39)). For a single experiment, the regular parameter $W_G = \alpha_0 \mathrm{R}T$ can be simply calculated as $W_G = G_{\mathrm{m}}^E / x_1 x_2$. A more complex mixing model would require multiple experiments from which a set of G_{m}^E values can be estimated, and the interaction parameters can be regressed using the least squares techniques.

Equilibrium molalities of dissolved salts can be measured; mean aqueous activity coefficients can also be measured with isopiestic techniques, or can be calculated from individual ion activity coefficients obtained using the Debye-Hückel, Davies, SIT, Pitzer, or Extended UNIQUAC equations (see Section II.1.2.1). For highly soluble salt-water systems, the Pitzer equations have routinely been used ([1984HAR/MOL], [1990FIL/RUM], [1994CHR/PET]). When the activity coefficients are calculated, the results of using equations like (II.199) will depend on the applicability of the aqueous electrolyte model to the system of interest. For instance, the Debye-Hückel ion associa-

tion models can be used with reasonable accuracy up to 0.1 - 0.4 m effective ionic strengths. The SIT model can be used in simple electrolytes up to 3 m ionic strength. The most complex Pitzer model is applicable to mixed electrolytes of any ionic strength with a good accuracy. The same is expected to be true for the Extended UNIQUAC electrolyte model ([1997THO], [2005THO]) which has only binary interaction coefficients, the extensive database of which is not yet available. More detail can be found in Section II.1.2.1.3.

Calculations using Eq. (II.200) can be illustrated for the K(Cl,Br)-H_2O system using the data selected from Table I of [1956MCC/WAL]. The data which include mean aqueous activity coefficients of KCl and KBr determined from isopiestic measurements is presented in Table II-3. The calculations resulting from Eqs (II.198) and (II.199) with the estimated values of the regular parameter W_G and the end-member solubility products are given in Table II-4 and Table II-5, where it is seen that the estimated W_G values are higher for the first three x_1 values (at low KCl fractions in the solid) than for the remaining six x_1 values. The reason for this difference is not clear; perhaps, it is due to some asymmetry in the shape of excess energy; the experimental data may also have uncertainties, possible biases, *etc*., that may not be included in any reported measurement precision. Thus, the average and standard deviation were calculated also without the first four experimental points, yielding a smaller mean W_G = (3.3 ± 0.3) (2σ) kJ·mol^{-1} with much smaller standard deviation σ.

In the dimensionless scale, this value of Margules parameter corresponds to α_0 = (1.33 ± 0.12). The solubility products of end-members KCl and KBr can be taken right away from the ln a_1 and ln a_2 "pure solution" values in Table II-4.

Table II-3: Experimental data on Aq-SS partitioning of K(Cl,Br) at 25 ºC (from [1944FLA/BUR]), cited from Table I in [1956MCC/WAL].

$x_{1(KBr)}$	$x_{aq(KBr)}$	$m_{KCl} + m_{KBr}$	$\gamma_{\pm(KCl)}$	$\gamma_{\pm(KBr)}$
0	0	4.869	0.588	–
0.1	0.315	5.460	0.605	0.628
0.2	0.450	5.830	0.612	0.634
0.3	0.505	6.003	0.615	0.637
0.4	0.550	6.040	0.617	0.639
0.5	0.586	6.070	0.618	0.640
0.6	0.625	6.120	0.618	0.641
0.7	0.675	6.200	0.620	0.642
0.8	0.745	6.125	0.620	0.641
0.9	0.840	5.945	0.618	0.640
1	1	5.764	–	0.636

Table II-4: Calculations using Eqs. (II.199), (II.200) and data from Table II-3.

x_w	ln $a_{1(KCl)}$	ln $a_{2(KBr)}$	ΣΠ	G_m(mix)	G_m^E	W_G
0.9194	2.1037	–	8.1966	0	0	–
0.9104	2.2845	0.1619	10.996	–0.2007	0.6052	6.7248
0.9050	2.3208	1.0052	12.917	–0.3592	0.8813	5.5082
0.9024	2.2556	1.4786	13.927	–0.5691	0.9452	4.5011
0.9019	2.1202	1.7848	14.291	–0.7820	0.8864	3.6934
0.9014	1.9510	2.0210	14.582	–0.9046	0.8137	3.2547
0.9007	1.7443	2.2228	14.955	–0.9146	0.7538	3.1407
0.8995	1.4891	2.4061	15.523	–0.7904	0.7239	3.4473
0.9006	1.0592	2.5122	15.216	–0.6884	0.5521	3.4507
0.9033	0.3000	2.5672	14.379	–0.5163	0.2896	3.2179
0.9059	–	2.5981	13.439	0	0	–

Notes: x_w is the mole fraction of water in aqueous phase, $x_w = 55.5084/(55.5084 + m_{KCl}+m_{KBr})$; the Lippmann total solubility product ΣΠ is calculated as $\Sigma\Pi = a_1'' + a_2''$; G_m(mix) (in kJ·mol^{-1}) is calculated using Eqs. (II.200) and (II.198); G_m^E (in kJ·mol^{-1}) is calculated from Eq. (II.200).

Table II-5: Regular Margules parameter W_G (kJ·mol^{-1}) found from the last column of Table II-4.

$\langle W_G \rangle_9$	4.104
σ_9	1.25
$\langle W_G \rangle_5$	3.302
σ_5	0.14

Notes: $\langle W_G \rangle_9$ means the average and σ_9 the standard deviation over all nine values; $\langle W_G \rangle_5$ and σ_5 for the last five values (at $x_1 > 0.4$), respectively.

Experimental Lippmann total solubility products ΣΠ can be found simply by summing up the activities of KCl and KBr in aqueous solution. This follows from $\Sigma\Pi = \{K^+\}\left(\{Cl^-\} + \{Br^-\}\right)$ (Eq. (II.147) written for this system), or $\Sigma\Pi = \{K^+\}\{Cl^-\} + \{K^+\}\{Br^-\} = a''_{1(KCl)} + a''_{2(KBr)}$ using the definition of activity of a dissociated salt. Now, one can construct a Lippmann diagram presented on Figure II-16, which compares well with that given by [1990GLY/REA].

Figure II-16: Lippmann diagram plotted using data from Table II-4 (experimental ΣΠ values and $\log_{10}K_{KCl} = 0.914$; $\log_{10}K_{KBr} = 1.13$) and Table II-5 ($W_G = 3.3$ kJ mol^{-1}).

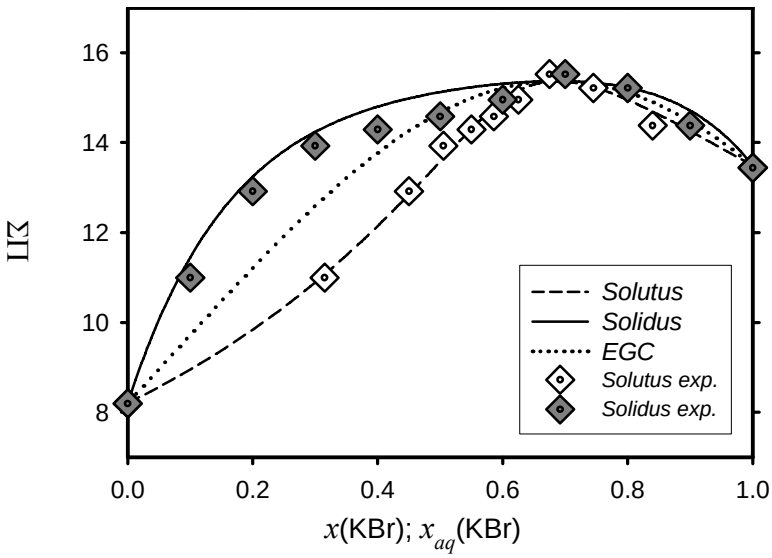

II.1.3.2 Dual Thermodynamic retrieval calculations

This method, described recently in [2004KUL/BER2], [2006KUL], can be considered as an extension and a generalisation of the "activity ratios" technique. The DualTh methods exploit the ability of modern GEM algorithms to compute the dual solution values u_i – the chemical potentials of stoichiometry units (see Section II.1.2.4, Eqs. (II.180), (II.182)) – in multiphase Aq-SS systems of any complexity. For a *j*–th solid solution end-member, the generic dual thermodynamic Equation (II.189) can be rearranged as:

$$\mu_j^{\circ} + \mathrm{R}T \ln f_j = \mu_j^{(u)} - \mathrm{R}T \ln x_j \qquad \text{(II.201)}$$

where $\mu_j^{\circ} = g_{j,T}^{\circ}$ is the standard molar Gibbs energy of the pure end-member, $\mu_j^{(u)} = \mathrm{R}T \sum_{i \in N} a_{ij} u_i$ is the dual chemical potential of end-member, f_j is its rational activity coefficient, and x_j is the (independently known) end-member mole fraction in the solid mixture phase.

The equilibrium criterion behind Eq. (II.201) is that the chemical potential of an independent component (element) is the same in the solid solution and the coexisting aqueous phase. Hence, the value $\mu_j^{(u)}$ can be obtained by solving a GEM speciation problem (Eq. (II.177)) only for the part of the system *without the solid solution of interest*, given that the bulk composition of that part is known or can be retrieved from ex-

perimental data. Then, one unknown parameter on the left-hand side of Eq. (II.201) can be immediately calculated. This idea (in a more formal notation) has been first expressed by Karpov *et al.* [2001KAR/CHU] and has already been used in several GEM applications ([2000KUL/KER], [2002KUL/KER], [2005CUR/KUL]).

II.1.3.2.1 Algorithm of the single DualTh calculation at equilibrium

The main DualTh criterion at equilibrium consists in the equality of chemical potentials of independent components in all coexisting phases. The DualTh calculation (in particular, for the Aq-SS system) can be performed using a simple algorithm, modified after [2001KAR/CHU]:

1. Define a *basis subsystem*, *i.e.*, a set L' of chemical species belonging to the aqueous phase and/or all other equilibrium phases with known g^o and activity coefficients γ for all components, but *excluding* any dependent components having these properties unknown.
2. Calculate the equilibrium state in the *basis subsystem only* from its known bulk composition $n'^{(b)}$ using the GEM algorithm to obtain the dual solution vector u' of chemical potentials of independent components.
3. Define a *non-basis subsystem*, *i.e.*, a set L^* of solid-solution end-members of interest with unknown g^o_j or f_j, $j \in L^*$, $n(L^*) \geq 1$.
4. From the known bulk composition $n^{(b)*}$ of the non-basis subsystem, calculate mole fractions $x_j, j \in L^*$ for all candidate end-member stoichiometries from the set L^*.
5. For each component from the non-basis subsystem: if its standard molar Gibbs energy g^o_j is known then use Eq. (II.202) to retrieve the activity coefficient f_j; if the activity coefficient f_j is known then use Eq. (II.206) to obtain a g^o_j estimate; and for a hypothetical trace end-member stoichiometry, use Eq. (II.209) to calculate the apparent molar Gibbs energy g^*_j.

Calculations at steps 4 and 5 are simple and can be done on a spreadsheet after computing all the basis subsystem equilibria at step 2 using the GEM code.

II.1.3.2.2 Retrieval of activity coefficients and mixing parameters

The DualTh equation for this case results from a rearrangement of Eq. (II.201):

$$\ln f_j = \frac{\left(\mu_j^{(u)} - g_j^o\right)}{RT} - \ln x_j \qquad \text{(II.202)}$$

It is implied that end-member stoichiometry and g^o_j value are known; the mole fraction x_j can be calculated from the known bulk composition of the solid solution; and the rational activity coefficient f_j is referenced to Raoult's law (*i.e.*, $f_j = 1$ when $a_j = x_j$). As shown in Section II.1.1, many solid solutions do not necessarily obey Raoult's law

even if there is no heat of mixing, no ordering effects, and the mixing of atoms on sublattices occurs randomly. For example, the clinoptilolite solid solution is expressed by (1) $Na_6Al_6Si_{30}O_{72}(H_2O)_{20}$ and (2) $K_6Al_6Si_{30}O_{72}(H_2O)_{20}$ end-members; for the statistically ideal mixing, $a_1 = x_1^6$ and $a_2 = x_2^6$ (see Eq. (II.35)).

These activity-composition relationships depend, in general, on how the stoichiometries of end-members are written. For implementation reasons, in computer-aided (GEM or LMA) solvers, the only kind of assumed ideal behaviour is Raoult's law ($a_j = x_j$), to which also Henry's law can be reduced by considering the "infinite dilution" activity coefficient term together with the standard chemical potential term (see Eq. (II.94)). Hence, in modelling Aq-SS chemical equilibria using the above clinoptilolite solid solution, the "activity coefficient value" calculated *e.g.*, from Eq. (II.202) will consist of two parts ($f_j = \lambda_j^{(id)} \cdot \lambda_j^{(E)}$): the formal "ideal mixing" part $\lambda_j^{(id)} = a_j^{(id)} / x_j = x_j^5$, and the "partial molar excess energy" part $\lambda_j^{(E)} = \exp\left(\overline{G}_j^E(x_j, x_{k\neq j}, \alpha)/\mathrm{R}T\right)$ where α stands for the necessary interaction parameters. Often, the formal activity coefficient $\lambda_j^{(id)}$ can be reduced to unity (Raoult's law) by an appropriate scaling of end-member stoichiometry (for the clinoptilolite example, by division by 6). This is not possible, however, for minerals like garnets with non-equal number of sublattice sites, for which complex activity-composition relationships must be directly accounted for *via* complex functions for activity coefficients and mixing energies (see Section II.1.1). For clarity, the discussion below will be restricted to Raoultian solid solution systems. Interpretation of ln f_j values estimated using Eq. (II.202) depends on the number of available experiments at different solid compositions, and on the non-ideal mixing model of choice (see Section II.1.1.4).

From one experiment in a binary solid solution-aqueous system (and two values of activity coefficients f_1 and f_2 estimated using Eq. (II.202)), the system of Eqs. (II.44) and (II.45) can be solved for the Margules parameters W_{12} and W_{21}:

$$W_{12} = \mathrm{R}T\left[\frac{2\ln f_2}{x_1} + \frac{\ln f_1}{x_2^2}\left(x_2 - x_1\right)\right];$$
$$W_{21} = \mathrm{R}T\left[\frac{2\ln f_1}{x_2} + \frac{\ln f_2}{x_1^2}\left(x_1 - x_2\right)\right] \qquad \text{(II.203)}$$

Clearly, if the calculated W_{12} and W_{21} values are similar, the regular binary mixing model can be used, with a parameter estimated as an average of values found from both activity coefficients:

$$\frac{W_G}{\mathrm{R}T} = \alpha_0 = \frac{1}{2}\left(\frac{\ln f_1}{x_2^2} + \frac{\ln f_2}{x_1^2}\right) \qquad \text{(II.204)}$$

Alternatively, the subregular Redlich-Kister interaction parameters can be found by solving together Eqs. (II.40), (II.41) truncated to the first two terms:

$$\alpha_0 = \frac{1}{2}\left[\frac{\ln f_1}{x_2^2}(3x_2 - x_1) + \frac{\ln f_2}{x_1^2}(3x_1 - x_2)\right];$$
$$\alpha_1 = \frac{1}{2}\left(\frac{\ln f_1}{x_2^2} - \frac{\ln f_2}{x_1^2}\right) \qquad \text{(II.205)}$$

From several $n(Q)$ experiments (indexed with q) performed at different solid phase compositions, it is possible to calculate the activity coefficient values $f_{j,q}$ using the DualTh Eq. (II.202) and then estimate the interaction parameters using the least squares fitting program. From activity coefficients estimated using Eq. (II.202), the molar excess Gibbs energy of mixing can be found:

$$G_{\mathrm{m}}^{E} = \mathrm{R}T\sum_j x_j \ln f_j \qquad \text{(II.206)}$$

From a single experiment, one (regular) mixing parameter for a binary solid solution can be calculated: $W_G = G_{\mathrm{m}}^{E} / x_1 x_2$. From several experiments, the interaction parameters can be regressed from G_{m}^{E} values for a particular model for excess Gibbs energy, *e.g.*, Eq. (II.39) or (II.42), using the least squares methods (see Section II.1.3.3 below).

II.1.3.2.3 Retrieval of end-member standard molar Gibbs energy and solubility product at equilibrium

The DualTh equation for this case is obtained by rearranging Eq. (II.201):

$$g_j^{\mathrm{o}} = \mu_j^{(u)} - \mathrm{R}T\left(\ln x_j + \ln f_j\right) \qquad \text{(II.207)}$$

This equation implies that the bulk composition (to calculate x_j) and the parameters of mixing model (to calculate f_j) of the solid solution phase are independently known. In some ionic structures (carbonates, sulphates), the binary non-ideality parameters can be semi-empirically predicted or estimated ([1980LIP], [2000BEC/FER], [2000GLY]). If the structure is ill-defined or it is not possible to estimate parameters of mixing from independent data then a formally ideal mixing model can still be applied. In any case, the stoichiometry of all end-members must be known or assumed for the calculation of x_j from the solid bulk composition. This may be a non-trivial task for a reciprocal solid solution [1978WOO/NIC].

The retrieved value of end-member g_j^{o} can be converted into a thermodynamic equilibrium constant, for instance (for a dissolution reaction) into a solubility product K_S, using the fundamental relation

$$\log_{10} K_S = -\,0.4343\,\frac{\Delta_{\mathrm{r}} G_{\mathrm{m}}^{\mathrm{o}}}{\mathrm{R}T} \qquad \text{(II.208)}$$

Other g^{o} values (of aqueous ions, complexes, gases or other solids) needed to compute $\Delta_{\mathrm{r}} G_{\mathrm{m}}^{\mathrm{o}}$ of reaction are available from thermodynamic data bases.

II.1.3.2.4 Retrieval of apparent molar Gibbs energy for a trace end-member

Incorporation of trace hazardous elements into solid solutions is an important geochemical topic from the waste management viewpoint. Especially in the case of heterovalent substitutions (*e.g.*, Eu^{III} in $CaCO_3$), the trace end-member may not exist as a pure solid substance; hence, a hypothetical stoichiometry of unknown stability may have to be tested. If the structural mechanism of incorporation is not known then the activity coefficient cannot be predicted. Although both parameters on the left-hand side of Eq. (II.201) may be unknown, their sum – the apparent molar Gibbs energy $g^*_{Tr} = g^\circ_{Tr} + \mathrm{R}T \ln f_{Tr}$ – can always be found as:

$$g^*_{Tr} = \mu^{(u)}_{Tr} - \mathrm{R}T \ln x_{Tr} \tag{II.209}$$

At trace mole fractions ($x_{Tr} < 10^{-3}$), the activity coefficient f_{Tr} can be taken as constant even in a strongly non-ideal mixing model. Therefore, the g^*_{Tr} estimate should have the same value if calculated from multiple experiments along the trace metal incorporation isotherm. The non-ideality does not change the isotherm slope, just shifts its position up or down relative to the "ideal" isotherm obtained at unity activity coefficients.

Why is the activity coefficient f_{Tr} approximately constant at trace mole fractions of the end-member? This can be checked, for instance, using Eqs. (II.44) and (II.45) where the mole fraction of major end-member (M or 1) is set to 0.999 and that of trace end-member Tr is set to 0.001:

$$\mathrm{R}T \ln f_M = \left(2W_{TrM} - W_{MTr}\right)\cdot 10^{-6} + 2\left(W_{MTr} - W_{TrM}\right)\cdot 10^{-9} \approx W_{TrM}\cdot 10^{-6}$$

$$\mathrm{R}T \ln f_{Tr} = \left(2W_{MTr} - W_{TrM}\right)\cdot 0.998 + 2\left(W_{TrM} - W_{MTr}\right)\cdot 0.997 \approx W_{TrM}$$

Here it was assumed that interaction parameters W_{TrM} and W_{MTr} are of the same order of magnitude ($W_{TrM} = W_{MTr}$ in the case of the regular mixing model) and that the absolute value of $W_{TrM}/(RT)$ or $W_{MTr}/(RT)$ does not exceed 10. The activity coefficient f_M of the major end-member is practically unity and that of the trace end-member f_{Tr} is (with a good precision) a constant equal to $\exp[W_{TrM}/(\mathrm{R}T)]$. Thus, at trace mole fractions, the analysis of non-ideal mixing becomes relatively simple, and the activity of a dilute end-member can be well approximated using Henry's law and the dilute solid solution model (see Eqs. (II.52) – (II.56)).

As an interesting alternative, especially in the case of heterovalent substitutions, the DQF formalism (see Eqs. (II.63) – (II.70)) can be used, if the stability and stoichiometry of trace end-member are independently known.

II.1.3.2.5 Dual-Th retrieval calculations at minimum stoichiometric saturation

At low temperatures, some crystalline solid solutions are known to dissolve in water (or in a background electrolyte) as solids of fixed composition. If the formation of secondary solid phases is kinetically inhibited, this congruent dissolution process slows down

to a metastable state of *minimum stoichiometric saturation* ([1985GAM], [1990GLY/REA], [1992KON/GAM], [2000GLY]), the relevance of which is still debated [2000GAM/KON]. Nevertheless, it seems that sparingly soluble solid solutions with similar end-member solubility products are prone to reaching the minimum stoichiometric saturation state at room temperatures and experimental times of about a week [1985GAM]. On a Lippmann diagram, the minimum stoichiometric saturation states fall to the "equal–G curve" EGC [1992KON/GAM], the criteria of which are (see also Eqs. (II.132) and (II.133) or Eqs. (II.141)): (i) the equality of end-member mole fractions

$$x_j^{(BS)} = x_j^{(NS)} = x_j; \tag{II.210}$$

and (ii) the equality of integral Gibbs energies of mixture in both solid and in aqueous phases

$$G_{\mathrm{m}}^{(NS)} = \sum_j \mu_j^{(NS)} x_j = G_{\mathrm{m}}^{(BS)} = \sum_j \mu_j^{(BS)} x_j \tag{II.211}$$

where the superscript $^{(NS)}$ denotes the value obtained for the non-basis subsystem (solid solution), and the superscript $^{(BS)}$ marks the value derived from the equilibrium in the basis subsystem (aqueous electrolyte) alone. There is no true equilibrium, thus chemical potentials of an independent component are not necessary equal in both parts of the system, and a separate value of $\mu_j^{(NS)}$ is not necessary equal to $\mu_j^{(BS)}$. The bulk composition of solid solution $^{(NS)}$ and, hence, the mole fractions of end-members x_j, are assumed to be experimentally known in all cases.

If the mixing model for the solid is known then the molar excess Gibbs energy can be calculated as function of end-member mole fractions, and Eq. (II.211) can be rearranged for estimating the g^o value of one k–th end-member:

$$g_k^{\mathrm{o}} = \frac{G_{\mathrm{m}}^{(BS)} - G_{\mathrm{m}}^{E}}{x_k} - \frac{\mathrm{R}T}{x_k} \sum_j x_j \ln x_j - \frac{1}{x_k} \sum_{j \neq k} x_j g_j^{\mathrm{o}} \tag{II.212}$$

The simplest cases are $G_{\mathrm{m}}^{E} = 0$ for the ideal mixing, and $G_{\mathrm{m}}^{E} = W_G x_1 x_2$ for the regular binary model.

In the much more usual case, the solubility products or the standard molar Gibbs energies of all solid solution end-members are known. The excess Gibbs energy of mixing can be retrieved by rearranging Eq. (II.211) as:

$$G_{\mathrm{m}}^{E} = G_{\mathrm{m}}^{(BS)} - \mathrm{R}T \sum_j x_j \ln x_j - \sum_j x_j g_j^{\mathrm{o}} \tag{II.213}$$

keeping in mind that

$$\sum_j x_j \mu_j = G_{\mathrm{m}} = G_{\mathrm{m}}^{\mathrm{o}} + G_{\mathrm{m}}^{Id} + G_{\mathrm{m}}^{E} = \sum_j x_j g_j^{\mathrm{o}} + \mathrm{R}T \sum_j x_j \ln x_j + \mathrm{R}T \sum_j x_j \ln f_j \,.$$

Further on, the interaction parameters can be found from the appropriate equations such as (II.39) or (II.44), using the least squares fitting if many solubility or partitioning experiments are available. The regular interaction parameter can be obtained even from a single experiment:

$$W_G = \frac{G^E_{\mathrm{m}}}{x_1 x_2} \tag{II.214}$$

although there is no way of assessing the uncertainty of such W_G estimate or even the adequacy of regular model to the solid mixture of interest. More complex mixing models would require application of least squares techniques to DualTh results from several experiments performed at different solid phase compositions.

II.1.3.2.6 Statistical Dual-Th calculations

As long as the aqueous thermodynamic model, regardless of its complexity, remains adequate for the (experimental) system, the GEM dual solution vector u can be applied to any set of possible solid solution end-member stoichiometries for computing their chemical potentials. Perhaps, this is the main advantage of DualTh calculations, which, in the case when many experiments at different solid phase compositions are available, can be enhanced by simple statistical procedures. The statistical DualTh method variant (described in detail in [2006KUL]), can select *optimal* end-member stoichiometries together with the standard molar Gibbs energies (or solubility products) and their uncertainty intervals.

Briefly, a statistical DualTh calculation can be done when several $n(Q)$ Aq-SS partitioning experiments have been performed at different solid phase compositions, and their results can be arranged into two input matrices: a matrix $B^{(\mathrm{BS})}$ composed of $n(Q)$ elemental bulk compositions of basis (aqueous) subsystems, and a matrix $B^{(\mathrm{NS})}$ composed of $n(Q)$ elemental bulk compositions of non-basis subsystems – solid solutions of interest. The $B^{(\mathrm{BS})}$ matrix is used only in GEM calculation of a $U^{(\mathrm{BS})}$ matrix containing dual-solution chemical potentials of elements for all $n(Q)$ experiments. The last part of input data consists in one or more $A^{(\mathrm{NS})}$ matrices containing the elemental stoichiometry of each of $n(M)$ end-member candidates that include all solid solution end-members (2 for binary, 3 for ternary *etc*.) plus some alternative stoichiometries of the end-member(s) of interest stability and stoichiometry of which must be determined.

From the $U^{(\mathrm{BS})}$ and $A^{(\mathrm{NS})}$ matrices, the dual chemical potential $\mu^{(u)}_{m,q}$ is computed for each m–th end-member candidate in each q–th experiment. From the $B^{(\mathrm{NS})}$ and $A^{(\mathrm{NS})}$ matrices, the mole fraction $x_{m,q}$ of m–th end-member candidate in q–th experiment is calculated (this may not be trivial for reciprocal solid solutions). Next, the above algorithm of single DualTh calculation in its appropriate variant is applied to each q–th experiment, resulting in one of the estimate matrices $G^{\mathrm{o}}_{NS} = \left\| g^{\mathrm{o}}_{qm} \right\|$ (standard molar Gibbs energies), $G^{*}_{NS} = \left\| g^{*}_{qm} \right\|$ (apparent molar Gibbs energies) or $W^{(r)}_{NS} = \left\| W_{qr} \right\|$ (mixing model interaction parameters). Rows in either matrix correspond to experiments, and columns to DualTh-estimated parameter values, which within a row are expected to be (almost) equal in the *optimal* case. From this idea, two simple statistical criteria follow immediately: the "optimal" end-member stoichiometry (or mixing model) must display (1) the smallest standard deviation σ and (2) no systematic trend within a column. If these cri-

teria are met for a given column, then the respective mean value of the parameter with 2σ uncertainty interval (and optionally the respective end-member stoichiometry) can be taken as a result of the whole statistical DualTh exercise.

There are some advantages of the inverse modelling DualTh methods over the estimation of G_m^E from equations like (II.200). It is the simplicity of DualTh determination of equilibrium chemical potential of a solid solution end-member using Eq. (II.177) which does not involve any aqueous molalities or activity coefficients directly. The DualTh equations do not depend on the complexity of the basis subsystem; the only requirement is that the underlying thermodynamic model is adequate for the system of interest. The parameterised non-basis subsystem can be included later into the GEM forward model for checking, forward modelling predictions, or sensitivity studies, if necessary.

II.1.3.2.7 Example: Eu^{III} in calcite

Trivalent europium, Eu^{III}, is a lanthanide element frequently used in laboratory studies as an analogue to Am^{III}, Cm^{III} and Pu^{III}, the safety-relevant actinides. It is known that the interaction of trace actinides or lanthanides with calcite rapidly produces dilute solid solutions, either through co-precipitation from an oversaturated solution, or through recrystallisation of preexisting calcite. This process may be complex for ions such as Eu^{3+} of charge different from that of Ca^{2+} (*heterovalent* substitution). In this case, the end-member stoichiometry is not trivial since formulae and structures of pure Eu-solids do not have much in common with calcite.

Statistical DualTh calculations can be helpful in determining the optimal stoichiometry and apparent standard molar Gibbs energy of Eu-containing end-member in the Eu-calcite solid solution (details are given in [2005CUR/KUL]). Only one data set (of three) is reproduced in Table II-6, namely, the data from co-precipitation experiments at $p_{CO_2} \approx 1$ bar and 25 ºC in Na-Ca-HCO_3-ClO_4 solutions of about 0.1 M electrolyte concentration and pH ~ 6, obtained from [2004LAK/STI]. From this data, using the Davies equation (II.110) and thermodynamic data from GEMS version of Nagra-PSI data base [2002HUM/BER], the dual elemental chemical potentials u_i, as described in Section II.1.2.4, (Table II-6) were calculated.

Four Eu solids exist, $Eu_2(CO_3)_3$, $EuOH(CO_3)$, $EuNa(CO_3)_2$, $Eu(OH)_3$, with known solubility products compiled in Table 5 in [2005CUR/KUL] (g°_{298} values given in Table II-7 below), from which the standard molar Gibbs energy of formation for the corresponding Eu end-members were calculated. Additionally, three hypothetical Eu end-member stoichiometries can be considered (Table II-7). For all seven end-member candidates, the DualTh calculations of apparent molar Gibbs energy have been performed using Eq. (II.209), with the results presented in Table II-7. This table also contains averages and standard deviations for each end-member stoichiometry together with standard molar Gibbs energy values of four known europium carbonate minerals.

DualTh values of molar Gibbs energy function for $CaCO_3$ (or $2CaCO_3$, $3CaCO_3$) end-members are not listed in Table II-7 because in all cases they were close to the standard molar Gibbs energy of pure calcite (– 1129.2 kJ·mol^{-1}) to within 0.05 kJ·mol^{-1}.

Table II-6: Final Eu molalities (m_{Eu}) and calculated Eu cationic mole fractions (χ_{Eu}) in calcite overgrowths precipitated at p_{CO_2} ≈1 bar and 25 ºC, together with dual chemical potentials.

exp. #	$\log_{10} m_{Eu}$	$\log_{10} \chi_{Eu}$	u_{Eu}	u_{Na}	u_C	u_O	u_H	u_{Ca}
3n	– 9.37	– 4.17	– 345.7	– 138.4	– 139.9	– 9.6	– 43.0	– 286.8
4n	– 9.96	– 5.18	– 347.7	– 138.4	– 140.9	– 9.1	– 43.3	– 287.3
5n	– 9.26	– 4.10	– 346.0	– 138.3	– 140.7	– 9.2	– 43.2	– 287.2
6n	– 9.03	– 4.29	– 345.5	– 138.4	– 140.8	– 9.1	– 43.3	– 287.3
7n	– 9.82	– 4.94	– 347.3	– 138.4	– 140.8	– 9.2	– 43.3	– 287.3
8s	– 9.27	– 4.64	– 345.9	– 137.6	– 140.5	– 9.3	– 43.2	– 287.1
9s	– 9.39	– 4.68	– 346.2	– 137.7	– 140.6	– 9.3	– 43.2	– 287.1
10n	– 9.18	– 4.23	– 346.0	– 138.4	– 141.0	– 9.1	– 43.3	– 287.3
11n	– 8.82	– 3.92	– 345.3	– 138.5	– 141.2	– 9.0	– 43.4	– 287.4
12s	– 8.18	– 3.23	– 344.0	– 138.5	– 141.4	– 8.9	– 43.4	– 287.6
13s	– 9.37	– 4.60	– 346.0	– 137.4	– 140.4	– 9.4	– 43.2	– 287.0
14s	– 9.08	– 4.19	– 345.4	– 137.5	– 140.5	– 9.3	– 43.2	– 287.1
15s	– 8.54	– 3.80	– 344.1	– 137.5	– 140.3	– 9.4	– 43.2	– 287.0
16s	– 8.89	– 4.10	– 345.0	– 137.6	– 140.5	– 9.3	– 43.2	– 287.1
17s	– 8.32	– 3.53	– 343.6	– 137.5	– 140.3	– 9.4	– 43.2	– 287.0
18s	– 8.85	– 4.13	– 345.6	– 138.5	– 141.5	– 8.8	– 43.4	– 287.6
19s	– 8.33	– 3.42	– 344.5	– 138.5	– 141.5	– 8.8	– 43.4	– 287.6
20s	– 8.16	– 3.41	– 344.1	– 138.5	– 141.5	– 8.8	– 43.5	– 287.6
21s	– 8.96	– 4.14	– 346.0	– 138.5	– 141.5	– 8.8	– 43.4	– 287.6
22s	– 8.55	– 3.83	– 344.9	– 138.2	– 141.5	– 8.8	– 43.5	– 287.6
23s	– 9.53	– 4.54	– 347.3	– 138.3	– 141.5	– 8.8	– 43.4	– 287.6

Note: respective dual elemental chemical potentials u_i (dimensionless) were calculated using GEM--Selektor for basis (aquatic) subsystems. Data from Table 3 of [2005CUR/KUL], with correction of a cut and paste error for experiments 21s, 22s and 23s.

Inspection of Table II-7 reveals that the largest standard deviation is computed for the $Eu_2(CO_3)_3$ end-member stoichiometry. In addition, there is a correlation between the g^*_{298} estimate and the mole fraction of Eu. These facts point to the violation of both statistical DualTh criteria, so this Eu end-member must be discarded.

Table II-7: Apparent molar Gibbs energies (g^{*}_{298}) estimated for seven Eu end-member candidates using Eq. (II.209) from dual elemental chemical potentials given in Table II-6.

exp.#	g^{o}_{298} for candidate Eu end-members (kJ·mol^{-1})						
	$Eu_2(CO_3)_3$	$EuOH(CO_3)$	$EuNa(CO_3)_2$	$Eu(OH)_3$	$EuH(CO_3)_2$	$EuO(OH)$	$EuO(CO_3)_{0.5}$
12s	– 2937.3	– 1380.3	– 2012.1	– 1223.1	– 1776.4	– 985.9	– 1064.5
20s	– 2935.9	– 1379.1	– 2010.7	– 1221.9	– 1775.2	– 984.7	– 1063.3
19s	– 2937.8	– 1380.1	– 2011.7	– 1222.9	– 1776.2	– 985.7	– 1064.3
17s	– 2937.5	– 1379.6	– 2009.7	– 1222.4	– 1775.7	– 985.2	– 1063.8
15s	– 2938.2	– 1379.2	– 2009.1	– 1222.0	– 1775.3	– 984.8	– 1063.4
22s	– 2937.8	– 1378.9	– 2009.7	– 1221.6	– 1775.0	– 984.5	– 1063.1
11n	– 2940.7	– 1380.0	– 2012.0	– 1222.8	– 1776.1	– 985.6	– 1064.2
5n	– 2944.6	– 1381.5	– 2013.4	– 1224.3	– 1777.6	– 987.1	– 1065.7
16s	– 2940.5	– 1379.4	– 2009.5	– 1222.2	– 1775.6	– 985.1	– 1063.7
18s	– 2939.7	– 1379.0	– 2010.7	– 1221.8	– 1775.1	– 984.6	– 1063.2
21s	– 2941.3	– 1379.7	– 2011.3	– 1222.5	– 1775.8	– 985.3	– 1063.9
3n	– 2945.4	– 1381.7	– 2014.2	– 1224.5	– 1777.8	– 987.3	– 1065.9
14s	– 2942.1	– 1380.0	– 2009.9	– 1222.8	– 1776.1	– 985.6	– 1064.2
10n	– 2942.9	– 1380.3	– 2012.1	– 1223.0	– 1776.4	– 985.9	– 1064.5
6n	– 2940.8	– 1379.1	– 2010.9	– 1221.9	– 1775.2	– 984.7	– 1063.3
23s	– 2945.2	– 1380.5	– 2011.8	– 1223.3	– 1776.6	– 986.1	– 1064.7
13s	– 2943.0	– 1379.3	– 2009.1	– 1222.1	– 1775.4	– 984.9	– 1063.5
8s	– 2941.8	– 1378.5	– 2008.7	– 1221.3	– 1774.6	– 984.1	– 1062.7
9s	– 2942.8	– 1379.0	– 2009.2	– 1221.8	– 1775.1	– 984.6	– 1063.2
7n	– 2946.2	– 1379.9	– 2011.7	– 1222.7	– 1776.0	– 985.5	– 1064.1
4n	– 2946.4	– 1379.3	– 2011.2	– 1222.1	– 1775.4	– 984.9	– 1063.5
mean $\pm\sigma$	– (2941.3 ± 3.2)	– (1379.7 ± 0.8)	– (2010.9 ± 1.5)	– (1221.5 ± 0.8)	– (1775.8 0.8)	– (985.3 ± 0.8)	– (1063.9 ± 0.8)
g^{o}_{298} $\pm\sigma$	– (2932.7 ± 1.7)	– (1383.6 ± 0.6)	– (2009.2 ± 4.0)	– (1201.0 ± 1.7)	n.d.	n.d.	n.d.

Mean and standard deviation values from Table 8 of [2005CUR/KUL], with corrections according to those in Table II-6

Values of g^{o}_{298} (kJ·mol^{-1}) were calculated from published solubility products given in Table 5 of [2005CUR/KUL].

n.d. means "no data available".

The next stoichiometry, $EuOHCO_3$, yielded a reasonable standard deviation and the g^{*}_{298} value 4.6 kJ·mol^{-1} more positive than the g^{o}_{298} of the corresponding pure phase. This difference would correspond to the regular interaction parameter α_0 = 4.6/2.479 = 1.856 – quite in the range reported for carbonate solid solutions. Unfortunately, the DualTh values for this stoichiometry obtained for two other experimental data sets are quite different, and this end-member candidate had to be discarded. The $EuNa(CO_3)_2$ end-member candidate produced the g^{*}_{298} value almost the same as that for the respective pure mineral, formally a good choice, but it also had been discarded be-

cause of the absence of convincing evidence on Na incorporation in calcite coupled with Eu uptake [2005CUR/KUL].

The $Eu(OH)_3$ end-member stoichiometry leads to an estimated g^*_{298} value which is 20.7 kJ·mol^{-1} more negative than the solubility product of Eu hydroxide. If the difference is attributed to non-ideality of mixing, it would correspond to the value of Redlich-Kister parameter equal to $\alpha = -8.35$, quite unusual for carbonate systems where positive excess Gibbs energies of mixing prevail. It is concluded that $Eu(OH)_3$ is not suitable as end-member to describe this set of experimental data.

Three remaining stoichiometries (Table II-7) which are not known to exist as pure solids show relatively small DualTh statistical scatter and no regular trend (perhaps, the last candidate $EuO(CO_3)_{0.5}$ is worse than two others). Thus, it is not possible to select one of two stoichiometries as optimal without considering other experimental data sets. This comparison [2005CUR/KUL] shows that the DualTh estimates for $EuH(CO_3)_2$ is almost the same for the pH~6 and pH~8 data sets but that for the pH~13 data set is more than 120 kJ·mol^{-1} different. The DualTh estimate for EuO(OH) or $Eu(OH)_3$ is very much the same for the pH~13 and pH~8 data sets but about 28 kJ·mol^{-1} different for the pH~6 data set (Table II-8).

Table II-8: Mean end-member standard Gibbs energies of formation g^o_{298} (kJ·mol^{-1}) derived from Dual-Th calculations for the three considered datasets (from [2005CUR/KUL]), with corrections according to those in Table II-6 and Table II-7.

Stoichiometry	pH~6	pH~8	pH~13
$Eu_2(CO_3)_3$	– (2941.3 ± 3.2)	– (2921.8 ± 1.4)	– (3106.6 ± 6.0)
$EuOHCO_3$	– (1379.7 ± 0.8)	– (1364.1 ± 1.0)	– (1425.5 ±1.7)
$EuNa(CO_3)_2$	– (2010.9 ± 1.5)	– (1994.5 ± 1.0)	– (2088.8 ± 1.7)
$Eu(OH)_3$	– (1222.5 ± 0.8)	– (1192.5 ± 1.0)	– (1193.3 ± 1.7)
$EuH(CO_3)_2$	**– (1775.8 ± 0.8)**	**– (1774.6 ± 1.0)**	– (1896.6 ± 1.7)
EuO(OH)	– (985.3 ± 0.8)	**– (955.3 ± 1.0)**	**– (956.1 ± 1.7)**
$EuO(CO_3)_{0.5}$	– (1063.9 ± 0.8)	– (1041.0 ± 1.0)	– (1072.2 ± 1.7)

Figure II-17: Experimental results (symbols) compared with predicted isotherms (lines) based on the same ternary $EuH(CO_3)_2$-$EuO(OH)$-$CaCO_3$ ideal solid solution model with g°_{298} values of −1773, −995, and −1129.2 kJ·mol^{-1}, respectively [2005CUR/KUL]. χ_{Eu} denotes the cationic fraction of europium in Eu-calcite. Horizontal lines define the solubility limits set by pure Eu-solids under the relevant experimental conditions.

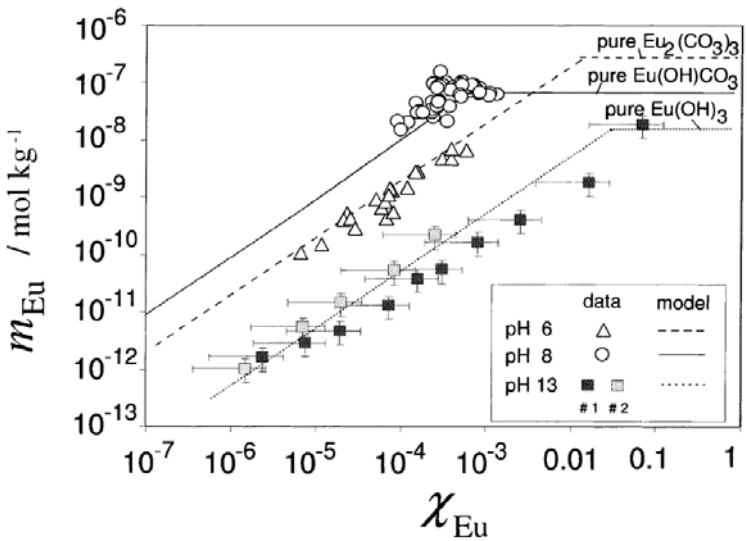

No plausible single end-member stoichiometry and apparent molar Gibbs energy was able to describe the uptake of Eu in all three series of experiments. Thus, it was concluded that two Eu end-members $EuH(CO_3)_2$ and $EuO(OH)$ must be considered together with calcite in a ternary "quasi-ideal" solid solution model which describes well all three experimental data sets (Figure II-17). Modeled equilibria for the pH ~8 data include the Eu-calcite ternary phase, in which both Eu end-members are present in approximately equal mole fractions. At the conditions of pH ~6 data, the mole fraction of $EuO(OH)$ end-member is very small, while at the conditions of pH ~13 data, the $EuH(CO_3)_2$ end-member is almost absent from the model Eu-calcite solid solution phase.

II.1.3.3 Graphical fitting and regression methods

The straightforward way of retrieving model parameters consists in plotting predicted model curves against the experimental values of a chosen property of the Aq-SS system. The goodness of fit is estimated visually; if necessary, the input model parameter value is adjusted and the whole operation (a series of model calculations, plotting) is repeated.

Lippmann diagrams are particularly easy and convenient to perform this kind of fitting in aqueous-binary solid solution systems if both end-members are present in the solid phase in non-trace mole fractions. As seen on Figure II-16, the regular parameter value around 3 kJ·mol^{-1} could be easily found also by means of graphical fitting. At trace end-member concentrations, the fitting with isotherm plots (like Figure II-17) is, perhaps, more convenient, at least if the trace end-member (apparent) solubility product must be retrieved. The model isotherm line(s) should be computed from the thermodynamic Aq-SS model that includes also the solid solution of interest.

A drawback of graphical fitting is that there is no formal (numerical) criterion of the goodness of fit as in data regression methods or in computer programs like FITEQL [1996HER/WES]. However, visual estimation of the quality of fit is still useful because different "weights" are heuristically assigned to different parts of the plot and outlying points are usually taken with less "weight" into consideration. However, possibilities of graphical fitting of more than one input parameter simultaneously are rather limited; in this case, least squares methods seem to be preferable.

II.1.3.3.1 Weighted least-squares and Bayesian estimation techniques

Statistical least-squares methods (LSM, *e.g.*, [1978BOX/HUN]) called also "data regression" methods can yield robust estimates of *e.g.*, interaction parameters, if a sufficient number of Aq-SS experimental points at different compositions are available. In general, such methods minimise the (scalar) error function

$$E(p) = \left[f(p) - y\right]^T C_y^{-1} \left[f(p) - y\right] \tag{II.215}$$

where y is a vector of experimental data (*e.g.*, $n(Q)$ distribution coefficients or excess Gibbs energy $G^E_{m,q}$ values), p is a vector of $n(M)$ adjustable parameters (*e.g.*, Redlich-Kister or Margules parameters), and C_y is the covariance matrix of the experimental data vector y. The inverse C_y^{-1} of C_y equals the weighting matrix.

Königsberger [1991KON] has suggested an improved "Bayesian least squares" technique of thermodynamic parameter estimation, also implemented as a subroutine in the ChemSage modeling code [1995KON/ERI]. In this technique, the objective function $E(p)$ consists of two parts: (1) the difference between the predicted and experimental data (Eq. (II.215)), and (2) the difference between estimated (p) and *a priori* parameter values (p^o):

$$E(p) = \left[f(p) - y\right]^T C_y^{-1} \left[f(p) - y\right] + \left[p - p^o\right]^T C_{p^o}^{-1} \left[p - p^o\right] \tag{II.216}$$

where $C_{p^o}^{-1}$ equals the weighting matrix for the *a priori* parameters vector. In this way, the user is able to weight the two parts of the deviation function $E(p)$ differently, depending on whether more confidence is put on the experimental data or on the inherent model properties that can often be independently estimated or predicted. The *a priori* uncertainties can also improve the convergence of numerical least-squares methods, especially when parameters of different magnitude are adjusted simultaneously.

Due to a quick progress of the atomistic modelling of mixing in solid solution structures ([2000BEC/FER], [2002BEC/POL]), more predicted parameters can be collected into the *a priori* vector (Eq. (II.216)). This points to a potential importance of Bayesian estimation approach, which can also be applied to the results of DualTh retrieval of solid solution parameters, thus enhancing the quality of "statistical" DualTh techniques. However, the effect of advanced regression methods applied to solubility data on (sparingly soluble) Aq-SS systems is often marred by the scarcity of experimental points at different solid compositions and their large uncertainty that usually limits the solid solution model to the regular formalism. In contrast to that, the electrochemical potentiometry methods can yield much more precise data that can be fitted to subregular or more complex mixing models (see below).

II.1.3.4 Retrieval of excess Gibbs energy from electrochemical measurements

The difference between the chemical potentials of pure solid and its solid solution with another end-member in (metastable) equilibrium with aqueous solutions of the same ionic strength and with the same atmospheres can be determined using emf measurements in parallel in two or three electrochemical cells ([1990KON/GAM], [1994ROC/CAS], [1998MCB/ROC]). Such experiments yield results that are much more precise than any results of "classic" solubility measurements (Section II.2.2), which has been demonstrated for the (Mn,Co)CO_3-aqueous system by Königsberger and Gamsjäeger [1990KON/GAM] and for the (Ca,Cd)CO_3-aqueous system by Rock *et al.* [1994ROC/CAS] and McBeath *et al.* [1998MCB/ROC]. The latter paper also contains a detailed description of the experimental setup with measured, intermediate and final calculated data. As these authors claimed, when applicable, the "double cell" method has several advantages over conventional solubility measurements:

1. It provides direct thermodynamic data rather than that derived from small differences between large numbers.
2. The precision of the measured cell voltages for reversible double cells is in the range of ± 0.05 to 0.50 mV, which makes the method sufficiently sensitive to detect small changes in the Gibbs energies.
3. Calculation of the Gibbs energies does not require a model for speciation of solutes in complex mixtures.
4. No correction for a liquid-liquid junction potential is required as the cell does not bring two different electrolyte solutions into direct contact.
5. The reversibility of the cell reaction can be established reliably. Finally, slow incongruent dissolution of $Ca_xCd_{1-x}CO_3$(s) to yield $CdCO_3$(s) does not necessarily invalidate the double-cell results because pure otavite is necessary to the electrode junction ([1994ROC/CAS], [1998MCB/ROC]).

As an example of retrieval, let us consider the electrochemical "potentiometer" setup for measuring excess Gibbs energies in Co–Mn mixed carbonates at stoichiometric saturation with aqueous $CoCl_2$, $MgCl_2$ solutions and the $0.8H_2$ $0.2CO_2$ atmosphere at 1 bar and 323.15 K [1990KON/GAM]. In their work, the following three cells were used:

$$\mathrm{Pt|H_2(g,}\,p_{\mathrm{H_2}}\mathrm{);CO_2(g,}\,p_{\mathrm{CO_2}}\mathrm{)|CoCl_2(aq,}m\mathrm{)|CoCO_3(s)|AgCl|Ag} \quad \text{(A)}$$

$$\mathrm{Pt|H_2(g,}\,p_{\mathrm{H_2}}\mathrm{);CO_2(g,}\,p_{\mathrm{CO_2}}\mathrm{)|CoCl_2(aq,}(1-x)m\mathrm{);MnCl_2(aq,}xm\mathrm{)|Co_{1-}}_x\mathrm{Mn}_x\mathrm{CO_3(s)|AgCl|Ag} \quad \text{(B)}$$

$$\mathrm{Pt|H_2(g,}\,p_{\mathrm{H_2}}\mathrm{);CO_2(g,}\,p_{\mathrm{CO_2}}\mathrm{)|MnCl_2(aq,}m\mathrm{)|MnCO_3(s)|AgCl|Ag} \quad \text{(C)}$$

As seen from the schemes A, B and C, the pure and mixed solid carbonates were equilibrated with H_2-CO_2 gas mixtures of the same composition and aqueous chloride solutions of the same total molality. In addition, the mole fractions $x = [Mn^{2+}]/([Co^{2+}]+[Mn^{2+}])$ were the same in the solid and aqueous phases. The measured emf of cells are related to the reaction

$$\mathrm{H_2(g) + 2AgCl(s) \rightleftharpoons 2H^+(aq) + 2Cl^-(aq) + 2Ag(s)} \quad \text{(II.217)}$$

with the respective pH determined by the reaction

$$\mathrm{Co_{1-}}_x\mathrm{Mn}_x\mathrm{CO_3(s) + 2H^+(aq) \rightleftharpoons (1-x)Co^{2+}(aq) + xMn^{2+}(aq) + H_2O(l) + CO_2(g)} \quad \text{(II.218)}$$

where $x = 0$ in the cell A and $x = 1$ in the cell C. This leads to the mass action law equation (braces denote activities)

$$\{\mathrm{H^+}\}^2 = \frac{\left(\{\mathrm{Co^{2+}}\} + \{\mathrm{Mn^{2+}}\}\right) p_{\mathrm{CO_2}}}{\Sigma K_{\mathrm{Co_{1-}}_x\mathrm{Mn}_x\mathrm{CO_3}}} \quad \text{(II.219)}$$

which contains the (Lippmann) total solubility constant $\Sigma K_{\mathrm{Co_{1-}}_x\mathrm{Mn}_x\mathrm{CO_3}}$ defined as:

$$\Sigma K_{\mathrm{Co_{1-}}_x\mathrm{Mn}_x\mathrm{CO_3}} = \left(\{\mathrm{Co^{2+}}\} + \{\mathrm{Mn^{2+}}\}\right) \cdot \{\mathrm{CO_3^{2-}}\} \quad \text{(II.220)}$$

(identical in form with Eq. (II.147)). At $x = 0$ and $x = 1$, Eq. (II.220) turns into solubility products of pure $CoCO_3$(s) and $MnCO_3$(s), respectively.

The measured emf difference

$$\Delta E = E_B - (1-x)E_A - xE_C \quad \text{(II.221)}$$

depends on $\{H^+\}$ as

$$2\mathrm{F}\Delta E = -\mathrm{R}T[\ln\{\mathrm{H^+}\}_B^2 - (1-x)\ln\{\mathrm{H^+}\}_A^2 - x\ln\{\mathrm{H^+}\}_C^2] \quad \text{(II.222)}$$

(F is the Faraday's constant) because pH_2 is equal in all three cells and $\ln\{\mathrm{Cl^-}\}_B - (1-x)\ln\{\mathrm{Cl^-}\}_A - x\ln\{\mathrm{Cl^-}\}_C \approx 0$. Inserting Eq. (II.219) into Eq. (II.222) results in

$$2\mathrm{F}\Delta E = \mathrm{R}T[\ln\Sigma K_{\mathrm{Co_{1-}}_x\mathrm{Mn}_x\mathrm{CO_3}} - (1-x)\ln K_{\mathrm{CoCO_3}} - x\ln K_{\mathrm{MnCO_3}}] \quad \text{(II.223)}$$

The right-hand side of Eq. (II.223) is the molar excess Gibbs energy G_m^E expressed through the Lippmann total solubility product (see Eq. (II.149)). Therefore,

$$G_m^E = 2F\Delta E \qquad \text{(II.224)}$$

[1990KON/GAM]. This equation has an advantage that it does not contain solubility products of the pure end-members, and the emf difference is directly measurable with good precision. The measured data are given in Table II-9. When $G_m^E / x(1-x)$ is calculated from Eq. (II.224) and plotted *vs.* x (the mole fraction of $MnCO_3$), the data fall on a straight line (Figure II-18). It is seen on this plot that the data obtained from conventional dissolution experiments ([1985GAM]) show a much larger scatter around a mean value which does not seem to depend on x. Thus, solubility data can be explained simply by a regular mixing model:

$$G_m^E = x(1-x)\cdot A_0$$

where A_0 = (3.4 ± 1.6) kJ·mol^{-1}. However, measurements with galvanic cells as chemical potentiometer (Table II-9) show a rather small scatter, and the regression slope on Figure II-18 suggests the subregular mixing:

$$G_m^E = x(1-x)\cdot[A_0 + A_1(2x-1)] \qquad \text{(II.225)}$$

Regressed parameters are A_0 = (3.74 ± 0.04) kJ·mol^{-1} and A_1 = – (0.72 ± 0.07) kJ·mol^{-1}. The huge difference in precision of data obtained by conventional solubility and galvanic cells measurements is also clearly seen on the Lippmann diagram on Figure II-19 which has a shape identical with that of the example diagram shown on Figure II-7.

Table II-9: Measured ΔE values and calculated G_m^E values for the $Co_{1-x}Mn_xCO_3$ solid solutions (data from Table 3 of [1990KON/GAM]).

x (Mn)	ΔE (mV)	G_m^E (kJ·mol^{-1})	$G_m^E / x(1-x)$ (kJ·mol^{-1})	$\ln \Sigma^* K_{p,s,0}$
0.391	4.53	0.874	3.67	17.03
0.391	4.65	0.898	3.77	17.04
0.391	4.96	0.957	4.02	17.06
0.880	1.71	0.329	3.12	17.02
0.880	1.78	0.343	3.25	17.03
0.093	1.81	0.349	4.14	16.72
0.093	1.98	0.383	4.54	16.74
0.093	1.94	0.375	4.44	16.73
0.807	2.74	0.530	3.40	17.07
0.807	2.68	0.517	3.32	17.06
0.727	3.34	0.645	3.25	17.08
0.851	2.18	0.421	3.32	17.05

Note: concentration solubility constants $\Sigma^* K_{p,s,0}$ [1985GAM] refer to the reaction (II.218). They are related to total solubility constants (Eq. II.200) as $\ln \Sigma^* K_{p,s,0} = \ln 10 (\log_{10} \Sigma K_{Co_{1-x}Mn_xCO_3} + 17.24)$ (see Table II-2).

Figure II-18: $G_m^E / x(1-x)$ *vs.* $x(MnCO_3)$ of the system $Co_{1-x}Mn_xCO_3$. Circles, results from measurements with galvanic cells; solid line, linear regression analysis leading to values A_0 and A_1 in Eq. (II.225); crosses, results from conventional solubility measurements, dashed and dotted lines correspond to mean value and standard deviation of conventional data (from [1990KON/GAM]).

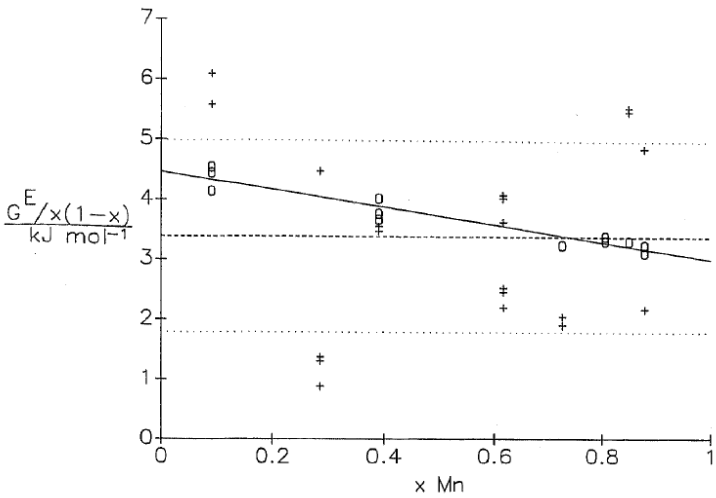

II.1.3.5 Estimation of interaction parameters from the position of miscibility gaps

Field or laboratory observations of compositional limits in coexisting solid solution phases (*e.g.*, carbonates, sulphates) can be recast into positions of miscibility gaps, spinodal gaps, critical points (see more in Section II.1.1) and interpreted in terms of excess energies of mixing and interaction parameters [2000GLY] even when direct solubility data are not available. The respective calculations for quasi-binary Aq-SS systems can be done with help of the MBSSAS code [1991GLY]. The code can compute regular or subregular Redlich-Kister, Guggenheim or Thompson-Waldbaum (Margules) parameters from (1) miscibility (binodal) gap data, (2) spinodal-gap data, (3) critical temperature and critical mole fraction data, *etc*.

Figure II-19: Solid-solute phase diagram of Co-Mn carbonates at 323 K. Circles, results from measurements with galvanic cells (Table II-9); crosses, results from conventional solubility measurements; solid line, equal–G curve; dashed lines, solidus (upper) and solutus (lower) representing thermodynamic equilibrium (from [1990KON/GAM]).

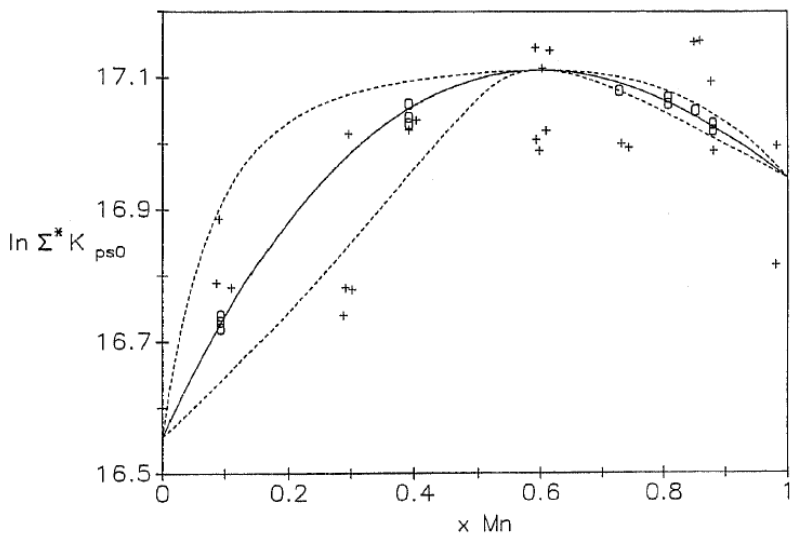

II.1.3.5.1 Miscibility gap data

Let the mole fractions $x_{BL,1}$ and $x_{BL,2}$ (or $x_{CL,1}$ and $x_{CL,2}$) define the compositional boundaries of a binodal miscibility gap. If Redlich-Kister parameters α_0 and α_1 are known (one of those must be positive), the position of miscibility gap (*i.e.*, $x_{BL,1}$ and $x_{BL,2}$) can be found from direct calculation of equilibrium using the GEM algorithm (see Section II.1.2.4) also in ternary, quaternary and higher order solid solution-aqueous systems. For binary solid solution, the MBSSAS code calculates the miscibility gap boundaries by iteratively solving the following set of transcendental equations:

$$\frac{x_{BL,1}}{x_{BL,2}} = \exp[\alpha_0\left(x_{CL,2}^2 - x_{CL,1}^2\right) + \alpha_1\left(3\left(x_{CL,2}^2 - x_{CL,1}^2\right) - 4\left(x_{CL,2}^3 - x_{CL,1}^3\right)\right)] \qquad \text{(II.226)}$$

$$\frac{x_{CL,1}}{x_{CL,2}} = \exp[\alpha_0\left(x_{BL,2}^2 - x_{BL,1}^2\right) + \alpha_1\left(3\left(x_{BL,2}^2 - x_{BL,1}^2\right) - 4\left(x_{BL,2}^3 - x_{BL,1}^3\right)\right)] \qquad \text{(II.227)}$$

In the MBSSAS code, the above set of equations are also optionally solved for interaction parameters, if the binodal boundaries (*e.g.*, $x_{BL,1}$ and $x_{BL,2}$) are given. These calculations are conditional on the prior determination of a spinodal gap [1991GLY]

which defines the boundary between intrinsically unstable solid solution compositions and metastable compositions (see Section II.1.1). In the MBSSAS code, the presence of spinodal gap is tested using the condition

$$\frac{\partial^2 G_{\mathrm{m}}^{M}}{\partial x_{BL}^2} = 0 \tag{II.228}$$

where $G_{\mathrm{m}}^{M} = G_{\mathrm{m}}^{Id} + G_{\mathrm{m}}^{E}$ is the molar Gibbs energy of mixing ($G_{\mathrm{m}}^{Id} = \mathrm{R}T\left(x_{BL}\ln x_{BL} + x_{CL}\ln x_{CL}\right)$). Substituting the subregular Redlich-Kister expression for G_{m}^{E} (Eq. (II.39)) and differentiating leads to the following equation to be solved numerically:

$$-12\alpha_1 x_{BL}^3 + \left(18\alpha_1 - 2\alpha_0\right)x_{BL}^2 + \left(2\alpha_0 - 6\alpha_1\right)x_{BL} - 1 = 0 \tag{II.229}$$

If Redlich-Kister parameters α_0 and α_1 are known then x_{BL} determining the position of spinodal gap can be calculated. Optionally, the MBSSAS code computes the parameters α_0 and α_1 by solving Eq. (II.229) as expressed at each of the two spinodal compositions [1991GLY].

As seen above, miscibility limits as observed from mineralogical compositions can be used to estimate interaction parameters in the absence of more accurate laboratory data. However, this approach has several drawbacks. The maximum mole fraction of trace component found may be smaller than the binodal gap fraction. In this case, if the solid solution is stable, the calculated excess energy will be overestimated. Conversely, if the analyzed "limiting" composition really represents a mechanical mixture rather than a solid solution mineral, the excess Gibbs energy may be underestimated. If the mineral was formed at much higher temperatures than the temperature of interest and if the mineral is unreactive at lower temperature then the maximum solid-solution mole fraction observed may be metastable or even unstable. The temperature of formation may not be known; if a lower temperature is assumed, the excess energy will be underestimated. A partial solid solution series may not be isomorphous, *i.e.*, end-members may not have the same structure (see Section II.1.1). In that case, the excess energy parameters must be estimated only on one side of the miscibility gap; on the other side, a different model will apply. Alternatively, the DQF formalism (Eqs. (II.63)-(II.70)) can be used.Yet, the mixing parameters estimated from the miscibility gap data are an improvement over the assumption of the Raoultian ideal mixing. One should keep in mind that such estimates have large uncertainty. Glynn [2000GLY] does not recommend estimating interaction parameters from spinodal gap compositions because of difficulties in distinguishing between intrinsically unstable and metastable solid solution compositions, especially in low-temperature systems.

II.1.3.5.2 Critical mixing-point data

Critical mixing-point data can also be used to calculate the non-ideality of a solid-solution series. The critical temperature of mixing, T_c, refers to the lowest possible tem-

perature at which a complete solid solution series may form. In a regular binary solid solution series, a miscibility gap at $x_{BA,c} = 0.5$ can only occur if $\alpha_0 > 2$. The following relation can be derived ([1980LIP], [2000GLY]):

$$\alpha_0 = 2\frac{T_c}{T} \tag{II.230}$$

where T is the current temperature. Thus, the regular interaction parameter can be calculated from Eq. (II.230) as a first approximation. If the critical mole fraction of mixing $x_{BL,c}$ is known then two Redlich-Kister or Margules subregular parameters can be calculated. Because of the usual lack of excess entropy and excess enthalpy data, such calculations commonly assume that the molar Gibbs energy of mixing decreases with increasing temperature because of the increase in the TS_m^{Id}, the ideal entropy of mixing term. At the critical temperature of mixing, this term becomes sufficiently large to overcome the positive ΔH_m term, and the miscibility gap disappears.

In a binary solid solution, at a critical temperature of mixing, two general relations must apply [1986GUG]:

$$\frac{\partial^2 G_m^E}{\partial x_{BL,c}^2} = \frac{-RT_c}{x_{BL,c}\left(1-x_{BL,c}\right)} \tag{II.231}$$

$$\frac{\partial^3 G_m^E}{\partial x_{BL,c}^3} = \frac{-RT_c\left(2x_{BL,c}-1\right)}{x_{BL,c}^2\left(1-x_{BL,c}\right)^2} \tag{II.232}$$

Substituting the second and third derivatives of the Guggenheim subregular excess Gibbs energy function (II.39) with parameters $A_0 = RT_c\alpha_0$ and $A_1 = RT_c\alpha_1$ results in the following equations:

$$\frac{-RT_c}{x_{BL,c}\left(1-x_{BL,c}\right)} = -12A_1x_{BL,c} + 6A_1 - 2A_0 \tag{II.233}$$

$$\frac{-RT_c\left(2x_{BL,c}-1\right)}{x_{BL,c}^2\left(1-x_{BL,c}\right)^2} = -12A_1 \tag{II.234}$$

Solving those yields the critical mole fraction and the critical temperature [1991GLY]:

$$x_{BL,c} = 0.5 + \frac{-A_0 + \sqrt{A_0^2 + 27A_1^2}}{18A_1} \tag{II.235}$$

$$T_c = \frac{1}{R}\left(12A_1x_{BL,c} - 6A_1 + 2A_0\right)x_{BL,c}\left(1-x_{BL,c}\right) \tag{II.236}$$

Conversely, the Guggenheim interaction parameters A_0 and A_1 can be found from the critical temperature and mole fraction [1991GLY] by solving Eq. (II.234) for A_1

$$A_1 = \frac{RT_c\left(2x_{BL,c}-1\right)}{12x_{BL,c}^2\left(1-x_{BL,c}\right)^2} \tag{II.237}$$

and substituting it into Eq. (II.233) to find A_0:

$$A_0 = \frac{RT_c}{2x_{BL,c}\left(1-x_{BL,c}\right)} - \frac{A_1}{3}\left(2x_{BL,c}-1\right) \tag{II.238}$$

For the regular mixing model, the above two equations reduce to $x_{BL,c} = 0.5$, $A_1 = 0$ and $A_0 = 2RT_c$.

As noted by Glynn [1991GLY], the MBSSAS calculations based on equations (II.233) to (II.238) depend on a questionable assumption that the Guggenheim parameters A_0 and A_1 do not vary as a function of temperature. This is equivalent to the assumption that the Redlich-Kister parameters α_0 and α_1 vary inversely with temperature. An estimate of the maximum possible α_0 value for ionic crystals can be obtained by using the highest temperature of melting of ionic solids (1700 ºC for alkaline-earth carbonates and sulphates) for the critical temperature. This maximum value $\alpha_0 \approx 13$–14 leads to a minimum binodal mole fraction of about 10^{-6}, which agrees with the observation that the purest chemical reagents are at best 99.999% pure [2000GLY].

II.1.3.6 Estimation of interaction parameters from distribution coefficients

This method has been used *e.g.*, by Glynn [1990GLY] to determine the excess Gibbs energy parameters for the Ag(Cl,Br)-aqueous system, and by Glynn and Reardon [1990GLY/REA] to confirm the known value of α_0 for the (Ca,Zn)CO_3-aqueous system. The estimation of excess Gibbs energy parameters from distribution coefficients was used also by Glynn *et a.l* [1992GLY/REA] for the Na(Cl,Br) system and by Glynn and Reardon [1992GLY/REA2] for the K(Cl,Br) system. For binary systems, the related calculations are also implemented in the MBSSAS code (Glynn 1991) which uses the definition of distribution coefficient in Eq. (II.154), as follows. Substituting the equations for solid activity coefficients f_{BL} and f_{CL} using the Guggenheim subregular model (Eqs. (II.39)) at two known different solid compositions $x_{BA,1}$ and $x_{BA,2}$ results in two equations:

$$D_1 = \frac{K_{CA}}{K_{BA}}\exp[\left(2x_{BA,1}-1\right)\alpha_0 + \left(6\left(x_{BA,1}^2 - x_{BA,1}\right)+1\right)\alpha_1] \tag{II.239}$$

$$D_2 = \frac{K_{CA}}{K_{BA}}\exp[\left(2x_{BA,2}-1\right)\alpha_0 + \left(6\left(x_{BA,2}^2 - x_{BA,2}\right)+1\right)\alpha_1] \tag{II.240}$$

which can be solved for the α_0 and α_1 parameters using known values of distribution coefficients D_1 and D_2.

There are two drawbacks of this approach. (1) The ratio of the ionic component activities in the coexisting aqueous (or non-aqueous) phase must be known to calculate distribution coefficients (compare with the "activity ratios technique", Section II.1.3.1), and (2) the measured distribution coefficients must represent the thermodynamic equilibrium between aqueous and solid phases [2000GLY]. The latter is often difficult to prove, especially with respect to carbonate systems where the partitioning may strongly depend on precipitation/recrystallisation rates [1981LOR], [1998RIM/BAL], [1999CUR].

II.2 Experimental and analytical aspects

The theoretical background of the thermodynamics of Aq-SS systems is well established (see Section II.1.1), and advanced numerical methods have been developed to describe such systems quantitatively (see Sections II.1.2, II.1.3). However, applying these concepts successfully to *real world* problems requires actual thermodynamic data as a baseline for geochemical modelling. Such thermodynamic data can be obtained either from laboratory experiments with synthetic compounds or from analysis of naturally occurring solid solution phases. Here, the focus will be on how to derive thermodynamic data from co-precipitation experiments using synthetic systems at relatively low (waste repository relevant) temperature $T < 373$ K. There will be some emphasis on high temperature synthesis as well as on samples from natural systems.

Characterising the aqueous solution and the solid phase on a molecular level is a prerequisite for deriving thermodynamic data. It is also crucial to prove that a Aq-SS system represents equilibrium conditions. Furthermore, synthesising solid solution phases from aqueous solution involve various pitfalls which need to be identified before one starts to interpret experimentally obtained data in terms of Aq-SS thermodynamics. Therefore, the intention of this chapter is to provide a critical overview of analytical techniques which are typically used to characterise the aqueous solution and the solid solution phase and how one obtains baseline/raw (*i.e.*, molecular level information) data for the thermodynamic description of such a system. First of all, synthesis procedures as well as some fundamental aspects of co-precipitation experiments in aqueous solution will be discussed. Special emphasis will be made on radionuclides/actinides in the trace level concentration range.

Throughout this chapter, the formation of simple binary solid solutions (B,C)A in aqueous solution will be described in terms of a distribution coefficient:

$$D = \frac{x_{BA} / x_{CA}}{\{B^+\} / \{C^+\}} \qquad \text{(II.241)}$$

where $\{B^+\}$ and $\{C^+\}$ are the aqueous activities and x_{BA} and x_{CA} are the mole fractions BA and CA in the solid. This is not the same as partitioning coefficient k_D used in pres-

entation of experimental data, which has the same form as D but total dissolved concentration $[B^+]$, $[C^+]$ instead of activities as in Eq. (II.241).

II.2.1 Co-precipitation experiments in aqueous solution

Synthesising solid solution compounds from aqueous solution is ultimately linked to fundamental aspects of crystal growth and the experimental procedure. Although with respect to the NEA TDB project one is ultimately interested in thermodynamic data (which are independent of the reaction path), co-precipitation experiments are usually done in a supersaturated non-equilibrium system. Therefore, it is important to demonstrate that experimentally obtained data from such an experiment on element partitioning from aqueous solution into a solid solution phase represent equilibrium conditions.

In the following, various complications will be outlined, which may obscure experimental data on Aq-SS systems. Most of these complications are related to kinetic aspects of co-precipitation experiments at repository relevant temperatures. They arise from the fundamental problem that one wants to derive thermodynamic data on Aq-SS equilibria from supersaturated systems which are not in equilibrium (otherwise the solid solution phase would not form). However, it is NOT intended to include kinetics into the NEA TDB solid solution Guidelines. Nevertheless, experimental data need to be evaluated critically!

II.2.1.1 Limitations and points to notice

(1) One key aspect of co-precipitation is related to a solution-boundary-layer process during mineral precipitation in aqueous solution [1998RIM/BAL]: dissolved species have to be transported from the bulk solution to the mineral surface, where they attach/adsorb to certain surface sites and eventually become part of the crystal structure. In case of a rather static solution (without mechanical mixing/stirring) the compounds will reach the growing mineral surface *via* diffusion. If the mineral precipitation rate is faster compared to the diffusion rate, the solution adjacent to the mineral surface will become depleted in the species that become incorporated into the growing crystal. As a consequence, a concentration gradient will evolve and the chemical composition of the bulk solution, which is usually analysed, differs from the chemical composition of the solution in contact with the growing mineral surface.

Applying this concept to co-precipitation, it is obvious that the ratio of the involved species in the solution in contact with the growing mineral surface might change depending on their diffusion coefficients and the actual distribution coefficient. In case the co-precipitation rate is higher than the diffusion rate of the involved species, as well as their diffusion coefficients, the analysed bulk solution does not represent the solution in contact with the mineral surface, in particular, with respect to the activity ratio $\{B^+\}/\{C^+\}$. This effect is the more pronounced the larger the precipitation rate and the larger or smaller the distribution coefficient is.

(2) Another process also affects co-precipitation even when one can establish an experimental setup where radionuclide uptake is surface reaction controlled (thus excluding diffusion control). Mineral precipitation in aqueous solution is driven by the chemical potential gradient, and this is, of course, in principle also true for co-precipitation experiments. However, at high precipitation rates, dissolved species might become incorporated into a growing mineral due to physical trapping rather than chemical coordination [2001WAN/XU]: adsorbed radionuclides can become overgrown before they desorb, depending on their adsorption/desorption behaviour and the precipitation dynamics on a growing mineral surface (*e.g.*, kink site formation). Near-equilibrium distribution coefficients can be significantly higher (*e.g.*, Mn^{2+}/calcite) or lower (*e.g.*, Sr^{2+}/calcite) than 1 [1999CUR], [1998RIM/BAL]. In both cases, at high precipitation rates the distribution coefficients tend to increase/decrease towards 1. Various studies have shown that the distribution coefficient can change by 1 or 2 orders of magnitude due to this kinetic trapping effect.

Since the incorporation of radionuclides at high precipitation rates is entirely controlled by kinetic trapping, the composition of the precipitated compound may even have an intermediate composition that lies within the mixing gap. In such a case, the composition cannot be used to derive for example Margules or Guggenheim or other parameters, or in dual thermodynamic calculations

(3) Closely linked to these two kinetic effects on co-precipitation is the chemical homogeneity of synthesised solid solution phases. Compositional zoning is a common phenomenon in natural, as well as synthetic compounds, precipitated in the presence of a radionuclide (or a trace metal).

Within a single crystal, internal chemical heterogeneities can define sector zones. **Sector zoning** is linked to differential trace component uptake as a consequence of preferential incorporation at specific surface sites on a growing mineral face ([1992FOU/REE], [1990PAQ/REE], [1995PAQ/REE]). Ultimately, the mineral surface structure controls the incorporation of the trace component. Sector zoning is a macroscopic evidence for non-equilibrium conditions. It occurs under low or moderate degree of supersaturation below the roughening transition (without heterogeneous nucleation). Treating sector-zoned minerals as homogeneous phases yields only an average value which cannot be used to derive thermodynamic data.

Many natural and synthetic minerals exhibit **oscillatory zoning**, with their chemical composition varying along a core-to-rim profile [2002LHE/JAM], [1997PRI/FER], [1993PRI/PUT], [1992PUT/FER]. Such spatio-temporal patterns arise by self-organisation. Non-linear couplings of the parameters affecting diffusion controlled mineral precipitation in aqueous solution can result in self-organised patterns. Again, such minerals are not chemically homogeneous and cannot be used to derive thermodynamic data. However, the surface of such zoned minerals can be in equilibrium with the adjacent aqueous solution.

(4) Co-precipitation experiments are usually performed in more or less supersaturated aqueous solutions. In addition to the solid solution phase of interest, other phases may also simultaneously precipitate. Depending on the crystallinity, particle size, *etc*. of such an additional phase and the analytical effort, as well as the detection limit of the used methods (see Section II.2.3), one might overlook the presence of certain phases. However, the radionuclide of interest might have a high affinity to that phase. Quite often, co-precipitation experiments are being performed without studying the precipitated solid in detail. In fact, the solid composition is derived from the compositional changes of the aqueous solution assuming that a homogeneous solid has formed. The precipitation of an unidentified phase may cause experimental data to be misinterpreted with respect to Aq-SS thermodynamics.

(5) Precipitation experiments in supersaturated solutions may involve the formation of metastable precursor phases. The solid phase of interest will form after a solid state phase transformation or dissolution/reprecipitation processes. Of course, this holds also true for co-precipitation experiments. In fact, the presence of radionuclides may even favour the formation of the precursor phases. A very prominent example is the precipitation of calcite ($CaCO_3$) and its potential precursor phase vaterite [2000WOL/KON]. The transformation of vaterite into calcite occurs at room temperature within hours. As a consequence, one would not necessarily detect that vaterite had occurred in a co-precipitation experiment. The distribution coefficient as determined from the composition of the aqueous phase and the composition of the calcite would be controlled by a number of parameters other than the thermodynamics of calcite: The interaction of the radionuclide of interest with vaterite during co-precipitation, and the behaviour of the radionuclide during the vaterite/calcite phase transformation. Another prominent example represents goethite/hematite and its precursor phase ferrihydrite. In contrast to the $CaCO_3$ system, ferrihydrite can be kept metastable at room temperature.

(6) In addition to these experimental aspects under non-equilibrium conditions, there seems to be a consensus that once a solid solution has been co-precipitated with a certain atomistic configuration, there is no possible reconfiguration *via* solid state diffusion possible, in order to achieve a configuration that represents equilibrium. Kinetic effects such as phase homogeneity, exsolution, compositional zoning, *etc*. as outlined above will be kept frozen at temperature conditions of interest here (< 100 ºC).

However, over time such non-equilibrium Aq-SS systems will evolve towards equilibrium —at least with respect to the surface *via* dissolution/reprecipitation processes. Depending on the reactivity of the solid phase, this might take quite long (considering typical timescales for laboratory studies). Without a doubt, thermodynamic equilibrium with a homogeneous solid phase is for many systems difficult to achieve at room temperature conditions. However, this approach requires that the entire mineral surface is homogeneous —at least within the topmost monolayer in contact with the aqueous solution.

Various co-precipitation techniques have been established to synthesise solid solution phases in aqueous solution. With the above potential complications outlined, the synthesis procedures will be critically discussed.

II.2.1.1.1 Synthesis procedures

(1) Probably, the most common way to synthesise solid solution phases is by simple ***batch type*** experiments. At least two different solutions containing the required species will be mixed, thus producing a supersaturated solution with respect to the solid solution of interest. For example, in co-precipitation experiments with calcite as one endmember, one would start with one solution containing $CaCl_2$ and possible the radionuclide of interest. A second solution will be prepared with, *e.g.*, $NaHCO_3$. The solubility of $CaCl_2$ and $NaHCO_3$ is significantly higher than of $CaCO_3$, therefore, upon mixing these two solutions, one produces a supersaturated solution with respect to calcite. With such an experimental setup, one starts with a high degree of supersaturation. Finally, such an Aq-SS system will develop towards equilibrium, and the surface of the synthesised material may be in equilibrium with the aqueous solution. However, the co-precipitated solid phase will be chemically zoned in the case if the distribution coefficient is be not 1.

Similarly, quite often, solid compounds (*e.g.*, $CaCl_2$, $NaHCO_3$ and a radionuclide of interest in case one wants to synthesise calcite-based phases) are added to an aqueous solution, where they dissolve and a supersaturated solution with respect to calcite will evolve. Such a setup has been quite often used in hydrothermal reaction vessels, since it can be used in a closed system. However, the degree of supersaturation is controlled by the balance of dissolution of the initial compounds and the co-precipitation of the solid solution phase. Again, with such a setup, the solid solution phase might be chemically zoned, with the surface potentially in equilibrium with the aqueous phase.

These two types of experiments include homogeneous/heterogeneous nucleation of the solid solution phase (which requires a high degree of supersaturation). In order to avoid nucleation, one can perform such experiments with a suspension of seed crystals, thus inducing crystal growth/co-precipitation. Introducing such seed crystal requires a careful characterisation of their surfaces. The presence of impurities should be excluded. Also, it should be ensured that one does not use freshly ground particles, because such particles tend to interact strongly with almost any species in the aqueous solution due to high energy surface sites. These high energy sites are generated at crystal surfaces due to the mechanical stress during grinding (surface defects). Preconditioning of such crystals in an aqueous solution with similar chemical composition being used in the actual co-precipitation experiment is a good strategy to remove these surface high energy sites.

A typical feature of these kinds of experiments is the fact that the chemical composition of the aqueous solution will change during the synthesis procedure as a consequence of the co-precipitation process. The solid solution phases may be chemically zoned.

(2) This drawback can be overcome by ***batch type constant composition methods*** where one monitors compositional changes in the aqueous solution and adds a sufficient amount of required reactants in order to keep the chemical composition of the aqueous phase constant. Compositional changes in the aqueous phase are typically measured in real-time *via* a pH electrode (in case co-precipitation involves a change in pH), ion selective electrodes or even simple conductivity measurements.

A potential drawback of these types of experiments is that one has to add the required compounds drop-wise in form of small amounts of high concentrated solutions in order to keep the volume in the reaction vessel almost constant. However, adding a high concentrated solution into the reaction vessel might induce *e.g.*, nucleation processes rending the experiment temporarily not well controlled.

(3) Another elegant way of synthesising solid solution phases is by ***counter diffusion experiments*** [1997PRI/FER], [1993PRI/PUT]. A U-tube is filled with a porous medium such as a silica gel and the two ends of the U-tube are filled with two solutions. The species in the two reservoirs will diffuse through the porous medium towards each other, and precipitation occurs when a supersaturated solution has developed. With such a setup, co-precipitation is controlled by diffusion. It has been demonstrated that the solution composition in the pore space can be determined. However, it is not clear to what extend the silica gel affects the presence of dissolved species (either by complexation in solution or surface adsorption).

(4) Many of the drawbacks involved in the above mentioned techniques can be overcome by performing co-precipitation experiment in a ***mixed flow reactor***. A reaction vessel is fed by three or more independent solution reservoirs, containing the required species for co-precipitation. The reactor contains a suspension which is stirred with a suspended stirring bar. One can prove experimentally that the stirring rate is sufficient for surface reaction- controlled co-precipitation (thus excluding diffusion). Since the suspension in the reactor is constantly fed by the reservoirs at a constant rate, the chemical composition of the aqueous solution in the reactor remains constant. Under these conditions the surfaces of the seed crystals will be conditioned and steady state conditions will evolve. This setup can also be adapted to hydrothermal conditions ($t >$ 100 ºC).

This experimental procedure ensures that homogeneous solid solution phases can be synthesised in aqueous solution at repository relevant temperatures. Also, distribution coefficients can be obtained under well defined experimental conditions and, in particular, kinetic effects can be studied systematically. The precipitation rates can be made small.

With respect to experimental studies on Aq-SS systems it seems crucial that one understands the involved reaction mechanisms that occur throughout an experiment on a molecular level. In particular, when working under low (room) temperature conditions in aqueous systems, kinetic effects, the formation of precursor phases and metastability effects have to be critically taken into account and ruled out before treating experimental results as thermodynamic data. Ultimately, it depends on what kind of further experiments will be done with the co-precipitated solid solution phases.

II.2.2 Solubility measurements in aqueous solutions

Aq-SS equilibria can be approached experimentally by means of solubility measurements. In contrast to solubility measurements of pure compounds (end-members), solubility measurements of solid solution phases are more complex and potentially involve a number of experimental pitfalls. In this section, three solubility concepts for Aq-SS systems will be introduced and discussed for a simple binary Aq-SS system (B,C)L – *e.g.*, $(Ba,Sr)SO_4$, Barite-Celestite:

(1) Thermodynamic equilibrium

(2) Primary saturation

(3) Stoichiometric saturation .

As introduced in Chapter II.1.2, the Lippmann theory provides a straightforward thermodynamic description of binary Aq-SS systems based on the total solubility product ΣΠ [1990GLY/REA] (see also Eq. (II.147)):

$$\Sigma\Pi = \{L^-\}\left(\{B^+\} + \{C^+\}\right) \tag{II.242}$$

where $\{L^-\}$, $\{B^+\}$ and $\{C^+\}$ are the activities of L^-, B^+ and C^+ in the aqueous solution. For a solid solution in equilibrium with an aqueous solution, the solid phase is described by the solidus equation (Eq. (II.148)):

$$\Sigma\Pi_{eq} = K_{BL} x_{BL} f_{BL} + K_{CL} x_{CL} f_{CL} \,, \tag{II.243}$$

K_{BL}, K_{CL} are the solubility products of the end-members, x_{BL}, x_{CL} are the mole fractions and f_{BL} and f_{CL} are the activity coefficients of the solid phase. Similarly, the aqueous phase (in equilibrium with the solid solution phase) is described by the solutus equation (II.150):

$$\Sigma\Pi_{eq} = \frac{1}{\dfrac{x_{B,aq}}{K_{BL} f_{BL}} + \dfrac{x_{C,aq}}{K_{CL} f_{CL}}} \tag{II.244}$$

where $x_{B,aq} = \{B^+\}/(\{B^+\}+\{C^+\})$ and $x_{C,aq} = \{C^+\}/\{B^+\}+\{C^+\})$ are the mole fraction B^+ and C^+ in the aqueous solution.

II.2.2.1 Thermodynamic equilibrium solubility

An aqueous solution with a total solubility product ΣΠ as defined by the solutus equation is in thermodynamic equilibrium with a solid solution phase with a composition that gives the same ΣΠ following the solidus equation. In case of the (Ba,Sr)SO_4-H_2O system as shown in Figure II-20, an aqueous solution with a composition defined by an aqueous mole fraction $X_{Ba,aq}$ of 0.10000 (point P1, Figure II-20) and a ΣΠ of 1.07×10^{-9} is in equilibrium with a solid solution phase with a mole fraction x_{Barite} of 0.99948.(point P2, Figure II-20). An aqueous solution in thermodynamic equilibrium with respect to a solid solution will be undersaturated with respect to both/all end-members.

Figure II-20: Lippmann diagram for the (Ba,Sr)SO_4-H_2O system: $\log_{10}K_{sp}(BaSO_4)$ = – 9.97; $\log_{10}K_{sp}(SrSO_4)$ = – 6.63 and a_0 = 2.0 (after [2000GLY]).

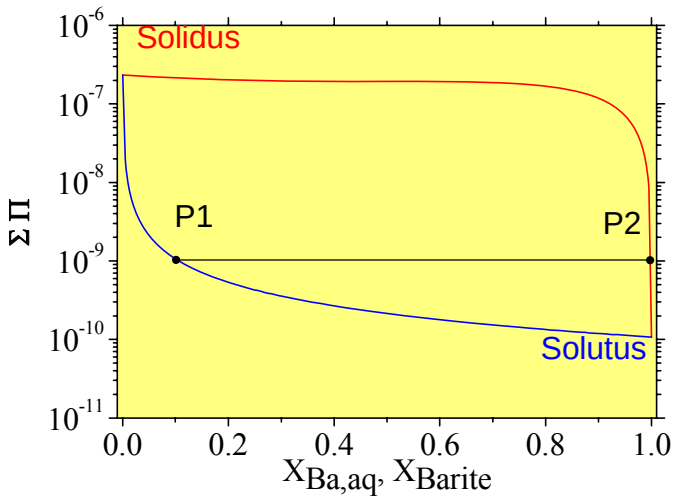

From an experimental point of view, one would add a homogeneous solid solution phase to an aqueous solution with an initial ΣΠ = 0. Under these conditions and if the solid solution phase dissolves congruently (stoichiometrically), $x_{Ba,aq}$ will be equal to x_{Barite} of the dissolving solid solution. However, many complex minerals, such as silicates, do not dissolve congruently, *i.e.*, secondary phases may form during such dissolution experiments and the macroscopically obtained element release will be apparently non-congruent. Without these complications, congruent dissolution will proceed until ΣΠ of the aqueous solution reaches the solutus line (Figure II-21). As soon as the solutus curve is reached, a new solid solution phase with a different composition than that of

the dissolving phase will precipitate according to the thermodynamic equilibrium as defined by the solutus and solidus equation (Figure II-20, point P1 and P2). This situation is called the primary saturation state [1978GAR/WOL], [1990GLY/REA] with a value of ΣΠ given by:

$$\Sigma\Pi_{ps} = \frac{1}{\frac{x_{BL}\, f_B}{K_{BL}\, f_{BL,y}} + \frac{x_{CL}\, f_C}{K_{CL}\, f_{CL,y}}} \qquad \text{(II.245)}$$

where $f_{BL,y}$ and $f_{CL,y}$ are the activity coefficients of BL and CL in the precipitating secondary solid solution that is in equilibrium with the aqueous solution. f_B and f_C account for possible differences in aqueous speciation and activity coefficients of B^+ and C^+.

Figure II-21: Congruent dissolution and primary saturation state, $\Sigma\Pi_{ps}$, in the $(Ba,Sr)SO_4$-H_2O system: $\log_{10} K_{sp}(BaSO_4) = -9.97$; $\log_{10} K_{sp}(SrSO_4) = -6.63$ and $a_0 = 2.0$ (after Glynn [2000GLY]).

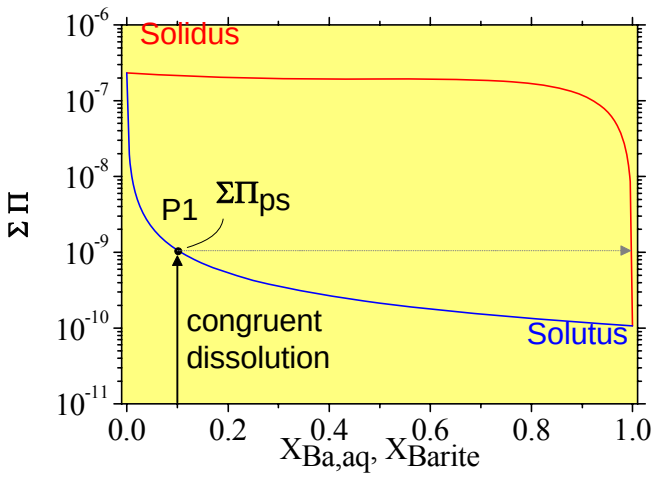

Excess Gibbs energy data on Aq-SS systems are ideally obtained from measuring solid solution solubility at equilibrium. However, especially at relatively low temperature (*e.g.*, < 100 ºC) it is usually difficult to establish "true" equilibrium conditions [1987PLU/BUS]. On the other hand, it has been demonstrated that with highly soluble solid solution phases (*e.g.*, Na(Cl,Br)-H_2O) it can be achieved [1990GLY/REA]. Ultimately, the dissolution/reprecipitation (recrystallisation) kinetics controls whether equilibrium can be established or not.

In many cases, the Aq-SS system may stay in a metastable state (at least with respect to typical laboratory time-scales), and the solid solution does not adjust its composition in response to compositional changes in the aqueous solution. In particular when the precipitation of a secondary solid solution is inhibited at the primary saturation state and stoichiometric dissolution proceeds. However, this situation opens new possibilities to obtain thermodynamic data on Aq-SS systems and leads to the stoichiometric saturation state/solubility concept.

II.2.2.2 Stoichiometric saturation

Stoichiometric saturation was introduced as a pseudo-equilibrium state [1977THO/PLU]. In contrast to the thermodynamic equilibrium solubility concept (Lippmann approach), where the solid solution composition is variable depending on the composition of the aqueous solution, here the composition of the solid solution phase remains invariant (due to kinetic restrictions). It only applies to observations of static batch type experiments with a short equilibration time, high solid-to-aqueous solution ratio, low solubility of the solid and congruent dissolution behaviour of the solid solution. It implies no significant recrystallisation of the initial solid or precipitation of a secondary solid-phase. In such a case, the solid solution phase can be treated as a phase with fixed chemical composition. And a simple solubility product for a solid solution $B_{1-x}C_xA$ can be defined:

$$IAP_{SS} = \frac{\{C^+\}^x \{B^+\}^{1-x} \{A^-\}}{1} = K_{SS} \tag{II.246}$$

For thermodynamic equilibrium, a single aqueous composition $x_{B,aq}$, $\Sigma\Pi_{eq}$ can be related to one solid solution composition x_{BA}, $\Sigma\Pi_{eq.}$. For stoichiometric solubility, a solubility variable $\Sigma\Pi_{ss}$ for a solid solution with invariant composition $B_{1-x}C_xA$ can be related to K_{ss} and the aqueous composition $x_{B,aq}$ and $x_{C,aq}$ over the full composition range:

$$\Sigma\Pi_{SS}(x_{B,aq}, x_{X,aq}) = \frac{K_{SS}}{x_{B,aq}^{1-x} \; x_{C,aq}^{1-x}} \tag{II.247}$$

$1–x$ and x refer to the invariant composition of the solid solution with K_{ss}. Each stoichiometric saturation curve (for every solid solution composition) has a minimum at $x_{B,aq.} = 1–x$ and $x_{C,aq} = x$ (Figure II-22).

Figure II-22 illustrates this situation for five different solid solution compositions in the system $(Ba,Sr)SO_4$-H_2O with x_{Barite}=0.1, 0.3, 0.5, 0.7 and 0.9. If congruent dissolution proceeds beyond the primary saturation state, apparently no new solid solution phase with a new compositions according to this solid solution – aqueous solution equilibrium has precipitated/nucleated. There seems to be a kinetic/metastable restriction for the formation of that new phase. As a consequence, congruent dissolution proceeds until the so-called stoichiometric solubility with respect to the dissolving solid

solution as defined by its solubility product K_{SS} and the minimum of the stoichiometric saturation curves, $\Sigma\Pi_{ss}$.

Figure II-22: Stoichiometric saturation curves in the system $(Ba,Sr)SO_4$-H_2O for x_{Barite}= 0.1, 0.3, 0.5, 0.7 and 0.9. Dissolution (indicated by grey arrows) proceeds until the minimum stoichiometric saturation is reached. For every composition, a stoichiometric saturation curve is a function of the composition of the aqueous solution, $x_{Ba,aq.}$ The minimum of each stoichiometric saturation curve is identical with the composition of the solid solution and is indicated by black points.

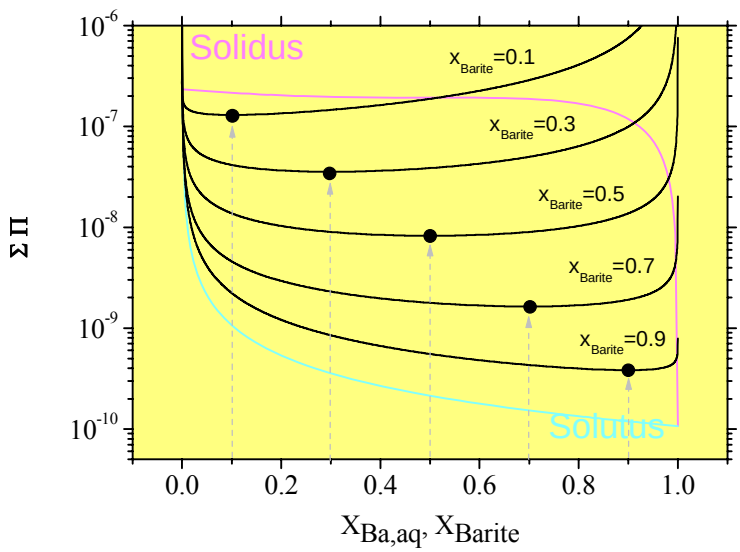

Connecting the minimum values of the series of stoichiometric saturation curves from $x = 0$ to $x = 1$ (Figure II-22) yields the minimum stoichiometric saturation curve, [1990GLY/REA], or "equal-G" curve, [1992KON/GAM], as shown in Figure II-23. The minimum stoichiometric saturation curve, $\Sigma\Pi_{ms}$, is a function of the end-member solubility products and of the excess Gibbs energy of mixing, G_m^E as defined in Eq. (II.152):

$$\Sigma\Pi_{ms} = K_{BA}^{1-x} K_{CA}^{x} \exp\left(\frac{G_m^E}{RT}\right) \qquad \text{(II.248)}$$

Whether minimum stoichiometric saturation has been achieved in an experiment can be easily checked: (1) Does the aqueous solution represent the stoichiometry of the dissolving solid solution? (2) Has the dissolution stopped (because it has reached

the solubility limit, defined by K_{SS})? This can be tested by a series of batch-type dissolution experiments.

Figure II-23: Minimum stoichiometric saturation curve in the system (Ba,Sr)SO_4-H_2O. The minima of the stoichiometric saturation curves in Figure II-22 are indicated by black points.

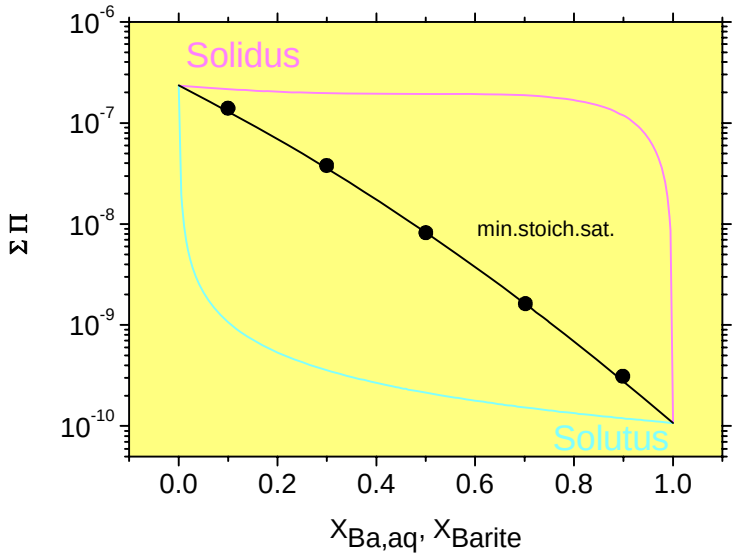

To conclude, it may appear to be unusual to derive thermodynamic data from a system that is apparently NOT in thermodynamic equilibrium but in a metastable pseudo-equilibrium state that cannot evolve —at least temporarily— towards equilibrium due to "kinetic restriction" [1977THO/PLU], [2000GLY]. In fact, various authors have criticised this approach in the past (see [1990GLY/REA]). However, for a number of systems, minimum stoichiometric solubilities have been successfully determined and allowed to derive thermodynamic data on solid solution excess Gibbs energy. There seems to be a consensus though that this approach can only be applied to dissolution experiments and not to co-precipitation experiments [1990GLY/REA].

In principle, deriving thermodynamic data from Aq-SS system *via* solubility measurements, one has to decide two fundamentally different approaches with distinct working hypothesis:

(1) Applying the stoichiometric saturation concept requires that the solid solution is treated as a pure-phase solid (with fixed composition). Such an experiment re-

quires a sufficiently high solid/aqueous solution ratio, relatively low solubility of the solid, and sufficiently short equilibration time.

According to Glynn [2000GLY], stoichiometric saturation measurements are the most promising technique for the estimation of thermodynamic mixing parameters at low temperatures from a (practical) experimental perspective. However, Glynn [2000GLY] points out, that most experimental data on stoichiometric saturation have not been verified by a second independent method.

(2) On the contrary, if one treats the solid as a solid solution with variable composition, which can be adjusted in response to the composition of the aqueous solution, true thermodynamic equilibrium can be studied. From the thermodynamics perspective, measuring solid solution solubilities at thermodynamic equilibrium are the ideal method to obtain excess Gibbs energy of mixing data [2000GLY]. However, the thermodynamic equilibrium may be applicable if the solid solution has a relatively high solubility and reactivity in aqueous solution. Also, a low solid/aqueous solution ratio has been chosen. However, compositional adjustments of the solid with respect to the aqueous solution may take a long equilibration time. From the experimental perspective it is straightforward to judge whether compositional adjustments have occurred in a series of batch-type dissolution experiments or not. It can be difficult though, to decide, whether true thermodynamic equilibrium has been established. It is believed that the closest approach to equilibrium can be achieved in constant-addition co-precipitation experiments at very low precipitation rates.

In some cases, a surface layer may have newly formed during a batch-type experiment on the solid with a chemical composition that is in equilibrium with the aqueous solution. In such a case, the primary saturation concept may apply; independent characterisation of the surface layer composition and structure will be crucial.

II.2.3 Solid phase characterisation

What is a well defined solid solution phase? This is, without a doubt, one of the key questions when experimental data on Aq-SS equilibria need to be evaluated. This section is intended to provide an overview of state of the art analytical techniques to characterise solid solution phases chemically as well as structurally and to obtain thermodynamic mixing data with respect to Aq-SS equilibria. Also, with respect to nuclear waste repository relevant conditions, in particular in the far-field, structural incorporation of radionuclides at trace concentration levels will be considered. It is not intended to provide an exhaustive compilation of all analytical techniques, but rather to outline some of the key aspects which need to be clarified when deriving thermodynamic data.

One key aspect will be focused on direct measurements of the thermodynamic mixing functions of the Gibbs energy, enthalpy, volume, vibrational and configurational entropy (for a detailed introduction see Section II.1.1):

$$\Delta_r G_m(p,T,\text{mix}) = \Delta_r H_m(T,\text{mix}) - \Delta_r S_m(T,\text{mix}) + \int_1^P \Delta V_T^{mix}\left(p,\text{mix}\right) dP$$

Measuring thermodynamic properties directly requires an extensive sample characterisation programme in order to ensure the derived thermodynamic data are actually related to a homogenous solid solution phase. Since direct measurements of thermodynamic mixing data typically require macroscopic amounts of a solid solution compound, its ***chemical homogeneity*** is a critical issue, which is quite often not carefully considered. In principle, four questions regarding chemical homogeneity need to be verified:

(1) Does the solid solution phase consist exclusively of the solid solution phase of interest, or are there minor/trace amounts of additional phases present? In particular, when studying Aq-SS systems, co-precipitation experiments are performed at relatively low temperature (< 100 ºC). In such experiments, the aqueous phase might be supersaturated with respect to more than one phase (see Section II.1.1). Similar situations may arise during dissolution tests (see Section II.2.2), when the stoichiometric solubility concept does not apply and precipitation of a new solid solution phase, as well as additional secondary phases, occurs.

Identification of the mineral phases present in a co-precipitation reaction product or a sample from a natural low temperature (< 100 ºC) aqueous system is typically performed routinely using ***powder x-ray diffractometry (XRD)***. Furthermore, XRD provides information about quantitative determination of phase percentages, crystal structure of unknown phases, particle size distribution, crystal-chemical and lattice strain information. However, with respect to phase identification, powder XRD has a low detection limit compared to other analytical methods. Although it is difficult to provide an exact number, since the diffraction peak intensities highly depend on the type of atoms involved (Z), the crystallinity, the particle size, and the symmetry of the crystal structure, a good rule of thumb is a detection limit around 1 wt%. In case of a crystalline actinide compound with its heavy elements in a matrix of minerals with a small average atomic number, the detection limit can be somewhat higher. Many actinides tend to form colloidal nanophases in aqueous systems (amorphous as well as crystalline). The detection limit for such systems is strongly affected by the crystallinity and by the particle size. The width of diffraction peaks is highly correlated with the particle size – with decreasing particle size, the peak width increases (Scherrer equation). Considering again an actinide compound (1 wt%) in a light matrix, the detectable particle size limit should be around 50 – 100 nm. On the contrary, for a pure crystalline actinide nanophase, significantly smaller particles could be detected. An amorphous actinide compound, such as many actinide oxy/hydroxides, cannot be detected by XRD methods at all, since they lack of sufficiently large scattering domains. The typical amount of sample required is in the range of 2−20 mg [1989BIS/POT]. However, the minimum sample volume needed for diffraction experiments has decreased considerably with recent developments of intense x-ray sources (*e.g.*, rotating anodes, synchrotron radiation). A full crys-

tal structure determination has been performed on a kaolinite single crystal of 0.8 μm^3 size [1999NED/BUR].

Phase composition can also be analysed by ***infra-red (IR) and Raman spectroscopy***. In contrast to XRD methods, IR and Raman spectroscopy provide information about the local structure, such as the site symmetry, coordination number, local chemical and crystallographic environment [1988MCM/HOF]. These methods do not depend on long-range periodicity/crystallinity and are applicable to amorphous materials. They are also sensitive to vibrational modes of pairs of atoms or molecular groups. Intensity of absorption (IR) or scattering (Raman) as a function of frequency/wavenumber provides key information to identify unknown phases. For a vibrational mode to be IR (Raman) active, the oscillating electric field of the incident beam must be able to interact directly with a changing molecular dipole moment (polarisability tensor component) associated with the vibration. IR and Raman spectra of a material can be quite different, and both methods are complementary. A set of vibrational modes is a characteristic fingerprint of the chemistry and structure of the molecular groups in a sample. The actual identification has to be made by comparison with reference spectra. In minerals, specific molecular groups such as hydroxyl groups, water molecules, as well as oxyanions (carbonate, sulphate, nitrate groups), give intense IR and Raman peaks. Since the exact frequency of a IR/Raman vibrational mode depends on the actual mineral structure, individual minerals can be identified. However, in complex mineral structures, molecular groups are not necessarily easy to identify, and understanding complex spectra requires a detailed knowledge of vibrations in crystals. Although it is difficult to define exact analytical limits easily, one can clearly state that the detection limits are lower than for XRD – presuming IR/Raman active modes are present. A combination with light microscopy adds spatial resolution to IR and Raman spectroscopy, in particular when used with a synchrotron light source (*e.g.*, at ANKA, Karlsruhe).

Complementary to diffraction and spectroscopy methods, electron microscopy, as well as atomic force microscopy can provide crucial information about the potential occurrence of secondary phases other than the solid solution phase of interest, in particular, due to their spatial resolution.

The presence of additional secondary phases, as well as compositional inhomogeneities within individual crystals, can be identified with high resolution electron-beam instruments such as ***scanning electron microscopy (SEM), transmission electron microscopic (TEM), or electron-beam microprobe (EMP)***. Typically, these instruments are provided with analytical equipment such as EDX or WDS detectors, which analyse X-rays generated upon electron beam – sample interactions. They allow spatially resolved chemical (and structural) sample characterisation. The EDX detectors typically provide an analytical precision ~1%, whereas WDS detectors have a much lower precision $\ll 1\%$. The spatial resolution of the analysed surface area with SEM has a diameter in the range of 1-3 µm, whereas TEM provides analytical information from an area with a diameter in the lower nanometer range. In addition to the chemical analysis, TEM can

be used to identify unknown phases using electron diffraction. The area of interest lies in the Ångström range. TEM has been very successfully applied in environmental geochemistry to identify trace metals occurring in nanophases in iron oxyhydroxide-rich sediments, as opposed to adsorbed trace metals [1999HOC/MOO], [2005HOC/MOO]. In particular, with respect to studying Aq-SS systems, colloidal nanophases are frequently encountered (especially when working with actinides or non-radioactive chemical homologues). One drawback of electron microscopy techniques is certainly the extensive sample preparation, which, depending on the question one is trying to answer, can be quite time consuming.

Atomic force microscopy (AFM) provides high resolution information of the nanotopography of any solid surface. Also, it can be applied in aqueous solution (no vacuum required) - in-situ nano-scale observations of crystal growth/co-precipitation processes are possible. With respect to co-precipitation experiments, the formation of secondary phases other than the solid solution phase of interest can be studied on a molecular level in-situ and in real-time [2004SCH/HAR], [2004SCH/PUT]. Also, the actual crystal growth mechanisms (step/spiral growth *vs*. heterogeneous nucleation) can be identified as a function of the solution composition. However, AFM does not provide chemical information.

Without a doubt, a whole range of analytical techniques are valuable to identify ALL the mineral phases present in a sample. In addition to the presence of such secondary phases other than the solid solution phase of interest (as outlined above), two more questions related to chemical inhomogeneity within individual crystals have to be carefully addressed and ruled out before further thermodynamic interpretation is performed. Both are related to metastable – non-equilibrium situations, which are quite common when working with aqueous low temperature (< 100 ºC) systems.

(2) Does the solid solution phase exhibit **compositional zoning** (*e.g*., oscillatory zoning or a simple spatial concentration gradient with respect to one or more radionuclides within individual crystals)? Such compositional zoning can be considered as a consequence of changing conditions during the synthesis or during formation in nature [2002LHE/JAM].

(3) Does the solid solution phase exhibits **compositional sector zoning** as a consequence of preferential radionuclide incorporation during the synthesis or formation in nature [1992FOU/REE], [1990PAQ/REE], [1995PAQ/REE]. Such differential radionuclide uptake is a consequence of selective adsorption/incorporation of certain radionuclides at certain sites at the mineral/aqueous solution interface.

Compositional zoning –sector zoning or oscillatory zoning– is a clear indication that thermodynamic non-equilibrium conditions are reflected in such an inhomogeneous solid solution compound. However, at high temperatures (several hundred degrees C) such inhomogeneities can re-equilibrate *via* solid state diffusion processes. On the contrary, at relatively low temperature conditions as considered relevant for a nu-

clear waste repository system (< 100 ºC), solid state diffusion is not an effective process, and chemical inhomogeneities will persist. All techniques mentioned above with the capability to provide spatially resolved chemical/structural analysis are suitable to clarify sample homogeneity.

Upon cooling, solid solution phases develop exsolution and spinodal decomposition features and develop chemical, as well as structural, inhomogeneities concomitant by complex microstructures. Therefore, another important question with respect to homogeneity arises:

(4) Does the sample exhibit exsolution related to a mixing gap below a critical temperature? Or, are there indications for spinodal decomposition features as a consequence of re-equilibration process upon cooling?

All four aspects of compositional homogeneity as described above certainly interfere with respect to the interpretation of spectroscopic data of structurally incorporated radionuclides (*e.g.*, XAFS, TRLFS). Most spectroscopic methods integrate over the entire sample. However, spatially resolved spectroscopic methods are able to overcome these problems (TEM-EELS, μXAFS, *etc*. – see below).

Once the chemical homogeneity has been verified, the **exact chemical composition** of the solid solution phases can be determined including the redox state of the involved species. ***SEM-EDX*** and ***EMP-WDS*** (see above) are used routinely to analyse the chemical composition non-destructively. Similarly, ***X-ray fluorescence (XRF)*** spectroscopy provides also non-destructive chemical analysis. However, routine instruments do not provide any spatial resolution. More recent developments have introduced ***micro XRF*** either using conventional X-ray sources (with a analytical sensitivity in the ppm range), but also synchrotron-based X-ray sources with a much lower analytical limit and a spot size with a diameter of around 5 μm.

Also, knowing the ***redox state*** of structurally incorporated radionuclides (in particular, some of the actinides – *e.g.*, Pu) is of key importance. The ***X-ray absorption near edge structure (XANES)*** provides detailed information about the redox state and the coordination chemistry, contained in the X-ray absorption spectrum from a few eV above the pre-edge to ~50 eV above the edge [1988BRO/CAL]. When a valence electron is removed from an atom, screening of core electrons provided by the valence electrons is reduced, and the core levels become more tightly bound. This change generates a shift in pre-edge and bound-state edge features. The pre-edge feature for iron in Fe(III) minerals is generally 2-3 eV higher in energy then the corresponding feature in Fe(II). The analysis of XANES for valence-state information is made easier when the element of interest occurs in discrete tetrahedral clusters. The detection limit for a heavy element like Pu in a relatively light matrix would be around 200 ppm.

Complementary to the analytical techniques for studying a solid phase, the chemical composition of a homogeneous solid solution phase can be determined using

the full range of techniques for analysing aqueous solutions (after dissolving the sample) – ICP-MS, ICP-OES, AAS, IC, *etc.* (see Section IV). The analytical limits clearly depend on the technique, but also the required dilution level. Generally, most radionuclides can be quantified at ultra trace concentration levels.

After the ***chemical homogeneity of a solid solution compound has been verified*** and its ***chemical composition determined***, the **crystal structure** and the atomic scale scheme how ions occupy distinct crystal lattice sites needs to be determined. These structural aspects also include the determination of the actual substitution mechanism, as well as the associated long-range order (LRO) and short-range order (SRO) phenomena. In order to obtain a complete description of a mineral structure, measurements over long AND short correlation length must be made.

- **X-ray diffraction (XRD)**

It is well known, that many simple binary solid solution systems follow one of the two crystal chemical rules: (1) Vegard's rule –the additivity of lattice parameters or interatomic distances and (2) Retger's rule –the additivity of molar volumes [2001URU]. Both rules are reflected in the averaging structural picture as provided by experiments [2001OBE]. Even with the smallest crystals, XRD averages over a significant number of unit cells. Structure refinement procedures allow a determination of the geometric relations between atoms in a crystal, provide information on the average chemical composition at each structural site and on the state of order/disorder. Such structural studies provide information on site occupancy whih is linked to the configurational entropy of a solid solution phase. Therefore, it gives indication about the occurrence of miscibility gaps, as well as phase transitions. At high temperature, solid solution phases show perfect mixing behaviour (see Chapter II). However, at lower temperatures exsolution and ordering phenomena occur. As temperature drops, a mixing gap may evolve and two solid solution phases form, which are easily detectable with XRD techniques. Cations may prefer certain sites within a crystal structure as temperature drops, which, eventually, may cause phase transitions and symmetry changes, which are also detectable with XRD methods. In the case of a coupled substitution on one lattice site, cations may order in a way to avoid adjacent equally charged ions – thus developing a superlattice.

Unit cell parameters can be measured by powder and single-crystal methods. Changes in unit cell parameters are crucial for understanding structural adjustments to atomic substitutions that allow a given substitution to occur in a given mineral structure, since geometric/vibrational properties of a structure depend on the atomic fractional coordinates. Determinations of unit-cell volume are also crucial for thermodynamic studies. Non-linear behaviour of the unit cell parameters is often difficult to measure, if the experimental accuracy is not good. Following Oberti [2001OBE], for high quality crystals the standard uncertainty is about 1 on the third or 5 on the fourth digit when dealing with unit cell edges of about 10 Å.

X-ray structure refinement procedures allow a precise determination of: (1) the number and coordination of structural sites, (2) the scattering power at each site (which is linked to the average atomic number) and (3) the coordination geometry at each structural site. On the basis of an analysis of the electronic and geometric properties of a structure, the cation distributions (site populations) can be derived [1983HAW], [1996KIR] and [1997KRO/LUE].

Similar to XRD, neutron diffraction has been used to study solid solution systems, mainly due to their non-systematic scattering characteristics of elements with similar atomic number (with almost identical x-ray scattering factor) and their efficient scattering with light elements.

In contrast to LRO (long range order) phenomena observed in diffraction experiments, SRO (short range order) phenomena are most often studied by spectroscopic techniques. Here, the focus will be on X-ray absorption spectroscopy and time resolved laser fluorescence spectroscopy, since they are frequently used when structurally incorporated radionuclides in a host mineral structure are studied. One of the key questions is related to the incorporation mechanism(s) and the incorporated species (valence state, simple ionic or complexed species).

- **X-ray absorption fine structure spectroscopy (XAFS)**

X-ray absorption fine structure spectroscopy (XAFS) provides a way to determine the local structural environment of trace amounts of radionuclides incorporated into a host mineral structure. The X-ray absorption spectrum is typically divided into two regimes: X-ray absorption near-edge spectroscopy (XANES) and extended X-ray absorption fine-structure spectroscopy (EXAFS). A XAFS measurement gives the energy dependence of the absorption coefficient at and above the binding energy of a known core-level of a known atomic species. In general, one can say that XANES is very sensitive to chemical aspects of the selected atom (oxidation state, coordination polyhedron), whereas EXAFS is more sensitive to interatomic distances, coordination number and species of the atoms surrounding the absorbing atom of the 1^{st} and 2^{nd} (sometimes 3^{rd}) coordination sphere. It can be applied to crystalline as well as amorphous solids.

The identification of the local environment can be obtained by using XAFS spectra of reference compounds with known structure or simulation of spectra using programs like FEFF. FEFF performs *ab initio* multiple scattering calculations of extended X-ray absorption fine structure (EXAFS) and X-ray absorption near-edge structure (XANES) spectra for clusters of atoms. The code yields scattering amplitudes and phases used in many modern XAFS analysis codes.

With respect to the local structure within a solid solution phase, interatomic distances can be determined with a precision of ± 0.005 Å, presuming spectra with a high signal-to-noise level and of high k-space range [1988BRO/CAL]. This is also an important aspect when studying a radionuclide occupying more than one lattice site.

The precision level of coordination number information from least-squares fitting is of the order of ± 0.2 – 0.4. Information of the local structural disorder around an absorber can be obtained from the magnitude of the Debye-Waller factor in EXAFS. Differences in backscattering amplitude and in phase shift exist for atoms of significantly different atomic number. Therefore, different neighbouring atoms in a coordination shell can be distinguished. This is particularly important when studying solid solution systems with variations in short-range ordering. The detection limit with respect to concentrations of radionuclides depends on experiment geometry, the chemical composition of the host matrix, and the actual element. For example, for actinides incorporated into a calcium-carbonate matrix the detection limit would be around 500 ppm. Using on synchrotron sources high intensity insertion devices, such as wigglers, will allow studies of even more dilute systems (< 100 ppm) [1988BRO/CAL].

In summary, with respect to solid solution phases, one of the key advantages of EXAFS is certainly that SRO phenomena are probed quantitatively, whereas LRO phenomena cannot be detected.

- **Time resolved laser fluorescence spectroscopy (TRLFS)**

Time resolved laser fluorescence spectroscopy (TRLFS) provides, in principle, also information about the coordination sphere of certain radionuclides. Exceptional fluorescence properties have been observed for Cm(III), Am(III) as well as for Eu(III) as a non-radioactive chemical analogue. Light emission associated with fluorescence is due to electronic transitions within single ions, or energy transfer between closely associated ions in a structure [1988WAY]. Fluorescence energy and associated life time can be analysed. Changes in the peak maxima of the emission spectra indicate a change in the chemical environment or ligand field. Furthermore, changes in the life time indicate the presence of quenchers such as H_2O or OH^- molecules in the local coordination sphere.

In general, two of the key advantages of fluorescent techniques are (1) their sensitivity to extremely small concentrations and (2) its sensitivity to variations in site geometry [1988WAY]. However, fluorescence data are much more difficult to understand compared to XRD or XAFS data. They do not provide direct structural information (*e.g.*, bond length, coordination number, atomic number). Nevertheless, fluorescence of uranium, curium, americium and the rare earth elements has been studied quite extensively.

Most recently, Cm^{3+} fluorescence of aqueous species, adsorbed species as well as structurally incorporated Cm species have been studied very successfully. Cm has extraordinary fluorescence properties due to its large energy gap between the first $^6D_{7/2}$ excited state level and the ground multiplet $^8S_{7/2}$. A superior advantage is its high sensitivity down to 10^{-12} mol·dm^{-3}.

Recently, TRLFS on Cm^{3+} co-precipitated with various minerals has been studied successfully [2004BOS/RAB], [2002STU/FAN2], [2004STU/TIT], [2003TIT/STU].

In case of calcium-carbonate, it could be shown that at least two Cm species are structurally incorporated Cm^{3+} and $CmOH^{2+}$, thus indicating a complex substitution mechanism.

Two additional spectroscopic techniques have provided valuable information on solid solution phases. However, in the context of small amounts of radionuclides incorporated into a mineral host structure, they do not provide a sufficient detection limit and have not been applied to these issues:

- **Nuclear magnetic resonance (NMR) spectroscopy**

NMR spectroscopy also provides information about local coordination environment of a nuclide, based on differences between allowed spin states of atomic nuclei. Atomic nuclei with a magnetic moment (according to their spin quantum number) exhibit a splitting of their energy level when a strong external magnetic field is applied. Since the energy differences are in the radio frequency range, transitions between spin states can be induced by applying a radio frequency field to a sample exposed to a large static magnetic field. Magnetic resonance occurs when the radio frequency matches the difference in spin energy levels. The exact frequency of the resonance depends on the local structural environment *via* the chemical shift between the resonance frequency in a sample of interest and a reference sample. The shift in resonance frequency depends on the shielding of the external field [1988KIR], [1988STE].

There seems to be no straight-forward way to assign NMR peaks to specific structural sites or to extract details of the chemical and structural ligand field. Nevertheless, NMR spectroscopy has been very successfully applied to solve short range order (SRO)/configurational entropy phenomena in alumosilicates, in particular with respect to Al,Si ordering phenomena based on ^{29}Si and ^{27}Al NMR. Paramagnetic impurities in a sample (such as Fe and Mn) limit the application of NMR. There seems to be no work published on trace amounts of radionuclides (or chemical homologues) in a host mineral.

- **Infra-red (IR) spectroscopy**

Information about the width of individual phonon bands has been used to study the variation of the order parameter for a phase transition quantitatively. More recently, it has been shown that peak shifts and line-width variations of phonon spectra can be used to detect the structural response to any local changes associated not only with phase transitions, but also with cation substitution [2001CAR/BOF]. The underlying concept is that the mechanism by which most materials accommodate atoms of different size involves elastic distortions. Non-ideal mixing in solid solutions can be therefore understood in terms of local strain heterogeneities arising from the replacement of one cation by another. Such local distortions give rise to spectral broadening. Experimental evidence shows close correlation of IR peak broadening, calorimetric data in enthalpy of mixing and bulk modulus ([2000BEC/CAR], [2001BAL/CAR], [2001BAL/CAR2], [2004ROD/CAR]). This has been shown for various silicates, however not for oxides

and carbonates. This approach has not been applied to trace concentrations of radionuclides incorporated into a host mineral.

A comprehensive structural characterisation of a solid solution phase apparently requires the application of a range of techniques. Only a combination of diffraction and spectroscopic techniques seem to be able to provide a molecular level picture of SRO and LRO phenomena and to identify potentially complex substitution mechanisms. There is only a limited number of studies on low temperature (<100 ºC) solid solution systems where all those aspect on chemical homogeneity, as well as chemical and structural SRO/LRO phenomena, have been described at a sufficient level. Nevertheless, once these issues have been clarified, reliable thermodynamic mixing data can be determined by means of measuring heat capacities (*e.g.*, adiabatic calorimetry, differential scanning calorimetry, drop calorimetry) or measuring enthalpies *via* heat of solution calorimetry.

A special case is related to direct measurements of ***solid solution – aqueous solution equilibria***. As outlined in Section II.2.2, when a homogeneous solid solution phase is exposed to an aqueous solution, dissolution/reprecipitation process may be initiated which will result in a thin coating covering the original solid solution phase, but with a new chemical composition. The chemical composition of this coating may be in equilibrium with the aqueous solution. It can be derived indirectly from compositional changes in the aqueous solution. Direct measurements need to rely on surface sensitive analytical tools and certainly represent a real analytical challenge.

- **X-ray photoelectron spectroscopy (XPS)/Auger electron spectroscopy (AES)**

X-ray photoelectron spectroscopy (XPS)/Auger electron spectroscopy (AES) is used to obtain chemical, oxidation state and structural information in the near surface region (few to 100 Å) of a solid sample [1988HOC]. In XPS, photoelectrons from valence and core levels of near-surface atoms are ejected upon irradiation with soft X-rays. Photoelectron has a characteristic energy, depending on the actual atom, its oxidation state and, in many cases, on the local structural environment. Similarly, AES Auger electrons are generated from a sample surface by an electron beam. Consequently, AES also provides spatial resolution (the latter is not so good for XPS). It should be mentioned that neither XPS nor AES are frequently used to study solid solution samples after a co-precipitation experiment or a solubility test.

- **IR and Raman spectroscopy**

Combining IR and Raman spectroscopy with a cofocal light microscope provide spatially resolved phase analysis with a diameter of about 1 μm including all the advantages if IR/Raman spectroscopy. Furthermore, by varying the focal depth, a depth-resolved phase analysis can be performed. This is of particular interest when secondary phases form within a thin coating at a mineral/aqueous solution interface.

- **Calorimetry**

Calorimetry, the measurement of heat effects, is a fundamental tool of experimental thermodynamics. It provides data on heat capacities, entropies, and enthalpies and is thus complementary to solubility and other equilibrium measurements that provide Gibbs energies. Broadly speaking, calorimetry can be divided into two categories: the measurement of heat capacities and heats of phase transition within a material of constant composition, and the measurement of heats of reaction. Sometimes, the first category is called thermophysical and the second, thermochemical measurement.

To obtain the standard entropy of a phase at a reference temperature, usually 298 K, one needs to integrate the $C_{p,\mathrm{m}}/T$ function from as close to absolute zero as possible to the temperature of interest:

$$S_T^\circ - S_0^\circ = \int_0^T (C_{p,\mathrm{m}}/T)\mathrm{d}T$$

$$H_T^\circ - H_0^\circ = \int_0^T C_{p,\mathrm{m}}\mathrm{d}T$$

For a perfect crystal, $S_0^\circ = 0$. For a solid solution, the randomness in mixing ions on various sites implies a zero point entropy equal to the configurational entropy. This is generally not observed by low temperature heat capacity measurements because the disorder is "frozen in".

Cryogenic adiabatic calorimetry [1972ROB/HEM2] is the most accurate method for measuring low temperature heat capacities but it requires several grams of sample. In general, the instruments are custom built and the work is performed in a small number of specialised laboratories. It is capable of determining heat capacities with an accuracy of 0.1-0.5% and standard entropies with an accuracy of 0.5-1%. A cryogenic heat capacity module, based on the PPMS (Physical Properties Measurement System) platform commercially available through Quantum Design Inc., has recently come into increasing use for $C_{p,\mathrm{m}}$ measurements. Though not as accurate as cryogenic calorimetry, it has the advantage of using samples of about 100 mg. With careful operation, it can provide accuracy approaching 1% (appropriate protocols and pitfalls are discussed by Lashley *et al*. [2003LAS/HUN]). For very small samples (micrograms to milligrams), silicon-chip based calorimetry appears capable of accuracy of 3-5% [1994DEL/ABA]. The applicability of these newer methods to insulating mineral and ceramic powders is just being explored.

Differential scanning calorimetry (DSC) [1992BOE/CAL], [1982STE/WEI] provides heat capacity measurements from about 100 to 1700 K, with accuracy ranging from about 1% near room temperature to 3-5% at the highest temperatures [2005MOR/NAV]. Many commercial instruments are available for the range 100 to 1000 K, and several for higher temperatures. Differential thermal analysis to 2773 K can provide enthalpies of phase transitions with an accuracy of about 5-10% at the higher temperatures [2005NAV/BEN]. Drop calorimetry (where a sample of 10-100 g is

dropped from a high temperature furnace into a room temperature calorimeter) provides the heat content ($H_T - H_{298}$), differentiation of which gives the heat capacity [1982STE/WEI]. Accuracy is 0.5 - 1% in the best cases.

Despite the apparent maturity of the field of heat capacity measurement, the available data for end-member and solid solution phases relevant to nuclear materials are surprisingly incomplete. Many of the older data, used to calculate standard entropies of common materials, in fact rely on extrapolations from 50 K to absolute zero and also suffer from sample characterisation inadequate by modern standards. There are relatively few studies of solid solutions, so excess vibrational entropies of mixing are poorly constrained.

To obtain the heat of formation of a material, a chemical reaction must take place in a calorimeter which relates that phase to products of known thermodynamic properties. That reaction may be direct, as in reaction calorimetry of a metal to a sulphide [1988BRY/KLE] or indirect, involving a process in which reactants and products are each converted to the same final state, and a thermodynamic cycle is written to relate their enthalpies. This final state often involves the dissolution of the solids in an appropriate solvent, which can range from water or aqueous acid [1972ROB/HEM2] to a molten oxide at high temperature [1977NAV], [1997NAV]. Because many of the solids relevant to nuclear materials are not readily soluble (in terms of both solubility limits and kinetics of dissolution) in aqueous solvents near room temperature, the latter route, high temperature oxide melt solution calorimetry, has proven very useful [1977NAV], [1997NAV]. The Calvet high temperature reaction calorimeter and its calorimetric cell are shown schematically in the figure below.

The basic calorimetric technique involves dissolving a mineral, ceramic, or oxide mixture in molten lead borate at 973 K or 1073 K. The difference in the heat of solution (if the sample is pre-equilibrated at calorimetric temperature and then dissolved) or the difference in heat of drop solution (if the sample is dropped into the solvent from room temperature) between reactants and products give the enthalpy of reaction.

An example of a thermochemical cycle is shown below, for the determination of the enthalpy of formation of thorite, $ThSiO_4$ [2005MAZ/USH].

$$ThO_2(\text{thorianite, 298 K}) \rightleftharpoons ThO_2(\text{dissolved in lead borate, 1080 K}) \qquad \text{(II.249)}$$
$$\Delta_r H^\circ_m = (98.1 \pm 1.7)\ \text{kJ·mol}^{-1}$$

$$SiO_2(\text{quartz, 298 K}) \rightleftharpoons SiO_2(\text{dissolved in lead borate, 1080 K}) \qquad \text{(II.250)}$$
$$\Delta_r H^\circ_m = (49.9 \pm 0.8)\ \text{kJ·mol}^{-1}$$

$$ThSiO_4(\text{thorite, 298 K}) \rightleftharpoons ThSiO_4(\text{dissolved in lead borate, 1080 K}) \qquad \text{(II.251)}$$
$$\Delta_r H^\circ_m = (128.4 \pm 0.8)\ \text{kJ·mol}^{-1}$$

$$ThO_2(\text{thorianite, 298 K}) + SiO_2(\text{quartz, 298 K}) \rightleftharpoons ThSiO_4(\text{thorite, 298 K}) \qquad \text{(II.252)}$$

$$\Delta_r H^\circ_m(\text{II.252}) = \Delta_r H^\circ_m(\text{II.249}) + \Delta_r H^\circ_m(\text{II.250}) - \Delta_r H^\circ_m(\text{II.251}) = (19.7 \pm 2.1)\ \text{kJ·mol}^{-1}$$

Figure II-24: Geometry for gas flow-mixing (bubbling) drop-solution calorimetry in a high-temperature Calvet solution calorimeter. A, calorimeter liner, crucible assembly insertion point; B, Inconel protection tubes; C, Al_2O_3 insulation; D, thermopiles; E, isothermal Inconel block with heaters positioned around the outside surfaces; F, reaction zone; G, Inconel protection tube; H, SiO_2 glass liner; I, Al_2O_3 plug; J, SiO_2 glass crucible; K, platinum crucible; L, solvent ($2PbO{\cdot}B_2O_3$); M, gas bubbles; N, SiO_2 glass dropping tube for sample introduction; O, platinum tube for bubbling gas introduction; P, 5 mm separation between the bottom of the platinum crucible (K) and the platinum bubbling tube (O).

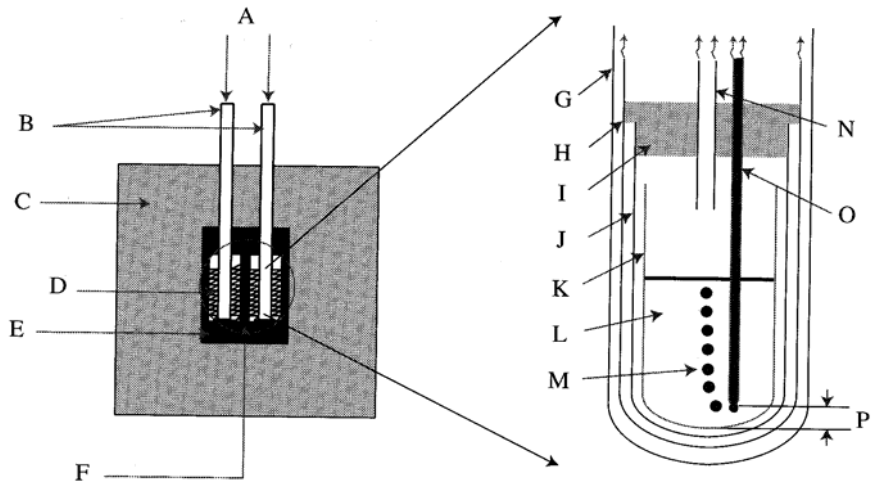

An important finding of this study is that thorite is energetically unstable relative to a mixture of oxides and that its synthesis and stability at high temperature is a result of a positive entropy of formation, suggested to be $\geq (8.9 \pm 3.3)\ \text{J·K}^{-1}\text{·mol}^{-1}$). The absence of low temperature $C_{p,\text{m}}$ data for thorite prevents an independent check on this entropy of reaction.

The uncertainty in heat of formation from oxides, on the order of $\pm 2\ \text{kJ·mol}^{-1}$ for a formula unit containing four oxygens, is fairly typical of that in oxide melt solution calorimetry. The precision in $\Delta_r G_m$ obtained from solubility or other equilibrium measurements often appears to be higher, on the order of $0.1\ \text{kJ·mol}^{-1}$. However, the accuracy in such determinations can be lower, is subject to proving that equilibrium is indeed attained, and often is affected by large uncertainties in the thermodynamic parameters for dissolved aqueous species. Furthermore, solubility measurements can often be performed only over a limited temperature range, making problematic the derivation

of both $\Delta_r H_m$ and $\Delta_r S_m$ from the temperature variation of $\Delta_r G_m$. Thus, in reality, equilibrium measurements of $\Delta_r G_m$ and calorimetric determinations of $\Delta_r H_m$ are complementary and together offer more certain proof of equilibrium and constraint of the $\Delta_r S_m$ of formation.

Though initially used for volatile-free ceramic samples [1977NAV], oxide melt solution calorimetry as a means of studying phases containing water and carbon dioxide was developed in the 1990s [1994NAV/RAP]. Thus clays [2001FIA/NAV], zeolites [2001YAN/NAV], and carbonates [1999NAV/DOO] can be studied.

The ability to dissolve small samples (5 mg) allows solution on refractory oxides which were too slow to dissolve, or which locally saturated the solvent and precipitated secondary phases, when larger samples (20 mg to 50 mg) were used in earlier studies [1977NAV]. One can now work with TiO_2 ([2003XU/SU], [2004HEL/USH]), ZrO_2 [2005PIT/USH], and lanthanides ([2002HEL/NAV], [2004HEL/USH]) and actinides ([2002HEL/NAV2], [2003HUG/HEL], [2005MAZ/USH]), using lead borate ($2PbO{\cdot}B_2O_3$) and sodium molybdate ($3Na_2O{\cdot}4MoO_3$) as solvent. Maintaining high oxygen fugacity by bubbling oxygen through the solvent also has led to success in an oxidative dissolution process for nitrides [1999LIA/TOP] and for iron, cobalt, manganese [2005GUI/NAV] cerium ([2002HEL/NAV2] and uranium ([2002HEL/NAV2], [2003HUG/HEL] phases of variable valence. These improvements dramatically extend the chemical variety of systems for which one can obtain reliable thermochemical data.

II.3 Cases of specific interest in relevant systems

II.3.1 Sulphates: the barite isostructural family and the incorporation of radioactive isotopes of Ra

II.3.1.1 Introduction to the barite isostructural family

Solid solutions involving the isostructural family of barite ($BaSO_4$) is one of the best studied solid solution series, as reflected by the extensive literature in a number of scientific fields (geology, geochemistry, crystallography, environmental sciences,…; [1971BRO/REN], [1983DEN/MIC], [1989GAL/DAN], [1990GLY], [1993FEL/RAI2], [1992PUT/FER], [1993PRI/PUT], [1997PRI/FER], [2000PRI/FER], [2002LHE/JAM], [2004ZHU]). Although barite is not strictly a rock–forming mineral, it is not rare in many geological environments ([2000HAN]) since its main components are usually found in both solid and aqueous phases. Barium is a minor and trace element in many common rocks such as limestones, dolostones, sandstones, granites and granodiorites, whereas sulphate is found in many evaporite minerals; as a result, many surface and ground waters carry them in solution, although the low solubility of barite (pK= 9.98; [1977BLO]) limits the transport of Ba^{2+} and sulphate in the same solution.

From the crystallographic point of view, barite isostructural family is orthorhombic and also includes celestite ($SrSO_4$), anglesite ($PbSO_4$) and hashemite ($BaCrO_4$) ([2000HAW/KRI]). In addition to Sr and Pb, a number of other cations are able to substitute for Ba^{2+} in the barite lattice. Such a substitution is controlled by the similarity in charge, ionic radius and electronegativity. As discussed below in the case of Ra^{2+}, the incorporation of some of these elements takes only place in trace amounts (*i.e.*, not forming *formal* mineral species) but becomes of special relevance for environmental issues. Anionic groups [MnO_4] and [SeO_4] readily substitute for sulphate in synthetic samples [1996CHA/HOW].

Despite the extensive work done on this system, some uncertainties still exist, even referring to the ideal/non ideal and complete/incomplete character of this solid solution family. The binary (Ba,Sr)SO_4 solid solution was initially considered a complete solid solution at room temperature (see [2000HAN] for reference list), although analytical data from natural samples shows a strong bimodal distribution into Ba-rich and Sr-rich end-members, with barite containing commonly less than 7 mol% $SrSO_4$ and celestite less than 4 mol% $BaSO_4$ ([1968HAN]). Precipitation experiments of (Ba,Sr)SO_4 solid solutions ([1938GOL], [1964STA], [1970CHU]) provided partition coefficients (D_{Sr-Ba}) at room temperature between $10^{-1.5}$ and 10^{-4} , that increase with increasing temperature [1964STA]. This means that Ba is strongly partitioned into the solid phase whereas Sr remains in solution. Interestingly, many D_{Sr-Ba} values are usually fairly higher than thermodynamic partition coefficients (K_{Sr-Ba}) assuming an ideal behaviour of the solid solution [2000HAN]. Prieto *et al.* [1997PRI/FER] also assumed an ideal behaviour and calculated the total solubility product (Figure II-25). They found that the precipitation of Sr-rich solid solutions was only possible from extremely Ba-poor aqueous solutions, and that a very wide range of solid solutions ($0.1 < x_{BaSO_4} < 0.9$) were in equilibrium with a very narrow range of aqueous solutions ($0.00005 < x_{Ba,\,aq} < 0.004$). The ultimate reason to explain this behaviour must be found in the large difference in the solubility products (three orders of magnitude) of the end-members, and in the existence of a miscibility gap. As a consequence, a bimodal trend of solid solution compositions results, as reported by Hanor [1968HAN] on natural samples.

Many other papers have concluded that the (Ba,Sr)SO_4 solid solution is not an ideal system at low temperatures, and a number of interaction parameter values have been reported (see review in [2000GLY], [2000HAN]). Based on compositional data from [1951PAL/BER], [2000GLY]. An extrapolated α_0 value of 2.34 at 25 ºC, considering a regular model. Another similar value, $\alpha_0 = 1.61$ (at 25 ºC), had early been reported from experimental data of [1989GAL/DAN]. A more complex model of non-ideality for this system was provided by Prieto *et al.* [2000PRI/FER]. They calculated the activity coefficients of the solid phases from theoretical calculations of thermodynamic mixing properties, since they consider that data from experimental methods or from natural miscibility gaps have many sources of uncertainty. These authors propose

a model with a five-term expansion of the Guggenheim excess Gibbs energy series, where $\alpha_0 = 8.15$, $\alpha_2 = 2.76$ and $\alpha_4 = -1.19$. As α_1 and α_3 are zeros, the distribution is the mixing properties are symmetrical around $x_{Sr} = 0.5$.

Figure II-25: (a) Lippmann diagram for an ideal (Ba,Sr)SO_4 solid solution at 25 ºC. This diagram is useful to plot the solubility products of solid solutions (see Section II.1). (b) Equilibrium $x_{Ba,\,aq} - x_{BaSO_4}$ (Roozeboom) plot. Note that a wide range of solid solution compositions are in equilibrium with a very narrow range of aqueous Ba^{2+} fractions. From [1997PRI/FER].

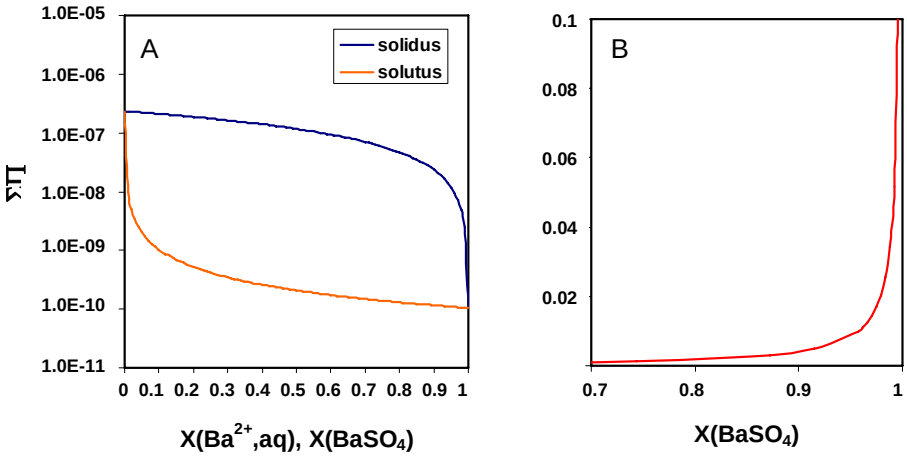

The (Ba,Pb)SO_4 binary solid solution has also received some attention because it was believed that this system may control the mobility/fixation of radium during the uranium ore processing ([1991KOR/PRE]; see next section for a more detailed explanation). Although the content of lead sulphate in barite in natural specimens is limited (up to 20%, [1951PAL/BER]), complete solid solutions in this system has been synthesised in some laboratory studies, even at a relative low temperature ([1967BOS/FRA], [2002WAN/LEE], [2005LEE/WAN]). However, it has been suggested that most precipitated solids are metastable and a miscibility gap exists between 25 and 75% $PbSO_4$ in the (Ba,Pb)SO_4 binary solid solution [1969TAK/YAN]. Based on the data from [1951PAL/BER], [1990GLY] recommended an interaction parameter $a_0 = 2.7$ at 25 ºC to describe the deviation from the ideality of this system. This value was also adopted by Kornicker *et al.* [1991KOR/PRE] to model their dissolution experiments.

The binary mixing properties of barite solid solutions ($BaSO_4$, $SrSO_4$, $PbSO_4$, $RaSO_4$ and $BaCrO_4$) from co-precipitation experiments have recently been re-evaluated by Zhu [2004ZHU]. By using corrections of Margules parameter, W, for the effects of the differences in the ionic properties of the other substituting ions, he was able to pre-

dict the behaviour of binary solid solution for metals for which no experimental data are available. Considering the presence of these metals into the solid solution as trace metals (*i.e.*, Raoult law is obeyed for the major metal and, therefore, its activity is considered as unity), he found that the trace component with lower solubility than the hosts has preference to its incorporation into the solid phase rather than in the aqueous phase. For the trace elements studied (Ra^{2+}, Ni^{2+}, Mg^{2+}, Cu^{2+}, Co^{2+}, Zn^{2+}, Fe^{2+}, Mn^{2+}, Eu^{2+}, Cd^{2+}, Ca^{2+} and Pb^{2+}), the calculated K_D values showed that radium is the most favourable metal to be incorporated into barite and celestite lattices. This high affinity of radium with respect to barite has very important implications in the evaluation of environmental pollution derived from wastes in some industrial and nuclear processes, as expanded in the next section.

II.3.1.2 The radium and its incorporation into the barite solid solution family: environmental implications

II.3.1.2.1 The radium-barium relationship in natural and anthropogenic environments

The relative abundance in nature and the low solubility of the end-members makes the barite solid solution family a potential sink of toxic and radioactive elements.

Perhaps, the co-precipitation between radium isotopes and barite precipitates is the best known example. Since the work of Doerner and Hoskins in 1925 [1925DOE/HOS], from which the theory of growth as incremental layers was defined (*Doerner-Hoskins logarithmic distribution law*), dozens of studies in several scientific disciplines have established a link between the concentration of radium and the precipitation of barite.

Radium has an ionic radius (1.43 Å) very similar to Ba^{2+} (1.36 Å), so that it is expected to be well accommodated in the barite lattice. Radium isotopes occurring in nature (^{224}Ra, ^{226}Ra, ^{228}Ra) are derived from 238–uranium and 232–thorium isotope decay. ^{226}Ra has by far the longest half-life (1622 years) and its migration through the geosphere may have a huge environmental significance since it is one of the major sources of radiological dose to human beings from U-bearing sources.

The role of barite as solubility-controlling phase of radium has been proposed in natural and in *anthropogenic* environments. First of all, barite is a common precipitated phase in the oil industry equipment, and it is formed when production waters in the oil fields are pumped out. The anomalously high radioactivity of these barites has long been known, and it is caused by the high content in radium isotopes and their decay products. Production waters, that are mixtures of formation waters and other types of waters injected during oil extraction operations, can contain tens to thousands of picocuries per liter ($pCi \cdot L^{-1}$) of dissolved ^{226}Ra ([1998FIS]), which is a concentration much higher than the maximum allowed for drinking water (5 $pCi \cdot L^{-1}$ total dissolved

radium in the U.S.[1]). Consequently, the mobility of radium is of special concern for its potential health risk. Soils in areas close to oil fields may contain elevated concentrations of radium, and its solubility is believed to be controlled by equilibrium with barite ([2001ZIE/OTT] and references therein). Barite scale is also considered as a high-risk material due to its radioactivity, and some studies have been carried out to minimise the pollution potential. In this regard, recently, Ceccarello *et al.* [2004CEC/BLA] synthesized a set of $(Ba,Sr,Ra)SO_4$ solid solutions from aqueous solutions with different initial [Sr]/[Ba] molar ratios, and they found that the presence of Sr^{2+} ions in the environment of formation inhibited the normal incorporation of ^{226}Ra in the barite crystals. According to them, the rate of incorporation of Ra in the $(Ba,Sr,Ra)SO_4$ solid solutions seems to be controlled by the degree of supersaturation with respect to celestite at the moment of nucleation and growth of the crystals.

Radium-bearing barite is also ubiquitous in other industrial wastes, such as the uranium mill tailings ([1987NIR]). Uranium is concentrated from ore minerals by leaching with sulphuric acid. Due to its relative low mobility during leaching conditions, radium is accumulated in the fine fraction of the waste, which is eventually stored in mill tailings. From these tailings, radium may be released to the soil, resulting in a serious concern due to its high radioactivity. The mobility of radium after storage have recently been evaluated in [1999MAR/AKB] and [2003MAR/CRU]. Martin and Akber [1999MAR/AKB] used the relative concentrations of radium isotopes to evaluate the absorption/desorption of radionuclides and secondary mineral formation in groundwater systems close to uranium mine tailings. Their data indicated that almost all ^{226}Ra was removed by the formation of barite solid solution. On the other hand, Martin *et al.* [2003MAR/CRU] concluded that dissolution of a solid $(Ba,Ra)SO_4$ solid solution controls the aqueous concentration of radium and barium in waste porewater, confirming previous data by Snodgrass and Hileman [1985SNO/HIL]. From microbiological studies, it is suggested that the radium and barium release is mediated by SO_4-reducing bacteria [1986LAN/MIL], [1986FED/WES].

Barite is also found as impurities in phospogypsum, which is a by-product from the manufacturing of phosphoric acid in phosphate fertilizer industry. Phospogypsum precipitates during the reaction of sulphuric acid with phosphate rock, and it may contain high levels of natural uranium-series radionuclides. Due to the fact that it is produced and stored in large amounts, phosphogypsum is considered as large potential source of radionuclides released to the geosphere, and, consequently, a number of studies have been devoted to its characterisation. In one of these studies, Rutherford *et al.* [1996RUT/DUD] found that one of the most problematic radioisotopes, ^{226}Ra, was probably part of $(Ba,Sr)SO_4$ solid solution impurities. On the other hand, in some plants, the manufacturing of phosphoric acid may use hydrochloric acid instead of sulphuric

[1] U.S. Environmental Protection Agency (1977). Quality Criteria for Water. Office of Water and Hazardous Materials, Washington, D.C., 256 p.

acid ([2001PAR/VAN]), resulting in the formation of $CaCl_2$-rich effluents that are discharged into surface waters. Part of the ^{226}Ra derived from the original phosphate rock mobilises as chloride complexes, resulting in a notable pollution of the surface waters. As a decontamination treatment, $BaCl_2$ and Na_2SO_4 are added to the effluents to precipitate $(Ba,Ra)SO_4$ solid solutions.

Other research fields that use the Ra-Ba sulphate solid solution are paleoceanography and climatology. The evaluation of many marine processes and their relationship with climatic phenomena requires precise dating of oceanic sediments. As an example, carbonate content fluctuations in marine sediments have been linked to atmospheric CO_2 changes but uncertainties still remain due to, in part, imprecise methods of dating of carbonate precipitates in oceans. In this regard, ^{226}Ra in marine barites has turned to be a very promising method of dating ([1996PAY/MOO], [2004BEC/REY]).

II.3.1.2.2 Numerical modelling involving $(Ba,Ra)SO_4$ solid solutions

The increasing knowledge of solid solution chemistry in the $(Ba,Ra,Sr,Pb)SO_4$ system has allowed the building of reactive transport models that include solid solutions instead of pure phases, which is, perhaps, the ultimate goal of Aq-SS research (and these Guidelines). Conventional reactive transport simulations use thermodynamic equilibrium and kinetic data of pure phases to explain the evolution of pollutants in water. However, most pollutants are found in trace concentrations that make unlikely the saturation with respect the pure solid phase. As illustrated above by the $(Ba,Ra)SO_4$ system and others ([1998BRU/DUR]), there are clear evidences that precipitation of pure phases of contaminants is rarely achieved. Langmuir and Melchior [1985LAN/MEL] found that deep brines in the Palo Duro basin (USA) were undersaturated by from 5 to 6 orders of magnitude with respect to pure $RaSO_4$, and they suggested that the radium solubility was limited by the formation of solid solutions in the $(Ba,Sr)SO_4$ system.

In view of the above, the effect of Aq-SS equilibrium on water chemistry is important enough to be considered in reactive transport modelling when simulating trace element migration. In a recent work, Zhu [2004ZHU2] implemented the thermodynamic and kinetic data of the $(Ba,Ra)SO_4$ solid solution system in reactive transport codes (EQMOD, [1992YEH], and PHREEQC, [1999PAR/APP]) and compared the data obtained when considering pure phases and solid solutions. His models included aqueous speciation and complexation, thermodynamic properties of solid and aqueous solutions and precipitation and dissolution kinetics. The obtained results clearly showed that Ra^{2+} concentrations in water differ several orders of magnitude whether equilibrium with a solid solution is considered or not. In one of these models, an oil-field brine was simulated to cool down from 100 to 25 ºC over five days. The numerical outcome showed a quick precipitation of a $(Ba,Ra)SO_4$ solid solution, implying a very significant decrease of radium in solution (Figure II-26). During the precipitation process, the solution was undersaturated with respect with pure $RaSO_{4(cr)}$.

Figure II-26: Plots showing the co-precipitation of radium with barite and their effects on the remaining oil-field brine in the model reported by [2004ZHU2]. Note that the incorporation of radium into barite solid solution as a trace metal takes place under conditions of undersaturation with respect to pure $RaSO_{4(c)}$.

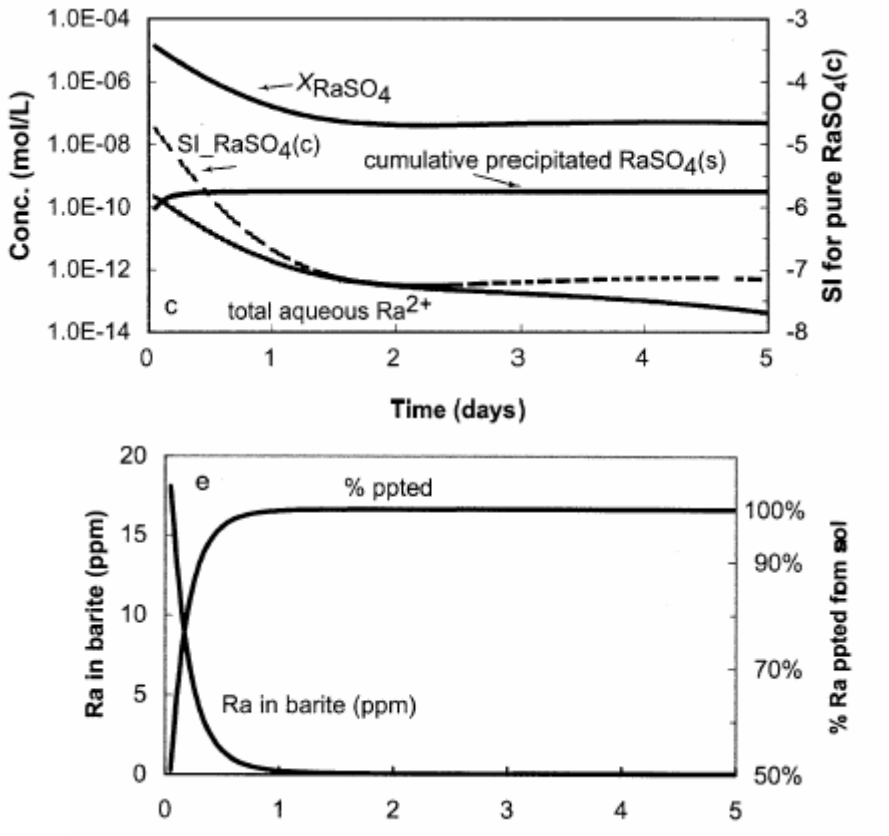

The effect of solid solution co-precipitation is also illustrated in the next example, which simulates in two dimensions the migration of radium-bearing effluent from a phosphate industry (Figure II-27). As explained above, some phosphate-manufacturing plants use HCl to treat ore to obtain phosphoric acid, resulting in effluents rich in calcium and, sometimes, in radium. In the example, the effluent coming from the plant flows through a sedimentary clay formation that contains a number of reactive minerals, mainly calcite and barite. Initially, clay porewater is equilibrated with the mineral paragenesis of the clay formation, but its composition changes, as long as the effluent migrates. For the sake of comparison, initial porewater composition (Table II-10) and mineral content is very similar to that reported by Wersin [2003WER] for the Opalinus Clay Formation, which has been investigated as a host–rock of HLN wastes. Berner and Curti

[2002BER/CUR] used the GEM approach (see Section II.1.2.4 in these guidelines) to calculate the retention of radium in a nuclear waste repository hosted by the Opalinus Clay. Their results showed that the solubility limit in the clay porewater considering the "conventional" approach, *i.e.*, the total concentration of dissolved radium being controlled by the least soluble pure phase ($RaSO_{4(c)}$), was 4.8×10^{-8} M. In contrast, ideal solid solution co-precipitation of radium with barite lowered the solubility limit to 8.2×10^{-12} M. The solubility limit was even lower, 7×10^{-13} M, if a more complex solid solution with four pure end-members (barite, celestite, gypsum and $RaSO_{4(cr)}$) was considered. However, this value is likely too low since the presence of $CaSO_4$ and and celestite end-member implies a positive non-ideality of the system and the overall solubility may be somewhat higher.

Figure II-27: Sketch of the example modelled to illustrate the effect of the radium co-precipitation with barite. A radium-bearing effluent is released from a phosphoric-manufacturing plant and interacts with the porewater of a clay formation. The concentration of barite in the rock is 0.0005 mol·(kg^{-1} porewater), except for a small portion close to the plant, where it reaches 0.1 mol·(kg^{-1} porewater).

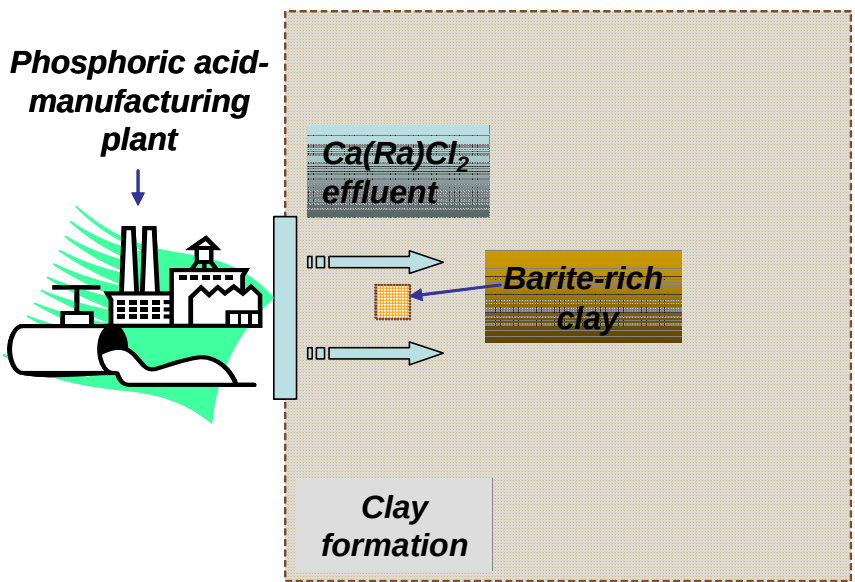

Table II-10: Initial composition of the clay porewater and of the radium-bearing effluent. Concentrations are in mol·kg^{-1} water.

	Effluent	Porewater
pH	7.2	7.2
C	1.0×10^{-10}	2.7×10^{-3}
Ca	1.0×10^{-2}	1.1×10^{-1}
Cl	2.0×10^{-2}	1.6×10^{-1}
K	1.0×10^{-10}	5.6×10^{-3}
Mg	1.0×10^{-10}	7.5×10^{-3}
Na	1.0×10^{-10}	1.7×10^{-1}
S	1.0×10^{-10}	6.0×10^{-2}
Ba	1.0×10^{-10}	1.0×10^{-4}
Sr	1.0×10^{-10}	1.0×10^{-4}
Ra	*1.0×10^{-6}*	*1.0×10^{-12}*

As in [2002BER/CUR], two different reactive transport simulations have been performed in the present example:

1/ $RaSO_4$ as a pure phase limiting the solubility of the radium.

2/ Formation of $(Ba,Ra)SO_4$ solid solution.

For a better observation of the co-precipitation effects, a number of important simplifications are considered:

- $(Ba,Ra)SO_4$ solid solution is considered as ideal.
- Calcite (initial concentration = 0.63 mol·kg^{-1} porewater) and barite (0.0005 mol·kg^{-1} porewater) are considered as reactive minerals. Celestite is not present initially but is allowed to precipitate if the solution is oversaturated with respect to this mineral. Gypsum is not allowed to dissolve or precipitate. The $\log_{10} p_{CO_2}$ is – 2.2.
- No decay of radium is implemented in the calculations, so that Ra concentration (or $RaSO_4$ precipitation) along the flow path is overestimated through time.
- The whole solid solution phase recrystallises in thermodynamic equilibrium with the aqueous solution. This assumption is forced by code limitations.
- No dissolution/precipitation kinetics is considered for any mineral phases.
- No exchange reactions between clay minerals and pore fluids are considered.

Kulik *et al.* [2004KUL/BER2] showed that the Ba/Ra in the precipitated solid solution has an important effect on the radium concentration in the solution (Figure II-28). To test this effect, the initial concentration of barite has been increased 200 times in a small portion of the modelled domain (see Figure II-27 for location).

Figure II-28: Effect of the Ba/Ra ratio on the radium concentration in solution. This ratio depends on the barium availability at time of (Ba,Ra)SO_4 precipitation. The solubility limit of radium if solution is equilibrated with pure $RaSO_4$ is also shown. From [2004KUL/BER2].

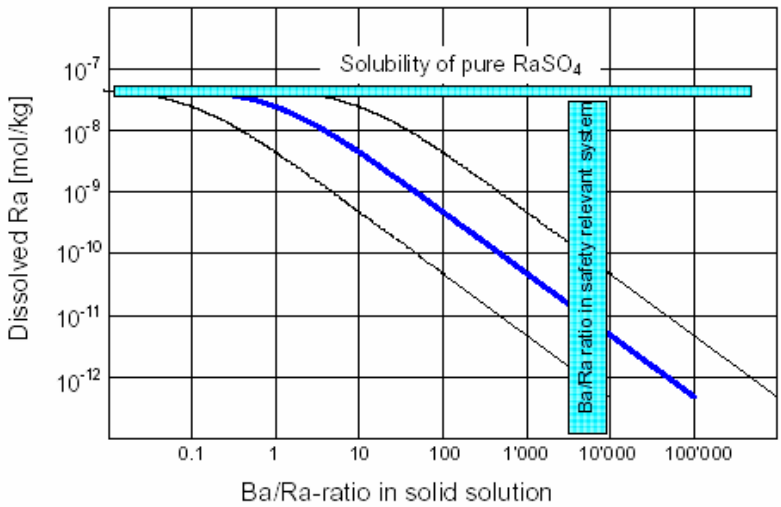

The simulations have been performed with the reactive transport code PHAST [2004PAR/KIP]. This code is the result of coupling a transport code, HST3D ([1997KIP]) and a geochemical code, PHREEQC [1999PAR/APP], and it is able to simulate multi-component, reactive solute transport in three-dimensional saturated groundwater flow systems. A number of boundary conditions are available (specified-head, flux and leaky conditions), and chemical reactions include homogeneous equilibria using an ion-association thermodynamic model, heterogeneous equilibria between the aqueous solution and minerals, gases, surface complexation sites, ion exchange sites, solid solutions, and kinetic reactions.

The modelled domain, which is 100m x 100m in extension, has been discretised into 924 elements. The minimum ΔX and ΔY is 2m and the maximum is 5m. The simulation time is 10,000 years.

The database used in the example is that of Nagra-PSI [2002HUM/BER]. The radium species considered are Ra^{2+}, $RaCl^+$, $RaOH^+$, $RaSO_4$(aq) and $RaCO_3$(aq).

The reactive transport calculations performed in the case 1 indicate that the initial concentration of radium carried by the effluent (1×10^{-6} mol·kg^{-1}) decreases one order of magnitude in the first 5 metres (Figure II-29), due to the precipitation of the pure radium sulphate phase (Figure II-30). Maximum radium concentration in porewater (*i.e.*, the solubility limit) reaches a stationary state around 8×10^{-8} mol·kg^{-1}. This value is close to the solubility limit reported by Berner and Curti [2002BER/CUR] ($[Ra]_{max} = 4.8\times10^{-8}$ mol·L^{-1}; see above). The difference between both values is caused by the lower radium concentration that is being added to the system in the model by Berner and Curti.

Figure II-29: Evolution of radium concentration through time along the flow direction (X) in the case 1. The plotted section corresponds to Y = 50 m. Note that the maximum radium concentration in porewater tends to stabilise when reaches values close to 8×10^{-8} mol·kg^{-1}, denoting the precipitation of a $RaSO_4$ solid.

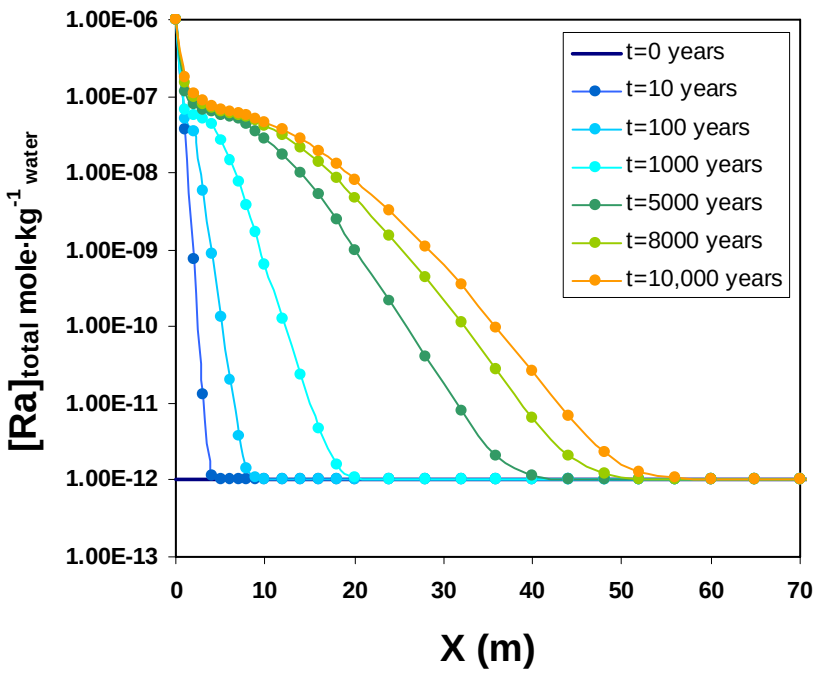

The solubility limit is much lower if the porewater is assumed to be equilibrated with a $(Ba,Ra)SO_4$ solid solution instead of pure phases (barite and $RaSO_4$). As observed in Figure II-31, the front of "Ra-polluted" water is less extensive and the maximum radium concentration is not higher than 1×10^{-9} mol·kg^{-1}. In the whole modelled domain, the radium concentration is, at least, three orders of magnitude lower than in the case considering pure solid phases. Interestingly, radium co-precipitation is en-

hanced in the area where barite is more concentrated, decreasing the solubility limit between two to three orders of magnitude with respect the zones with lower barite content (Figure II-31 and Figure II-32). This is caused by the higher supply of barium in solution due to the instantaneous dissolution of barite, which is subsequently reprecipitated as solid solution. Obviously, this complete recrystallisation of barite is unlikely to occur since kinetics may prevent barite to dissolve. Nevertheless, leaving apart kinetic influence, it is important to show the dependence of radium solubility limit on the Ba/Ra ratio in the solid solution, as already illustrated by Kulik *et al.* [2004KUL/BER2] (Figure II-28).

Figure II-30: Precipitation of $RaSO_4$ due to the inflow of a Ra-bearing effluent from the plant. The low solubility of pure radium sulphate ($\log_{10}K_s$= –10.38) and the relatively high concentration in sulphate in the porewater leads to the formation of $RaSO_4$ in areas close the effluent source.

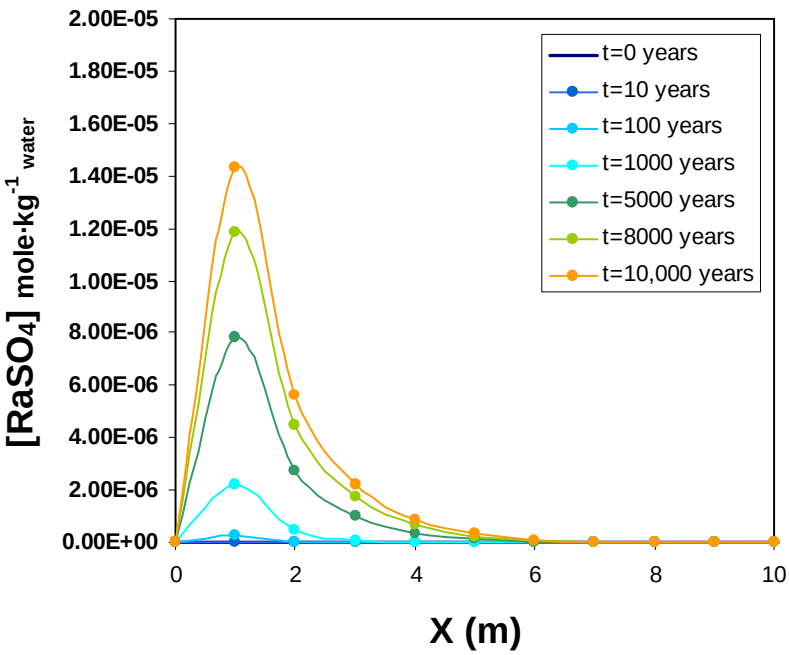

Figure II-31: Extension of the Ra-rich plume after 10,000 years in the two cases simulated. In the first case (top), porewater is equilibrated with a pure $RaSO_4$ phase, whereas in the second one (bottom), the radium solubility is controlled by the formation of the $(Ba,Ra)SO_4$ solid solution. In the latter case, the influence on the radium solubility of a zone with higher barite content is well observed (arrow). The source of the Ra-bearing fluid is indicated as a pale blue rectangle in the left margin of the domain.

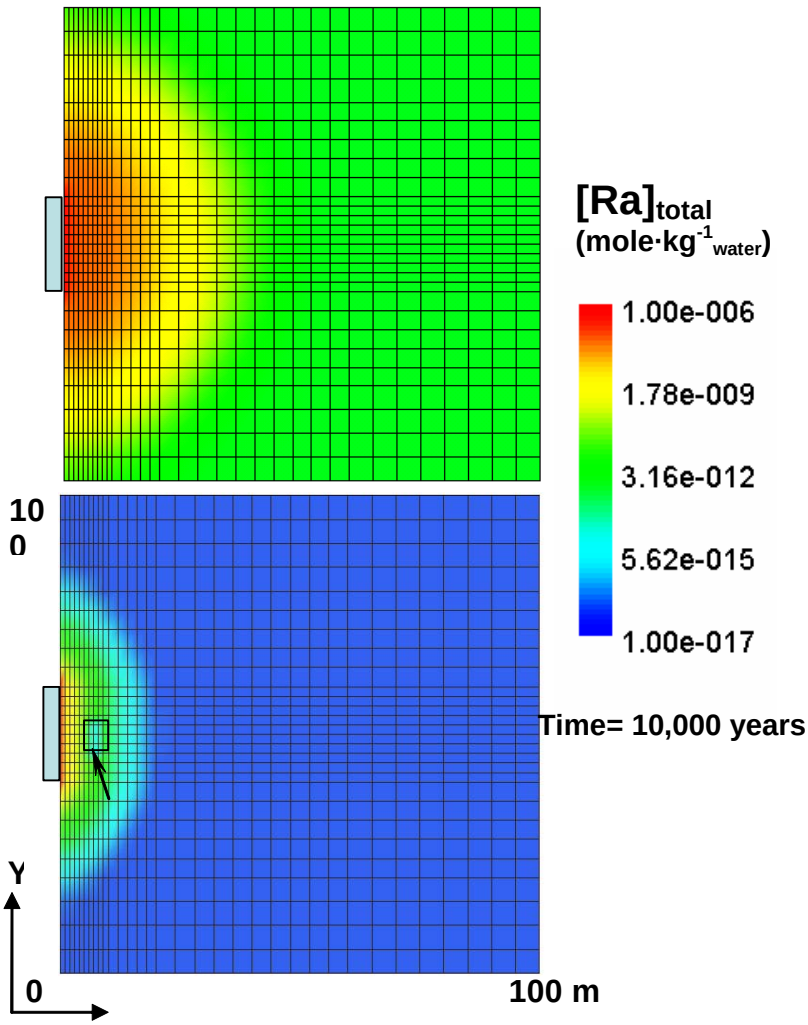

Figure II-32: Evolution of radium concentration through time along the flow direction (X) in the case 2. The plotted section corresponds to Y = 50m. Formation of the $(Ba,Ra)SO_4$ solid solution controls the radium concentration in solution. The sudden $[Ra]_{total}$ decrease from X = 6 to 8 m is caused by the existence of initial higher barite contents in the clay formation that leads to higher barium availability in the porewater (see text).

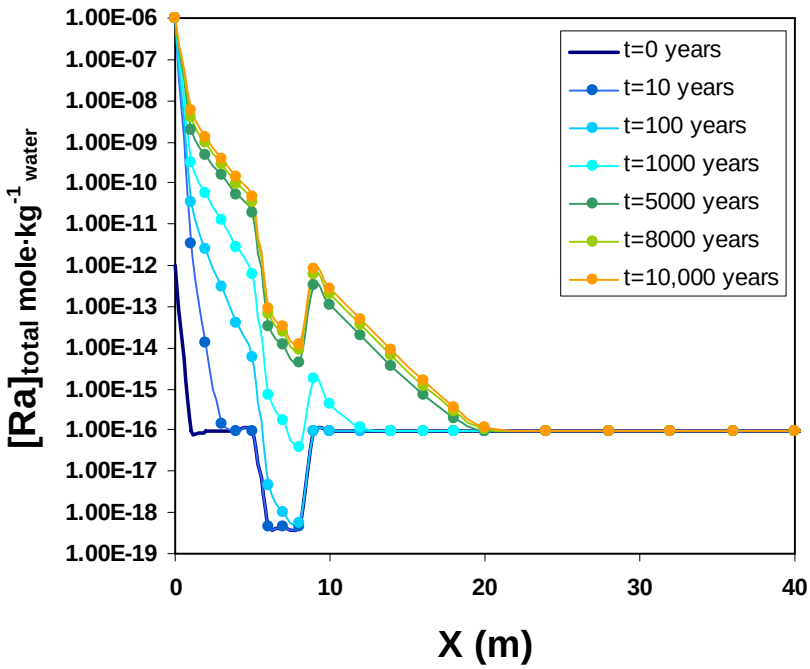

II.3.1.3 Conclusions

The results from the $(Ba,Ra)SO_4$ system and from other solid solution series strongly supports the idea that the knowledge on Aq-SS systems is essential when evaluating the behaviour of radionuclides in PA. Conventional numerical models failed in reproducing environmental data because most codes still use pure phases as solubility-controlling components. On the other hand, the studies on the barite isostructural family also show that much work on the thermodynamic properties of solid solutions remains to be done until a complete SS data base is built.

II.3.2 Cases study/Cement phases – Solubility of calcium silicate hydrates (C-S-H)

Ordinary Portland Cement (OPC) is the most widespread matrix material currently considered in disposal of low-to-intermediate level nuclear (and non-nuclear) waste ([1992BER], [1992REA], [1997GLA]).

Hydrated cements consist mainly of the *calcium silicate hydrate* phase (C-S-H in cement chemistry notation, where CaO is denoted as C, SiO_2 as S, and H_2O as H) of variable composition expressed with the C/S (Ca/Si molar) ratio, usually in the range $0.8 < C/S < 1.7$. The structure and stability of C-S-H has been the subject of a long debate because C-S-H is a major binder in the hydrated cement paste, and because it can immobilise many hazardous elements. The structure of C-S-H phases can be viewed as a distorted and fragmented structure of calcium hydrosilicates such as tobermorite or jennite ([2004RIC], [1992TAY]). However, the structural details of C-S-H are not yet fully understood because such phases have very small grain size, often X-ray amorphous (gel-like) and tightly intermixed in cured samples. This imposes a phase characterisation problem. At the same time, C-S-H structure is flexible enough to accommodate variable fractions of calcium and to provide exchange sites for various cations (Na, K, Cs, Sr, Al, Zn, …).

Thermodynamic modelling can calculate stable phase assemblages and metal partitioning between phases as a function of physicochemical conditions and bulk composition of the system. However, the system $CaO\text{-}SiO_2\text{-}H_2O$ poses some problems to thermodynamic modelling when C-S-H phases are involved. The C-S-H "gel" is, in fact, a less-polymerised metastable precursor of crystalline tobermorite or jennite, and it tends to convert into a more polymerised form with time or at elevated temperatures. C-S-H phases have significant and variable specific surface area (up to 200 $m^2 \cdot g^{-1}$ or more) which makes them reactive, prone to incongruent dissolution with preferential release of Ca upon acidification or carbonation of the system, or even upon decreasing solid/water (S/W) ratio, which leads to precipitation of more silica-rich secondary (but again metastable) C-S-H phases. This kind of incongruent, non-stoichiometric dissolution behaviour, typical for Aq-SS equilibria, must be duly addressed in any experimental work or physicochemical modelling related to cement-water interactions.

Kulik and Kersten [2001KUL/KER] have identified two alternative ways of thermodynamic modelling of partial-equilibrium Aq-SS systems such as $C\text{-}S\text{-}H\text{-}H_2O$. (i) One can assume end-member stoichiometries derived from stable mineral analogs such as tobermorite, jennite, or portlandite, and eventually include non-ideal behavior into solid solutions formed by these end-members, if this is needed for fitting experimental solubility data. (ii) One can seek for such C-S-H end-member stoichiometries and their standard molar Gibbs energy G^{o}_{m}(298.15 K) values that would make the ideal solid solution model possible to apply. However, the need for further extension to trace metal or radiotoxic element-doped (*i.e.*, multi-component) C-S-H systems makes the approach (i)

intractable in practice due to the necessity to introduce many (semi-empirical) interaction parameters with little hope to collect enough experimental data for finding parameter values with reasonable precision. For those reasons, the approach (ii) based on optimisation of ideal end-member stoichiometries to fit experimental data appears to be the only practically feasible opportunity [2001KUL/KER].

Next question was - how the stoichiometries of C-S-H model end-members can be substantiated regarding structures of C-S-H and crystalline minerals tobermorite or jennite? Both minerals are composed of layers of octahedrally-coordinated Ca ions intercalated with "dreierketten" chains of silicon-oxygen tetrahedra (see *e.g.*, [2004RIC]) in which each third "bridging" tetrahedron is looking out of the Ca-Si layer. In the C-S-H structure, many "bridging" silica tetrahedra are missing, especially in freshly precipitated C-S-H at room temperatures, which are essentially "dimeric" (Figure II-33-A). The missing silica tetrahedra sites possess charges that are compensated with Ca^{2+} or other cations. At high calcium concentrations, Ca-hydroxide "layers" can be additionally intercalated, forming Ca-rich C-S-H with C/S > 1.5. Upon aging, dissolved silica species attach to the "bridging" sites thus increasing the degree of polymerisation of C-S-H (from dimeric to about pentameric structures, especially at C/S ratios below 1 and/or at elevated temperatures). Aluminate ions can also attach to vacant "bridging" sites together with alkali ions, as shown schematically on Figure II-33-B.

Assuming that C-S-H gels contain at least two kinds of micro-domains of different structure, one related to that of tobermorite $[Ca_5Si_6O_{16}](OH)_2{\cdot}4(H_2O)$, and another to that of jennite $[Ca_9Si_6O_{18}](OH)_6{\cdot}8H_2O$, Taylor [1986TAY], [1993TAY] suggested the following chemical formula:

$$Ca_4[(Si_{6-\Delta}\boxtimes_{\Delta}O_{18-2\Delta})H_{2p}Ca_{2-p}]_q{\cdot}(OH)_{8(1-q)}\cdot mH_2O \qquad \text{(II.253)}$$

where ⊠ represents a vacant "bridging" tetrahedral site. The other parameters are constrained to $0 < \Delta < 2$, $0 < p < 2$, and $0.5 < q < 1$. The mean chain length is hence equal to $6/\Delta - 1$, so the fully-polymerised structures of tobermorite (with $q = 1$, $p = 1$) and jennite (at a Ca/Si = 1.5 with $q = 0.5$, $p = 1$) correspond to $\Delta \to 0$. On the other hand, many or all of the bridging tetrahedra can be absent in freshly precipitated C-S-H at an early reaction stage (dimeric C-S-H). Upon ageing or during a slow, diffusion-controlled preparation route, however, the bridging tetrahedra may become present to an increasing extent. Fujii and Kondo [1983FUJ/KON] described their solubility data at 30 ºC assuming the fully polymerised 14Å-tobermorite end-member stoichiometry, $5Ca(OH)_2{\cdot}6SiO_2{\cdot}5H_2O$, in the following denoted as "*Tob*" end-member. Compilation of the available experimental solubility data points to a minimum of dissolved Ca_{aq} in the aqueous phase in equilibrium with C-S-H of C/S ≈ 0.8 [1988BER2], [1987GAR/JEN]. This may suggest the existence of a Gibbs energy minimum for C-S-H gel close to the ideal tobermorite composition with C/S = 5/6 ≈ 0.833. Supposing that in such a C-S-H structure pentameric silica chains prevail [2000JEN], one obtains a somewhat different stoichiometry, $[Ca_4H_4Si_5O_{16}]{\cdot}(H_2O)_m$. According to Fujii and Kondo [1981FUJ/KON],

the water content m can be expressed in a simplified way as xCaO·SiO$_2$·(x+0.8)H$_2$O, which gives a bulk composition 4CaO·5SiO$_2$·8H$_2$O, resulting in m = 6 for this kind of end-member.

Figure II-33-A: "Dimeric" tobermorite-like structural motive of C-S-H (silica chain length equals 2); B. More polymerised C-S-H structure (chain length up to 5) with sorbed cations and tetrahedral aluminate ions; C. Additional Ca(OH)$_2$ layer in high-Ca C-S-H structure. The interlayer water molecules are not shown. Reprinted from [2004RIC], Copyright (2004), with permission from Elsevier.

A

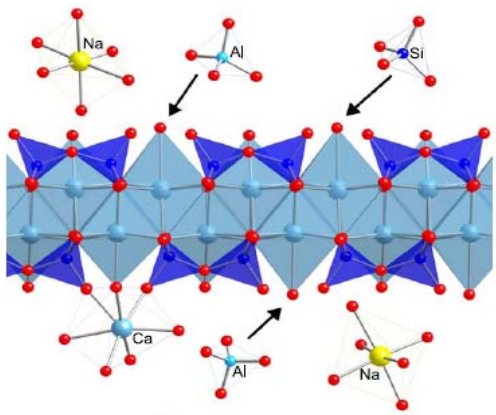

B

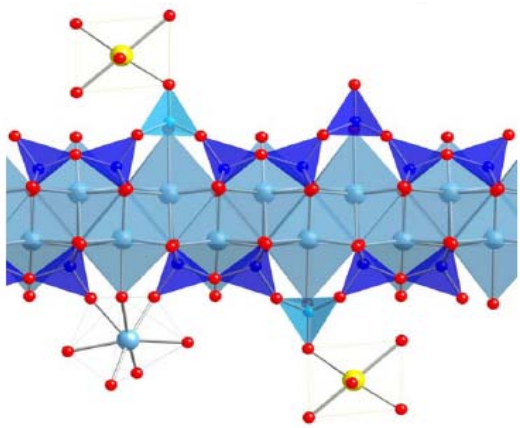

C

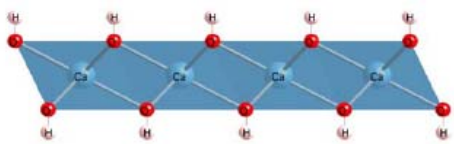

For the Ca-rich end-member, different sets of solubility data cover a range 1.4 < Ca/Si < 2.0 until saturation with crystalline portlandite is reached [1988BER2], [1987GAR/JEN], [1986JEN]. Pronounced solubility differences for samples of different preparation conditions and ageing can be accounted for by fitting the standard molar Gibbs energy G_m^o value for this end-member, or, more simply, by changing the C/S ratio in the end-member formula. For instance, the pentameric "Ca-rich" jennite-like C-S-H end-member "J5" would have a bulk formula $10CaO{\cdot}5SiO_2{\cdot}14H_2O$. The whole binary pentameric solid-solution series *T5 – J5* would then cover C-S-H compositions in $0.8 \le C/S \le 2.0$ interval.

Recent studies based on ^{29}Si-NMR data corroborate a two-phase model for C-S-H and suggest that 14 Å-tobermorite is a suitable structural model for low-Ca C-S-H at 0.8 < Ca/Si < 1.0 [1999GRU]. What happens with the structure at Ca/Si < 0.8 is less clear. Until the structural relationships in this silica-rich region will be clarified, solubility data can reasonably well be modelled assuming simply another (hypothetical) solid solution between amorphous silica and tobermorite-like C-S-H end-member. This approximation is warranted because of the potential role of low-calcium C-S-H phases as end-products of prograde reaction of cements with CO_2-containing groundwater, although not yet considered in detail.

The stoichiometries considered above suggest that the C-S-H solid solutions may not obey Raoult's law even at zero enthalpy of mixing (see Section II.1 for theoretical details). In such mixtures resembling "sublattice" solid solutions, the activities of end-members are proportional to non-unity powers of mole fractions [1969OAT]. However, as shown in Section II.1 and in [2001KUL/KER], this behaviour can often be reduced to "Raoultian" ideal mixing by the appropriate scaling of end-member stoichiometries and their solubility products or standard molar Gibbs energies. As the Raoult ideal law is used in almost all geochemical modelling codes for ideal mixtures, this opportunity to fit the solid solution model to solubility data is of a considerable practical interest, especially in the case of strongly incongruent mixtures with ill-defined structure, such as C-S-H phases.

Kulik and Kersten [2001KUL/KER] suggested that "fitting" of the ideal C-S-H solid solution model can be achieved by simply multiplying the stoichiometry of both end-members (and also their $\log_{10}K_{s,p}$ and G_m^o values) by scaling coefficients n_i, which are not necessarily equal for all end-members. This procedure will retain the same stability and solubility of both end-members, will make their activities in the ideal solution formally equal to mole fractions, but will change the calculated solubilities of intermediate solid phase compositions. In order to derive the scaling coefficients n_i for the C-S-H solid-solution system, the generic reactions should be written to determine standard thermodynamic properties of solid end-members. The C-S-H end-members can be described using isoelectric hydrolysis dissolution reactions, but with component formulae normalised per n_{Si} silicon atoms. Bulk tobermorite-like C-S-H stoichiometries can then be expressed as:

$$n_{Si}(SiO_2)n_{Ca}[Ca(OH)_2]n_{Ca}(H_2O) + 2n_{Ca}H^+ \rightleftharpoons 3n_{Ca}H_2O + n_{Ca}Ca^{2+} + n_{Si}SiO_2$$
$$\text{with } \log_{10}K = n_{Si}\log_{10}K_{Tob} \qquad \text{(II.254)}$$

where $n_{Ca} = 0.8\ n_{Si}$ for the pentameric (*T5*) and $n_{Ca} = 0.833\ n_{Si}$ for the fully polymerised (*Tob*) end-member structure models discussed above. Likewise, bulk jennite-like C-S-H stoichiometries can be expressed as:

$$n_{Si}(SiO_2)\ n_{Ca}[Ca(OH)_2]\ n_{Si}(H_2O) + 2n_{Ca}\,H^+ \rightleftharpoons (n_{Si}+2n_{Ca})H_2O + n_{Ca}Ca^{2+} + n_{Si}SiO_2$$
$$\text{with } \log K = n_{Si}\log K_{Jen} \qquad \text{(II.255)}$$

where the parameter n_{Ca} may in principle vary between 1.4 n_{Si} and 2.0 n_{Si}, in the range of C/S ratios known for the Ca-rich C-S-H phases. The mineral jennite has $n_{Ca} = 1.5\ n_{Si}$, while the "polymerised" Ca-tobermorite end-member (herewith called "Jen") with C/S = 10/6 has $n_{Ca} = 1.667n_{Si}$, close to the "pentameric" end-member variant "J5" with C/S = 8/5 ($n_{Ca} = 1.6n_{Si}$) or 9/5 ($n_{Ca} = 1.8n_{Si}$). The dimeric model end-member would have C/S = 3/2 ($n_{Ca} = 1.5n_{Si}$); the Grutzeck's ([1999GRU/KWA]) "sorosilicate-like" model end-member should have C/S = 2 ($n_{Ca} = 2n_{Si}$).

Eqs. (II.254) and (II.255) assume that the number of water molecules is equal to n_{Ca} at C/S < 1, and to n_{Si} at Ca/Si > 1, in order to keep it close to the ratios proposed in [1981FUJ/KON]. Note that the amount of crystallisation water in the end-member stoichiometry does not affect the calculated Aq-SS solubility curves, as long as the C-S-H phases remain fully hydrated.

If any standard molar thermodynamic property Θ(A) of one of the above mentioned end-members is determined at a certain value of n_{Si}(A) with a stoichiometry factor A, it can be converted using another "fractional" stoichiometry factor B at n_{Si}(B) by simple multiplication:

$$\Theta(B) = \frac{n_{Si}(B)}{n_{Si}(A)}\,\Theta(A) \qquad \text{(II.256)}$$

provided that the ratio n_{Ca}/n_{Si} = C/S remains constant; otherwise, standard thermodynamic properties must be refitted or redetermined. Equation (II.256) is simply a consequence of the additivity of chemical potentials; it provides constant stability/solubility of the end-members upon scaling of their stoichiometries.

Modelling of complex Aq-SS systems such as cement pore fluids or near-field interstitial waters requires application of computer codes (see Section II.2.). Programs based on the convex-programming GEM approach enable one to solve equilibria in any heterogeneous multi-component ideal or non-ideal Aq-SS system at full complexity. The aqueous ion-association thermodynamic model, used in this study together with the GEMS-PSI code and database (http://les.web.psi.ch/Software/GEMS-PSI/), considers aqueous speciation in the system Ca-Si-N-Cl-O-H-charge. Activity coefficients of aqueous species were calculated using the Debye-Hückel or Davies equations (II.2).

Thermodynamic data for solid phases (portlandite, $SiO_{2,am}$, plombierite *etc*.) can be found in literature ([2001KUL/KER], [2002KUL/KER], [2006LOT/WIN]).

The main test of any model is to demonstrate its ability for providing independent and reasonable predictions of existing experimental data. Many authors selected the C-S-H solubility data set [1965GRE/CHA] where the C-S-H samples were prepared by stirring hydrated silica and portlandite in suspension at 50 ºC for several weeks. Both the slow aqueous reaction route and the elevated temperature yielded rather mature, highly polymerised samples. An important precaution in the experiments of Greenberg and Chang [1965GRE/CHA] (but not by most others) was to exclude the formation and to verify by microprobe determination the absence of surface layer products different in composition from the bulk C-S-H phases. The resulting solution data for dissolved Ca_{aq} and Si_{aq} concentrations, as well as the pH data, show quite consistent trends and cover the whole compositional region of $0 < C/S < 1.9$, thus appearing quite suitable for model verifications.

From a thermodynamic point of view, the C-S-H system can be described using two ideal binary C-S-H-(I) and C-S-H-(II) solid solution phases [2001KUL/KER], [1997SIN/KUL]. Based on the above structural discussion on polymerised end-member compositions, for the Ca-rich C-S-H-(II) phase, two initial end-members $5Ca(OH)_2{\cdot}6SiO_2{\cdot}5H_2O$ (*Tob-II*) and $10Ca(OH)_2{\cdot}6SiO_2{\cdot}6H_2O$ (*Jen*) have been suggested. For another, Si-rich C-S-H-(I) phase, the amorphous silica $SiO_{2,am}$ (*SH*) and a tobermorite-like $5Ca(OH)_2{\cdot}6SiO_2{\cdot}5H_2O$ (*Tob-I*) end-members have been used. Initial estimates of the standard-state Gibbs energy g^o_{298} of those end-members were derived from earlier work [1997SIN/KUL] and then adjusted in GEM calculations of Aq-SS equilibria against the [1965GRE/CHA] solubility data. Equilibria at 1 bar, 25 ºC were calculated at bulk C/S ratios increasing from 0.01 to 2.0 at step 0.05 reproducing the experimental systems (8.05 g SiO_2 per 1 kg H_2O at varying additions of CaO). Portlandite appeared in the calculated equilibria only at $Ca/Si > 1.5$ and higher. The initial solubility products and g^o_{298} values for four end-members (at $n_{Si} = 1$) were ([2001KUL/KER]):

C-S-H-(I): $\log_{10}K_{SH} = -1.2$, $G^o_m(SH) = -849.45$ kJ·mol^{-1};

$\log_{10}K_{Tob\text{-}I} = 11.15$, $G^o_m(Tob\text{-}I) = -1823.38$ kJ·mol^{-1};

C-S-H-(II): $\log_{10}K_{Tob\text{-}II} = 11.15$, $G^o_m(Tob\text{-}II) = -1823.38$ kJ·mol^{-1};

$\log_{10}K_{Jen} = 29.133$, $G^o_m(Jen) = -2616.23$ kJ·mol^{-1}.

Based on Eqs (II.254) and (II.255), a systematic search for optimal C-S-H end-member stoichiometries was performed by changing the n_{Si} coefficients in the range $0.1 < n_{Si} < 6.0$, where only the upper value (6.0) fully corresponds to initially assumed "crystallographic" formula. Constant stabilities of pure end-members throughout the model run series were maintained by first establishing the $G^o_m(298.15\ K)$ from GEM calculations and solubility data at $n_{Si} = 1$ (see above) and then, for other n_{Si} values, by multiplying the initial value of $G^o_m(298.15\ K)$ by the new n_{Si} according to Eq. (II.256).

The results were plotted against experimental data points with dissolved Ca_{aq}, Si_{aq}, and pH *vs.* C/S ratio.

On Figure II-34, it is seen that C/S ratio in the most Ca-rich end-member stoichiometry ("Jennite") has a dramatic effect on the shape of dissolved Ca curve. The higher C/S the stronger "non-ideality" is introduced. Clearly, C/S in the "Jen" end-member should not exceed 10/6 or 1.667 if it is desired to have the ideal SS model applicable. This explains the final selection of the initial "Jen" stoichiometry $10Ca(OH)_2{\cdot}6SiO_2{\cdot}6H_2O$.

Figure II-34: Effect of changing C/S ratio in high-Ca ("Jennite") end-member of C-S-H(II) on the shape of Ca solubility curve of the ideal solid solution between "Tob" $5/6Ca(OH)_2{\cdot}SiO_2{\cdot}5/6H_2O$ and "Jen" $xCa(OH)_2{\cdot}SiO_2{\cdot}H_2O$ where x = 10/6; 11/6; 12/6 and 15/6 (numbers on plot lines). The G^o_m (298.15 K) value of "Tob" was kept constant while G^o_m (298.15 K) value of "Jen" was adjusted in each run to get into experimental region at 1.6 < C/S < 2 (experimental data from [1965GRE/CHA]).

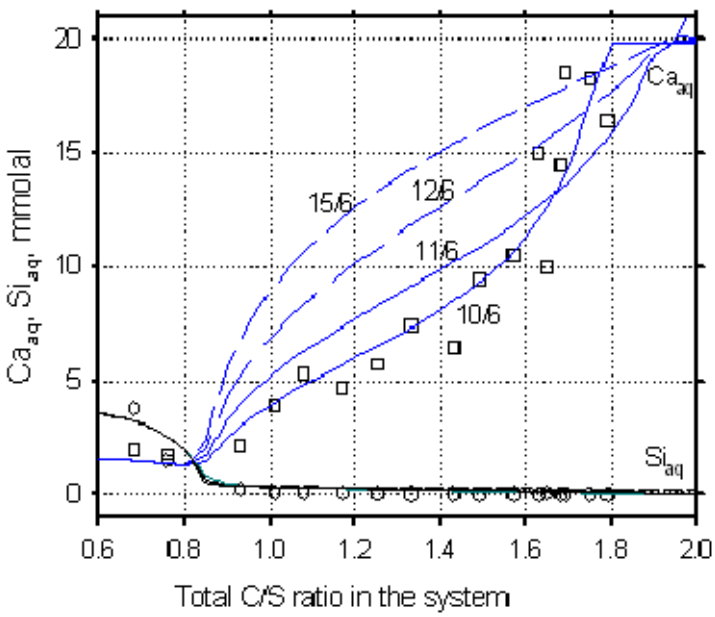

The impact of simultaneous scaling of all end-members (n_{Si} from 0.1 to 6) is seen on Figure II-35. "Crystallographic" end-member stoichiometries (n_{Si} = 6.0) produce unrealistic sigmoid shapes of dissolved Ca curve for the C-S-H-(II) ideal solid solution, and too high, box-like curves for the C-S-H-(I) solid-solution subsystems. However, n_{Si} values of 1.0 to 1.5 for C-S-H-(II) and 2 to 3 for the *Tob-I* end-member of

C-S-H-(I) solid solution lead to correct shapes and almost perfect fits to solubility data. Fractional end-member stoichiometries ($n_{Si} < 1$) yielded rather odd exponential curve shapes for C-S-H-(II) and too low, flat curves for the C-S-H-(I) solid solutio

Figure II-35: An example of impact of the normalisation factor n_{Si} (applied simultaneously to all four end-member stoichiometries) onto the shape Aq-SS curves for calculated total solubility of Ca and Si (lines) in the C-S-H-H_2O system as function of the total C/S ratio (from [2001KUL/KER] with minor modifications). The flat part of Ca curve at *ca*. 20 mmolal is due to appearance of a stable portlandite $Ca(OH)_2$ phase.

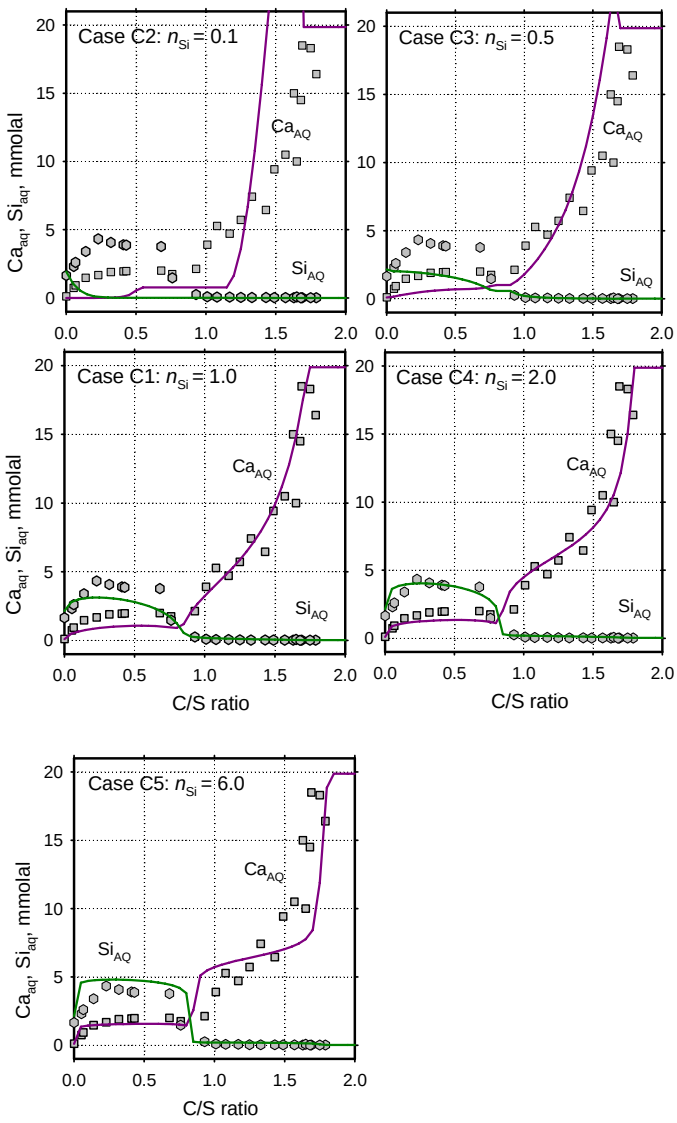

Further fine-tuning of the Aq-SS model ([2001KUL/KER], [2006LOT/WIN]) with different n_{Si} scaling of end-members results in good fits to dissolved Ca and pH data, with a slight overestimation of dissolved Si at C/S > 1 (Figure II-36). "Optimal" stoichiometries and G^{o}_{m} (298.15 K) values of end-members are given in Table II-11. It is seen that, even different aqueous thermodynamic data sets and activity coefficient equations have been used, the G^{o}_{m} (298.15 K) values of end-members differ in at most 2.2 kJ·mol^{-1} or 0.4 pK units, which can be taken as the estimate of uncertainty interval. Refitting of the Aq-SS model to other experimental data sets can be easily done by n_{Si} scaling and/or slight adjustment of G^{o}_{m} (298.15 K) value for the "Jen" end-member.

Table II-11: Optimised C-S-H solid solutions model [2001KUL/KER], [2006LOT/WIN]

Phase	End-member	n_{Si}	n_{Ca}	n_{H}	$\log_{10}K$	G^{o}_{m} (298.15 K) kJ mol^{-1}	G^{o}_{m} (298.15 K)[B] kJ mol^{-1}
C– S– H(I)	SH, SiO_2	1.0	0	0	– 1.20 [A]	– 849.45	– 848.90
	Tob– I	2.4	2.0	2.0	27.36	– 4372.70	– 4370.50
C– S– H(II)	Tob– II	1.8	1.5	1.5	20.52	– 3279.52	– 3277.87
	Jen	0.9	1.5	0.9	26.45	– 2353.32	– 2353.70

Portlandite $Ca(OH)_2$: G^{o}_{m} (298.15 K) = – 897.01 kJ·mol^{-1}. Coefficients n_{Si}, n_{Ca}, n_{H} refer to the bulk formulae $n_{Si}(SiO_2)\cdot n_{Ca}[Ca(OH)_2]\cdot n_{H}(H_2O)$. Values of $\log_{10}K$ refer to the reaction:

$$n_{Si}(SiO_2)\cdot n_{Ca}[Ca(OH)_2]\cdot n_{H}(H_2O) + 2n_{Ca}H^{+} \rightleftharpoons (2n_{Ca} + n_{H})H_2O + n_{Ca}Ca^{+2} + n_{Si}SiO_2.$$

A: reaction: SiO_2(quartz) $\rightleftharpoons$ SiO_2(SH).

B: data from [2006LOT/WIN] consistent with the Nagra-PSI chemical thermodynamic data base [2002HUM/BER] and Davies equation.

The simple ideal solid solution model of C-S-H provides good fits to available solubility data. At the same time, this Aq-SS model can readily reproduce (at least qualitatively) some important features of the C-S-H system, namely the re-equilibration in response to changing S/W ratio (dilution) or addition of CO_2 at fixed S/W (carbonation) [2002KUL/KER]. Both processes can be modelled (using a GEM computer code) as a sequence of equilibrium states controlled by a "process extent" variable.

Figure II-36: Solubility profile (A) and solid phase speciation (B) of C-S-H *vs.* C/S ratios at 1 bar 25 ºC modelled with GEMS-PSI code using two ideal solid solutions C-S-H(I) (end-members SH and Tob-I) and C-S-H(II) (end-members Tob-II and Jen) with G^{o}_{m} (298.15 K) values of end-members from the rightmost column of Table II-11. Graphic printouts from GEMS-PSI code.

(A) (B)

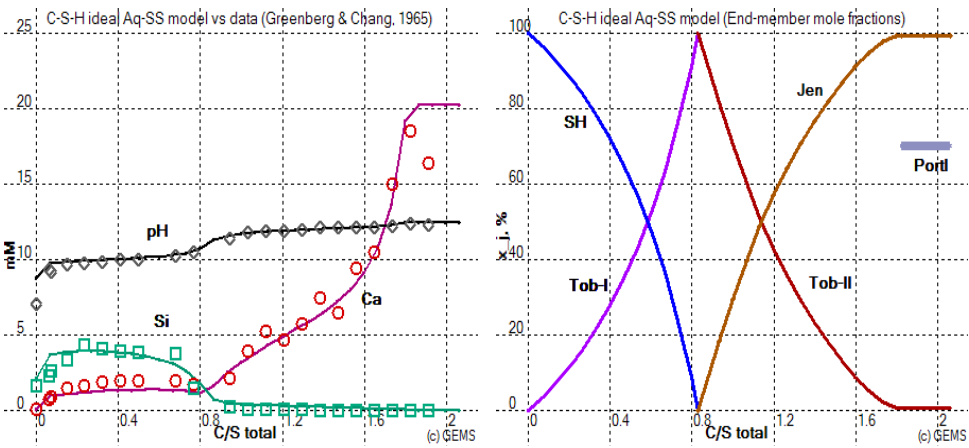

In the first case, the initial system recipe (at 1 bar 25 ºC) can be taken as 1 mol N_2 and 0.001 mol O_2 (to create CO_2-free atmosphere), 1 mol $Ca(OH)_2$, 0.5 mol SiO_2 and 100 g H_2O. The process extent variable is the decimal logarithm of amount of H_2O (grams) in the recipe, changing stepwise from 2.0 (100 g) to 6.0 (1000 kg). Simulation of this irreversible process of dilution using C-S-H(II) solid solution model similar to that given in Table II-11 results in Figure II-37-A. It is seen on this diagram that, as long as the excess portlandite is stable (13 millimoles at the beginning), the dissolved Ca molality and the C/S in C-S-H(II) phase remain constant. Upon complete dissolution of portlandite, the C-S-H(II) phase will incongruently dissolve while releasing Ca into aqueous solution and reprecipitating with more Si-rich composition. This will go on until complete dissolution of C-S-H solid at C/S about 0.8. Of course, such equilibrium "process-extent" model does not take into account any kinetic effects, dissolution and precipitation rates.

Under subsurface waste repository conditions, hydrated cements would react with CO_2-containing groundwater resulting in an incongruent dissolution of portlandite and C-S-H and precipitation of calcium carbonate. In this typical concrete weathering scenario ([1996LAN/HIL], [1997WAL/BIN]), any intercalated metal can be partially mobilised into aqueous solution, precipitate into its own oxide or carbonate phase, or get incorporated into a solid solution with ubiquitous calcite. GEM calculations can easily reproduce such chemical mass transfer, helping in (at least qualitative) prediction

of the possible metal re-partitioning between the near-field groundwater, C-S-H and carbonate solid solutions, or other solid phases.

Figure II-37-A: simulated impact of dilution on Ca solubility and C/S ratio in C-S-H(II) (portlandite is present only at high S/W ratios); B: simulated impact of CO_2 titration on Ca solubility, pH, and C/S ratio in C-S-H(II) (excess calcite phase is present throughout). GEMS-PSI printouts.

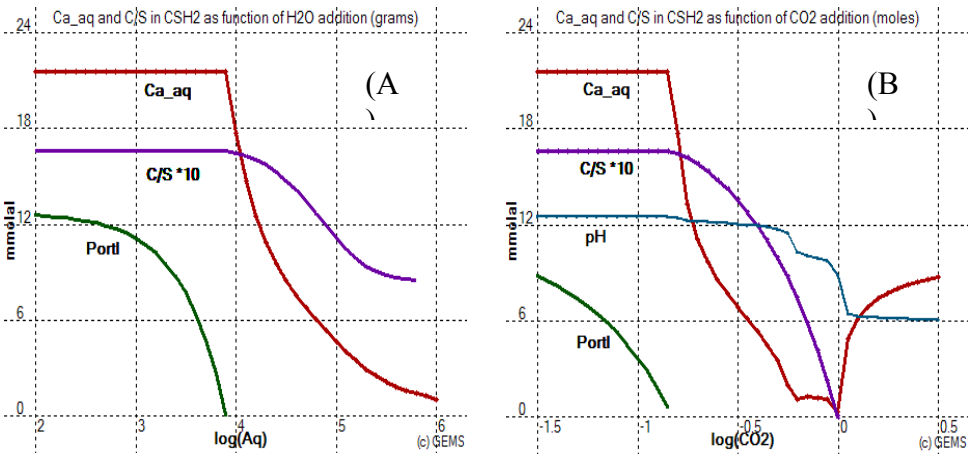

Figure II-37-B shows one such "process extent" calculation with the following initial recipe: 1 mol N_2 0.001 mol O_2 + 1 mol $Ca(OH)_2$ + 0.5 mol SiO_2 + 1 kg H_2O + $10^{-1.5}$ mol CO_2. Then the addition of CO_2 was incrementally increased up to $10^{0.5}$ mol. In presence of carbon dioxide, both C-S-H and portlandite are unstable with respect to calcite which works as a sink for Ca. At $\log_{10}(CO_2,\text{added}) < -0.5$, the diagram looks pretty similar to Figure II-37-A, but at higher additions of CO_2, the process goes further; at $\log_{10}(CO_2,\text{added}) < -0.25$, the C-S-H(II) phase is replaced by C-S-H(I) with C/S < 0.8, until it gets leached to almost pure SiO_2,am (SH) and completely dissolves at $\log_{10}(CO_2,\text{added}) \approx 0$. At this point, pH is about 8, and further addition of CO_2 just acidifies the remaining system calcite + gas + aqueous electrolyte which leads to decreasing pH (down to 6) and increasing dissolved Ca in equilibrium with calcite. Note that this simulation is qualitative because it does not account for the reaction rates and the impact of newly-forming calcite on porosity and permeability of cements.

How can the Aq-SS system for the C-S-H(II) binary solid solution phase described above be extended by introducing another end-member for a minor (trace) metal? This extension has been done for Zn ([2002KUL/KER]) using limited solubility data ([1999JOH/KER]) and evidence of Zn solid solution incorporation in C-S-H. A first step in this study was to seek for the Zn end-member stoichiometry and its G°_{m}(298.15 K) value consistent with Raoultian ideal mixing behaviour. The ideal model appears preferable for an extension to C-S-H-M system because of the lack of experi-

mental data precise enough to determine the interaction parameters needed for any non-ideal solid solution model. The challenge was that for the Zn-bearing end-member, stoichiometry and G_m^o (298.15 K) value must have been determined simultaneously.

Minerals hardystonite ($Ca_2ZnSi_2O_7$), clinohedrite ($CaZnSiO_4{\cdot}H_2O$), hemimorphite ($Zn_4Si_2O_7(OH)_2{\cdot}H_2O$) and junitoite ($CaZn_2Si_2O_7{\cdot}H_2O$) are natural silicates structurally similar to tobermorite. The tetrahedral $ZnO_2(OH)_2^{4-}$ ion can potentially occupy triple-chain (dreierketten) bridging sites instead of silica SiO_4^{4-} ions, thus leading to "Zn-substituted" C-S-H end-members like $[Ca_4H_4Si_4O_{14}Zn(OH)_2]{\cdot}(H_2O)_m$ [2002KUL/KER]. In the presence of portlandite, Ca-hydroxozincate phase (CHZ) can readily form. It is not yet clear to what extent these minerals can mix in solid solution series, and whether their fully hydrated analogues exist at room temperatures. However, one can consider these stoichiometries as potential candidates for Zn-containing C-S-H end-member. Other relevant solids include amorphous silica (SH), portlandite (CH), zincite (ZnO), and calcite.

Unfortunately, thermodynamic data for the Zn-Ca silicates and Zn-bearing C-S-H end-members are not available. The thermodynamic data evaluation technique called "statistical dual-thermodynamic calculation" (Section II.1.3.2.6) turned to be convenient for estimating these G_m^o (298.15 K) values from the available stoichiometries and solubility data, and to select the "optimal" Zn-bearing end-member stoichiometry [2002KUL/KER]. In these DualTh calculations, alternatively "clinohedrite" (*Clnh*, $SiO_2{\cdot}Ca(OH)_2{\cdot}Zn(OH)_2$) and "hardystonite" (*Hard*, $SiO_2{\cdot}Ca(OH)_2{\cdot}[Zn(OH)_2]_{0.5}$) end-members have been found to match best with the ideal ternary solid solution model (other two Zn-free end-members are "Tob" and "Jen" similar to that of C-S-H(II) end-members described above).

The ideal ternary solid solution models Clnh – Tob – Jen or Hard – Tob – Jen with G_m^o (298.15 K) values found from DualTh calculations ([2002KUL/KER]) can be tested in GEM calculations to follow how the composition of Zn-doped C-S-H phases react upon leaching or carbonation of the "cement" system. For instance, Figure II-38-A shows the "dilution profile" of aqueous – 1% Zn-doped C-S-H system (initial recipe similar to that for Figure II-37-A).

At s/w > $10^{-1.2}$ mol (kg H_2O)$^{-1}$, pH, dissolved Ca_{aq}, and Zn_{aq} are fixed by presence of excess portlandite and CHZ. These solids both disappear at s/w < $10^{-1.8}$, where Ca_{aq} and Zn_{aq} become controlled only by the Zn-C-S-H(II) phase of drastically changing composition (Figure II-38-B). Note that this change in solid solution composition coincides with a trough-like Zn_{aq} minimum of 2-3 orders of magnitude (Figure II-38-A). At different total Zn loadings, the Zn_{aq} minima are located at s/w ≈ 10^{-3} close to the maxima in mole fraction of Tob-II end-member. Experimental Aq-SS data (error bars in Figure II-39-A,B) are close to these minima, which indicates consistent behaviour of the Zn-C-S-H ideal solid solution model in all GEM model runs.

Figure II-38: Example of GEM model simulation of Zn-doped "cement" leaching at 1% Zn in *CSH* loading, using Zn-C-S-H(II) solid solution with hardystonite end-member, from [2002KUL/KER]. A: total aqueous solubilities of Ca_{aq}, Zn_{aq}, Si_{aq} and pH; bars at a s/w $\approx 10^{-3}$ correspond to the uncertainty intervals of experimental solubility data ([1999JOH/KER]), positioned along the abscissa according to the solid phase composition. B: mole fractions of end-members and presence of single-component solids (portlandite $Ca(OH)_2$ and Ca-zincate hydrate $CaZn_2(OH)_6{\cdot}2H_2O$ (CHZ)); hexagonal dots correspond to the solid phase composition in the solubility experiment for 1% Zn in C-S-H loading.

(A)

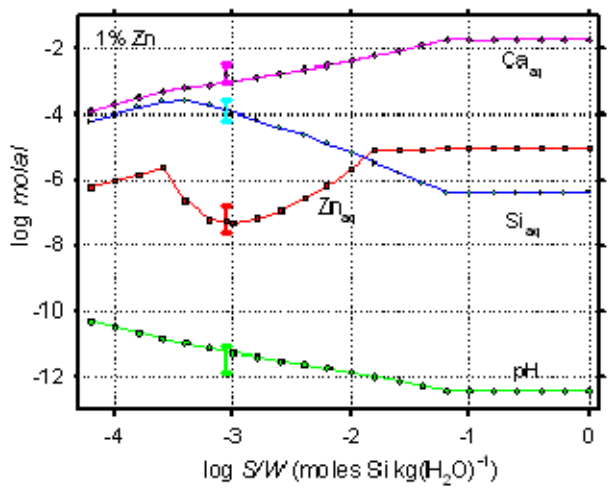

(B)

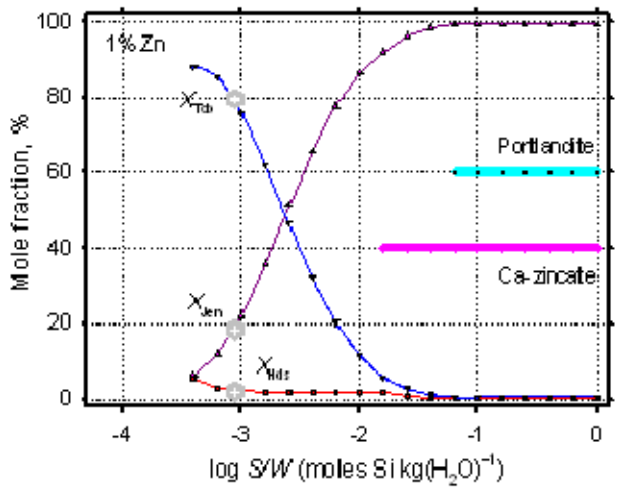

Figure II-39: GEM simulation runs of Zn-doped "cement" leaching at 1 bar 25 ºC, dependence of Zn_{aq} on Zn loading (z in %, numbers at the curves). A: with hardystonite-like, B: with clinohedrite-like Zn-C-S-H(II) end-member (from [2002KUL/KER]). Bars at s/w ≈ 10^{-3} correspond to the uncertainty intervals of experimental solubility data [1999JOH/KER].

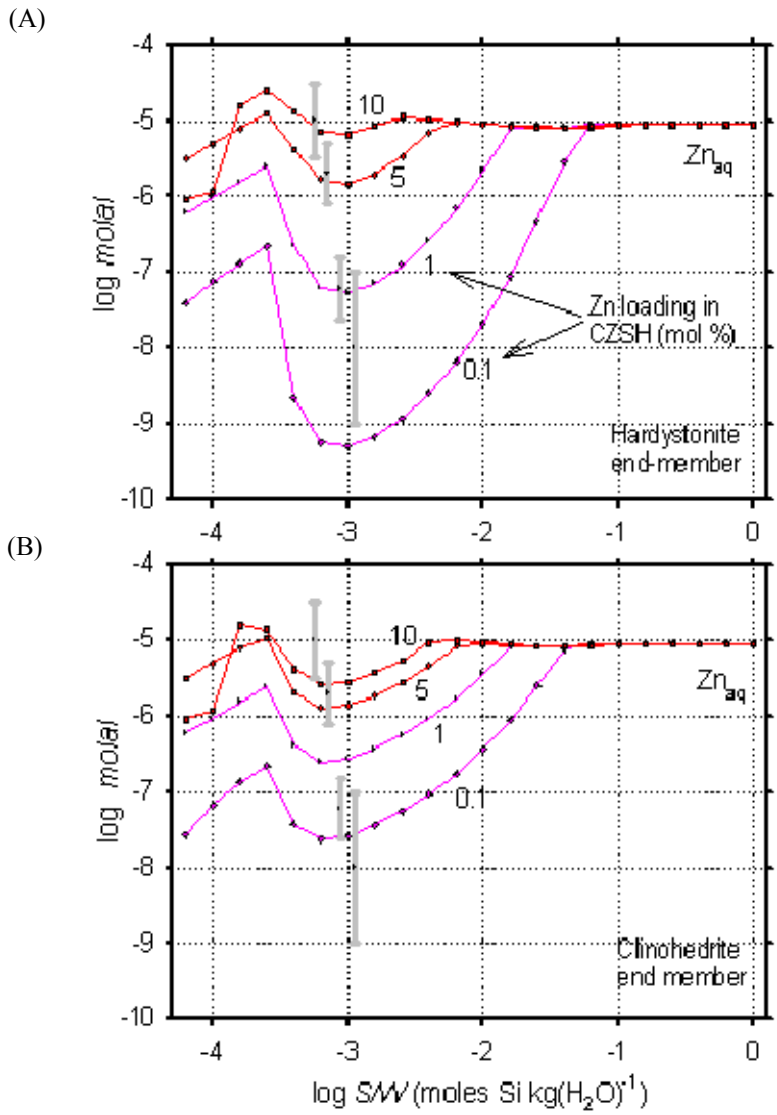

Further decrease in the s/w ratio results in complete dissolution of Zn-C-S-H phase at s/w < 10^{-4}. Calculations with the alternative clinohedrite Zn end-member produced similar plots, but with somewhat less pronounced minima in Zn_{aq} (Figure II-39–B). Evidently, the choice of another Zn-containing end-member stoichiometry leads to different trends of Zn_{aq} at trace Zn loadings. For instance, at 0.1% Zn loading in exchange for Ca, the hardystonite-like end-member model (Figure II-39-A) predicts about two orders of magnitude lower Zn_{aq} than that with the clinohedrite-like end-member (Figure II-39-B). At present, experimental data are insufficient to decide which of both end-members is more reliable. Nonetheless, these results clearly demonstrate the importance of the s/w ratio (*i.e.*, the ratio of actually reacted solid to aqueous phase mass) in modelling metal leaching upon weathering in cementitious repository systems.

The above examples demonstrate the potential of multicomponent ideal solid solution models of C-S-H (formulated in GEM approach) to describe incorporation of cations into the ill-defined structure of C-S-H phases. There is a good short-term perspective of extension of such Aq-SS models to include sorbed Na, K, Al, Sr and Cs because a critical body of experimental data has already been accumulated ([1990BRO], [1999GLA/HON], [2002GLA/HON], [1989MAC/LUK], [2006TIT/WIE]). To establish optimal end-member stoichiometries, the use of DualTh methods seems to be unavoidable.

Other Aq-SS systems relevant for cement disposal matrices include several groups of crystalline minerals that can form various solid solutions, thermodynamic models for which are under construction or still have to be put together. Here, we only list these minerals with some short comments.

AFt phases (ettringites) are considered important regarding the "sulphate attack" on cements, and also because they are known to incorporate hazardous anions such as chromate, selenate, arsenate and vanadate. Ettringite $Ca_6[Al(OH)_6{\cdot}12H_2O]_2(SO_4)_3(H_2O)_2$ has an unusual columnar structure, in which columns are built of Ca^{2+} ions, $Al(OH)_6^{3-}$ moieties and water molecules. The extra positive charge of columns is compensated by intercolumnar anions like sulphate. In place of $Al(OH)_6^{3-}$, $Fe^{III}(OH)_6^{3-}$, $Cr^{III}(OH)_6^{3-}$, and $Si(OH)_6^{2-}$ can be substituted; intercolumn sulphate anions can be exchanged with CO_3^{2-}, CrO_4^{2-}, SeO_4^{2-}, AsO_4^{3-}, VO_4^{3-}, $B(OH)_4^-$. Some thermodynamic data on $Si(OH)_6^{2-}$ substituted ettringite (thaumasite) and anion-substituted ettringites are available ([2003BAU/JOH], [1998BOT/BRO], [2004MAC/BAR], [1999PER/PAL], [2000PER/PAL]), but miscibility limits and interaction parameters of mixing are yet poorly known.

Layered Double Hydroxides (LDH) represent another important group of cement-relevant solid solution phases, which consist of two subgroups: AFm phases (Ca-Al LDH phases) and hydrotalcites (Mg-Al LDH phases).

In the AFm group, the M^{II} cation is Ca^{2+} and the M^{III} cation can be Al^{3+}, Ga^{3+}, Fe^{3+} or Sc^{3+}. Interlayer anions are usually CO_3^{2-}, SO_4^{2-}, Cl^-, OH^-, but can also be SO_3^{2-},

SeO_4^{2-}, CrO_4^{2-}, MoO_4^{2-}, $B(OH)_4^-$, Br^-, I^-. Some solubility products for fully substituted Ca-Al phases like $[Ca_2Al(OH)_6]CrO_4 \cdot 2H_2O$ are known (*e.g.*, [2003BAU/JOH]); some miscibility limits are also known [1989POL].

Mg-Al LDH phases have a common formula $[M^{II}_{1-x}M^{III}_x(OH)_2][A^{m-}_{x/m} \cdot nH_2O]$ with $0.17 < x < 0.45$ (typically, $x = 0.25$). In hydrotalcite group, relevant substitutions may occur in two cationic and in interlayer anionic positions. M^{II} cations can be Mg^{2+}, Fe^{2+}, Ni^{2+}, Co^{2+}, …; M^{III} cations can be Al^{3+}, Fe^{3+}, Cr^{3+}, Cm^{3+}, … Interlayer anions are represented by OH^-, Cl^-, NO_3^-, I^-, SO_4^{2-}, CO_3^{2-}, SeO_4^{2-}, TcO_4^-. Such minerals are also known as "anionic clays" because of high anion exchange capacity; they are important in waste geochemistry because of a unique role in sorbing hazardous anionic radionuclides and toxic elements. Structure of LDH phases is well known because many varieties are synthesised in catalysis chemistry [2001ROY/FOR]. However, surprisingly little is still known about solubility and miscibility of hydrotalcite-like LDH phases ([2005ALL/NAV], [2003JOH/GLA]) which certainly deserve more experimental work. This, in turn, would permit thermodynamic consideration of relevant Aq-SS systems involving LDH phases or ettringites in applications related to cement waste immobilisation.

II.3.3 Structural incorporation of trivalent actinides/lanthanides into Calcite

Calcite is a common mineral in most geological formations, which are currently studied for disposal of high level nuclear waste. It is a major component of clay rocks such as the Opalinus clay in Switzerland with 11% calcite [1998BRA/BAE] and the Bure argillite in France [2001AND]. Also, it is a key secondary alteration phase of cement based structural components within a waste repository system [1999ADL/MAD]. Therefore, calcite co-precipitation/solid solution formation and adsorption with actinides is an important aspect of a geochemically-based long-term safety analysis.

Calcite crystals formed in nature do contain significant amounts of rare earth elements (REE). REE distribution in marine limestone exhibit similar distribution patterns as normal seawater, which has led to the idea of direct REE co-precipitation [1977PAR/MOL], [2004TAN/OHT]. In hydrothermally formed calcite crystals from Iceland, up to 100 ppm Eu was detected. A concave normalised REE pattern was found with positive anomalies for Eu and Tb [2001HAB/NIK], which are supposed to reflect the REE composition of the hydrothermal fluids from which they were formed, thus also indicating direct co-precipitation. However, since the geochemical boundary conditions during calcite formation in natural systems are in many cases not well constrainted, the Aq-SS equilibria cannot be applied easily.

Co-precipitation of various trace metals with carbonate minerals has been studied experimentally for many years [1999CUR], [1998RIM/BAL]. In most co-precipitation studies, trace element uptake/incorporation by calcite was described in

terms of an empirical partition coefficient. Only a few studies were actually intended to workout the Aq-SS thermodynamics. Nevertheless, a substantial amount of thermodynamic data for divalent metal ion substitution into calcite as well as aragonite is available [2000GLY]. Furthermore, sorption studies with actinides (U(VI), Th(IV), Np(V), Pu(V)/Pu(VI) and Cm(III)) have been published [1992CAR/BRU], [2005MAR/STU], [1982SHA/MOR], [2002STU/FAN2], [2005ZAV/ROB].

Here, the main focus will be on experimental studies on structurally incorporated trivalent f-elements – primarily the actinides Pu(III), Am(III) and Cm(III) and in particular chemical homologues, but non-radioactive, rare earth elements (REE). Uptake of trivalent actinides, An(III), into a calcite host structure will be quantified in terms of a Henderson-Kracek partition coefficient, D:

$$D = \frac{x_{\mathrm{An(III)}} / x_{\mathrm{calcite}}}{\left[\mathrm{An(III)}\right] / \left[\mathrm{Ca}^{2+}\right]} \qquad \text{(II.257)}$$

$x_{\mathrm{An(III)}}$ and x_{calcite} represent the molar fractions of the actinide and Ca^{2+} in the precipitating solid. [An(III)] and [Ca^{2+}] are the molar concentrations in the aqueous solution. In case the free-drift batch-type sorption/uptake experiments were performed, the chemical composition of the aqueous solution will change and only a heterogeneous Doerner-Hoskins partition coefficient can be derived (see Chapter II).

Due to the similar ionic radii, the structural incorporation of trivalent actinides into calcite occurs presumably on a calcite lattice site *via* replacement of Ca^{2+}. However, this apparently implies a complex heterovalent substitution mechanism, which needs to be characterised on a molecular level before Aq-SS thermodynamics can be derived. Ultimately, experimental data on Aq-SS equilibria and spectroscopic data should provide a coherent picture.

In the following, a critical overview of published experimental studies on An(III)/REE co-precipitation will be presented. The first systematic experimental study on REE co-precipitation with calcite was published by Terakado and Masuda [1988TER/MAS]. They used a free-drift batch-type experimental setup to determine REE co-precipitation at room temperature (20-25 ºC). A Doerner-Hoskin partition coefficient of ~ 10 for all REE was derived. However, inherent to free-drift experiments is the fact that the solution composition changes throughout the experiment as a consequence of precipitation of a solid (see Section III.1). Consequently, it is difficult to relate the obtained partition coefficient to a particular solution composition. Also, it was noted by Zhong and Mucci [1995ZHO/MUC], that Terakado and Masuda established a very high initial degree of supersaturation at the beginning of their experiments. Under these conditions, nucleation of calcite occurred before subsequent calcite crystal growth. It is not clear, whether REE partitioning during nucleation follows the same rules as during crystal growth, which primarly involves the attachment of REEs to kink sites on a calcite surface. Further, recently Tsuno *et al*. [2002TSU/KAG] observed that the pres-

ence of REE in a highly supersaturated calcium carbonate solution affects precipitation. At 25 ºC, instead of pure calcite, a mixture of calcite and vaterite, a metastable polymorph of $CaCO_3$, precipitated. At slightly higher temperatures (50 ºC) almost 90% of the precipitated $CaCO_3$ was vaterite. Vaterite represents a precursor phase, which typically transforms into calcite and is quite often overlooked in experimental studies (due to the time span between the actual precipitation experiment and the application of analytical techniques). It was shown that the presence of REE in the aqueous solution and high degrees of supersaturation promotes the temporary formation of vaterite. This introduces a significant complication to REE co-precipitation experiments intended to derive data on REE partitioning and solid solution thermodynamics on the REE – calcite system. In such a case, the macroscopically observed REE uptake by the precipitating carbonate phases is controlled by REE/calcite as well as REE/vaterite interactions. The behaviour of REE during the vaterite – calcite phase transition is not clear at all. There are two more metastable $CaCO_3$ phases: ikaite and calcium carbonate-monohydrate which may also precipitate from a supersaturated calcium carbonate solution, but have not been studied that extensively.

Zhong and Mucci [1995ZHO/MUC] obtained REE partitioning data into calcite from (artificial) sea water using a constant addition experiments at 25 ºC. In contrast to the free drift experiments by Terakado and Masuda [1988TER/MAS], Zhong and Mucci established steady state conditions in their experiments. Also, it seems reasonable to assume that the (co-)precipitation kinetics were surface reaction controlled (and not transport/diffusion controlled), although this was not explicitly demonstrated. Since the solution composition was kept constant throughout the experiment, a homogenous REE-containing calcite phase precipitated onto calcite seed-crystals, where the REE incorporation was actually controlled by a reaction at the calcite – solution interface. The conditions were carefully chosen in order to ensure that the possible precipitation of $REE_2(CO_3)_3$ and $REEOHCO_3$ phases can be excluded.

A mean partition coefficient of 2340 for La and 65 for Yb was observed. The decreasing partitioning with increasing Z from La to Yb was explained by the size match between the REE and the calcite Ca^{2+} crystal lattice site. Within the calcite structure Ca^{2+} occupies a 6-fold oxygen coordinate lattice site, with a ionic radius of 1.00 Å, which is very similar to the ionic radius for 6-fold oxygen coordinated La with 1.032 Å. The lighter REE have a smaller ionic radius down to 0.868 Å for Yb (Eu: 0.947 Å) [1976SHA2].

In general, REE partitioning data in Zhong and Mucci's study also depended on the REE concentration in the aqueous solution. The $\log_{10}D$ increased linearly with $\log_{10}[REE]_{aq}$. For Eu, the partition coefficient varied between 200 at 10 nM Eu and 1400 at 170 nM Eu. This variation was however not linked with the variation in co-precipitation rate. In contrast to co-precipitation experiments with various divalent metal ions, REE co-precipitation seems not to show any dependence on the precipitation kinetics – at least in the investigated range of precipitation rates ($3.3 \cdot 10^{-10}$ – $4.5 \cdot 10^{-8}$

$mol \cdot g^{-1} \cdot s^{-1}$). It should be emphasised though, that the trivalent REE inhibit calcite precipitation significantly, due to their strong adsorption behaviour. Many divalent metal ions do not show this strong inhibitory effect. The precipitation rate effect on the partition coefficient is related to the link between metal ion adsorption/incorporation kinetics and calcite growth (Ca^{2+} / CO_3^{2-} attachment to crystal surface). Adsorption and co-precipitation of REE/calcite show similar trends, however REE partitioning (D) decreases from La to Lu significantly more compared to the distribution coefficient for adsorption (K_D). This indicates that co-precipitation is not simply related to adsorption, but involves more complex interfacial reactions (*e.g.*, dehydration, *etc.*) during crystal growth. From these observations, it is not clear, whether the measured REE partition coefficients represent equilibrium conditions, which is a prerequisite for deriving thermodynamic data on Aq-SS systems.

With respect to the Eu(III) incorporation or substitution mechanism, several macroscopic observations give at least some hints: (1) $\log_{10}(D_{REE})$ *vs.* $\log_{10}(D_{Na})$, (2) D_{REE} *vs.* $[REE]_{aq}$, (3) $\log_{10}(D_{REE})$ *vs.* $-\log_{10}(K_{sp,REE\text{-}carbonate})$.

Zhong and Mucci observed a correlation between the REE concentration in the precipitated carbonate and the partitioning of Na^+ from their artificial seawater solution. They suggest that this, at least, indicates that Na^+ might substitute for Ca^{2+} in parallel with the incorporation of Eu^{3+} in order to compensate for the charge. The observation was also taken as a hint that an actual calcite-like REE containing solid solution had formed. The coupled substitution reaction may be written as:

$$2Ca^{2+}_{calcite} \rightleftharpoons Na^{+}_{calcite} + Eu^{3+}_{calcite} \qquad \text{(II.258)}$$

For the light REE, they observed also a correlation between the partitioning coefficient and the REE concentration in the aqueous solution. Apparently, the heavy REE did not show this clear correlation. They explain this observation by a two-step incorporation reaction during co-precipitation. Upon attachment of a REE^{3+} onto a calcite surface site, there will be charge balance restrictions with respect to the possible precipitating ions in the vicinity. Only a monovalent or another REE^{3+} combined with a vacancy are allowed to attach next to a REE^{3+} surface site. Surface selectivity controls the correlation between partitioning coefficient and aqueous REE concentration. Since the heavy REE do not have such a high affinity to calcite surfaces (as indicated by their adsorption behaviour), they do not show this correlation. As long as the supersaturation/precipitation rate is not too high, this concept explains short-range ordering phenomena for light REE during co-precipitation from aqueous solution.

Furthermore, a clear negative linear correlation of REE partitioning coefficient with solubility of REE carbonates was found. For thermodynamic equilibrium, one expects that the distribution coefficient is related to the ratio of the solubility products of the REE-carbonate and calcite (see Chapter II) - $D^{o}_{REE} = \left[K^{o}_{sp(CaCO_3)}\right]^3 \Big/ \left[K^{o}_{sp(REE_2(CO_3)_3)}\right]$. However, Zhong and Mucci clearly state that they do not think that their observed REE

partitioning data represent necessarily thermodynamic distribution coefficients, however, the apparent correlation is quite striking.

Lakshtanov and Stipp [2004LAK/STI] studied the co-precipitation of Eu(III) with calcite using also a constant addition method. They used a similar experimental setup as Zhong and Mucci [1995ZHO/MUC], although the investigated range of precipitation rate was larger ($3.3\cdot10^{-10}$ – $4.5\cdot10^{-8}$ mol g^{-1} s^{-1}). The partition coefficient for an Eu concentration range between 0.1 – 6.9 nM was found to be (770 ± 290). Zhong and Mucci obtained at a Eu concentration of 10 – 170 nM a partition coefficient of 200 (for 10 nM Eu) up to 1400 (for 170 nM Eu). As Zhong and Mucci [1995ZHO/MUC], Lakshtanov and Stipp [2004LAK/STI] also did not observe any dependence of Eu partitioning into calcite as a function of the precipitation rate.

In addition to various precipitation rates, they used 2 different samples with a difference in particle size (10 - 20 µm and 2 - 100 µm). It is well known from the crystal growth community [1984CHE], that precipitation rates are affected by particle size, in particular, if the precipitation rate is transport controlled (rather than reaction controlled). It is argued that since there is no partition coefficient dependence on the precipitation rate, the measured partition coefficients do represent equilibrium conditions. Based on this assumption, various substitution mechanisms are tested with respect to the measured partition coefficient:

$$3Ca^{2+}_{calcite} \rightleftharpoons 2Eu^{3+}_{calcite} + vac_{calcite} \quad \text{(II.259)}$$

$$Ca^{2+}_{calcite} \rightleftharpoons EuOH^{2+}_{calcite} \quad \text{(II.260)}$$

$$2Ca^{2+}_{calcite} \rightleftharpoons Na^{+}_{calcite} + Eu^{3+}_{calcite} \quad \text{(II.261)}$$

Following the substitution scheme (II.259), they show that the experimental data followed the expected correlation between the aqueous Eu^{3+} concentration and the solubility product of the $Eu_2x(CO_3)_3$ end-member and the Eu mole fraction in the precipitated solid according to: $(Eu^{3+})^2(CO_3^{2-})^3 = K_{sp,Eu_2x(CO_3)_3} x_{Eu}^2$. Their experimental data follow this correlation, thus suggesting this substitution mechanism. Furthermore, since the experimental data also were compatible with the relation according to: $(Eu^{3+})(OH^-)(CO_3^{2-}) = K_{sp,EuOHCO_3} / K_{sp,EuOH}\, x_{EuOHCO_3}$, a substitution mechanism according to Reaction (II.260) was also assumed. However, in contrast to Zhong and Mucci [1995ZHO/MUC], Lakshtanov and Stipp [2004LAK/STI] did not observe any correlation between Na^+ and Eu^{3+} partitioning. Consequently they ruled out a substitution mechanism according to Reaction (II.260). In summary, from these co-precipitation experiments, a complex substitution scheme is proposed, based on a ternary system with the end-members $CaCO_3$ – $EuOHCO_3$ – $Eu_2(CO_3)_3$.

More recently, Tanaka *et al*. [2004TAN/OHT] published an experimental study on REE partitioning into calcite from constant addition experiments, also similar to [1995ZHO/MUC]. However, although they do not present partitioning data, but partitioning data normalised to Gd, it becomes clear that the results do not confirm earlier

published data. Zhong and Mucci found a decreasing partitioning coefficient with increasing Z from La (2340) to Yb (65), whereas Tanaka *et al*. found normalised REE pattern which show the highest relative partition coefficient for Sm and significantly smaller partition coefficients for lighter or heavier REE. They claim that this is due to the differences in the chemical composition of the aqueous solution (compared to [1995ZHO/MUC]. It is stated that in their experiments, $REECO_3^+(aq)$ is the most abundant species, whereas under the experimental conditions used by Zhong and Mucci $REE(CO_3)_2^-(aq)$ is the dominant species, thus explaining the difference in REE patterns. Unfortunately, the exact chemical composition of the aqueous solution is not presented in detail, and this statement cannot be verified. However, the $REECO_3^+(aq) / REE(CO_3)_2^-(aq)$ does not change very much as a function of the CO_3^{2-} concentration (within the investigated pH range). Furthermore, Tanaka *et al*. used a higher Eu concentration up to 100 ppb (= 680 nM, compared to 10-70 nM in [1995ZHO/MUC] study). They concluded that REE partitioning into calcite is actually controlled by REE carbonate complexation in solution. They do not provide a concept for the molecular level substitution mechanism. Also, since the chemical composition of the aqueous solution and of the precipitated solid solution phase is not documented in detail, it is not possible to derive thermodynamic data. REE fractionation during calcite co-precipitation exhibits different trends between the [1995ZHO/MUC] study and the [2004TAN/OHT] study.

Very recently, Curti *et al*. [2005CUR/KUL] derived a thermodynamic model of the Eu/calcite Aq-SS system based on batch-type Eu sorption experiments at pH 13 combined with the experimental data from [1995ZHO/MUC] as well as from [2004LAK/STI]. It is assumed that in their sorption experiments equilibrium was established between the aqueous solution and the reprecipitated/recrystallised Eu containing calcite surface coating. Further, the published REE co-precipitation experiments are also assumed to represent equilibrium, since there is apparently no correlation between precipitation rate and partition coefficient (see above). The Eu partitioning data could also not be described by simple binary Aq-SS systems. Further, they were also not able to fit their experimental data in terms of a Aq-SS systems with the end-members $CaCO_3$ – $Eu_2(CO_3)_3$ and $EuNa(CO_3)_2$, as [2004LAK/STI]. Instead, they used an advanced thermodynamic "inverse" modelling approach (DualTh GEM, see Chapter II.1.3.2)) and estimated G^*_{298} values for hypothetical end-members $EuO(OH)$, $EuH(CO_3)_2$ and $EuO(CO_3)_{0.5}$. Only an ideal ternary solid solution with these end-members allowed to model the experimental data consistently. Their thermodynamic approach leads to the assumption of incorporation of two distinctively different Eu species: (1) one involving a coupled substitution $2Ca^{2+} \rightleftharpoons H^+ + Eu^{3+}$ and (2) the incorporation of an Eu oxy hydroxo species. The predicted Eu hydroxo complex involves significant structural relaxation within the calcite host structure, with a 9-fold O coordination of Eu. However, this structural model has not been confirmed by direct measurements, although, time resolved laser fluorescence spectroscopy data (see below) seem to be compatible with some of these assumption. The EXAFS data by Elzinga *et al*. [2002ELZ/REE] and

Withers *et al*. [2003WHI/PEA] were performed with REE doped crystal that were grown at much lower pH conditions. (Ongoing work by Marques-Fernandes *et al*. on EXAFS measurements with Nd and Am doped calcite crystals grown at high pH will clarify this open question – Marques-Fernandes, pers. comm.).

To summarise, these studies have provided a substantial amount of data on empirical REE partitioning into calcite during calcite precipitation from aqueous solution at room temperature. Also, first attempts have been made to derive the molecular level substitution mechanism and a thermodynamic solid solution model. However, without direct structural information about the molecular level incorporation and substitution mechanism, the interpretation of macroscopic observations remains ambiguous. In particular, there seems to be no coherent substitution model suggested in the above-presented studies.

In the following, spectroscopic studies on structurally incorporated trivalent f-elements in calcite will be evaluated in particular with respect to the substitution mechanism(s) which are responsible for the experimentally observed element partitioning (as outlined above). The local coordination of some REE and An(III) in a calcite host structure was studied using extended X-ray absorption fine structure (EXAFS) spectroscopy, time resolved laser fluorescence spectroscopy (TRLFS) (for Eu(III) and Cm(III)) and IR spectroscopy by calcite [2002ELZ/REE], [2005MAR/STU], [1997PIR/FED], [2002STU/FAN2], [2003WHI/PEA].

Elzinga *et al*. [2002ELZ/REE] studied structurally incorporated Nd, Sm, Dy, Yb in calcite crystals co-precipitated from aqueous solution at room temperature using EXAFS spectroscopy. REE doped calcite crystals were prepared by a batch-type synthesis procedure, where precipitation is essentially transport/diffusion controlled. Although the pH remained constant in their experiments, the Ca and REE concentration of the aqueous solution changed during the synthesis. It was assumed that the incorporation mechanism does not change depending on the element concentrations through the experiments. Some of the studied crystals were chemically homogeneous, whereas some crystals did exhibit compositional zoning (see Section III.1) suggesting some kinetic effects during co-precipitation.

EXAFS spectra indicate that the studied REEs occupy a Ca lattice site within the calcite structure. For Dy and Yb they found the expected 6-fold oxygen coordination, whereas Nd and Sm seem to be 7-fold oxygen coordinated. Also, Nd-O and Sm-O distances are longer than what would be consistent with the sum of the ionic radii. 7-fold REE-oxygen coordination implies a significant distortion of the local calcite structure, which could be a consequence of a bidentate surface complex with a carbonate group. They also point out, that due to the similarities in ionic radius, a similar behaviour can be expected for Am^{3+} and Cm^{3+}. There was no indication of a REE in the 2nd coordination shell.

Withers *et al.*[2003WHI/PEA] characterised Nd doped calcite crystals, which were prepared by the same procedure as Elzinga *et al.* (see above) with temperature dependent near-IR and EXAFS spectroscopy. Their EXAFS data suggest that Nd occupies a Ca lattice site with a coordination number of 6.6 oxygen with a substantial local lattice dilation. Furthermore, a high Debye-Waller factor was obtained which indicates "some" difference from the ideal calcite structure. From IR measurements, they found a rather broad $^4F_{3/2}$ line without discrete structures (which is typical for other studied Nd doped crystals). This observation would be expected for a broad and continuous distribution of ligand-field environments, which are typical for glassy rather than crystalline host materials. Furthermore, it is pointed out that broad absorption bands have been frequently observed in REE co-precipitated crystals as a consequence of local lattice strain due to incorporated molecular water. Their IR spectra indicate H_2O related absorption bands in their Nd doped calcite crystals. However, these water absorption bands could also be linked with fluid inclusions. They concluded that the incorporation of a $NdOH^+$ species would very likely explain the observed IR spectra. It should be mentioned that small amounts of metastable vaterite were detected by powder XRD.

It is hypothesised that structurally incorporated Eu^{3+} in calcite should have a 6-fold oxygen coordination. Therefore, such a Eu containing calcite would be more stable than a Nd containing calcite with it is significant local structural deformation. However, this hypothesis is certainly very speculative.

Marques-Fernandes *et al.* [2005MAR/STU] characterised Cm(III) doped calcite crystals with TRLFS. The samples were co-precipitated in mixed flow reactor experiments under steady state conditions with a growth rate of $3.0 - 5.4 \cdot 10^{-6}$ mol g^{-1} s^{-1} at various pH conditions in aqueous solution. The emission of the 609 nm and 620 nm fluorescence lines show a significant red shift compared to the Cm(III) aquo ion and an increased life time, indicating that Cm(III) is incorporated into the calcite structure. Based on life time measurements, two distinctively different incorporated Cm(III) species can be identified.

One species with a life time of 2009 µs presumably represents a Cm(III) ion on a more or less regular Ca lattice site. However, splitting of the emission peak at low T (18 K), indicates variations of the local ligand field (*e.g.*, slight distortions of the first O coordination sphere). The TRLFS data would be compatible with a simple coupled substitution $2Ca^{2+}_{calcite} \rightleftharpoons Na^{+}_{calcite} + Cm^{3+}_{calcite}$, although a correlation between Na^+ and Cm^{3+} in the calcite samples was not observed in this study. Furthermore, the data would be also compatible with a substitution involving a vacancy according to $3Ca^{2+}_{calcite} \rightleftharpoons 2Cm^{3+}_{calcite} + vac_{calcite}$ as well as a coupled substitution according to $2Ca^{2+}_{calcite} \rightleftharpoons Cm^{3+}_{calcite} + H^{+}_{calcite}$ It can also not be excluded that Cm occupies some interstitial or defect site.

A second incorporated Cm species with a life time of 450-500 µs seems to be coordinated by at least 1 H_2O/OH^- species which causes a quenching of the fluorescence

life time. This second incorporated species would be compatible by a $CmOH^{2+}$ species, as proposed by [2004LAK/STI] as well as [2003WHI/PEA]. This species was found by Marques-Fernandes *et al*. particularly in samples that were precipitated at pH 13 conditions. This incorporated species also shows peak splitting at low T, indicating a variability of the local ligand field.

Although Marques-Fernandes *et al.* studied the Eu fluorescence in doped calcite crystals as well, the Eu fluorescence data does not provide as much detail as that for the Cm. However, it seems reasonable to assume that Cm and Eu behave crystal-chemically almost identical.

To summarise, one can clearly state that a substantial amount of macroscopic REE/An(III) co-precipitation data are available. Also, significant results from spectroscopic data have been published. However, some open questions still remain: ***What do we know about structural incorporation of REE/An(III) by calcite?*** Spectroscopic data clearly indicate that Eu becomes incorporated into the crystal structure of calcite. From macroscopic co-precipitation/sorption experiments and from spectroscopic measurements (on synthetic doped calcite crystals) it is clear that the incorporation is not a simple coupled substitution. It involves more than one incorporated species, presumably Eu^{3+} and $EuOH^{2+}$ occupying the Ca lattice site within the calcite structure. Local coordination involves 6 and/or 7 oxygen atoms. Multiple sites with variability of the ligand field (due to local distortions). ***What do we not know (but need to know)?*** Do the incorporated Eu species represent equilibrium? There seems to be some indication that this is not the case, and the question arises, how can one estimate/extrapolate to equilibrium conditions? Are the spectroscopically characterised Eu species in experimentally doped calcite crystals identical in all the different co-precipitation experiments (at least 3 different experimental procedures have been used)? To what extent do the experimental co-precipitation experiments reflect the conditions for naturally formed (and potentially equilibrated) calcite crystals? Some of the spectroscopic data are compatible with the model proposed by Curti *et al*. [2005CUR/KUL]. However, there are still some open questions, such as the proposed 9-fold oxygen coordination, which has not been verified by direct spectroscopic measurements.

In conclusion, it seems clear that there is not yet a coherent picture of Eu incorporation into calcite considering the macroscopic co-precipitation/sorption experiments. The thermodynamic approach developed by Curti *et al*. [2005CUR/KUL] seems to provide the most advanced thermodynamic Aq-SS concept, which is capable of handling complex substitution mechanisms in a multi-component system. The EXAFS, TRLFS, IR spectroscopic data do give to a large extent a coherent picture, although the exact substitution mechanism becomes not clear, in particular with respect to equilibrium conditions. Without a doubt, thermodynamic tools have been developed to handle even complex substitution/incorporation mechanisms as they seem to occur in Calcite (and once they have been characterised on a molecular level by direct measurements).

II.3.4 Solid solutions in the nuclear fuel cycle

II.3.4.1 Introduction

One of the fields where solid solutions thermodynamics becomes more relevant is the study of materials used in the nuclear fuel cycle. Most of the components involved, from the original ore recovered from nature (uraninite) to ceramic substances developed to stabilise and immobilise spent nuclear fuel, can be considered as solid solutions. In spite of the difficulty in handling this material, its characterisation has been reported in dozens of reports in the last two decades.

Knowledge of the physical chemistry of all the compounds involved in the nuclear fuel cycle is essential in performance assessment studies of potential future geological disposal systems, especially when dealing with the alteration and dissolution of spent fuel due to the potential risk of release of radioactive isotopes to the surrounding geosphere and biosphere. Such an assessment of spent nuclear fuel requires an understanding of the important time-dependent phenomena influencing its behaviour on a time-scale up to millions of years. This demanding goal requires the development and qualification of models predicting the long-term release rate of radionuclides usually referred to as "radionuclide source term models". The development of these models is based on the knowledge and understanding of the spent fuel alteration processes taking place in the spent fuel/water interface. From the last two decades, carefully controlled spent fuel dissolution experiments have been performed in the frame of several experimental national or international programmes [1983RYA/RAI], [1987GRA], [1987WIL/SHA], [1990WIL], [1991TAI/STR], [1992OLL], [1992STR], [1996GRA/LOI], [1997FOR], [1999BRU/CER], [2000GRA/LOI], [2003BRU/CER] for elucidating the mechanisms and processes governing radionuclides release from the fuel matrix. Many efforts have been also focused on the interpretation of the dissolution data generated within these experimental programmes both from a thermodynamic and kinetic point of view [1997FOR], [1998BRU/CER], [1999BRU/CER], [2003BRU/CER].

Radionuclide release processes are directly related to the way radionuclides are embedded in the spent fuel matrix. The knowledge on the chemical state of the fission products and actinides in the fuel matrix after the irradiation history is well established after numerous elemental analyses on irradiated fuels of different type and history.

The chemical nature and the geometrical distribution of some of these radionuclides in the spent fuel matrix has lead to apply the Aq-SS concepts to interpret the processes governing their aqueous behaviour, in spite of the complexity of these solids. The potential mechanisms controlling radionuclide dissolution from the UO_2 matrix include co-dissolution processes, as well as the potential phases that can control the retardation of the radionuclide once released, including the formation of secondary solid phases, or the co-precipitation with major components of the near field. Modelling studies have been performed in order to establish the most likely sequence of processes that

control the release of the radionuclides from the fuel and their solubility in the aqueous phase.

In this example, the most relevant nuclear fuel materials are first described to show the role of solid solution in their composition. In a second section, the dissolution of spent fuel is evaluated in terms of kinetic congruent dissolution and stoichiometric saturation concepts.

II.3.4.2 Solid solution in nuclear materials

II.3.4.2.1 Uraninite and non-irradiated fuel

The ultimate origin of the fuel used in nuclear reactor to obtain energy is uraninite, a naturally occurring mineral mined in some sedimentary (mainly sandstones) and crystalline (granitic pegmatites, carbonatites, peraluminous granites …) rocks. Its conventional mineralogical formula is UO_2, although the structural formula is much more complex [1992JAN/EWI], $(U^{4+}_{1-x-y-z}U^{6+}_{x}REE^{3+}_{y}M^{2+}_{z})O_{2+x-(0.5y)-z}$.

Such a complexity is mainly caused by the oxidation of U(IV) to U(VI) during the deposition and subsequent alteration and by the incorporation of elements from the radioactive decay. Main accessory-to-trace elements are Th, Pb, Ca and REE, although many others have been found. Uraninite forms an isostructural, continuous solid solution with thorianite (ThO_2). The Th content in natural uraninites is highly variable and clearly dependent on the deposition environment. Magmatic deposits typically contain the highest Th (and REE) concentrations, *e.g.*, up to 9.9 wt% ThO_2 at Palmottu deposit (Finland) [1992JAN/EWI]. In contrast, low-temperature, sedimentary deposits are virtually free of Th since the mobility of uranium is much higher in oxidised waters (transported as U(VI) complexes) than that of other elements with lower oxidation states.

Lead may reach contents in uraninite up to 20 wt% PbO, *e.g.*, at Oklo (Gabon) [1995JAN/EWI], although the incompatibility of this element in the uraninite lattice suggests that it occupies interstitial sites rather than forming true solid solutions [1992JAN/EWI]. Lead is eventually released from uraninite by forming, in reducing environments, galena (PbS) [1995JAN/EWI].

On the other hand, calcium may be found in relatively high contents in uraninite (as high as 12 wt% CaO [1981XU/WAN]), although it is suggested that it can be present as impurities forming other minerals like calcite [1994CAS/BRU]. Nevertheless, part of the calcium may enter in the uraninite lattice by forming pseudo-binary solid solutions $U_{1-x}Ca_xO_{2-x}$ (fluorite structure). In fact, experimental analysis by [1998PIA/TOU] showed $0.25 \leq x \leq 0.45$ in the temperature range of $20 \leq t\,(°C) \leq 1390$.

In a similar manner as Th, REE content in uraninites is strongly dependent on the redox state existing in the deposition environment [1985PAG/PIN], and it may vary from several ppm to several wt%.

Variable contents in Si, Al, P, Fe, Mg, Na and K have also been reported in a number of studies (see [1999FIN/MUR] and references therein), although in many cases it is believed that these elements are part of accessory minerals mixed with the uraninite rather than participate in the structural lattice. As an example, Si likely forms part of coffinite ($USiO_4 \cdot nH_2O$) inclusions.

Uraninite from ore is not directly used as fuel in nuclear reactors. This mineral is reacted with fluoride to form uranium(VI) fluoride which is enriched in ^{235}U. After this process, the fuel is reconverted to the oxide form to obtain the fuel pellets that will be used as nuclear fuel in the reactor.

II.3.4.2.2 Irradiated UO_2

The composition of irradiated fuel has been extensively studied. This is reflected by the substantial number of articles and reports that deal with the characterisation of this material. During irradiation, the fission of uranium and plutonium generates a number of products that can be classified into *fission products* and *actinides.* There is still an uncertainty on the spatial distribution and structure of the compounds integrating the irradiated fuel. The reason for that is found in the continuous changes underwent by the fuel during and after its irradiation, which lead [1988KLE3] to postulate that the key processes occurring when irradiation increases are:

1. Increase in the relative concentration of the fission products.
2. Changes in the oxygen-to-metal (O/M) ratio and the chemical potential of the oxygen.
3. Existence of radial variations in the fission product concentrations due to temperature gradients that generate thermal diffusion of the radionuclides.
4. Decay of the β-active fission products.

Despite these processes, there is a general consensus that fission products can be classified into four groups [1988KLE3] according to the nature of phases where they locate within the spent fuel matrix:

1. Fission gases (Kr, Xe, Br, I).
2. Metallic phases (Mo, Tc, Ru, Rh, Pd, Ag, Cd, In, Sn, Sb and Te),
3. Oxide phases (Rb, Cs, Ba, Zr, Nb, Mo and Te) and
4. Solid solutions in the fuel matrix (Sr, Zr, Nb, REE).

The relative distribution and nature of each fission product is essential to evaluate a potential dissolution of the fuel. Metallic precipitates seem to form solid solutions whose composition is dominated by molybdenum and ruthenium: Ru (Mo, Tc, Rh, Pd) [1985KLE/PAS], [1989KLE]. On the other hand, oxide precipitates also are found as complex solid solutions with the cubic perovskite structure whose main com-

position being $Ba(U, Zr, Mo)_3$ [2001POI/TOU]. The relative partition of Mo between metallic and oxide precipitates depends on the chemical potential of oxygen in the fuel, which, in turn, it is related to the fuel burn-up.

After irradiation, the UO_2 matrix contains about 3-4 wt% of fission products and actinides. Of these, about 30 wt% is believed to form solid solutions with the matrix. The structure of the matrix keeps defining a cubic fluorite-type lattice inherited from the original non-irradiated fuel.

II.3.4.2.3 Mixed oxide (MOX) and Rock-like oxide (ROX)

Plutonium and other actinides such as ^{237}Np, ^{241}Am, ^{243}Am, ^{244}Cm, which are generated in nuclear reactors, are the main contributors to radiotoxicity of spent fuel due to their long half-lives. Consequently, they are of special concern in the evaluation of the long-term performance of a geologic repository [2005EWI]. Several strategies have been developed to reduce the inventory of these actinides, such as reprocessing them in order to be reused in nuclear reactors, by the manufacturing of the Mixed-oxide (MOX) and Rock-like oxide (ROX) fuels, or the direct disposal in repositories by immobilisation into ceramic material. In both cases, the role of solid solutions seems to be of fundamental importance.

Mixed-oxide (MOX) fuels consist of the mixture of plutonium oxide (prepared from spent fuel) with UO_2. The mixture is sintered and, as a result, the fuel becomes a solid solution of $(U, Pu)O_2$ composition, with around 25-30 % PuO_2 [2004KLE]. After mixing again with UO_2 powder, the amount of PuO_2 in the MOX is between 3 and 5 % [2004KLE], [2001CAR/YOD]. This MOX fuel is burned again in the reactor. After irradiation, a duplex structure is observed in the MOX fuel: a $(U, Pu)O_2$ agglomerates embedded in a UO_2 matrix [2004KLE].

ROX fuels are multi-phase mixtures of compounds such as thoria (ThO_2), spinel ($MgAl_2O_4$), corundum (Al_2O_3) and yttria-stabilized zirconia (YSZ) (see review in [2001YAM/AKI]). Some of them (thoria and YSZ) have the ability of incorporate PuO_2 as solid solution.

II.3.4.3 Application of Aq-SS thermodynamics to spent fuel dissolution experimental data

As explained above, actinides and some fission products are typically associated with the major component of the spent fuel, uranium dioxide, forming a solid solution. Once in a repository, and in case of isolation failure of the engineered barriers, these radionuclides may be released to the aqueous phase due to the alteration of the spent fuel matrix.

The application of Aq-SS theory to interpret the results obtained from dissolution experiments with spent fuel or natural and synthetic analogues under different experimental conditions, as developed in the previous chapters, is rather difficult. This is

due to the uncertainty derived from the complexity of the spent fuel itself, where several solid solution systems seem to coexist (zirconates, UO_2 matrix …). In addition, many fundamental thermodynamic data are still missing for these end-members compounds.

One approximation to spent fuel dissolution may be the use of the stoichiometric saturation concept formally defined by Thorstenton and Plummer [1977THO/PLU] (as developed in Section II.2.2.2 in these Guidelines and defined in Section II.1.2.1). According to these authors, the composition of a solid solution may remain invariant during the dissolution of the solid phase owing to kinetic restrictions. Glynn [1990GLY] defines this concept as a pseudo-equilibrium state which may occur between an aqueous phase and a multi-component solid solution. The stoichiometric saturation model intends to explain concentrations in metastable Aq-SS systems when the congruent dissolution rate goes to zero; such could be the case of spent fuel dissolution since the solid is actually dissolving in the system, from an under-saturation situation. This concept assumes that a solid solution may behave as a pure (stoichiometric) phase. In the case of spent fuel dissolution, this process may be expressed in a general form as:

$$U_{1-x-y}Rn1_xRn2_yO_2 \rightleftharpoons (1-x-y)U + xRn1 + yRn2 + \dots \quad \text{(II.262)}$$

The term *congruent* implies that the transfer of ions from the solid to the aqueous phase occurs at an ionic ratio equal to that in the solid solution phase. If this assumption is valid, the aqueous concentration of each radionuclide may be expressed as a function of the aqueous concentration of the major component of the matrix and the molar fraction of the minor component in the solid, as follows:

$$[Rn1] = \chi \times [U] \quad \text{(II.263)}$$

where, $\chi = x/(1-x-y-...)$.

When the solid is dissolved and kinetic restrictions are not considered, the situation changes and the system evolves towards equilibrium by precipitation of secondary, pure or mixed, solid phases, changing the composition of the aqueous phase with respect to that of the solid, and consequently leading to incongruent dissolution processes.

In the next sections, several modelling studies are presented to show the application of solid solution thermodynamics to interpret the dissolution behaviour of several radionuclides from spent fuel dissolution experiments.

II.3.4.3.1 Strontium

Strontium has been proposed as an indicator of the extent of dissolution of the spent fuel matrix, since it is present in solid solution in the UO_2(s) matrix and does not form secondary phases upon dissolution. However, part of the strontium present in the fuel can also be found forming oxide precipitates (see Section II.3.4.3.2).

Most of the dissolution data reported in the literature indicate that strontium concentrations in solution from spent fuel dissolution experiments are clearly under-saturated with respect the most thermodynamically favoured solid phases able to precipitate under the experimental conditions of the tests [1997FOR], [1997BRU/CER2], [2003BRU/CER]. Therefore, the release of this radionuclide in solution is not controlled by the solubility of a particular secondary solid phase. Accordingly, modelling of the dissolution data has been done assuming a congruent co-dissolution approach of strontium with uranium as the main process governing the release of this radionuclide from the fuel matrix.

Bruno *et al.* [1999BRU/CER] reported strontium concentrations from spent fuel dissolution experiments in their study of radiolytic processes at the spent fuel/water interface. These authors explained the release of strontium from the fuel by the co-dissolution of this radionuclide with the major component of the matrix (Figure II-40). Test solutions are clearly under-saturated with respect to the precipitation of the most likely solid phases. The deviation from the expected behaviour in the first run (labelled "7.40.1") is explained by assuming that this radionuclide is not present at the inventory ratio in the UO_{2+x} oxidised surface layer of the unreacted fuel sample. Once this layer is depleted, Sr dissolves congruently with uranium which was positively identified in the unreacted fuel sample.

Figure II-40: Strontium concentrations determined in the leaching solution *vs.* strontium concentrations calculated assuming a congruent co-dissolution process (From [1999BRU/CER]).

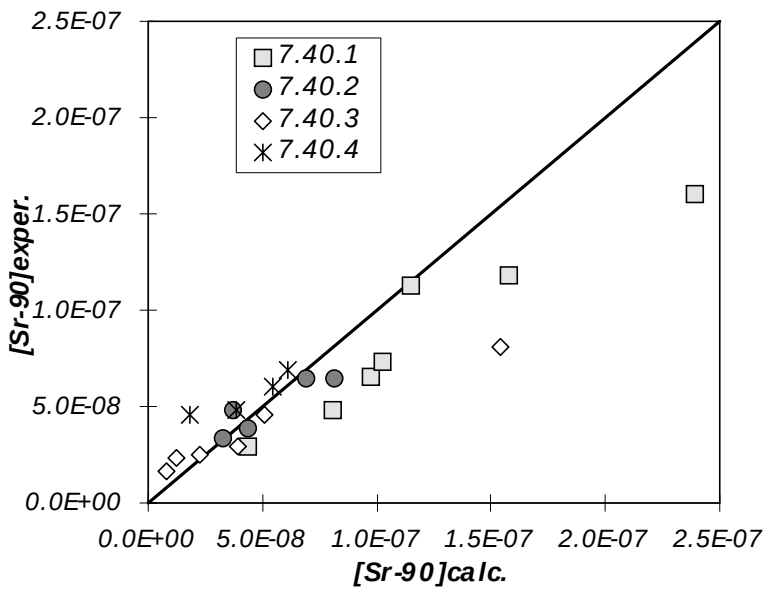

Analogous analysis was performed by Bruno *et al.* [2003BRU/CER] by including new experimental series carried out with different groundwater compositions, concluding that the release of strontium in most of the tests is controlled by its co-dissolution from the fuel matrix. Figure II-41 is a plot of ^{90}Sr *vs.* uranium concentrations measured at different time intervals in different experimental tests. The slope obtained (1.03×10^{-3}) by linear regression for the ^{90}Sr to U ratio from the aqueous solution data is quite close to the molar ratio in the spent fuel solid solution, [90Sr]/[U] = $(1.51 \pm 0.17) \times 10^{-3}$ indicating a congruent release of this radionuclide with the fuel matrix. The initial release of 10^{-8} mole·dm^{-3} was interpreted by the authors as an instant strontium release attributed to the enrichment of this radionuclide in the grain boundaries and gaps on the surface of the fuel [1997JOH/TAI].

Figure II-41: Strontium *vs.* uranium concentrations in all the tests with the exception of those reaching a steady-state for ^{90}Sr (from [2003BRU/CER]).

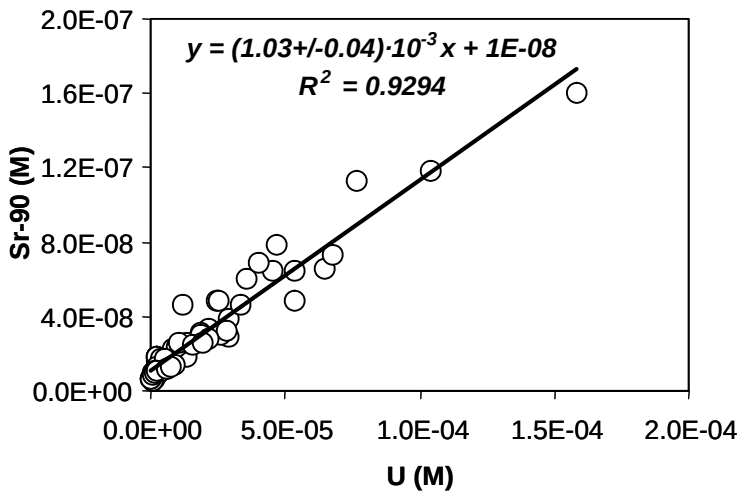

II.3.4.3.2 Barium

Barium, as strontium, is found mainly forming oxides in the fuel matrix, although it can also be found as a solid solution with the fuel matrix [1988KLE3]. Upon dissolution, concentrations of this element in solution as a function of time seem to follow the same trend as that for uranium [1997FOR]. In addition, solution concentrations are undersaturated with respect the precipitation of any secondary solid phase.

Because of the chemical analogy with strontium, dissolution data have been treated as discussed above for Sr. The ratios between measured and calculated data as-

suming co-dissolution with uranium are close to unity (Figure II-42) indicating that, as in the case of strontium, the main process governing the release of barium from the fuel matrix is a congruent co-dissolution with uranium.

Figure II-42: Barium concentrations calculated assuming a congruent co-dissolution process with uranium *vs.* the ones determined in the leaching solution. Data are taken from [1997FOR]. Black rounds stand for series 3 data, grey triangles stand for series 7 data and white diamonds stand for series 11 data (see [1997FOR] for explanation of series).

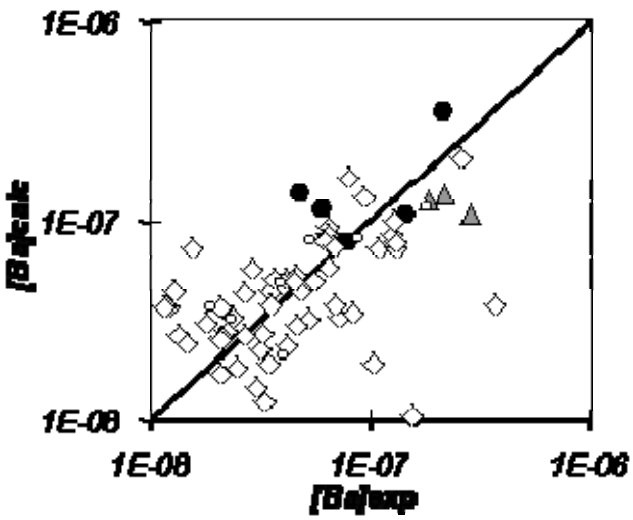

II.3.4.3.3 Neptunium

Neptunium concentrations measured in solution from spent fuel dissolution experiments [2003BRU/CER] showed the same trend as the uranium in most of the tests, indicating a congruent co-dissolution process of Np from the matrix (Figure II-43). The Np/U molar ratio in the aqueous phase $(4.8 \pm 0.1) \times 10^{-4}$ was quite close to the one calculated based on the molar ratio of the fuel sample, $[Np]/[U] = (5.6 \pm 0.9) \times 10^{-4}$.

As discussed by [1999BRU/CER], neptunium concentrations were undersaturated with respect to the $Np(OH)_4(s)$ phase although a general trend to saturation was observed as the dissolution reaction proceeded.

Figure II-43: Neptunium *vs.* uranium concentrations in all the experimental series (taken from [2003BRU/CER]).

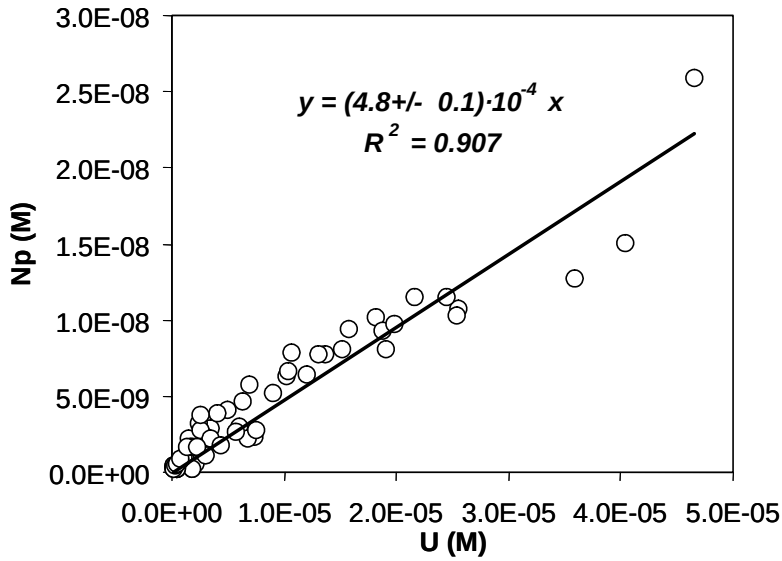

II.3.4.3.4 Plutonium

Bruno *et al.* [2003BRU/CER] also interpreted the data for plutonium and the results suggested that additional processes to matrix dissolution govern its overall behaviour at very short contact times. They indicated that this behaviour was mainly caused by the high stability of plutonium hydroxides. [1998BRU/CER] evaluated the Pu behaviour from spent fuel dissolution experiments by an initial at very short contact times congruent release of plutonium from the fuel matrix, followed by forming a $Pu(OH)_4$ poorly ordered solid phase (denoted as $Pu(OH)_4(coll)$), followed by the ageing of this phase to a more stable amorphous $Pu(OH)_4$ (am) phase.

Congruent dissolution of Pu(IV) from the matrix to form the predominant Pu(IV) aqueous complex was considered by these authors according to the following reaction:

$$PuO_2 + 2H_2O \rightleftharpoons Pu(OH)_4(aq) \qquad \text{(II.264)}$$

where *x* stands for the mole fraction of Pu present in the UO_2 matrix. Consequently, by assuming a congruent dissolution process, the authors calculated a dissolution rate given by the product of the *x* - the mole fraction of Pu in the matrix, - times the oxidative dissolution rate of the UO_2 matrix, R_{ox}.

$$R_0(Pu) = x \times R_{ox}(UO_2) \quad \text{(II.265)}$$

The kinetic modelling carried out by these authors assuming this initial congruent release of Pu with the matrix lead to the fitting of the experimental data depicted in Figure II-44.

Figure II-44: Comparison between the kinetic model and the experimental data. (from [1998BRU/CER].

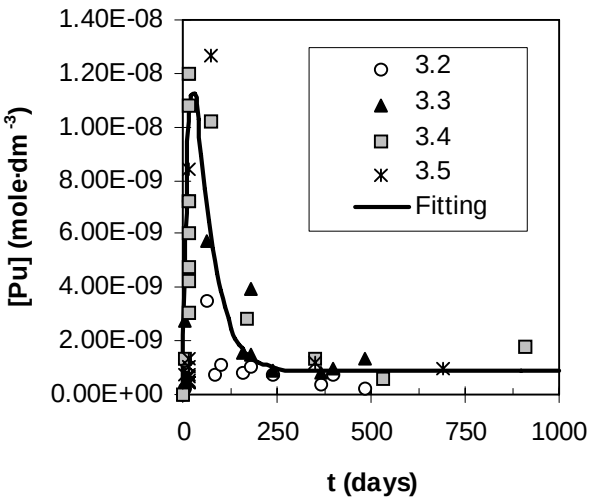

II.3.4.3.5 Lanthanides

The results obtained in spent fuel solid characterisation after irradiation [1988KLE3], [1995FOR], [1997FOR] show a homogeneous distribution of the lanthanides in the UO_2 fuel matrix in spite of the differences in oxidation state which have been obsreved for some of the lanthanides, *i.e.*, cerium which can be present as Ce(IV) oxide. Spent fuel dissolution data reported in [1997FOR] indicate that the concentrations of these radionuclides in solution are under-saturated with respect to the precipitation of any secondary lanthanide solid phase. The chemical similarity of the lanthanide elements leads to study the behaviour of these elements following a co-dissolution process with neodymium, based on the fact that this lanthanide is present in the largest amount in the fuel matrix. The results are given in Figure II-45.

Figure II-45: Calculated concentrations *vs.* the experimental ones assuming a congruent co-dissolution process of the minor lanthanides (europium samarium, gadolinium and lanthanum respectively with neodymium). Black circles stand for series 3 data, grey triangles stand for series 7 data and white diamonds stand for series 11 data (see [1997FOR] for data series explanation).

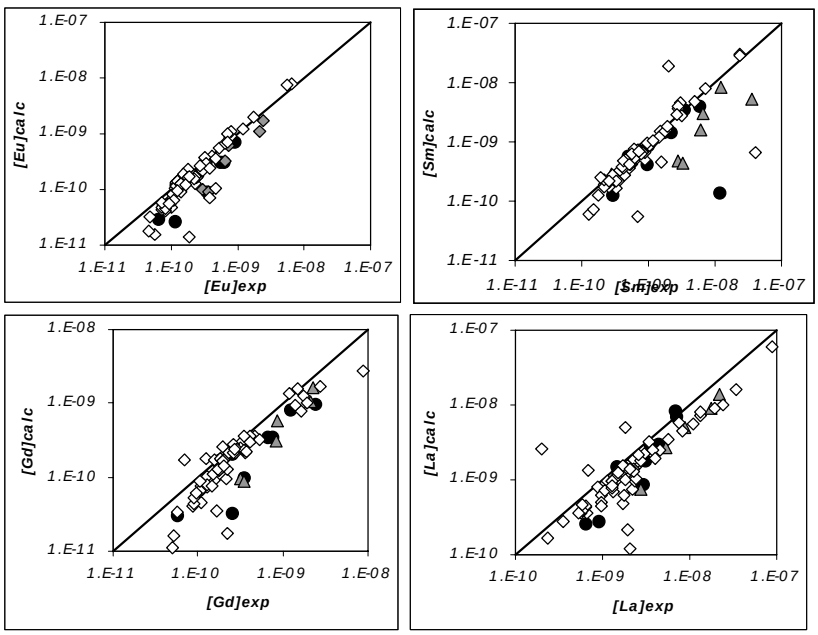

II.3.4.4 Final remarks

Even in a non-equilibrium situation, Aq-SS concepts presented in Section II of this document seem to provide an adequate framework for understanding the key processes controlling the dissolution behaviour of the minority radionuclides present in spent fuel. This framework is scientifically more satisfactory and more robust from the performance assessment point of view than the simple descriptive behaviour of dissolution tests. Further developments in this particular area should include the determination of the activity coefficients for the minor components of the solid solution in order to improve the initial ideal approximation with a more stringent thermodynamic approach. This is particularly critical for the case of Pu which makes up a significant mole fraction in UO_2 fuels and even more so in MOX fuels.

Bibliography

[1925DOE/HOS] Doerner, H., Hoskins, W. M., Co-precipitation of barium and radium sulphates, *J. Am. Chem. Soc.*, **47**, (1925), 662-675. Cited on pages: 25, 26, 158.

[1937KIE] Kielland, J., Individual activity coefficients of ions in aqueous solutions, *J. Am. Chem. Soc.*, **59**, (1937), 1675-1678. Cited on page: 68.

[1938GOL] Goldschmidt, B., Sur la précipitation mixte des sulfates de baryum et strontium, *C. R. Hebd. Séances Acad. Sci.*, **206**, (1938), 1110. Cited on page: 156.

[1944FLA/BUR] Flatt, R., Burkhard, G., Untersuchungen über Mischkrystallbildung in Lösungen. II. Die Systeme KCl + NH_4Cl + H_2O, KBr + NH_4Br + H_2O, KCl + KBr + H_2O und NH_4Cl + NH_4Br + H_2O bei 25°, *Helv. Chim. Acta*, **27**, (1944), 1605-1610. Cited on page: 107.

[1951PAL/BER] Palache, C., Berman, H., Frondell, C, *Dana's System of Mineralogy. v.II*, J. Wiley & Sons, New York, (1951). Cited on pages: 156, 157.

[1952GUG] Guggenheim, E. A., *Mixtures: the theory of the equilibrium properties of some simple classes of mixtures, solutions and alloys*, Oxford Clarendon Press, (1952), 270 pp.. Cited on page: 45.

[1956MCC/WAL] McCoy, W. H., Wallace, W. E., Free energies and entropies of formation of KCl-KBr solid solutions at 25°C, *J. Am. Chem. Soc.*, **78**, (1956), 5995-5998. Cited on pages: 105, 107.

[1958HAR/OWE] Harned, H. S., Owen, B. B., *The physical chemistry of electrolytic solutions*, 3rd. Edition, Reinhold Publishing Corporation, New York, (1958), 803 pp.. Cited on pages: 69, 72.

[1961GOL/HEA] Goldsmith, J. R., Heard, H. C., Subsolidus phase relations in the system $CaCO_3$-$MgCO_3$, *J. Geol.*, **69**, (1961), 45-74. Cited on pages: 57, 58.

[1964LAH/BOL] Lahav, N., Bolt, G. H., Self-diffusion of ^{45}Ca into certain carbonates, *Soil Sci.*, **93**, (1964), 293-299. Cited on page: 10.

[1964STA] Starke, R., Die strontiumgehälte der baryte, *Freiberg. Forschungsh C.*, **150**, (1964), 123. Cited on page: 156.

[1965GRE/CHA] Greenberg, S. A., Chang, T. N., Investigation of the colloidal hydrated calcium silicates. II. Solubility relationships in the calcium oxide-silica-water system at 25C, *J. Phys. Chem.*, **69**, (1965), 182-188. Cited on pages: 28, 174, 175.

[1967BOS/FRA] Boström, K., Frazer, J., Blankenburg, J., Subsolidus phase relations and lattice constants in the system $BaSO_4$- $SrSO_4$- $PbSO_4$, *Ark. Mineral. Geol.*, **4**, (1967), 447-485. Cited on page: 157.

[1967DAR] Darken, L. S., Thermodynamics of binary metallic solutions, *Trans. Metall. Soc. AIME*, **239**, (1967), 80-89. Cited on pages: 51, 52.

[1967DAR2] Darken, L. S., Thermodynamics of ternary metallic solutions, *Trans. Metall. Soc. AIME*, **239**, (1967), 90-96. Cited on page: 51.

[1967GUG] Guggenheim, E. A., *Thermodynamics: An advanced treatment for chemists and physicists*, 5th. Edition, Elsevier/North Holland, Amsterdam-New York, (1967), 390 pp.. Cited on pages: 37, 61, 62, 91.

[1967THO] Thomson, J. B., Thermodynamic properties of simple solutions, *Researches in geochemistry*, pp.340-361, Abelson PH. New York John Wiley and Sons, (1967). Cited on page: 45.

[1968HAN] Hanor, J. S., Frequency distribution of compositions in the barite-celestite series, *Am. Mineral.*, **53**, (1968), 1215-1222. Cited on page: 156.

[1969OAT] Oates, W. A., Ideal solutions, *J. Chem. Educ.*, **46**, (1969), 501-504. Cited on page: 172.

[1969TAK/YAN] Takano, B., Yanagisawa, M., Watanuki, K., Structure gap in $BaSO_4$-$PbSO_4$ solid solution series, *Mineral. J.*, **6**, (1969), 159-171. Cited on page: 157.

[1969THO] Thomson, J. B., Chemical reactions in crystals, *Am. Mineral.*, **54**, (1969), 341-375. Cited on page: 58.

[1970CHU] Church, T. M., Marine barite, Ph. D. Thesis, University of California San Diego, (1970). Cited on page: 156.

[1970GRE] Green, E. J., On the perils of thermodynamic modelling, *Geochim. Cosmochim. Acta*, **34**, (1970), 1029-1033. Cited on page: 105.

[1970ROB/STO] Robinson, R. A., Stokes, R. H., *Electrolyte solutions*, Butterworth, (1970), 571 pp., 2nd revised, 2002. Cited on pages: 66, 68.

[1970VAN/STO] Van Zeggren, F., Storey, S. H., *The computation of chemical equilibria*, Cambridge University, (1970), 176 pp.. Cited on page: 87.

[1971BRO/REN] Brower, E., Renault, J., The solubility and enthalpy of the barium-strontium sulfate solid solution series, New Mexico Bureau of Mines and Mineral Resources Circular, Report 116, 21, (1971). Cited on page: 155.

[1972GOL] Goldsmith, J. R., Cadmium dolomite and the system $CdCO_3$-$MgCO_3$, *J. Geol.*, **80**, (1972), 617-626. Cited on pages: 57, 58.

[1972ROB/HEM2] Robie, R. A., Hemingway, B. S., Calorimeters for heat of solution and low temperature heat capacity measurements, US Geological Survey Professional Paper, Report , (1972). Cited on pages: 24, 152, 153.

[1973ERI/ROS] Eriksson, G., Rosén, E., Thermodynamic studies of high temperature equilibria. VIII: General equations for the calculation of equilibria in multiphase systems, *Chem. Scr.*, **4**, (1973), 193-194. Cited on page: 60.

[1974BRO/SKI] Brown, T. H., Skinner, B. J., Theoretical prediction of equilibrium phase assemblages in multicomponent systems, *Am. J. Sci.*, **274**, (1974), 961-986. Cited on page: 60.

[1974TRU/JON] Truesdell, A. H., Jones, B. F., WATEQ, a computer program for calculating chemical equilibria in natural waters, *J. Res. U. S. Geol. Surv.*, **2**, (1974), 233-274. Cited on page: 68.

[1975ABR/PRA] Abrams, D. S., Prausnitz, J. M., Statistical thermodynamics of liquid mixtures: A new expression for the excess Gibbs energy of partly or completely miscible systems, *Am. Inst. Chem. Eng. J.*, **21**, (1975), 116-128. Cited on page: 70.

[1975URU] Urusov, V. S., Energetic theory of miscibility gaps in mineral solid solutions, *Fortschr. Mineral.*, **52**, (1975), 141-150. Cited on pages: 14, 80.

[1976SHA2] Shannon, R. D., Revised effective ionic radii in oxides and fluorites, *Acta Crystallogr., Sect. B: Struct. Sci.*, **B25**, (1976), 295-946. Cited on page: 186.

[1977BLO] Blount, C. W., Barite solubilities and thermodynamics quantities up to 300°C and 1400 bars, *Am. Mineral.*, **62**, (1977), 942-957. Cited on page: 155.

[1977HOV/WAL] Hovis, G. L., Waldbaum, D. R., A solution calorimetric investigation of K-Na mixing in a sanidine-analbite ion exchange series, *Am. Mineral.*, **62**, (1977), 680-686. Cited on page: 55.

[1977LIP] Lippmann, F., The solubility products of complex minerals, mixed crystals, and thee-layer clay minerals, *Neues Jahrb. Mineral. Abh.*, **130**, (1977), 243-263. Cited on pages: 18, 72, 78.

[1977NAV] Navrotsky, A., Progress and new directions in high temperature calorimetry, *Phys. Chem. Miner.*, **2**, (1977), 89-104. Cited on pages: 24, 25, 153, 155.

[1977PAR/MOL] Parekh, P. P., Möller, P., Dukski, P., Bausch, W. M., Distribution of trace elements between carbonate and non-carbonate phase in limestone, *Earth Planet. Sci. Lett.*, **34**, (1977), 39-50. Cited on page: 184.

[1977PEL/BAL] Pelton, A. D., Bale, C. W., Computational techniques for the treatment of thermodynamic data in multicomponent systems and the calculation of phase equilibria, *CALPHAD: Comput. Coupling Phase Diagrams Thermochem.*, **1**, (1977), 253-273. Cited on page: 60.

[1977THO/PLU] Thorstenson, D. C., Plummer, L. N., Equilibrium criteria for two-component solids reacting with a fixed composition in aqueous phase, *Am. J. Sci.*, **277**, (1977), 1203-1223. Cited on pages: 16, 32, 139, 141, 197.

[1978BOX/HUN] Box, G. E. P., Hunter, W. G., *Statistics for experimenters: An Introduction to design, data analysis, and model building*, New York, Wiley, (1978). Cited on page: 121.

[1978GAR/WOL] Garrels, R., Wollast, R., Discussion of equilibrium criteria for two-component solid reacting with fixed composition in an aqueous phase. Example: The magnesian calcites, *Am. J. Sci.*, **278**, (1978), 1469-1474. Cited on pages: 16, 138.

[1978WOO/NIC] Wood, B. J., Nicholls, J., The thermodynamic properties of reciprocal solid solutions, *Contrib. Mineral. Petrol.*, **66**, (1978), 389-400. Cited on pages: 43, 112.

[1980LIP] Lippmann, F., Phase diagrams depicting aqueous solubility of binary mineral systems, *Neues Jahrb. Mineral. Abh.*, **139**, (1980), 1-25. Cited on pages: 18, 19, 72, 78, 112, 128.

[1980WEI/HON] Weill, D. F., Hon, R., Navrotsky, A., The igneous system $CaMgSi_2O_6$-$CaAl_2Si_2O_8$-$NaAlSi_3O_8$: Variations on a classic theme by Bowen, *Physics of magmatic processes*, pp.49-92, Hargraves, R. B. Princeton Univ. Press, (1980). Cited on page: 44.

[1981FUJ/KON] Fujii, K., Kondo, W., Heterogeneous equilibrium of calcium silicate hydrate in water at 30°C, *J. Chem. Soc. Dalton Trans.*, **2**, (1981), 645-651. Cited on pages: 170, 173.

[1981HEL/KIR] Helgeson, H. C., Kirkham, D. H., Flowers, G. C., Theoretical prediction of the thermodynamic behavior of aqueous electrolytes at high pressures and temperatures: IV. Calculation of activity coefficients, osmotic coefficients, and apparent molal and standard and relative partial molal properties to 600°C and 5 kb, *Am. J. Sci.*, **281**, (1981), 1249-1516. Cited on pages: 68, 69.

[1981HON/HEN] Hon, R., Henry, D. J., Navrotsky, A., Weill, D. F., A thermochemical calculation of the pyroxene saturation surface in the system diopside-albite-anorthite, *Geochim. Cosmochim. Acta*, **45**, (1981), 157-161. Cited on page: 44.

[1981KAR] Karpov, I. K., *Computer-aided physico-chemical modeling in geochemistry*, Nauka publ., (1981), 247 pp.. Cited on pages: 60, 98.

[1981LOR] Lorens, R. B., Sr, Cd, Mn and Co distribution coefficients in calcite as a function of calcite precipitation rate, *Geochim. Cosmochim. Acta*, **45**, (1981), 553-561. Cited on page: 130.

[1981XU/WAN] Xu, G., Wang, A., Gu, Q., Zhang, J., Zhang, Z., Huang, Y., Some characteristics of uranium-oxides in China, *Bull. Mineral.*, **104**, (1981), 565-574. Cited on page: 194.

[1982HEN/NAV] Henry, D. J., Navrotsky, A., Zimmermann, H. D., Thermodynamics of plagioclase-melt equilibria in the system albite-anorthite-diopside, *Geochim. Cosmochim. Acta*, **46**, (1982), 381-391. Cited on page: 44.

[1982LIP] Lippmann, F., Stable and metastable solubility diagrams for the system $CaCO_3$-$MgCO_3$-H_2O at ordinary temperatures, *Bull. Mineral.*, **105**, (1982), 273-279. Cited on pages: 18, 78.

[1982MCB] McBride, M. B., Electron spin resonance investigation of Mn^{2+} complexation in natural and synthetic organics, *Soil Sci. Soc. Am. J.*, **46**, (1982), 1137-1143. Cited on page: 10.

[1982REE2] Reed, M. H., Calculation of multicomponent chemical equilibria and reaction processes in systems involving minerals, gases and aqueous phase, *Geochim. Cosmochim. Acta*, **46**, (1982), 513-528. Cited on pages: 90, 91.

[1982SHA/MOR] Shanbhag, P. M., Morse, J. W., Americium interaction with calcite and arragonite surfaces in seawater, *Geochim. Cosmochim. Acta*, **46**, (1982), 241-249. Cited on pages: 29, 185.

[1982STE/WEI] Stebbins, J. F., Weill, D. F., Carmichael, I. S. E., High temperature heat contents and heat capacities of liquids and glasses in the system $NaAlSi_3O_8$ - $CaAl_2Si_2O_8$, *Mineral. Petrol.*, **60**, (1982), 276-284. Cited on pages: 24, 152, 153.

[1983DEN/MIC] Denis, J., Michard, G., Dissolution d'une solution solide: Etude théorique et expérimentale, *Bull. Minéral.*, **103**, (1983), 307-316. Cited on pages: 16, 155.

[1983FUJ/KON] Fujii, K., Kondo, W., Estimation of thermochemical data for calcium silicate hydrate (C-S-H), *J. Am. Ceram. Soc.*, **66**, (1983), C220-C221. Cited on page: 170.

[1983HAW] Hawthorne, F. C., Quantitative characterisation of site-occupancies in minerals, *Am. Mineral.*, **68**, (1983), 287-306. Cited on page: 148.

[1983PEL/LIN] Pelton, A. D., Lin, P. L., Calculation of phase diagrams of the reciprocal quaternary systems Li, Na, K/CO_3, SO_4; Li, Na/CO_3, SO_4, OH; Li, K/CO_3, SO_4, OH and Na, K/CO_3, SO_4, OH, *CALPHAD: Comput. Coupling Phase Diagrams Thermochem.*, **7**, (1983), 295-303. Cited on page: 43.

[1983RYA/RAI] Ryan, J. L., Rai, D., The solubility of uranium(IV) hydrous oxide in sodium hydroxide solutions under reducing conditions, *Polyhedron*, **2**, (1983), 947-952. Cited on page: 193.

[1984CHE] Chernov, A. A., *Modern crystallography III. Crystal Growth.*, Springer, Heidelberg, Ed., (1984). Cited on page: 188.

[1984HAR/MOL] Harvie, C. E., Møller, N., Weare, J. H., The prediction of mineral solubilities in natural waters: The Na-K-Mg-Ca-H-Cl-SO_4-OH-HCO_3-CO_3-CO_2-H_2O system to high ionic strengths at 25°C, *Geochim. Cosmochim. Acta*, **48**, (1984), 723-751. Cited on pages: 69, 70, 106.

[1984ONE/NAV] O'Neill, H. St. C., Navrotsky, A., Cation distributions and thermodynamic properties of binary spinel solid solutions, *Am. Mineral.*, **69**, (1984), 733-753. Cited on pages: 55, 56.

[1984REE] Reeder, R. J., Crystal chemistry of the rhombohedral carbonates. In Carbonates: Mineralogy and chemistry., *Rev. Mineral.*, **11**, (1984), 1-48. Cited on page: 57.

[1984SVE] Sverjensky, D. A., Predicting Gibbs free energies of calcite-type carbonates and the equilibrium distribution of trace elements between carbonates and aqueous solutions, *Geochim. Cosmochim. Acta*, **48**, (1984), 1127-1134. Cited on page: 54.

[1985CAR/MCC] Carpenter, M. A., McConnell, J. D. C., Navrotsky, A., Enthalpies of ordering in the plagioclase feldspar solid solution, *Geochim. Cosmochim. Acta*, **49**, (1985), 947-966. Cited on page: 55.

[1985GAM] Gamsjäger, H., Solid state chemical model for the solubility behaviour of homogeneous solid Co-Mn- carbonate mixtures, *Ber. Bunsen-Ges.*, **89**, (1985), 1318-1322. Cited on pages: 78, 80, 81, 114, 124, 125.

[1985KLE/PAS] Kleykamp, H., Paschoal, J. O., Pejsa, R., Thümmler, F., Composition and structure of fission product precipitates in irradiated oxide fuels: Correlation with phase studies in the Mo-Ru-Rh-Pd and BaO-UO_2-ZrO_2-MoO_2 systems, *J. Nucl. Mater.*, **130**, (1985), 426-433. Cited on page: 195.

[1985LAN/MEL] Langmuir, D., Melchior, D., The geochemistry of Ca, Sr, Ba and Ra sulfates in some deep brines from the Palo Duro Basin, Texas, *Geochim. Cosmochim. Acta*, **49**, (1985), 2423-2432. Cited on page: 160.

[1985LAN/RIE] Langmuir, D., Riese, A. C., The thermodynamic properties of radium, *Geochim. Cosmochim. Acta*, **49**, (1985), 1593-1601. Cited on page: 26.

[1985PAG/PIN] Pagel, M., Pinte, G., Rotach-Toulhoat, N., Rare-earth elements in natural uranium-oxides, *Fortschr. Mineral.*, **63**, (1985), 174. Cited on page: 194.

[1985SNO/HIL] Snodgrass, W. J., Hileman, O. E., *On the geochemical mechanism controlling Ra-226 dissolution in uranium mill wastes (tailings)*, Beak Consultants Limited Publication, (1985). Cited on pages: 25, 159.

[1986FED/WES] Fedorak, P. M., Westlake, D. W. S., Anders, C., Kratochvil, B., Motkosky, N., Anderson, W. B., Huck, P. M., Microbial release of Ra-226 (2+) from (Ba,Ra)SO_4 sludges from uranium-mine wastes, *Appl. Environ. Microbiol.*, **52**, (1986), 262-268. Cited on page: 159.

[1986GUG] Guggenheim, E. A., *Thermodynamics*, Amsterdam, North Holland, (1986). Cited on page: 128.

[1986JEN] Jennings, H. M., Aqueous solubility relationships for two types of calcium silicate hydrate, *J. Am. Ceram. Soc.*, **69**, (1986), 614-618. Cited on page: 172.

[1986LAN/MIL] Landa, E. R., Miller, C. L., Updegraff, D. M. , Leaching of Ra-226 from U mill tailings by sulphate-reducing bacteria, *Health Physics*, **19**, (1986), 509-511. Cited on page: 159.

[1986SPO] Sposito, G., Sorption of trace metals by humic materials in soils and natural waters, *CRC Critical reviews in environmental control*, vol. 16, pp.193-229, CRC Press, (1986). Cited on page: 9.

[1986TAY] Taylor, H. F. W., Proposed structure for calcium silicate hydrate gel, *J. Am. Ceram. Soc.*, **69**, (1986), 464-467. Cited on page: 170.

[1986WES/ZAC] Westall, J. C., Zachary, J. L., Morel, F. M. M., *MINEQL: A computer program for the calculation of the chemical equilibrium composition of aqueous systems*, Department of Chemistry, Oregon State University, (1986), 91 pp., Version 1, Report 86-0. Cited on page: 87.

[1987BUR] Burton, B. P., Theoretical analysis of cation ordering in binary rhombohedral carbonate system, *Am. Mineral.*, **72**, (1987), 329-336. Cited on pages: 58, 59.

[1987CAP/BRO] de Capitani, C., Brown, T. H., The computation of chemical equilibrium in complex systems containing non-ideal solutions, *Geochim. Cosmochim. Acta*, **51**, (1987), 2639-2652. Cited on page: 37.

[1987CAP/BUR] Capobianco, C., Burton, B. P., Davidson, P. M., Navrotsky, A., Structural and calorimetric studies of order-disorder in $CdMg(CO_3)_2$, *J. Solid State Chem.*, **71**, (1987), 214-223. Cited on pages: 57, 58, 59.

[1987GAR/JEN] Gartner, E. M., Jennings, H. M., Thermodynamics of calcium silicate hydrate and their solutions, *J. Am. Ceram. Soc.*, **70**, (1987), 743-749. Cited on pages: 170, 172.

[1987GRA] Gray, W. J., Comparison of uranium release from spent fuel and unirradiated UO_2 in salt brine, *Sci. Basis Nucl. Waste Manage. X*, **84**, (1987), 141. Cited on page: 193.

[1987HAR/GRE] Harvie, C. E., Greenberg, J. P., Weare, J. H., A chemical equilibrium algorithm for highly non-ideal multiphase systems: Free energy minimization, *Geochim. Cosmochim. Acta*, **51**, (1987), 1045-1057. Cited on pages: 70, 95.

[1987NAV/CAP] Navrotsky, A., Capobianco, C., Enthalpies of formation of dolomite and of magnesian calcites, *Am. Mineral.*, **72**, (1987), 782-787. Cited on pages: 56, 57.

[1987NAV] Navrotsky, A., Models of crystalline solutions. Thermodynamic modelling of geologic systems: Minerals, fluids, and melts, Eds. Carmichael, I. S. E. and Eugster, H. P., *Reviews in Mineralogy, Mineral. Soc. Am.*, **17**, (1987), 35-69. Cited on page: 37.

[1987NIR] Nirdosh, I., A review of recent developments in the removal of ^{226}Ra and ^{230}Th from uranium ores and mill tailings, *Uranium*, **4**, (1987), 83-95. Cited on pages: 25, 159.

[1987PLU/BUS] Plummer, L. N., Busenberg, E., Thermodynamics of aragonite-strontianite solid solutions: Results from stoichiometric solubility at 25 and 76°C, *Geochim. Cosmochim. Acta*, **51**, (1987), 1393-1411. Cited on pages: 83, 138.

[1987POW] Powell, R., Darken's quadratic formalism and the thermodynamics of minerals, *Am. Mineral.*, **72**, (1987), 1-11. Cited on pages: 51, 52, 55.

[1987WIL/SHA] Wilson, C. N., Shaw, H. F., Experimental study of the dissolution of spent fuel at 85°C in natural groundwater, *Mater. Res. Soc. Symp. Proc.*, **84**, (1987), 123. Cited on page: 193.

[1987WOO] Wood, B. J., Thermodynamics of multicomponent systems containing several solid solutions, *Thermodynamic modeling of geological materials: Minerals, fluids and melts*, Carmichael, I. S. E., Eugster, H. P., Eds., pp.71-95, Mineralogical Society of America, (1987), Reviews in Mineralogy 17. Cited on page: 60.

[1988BER2] Berner, U., Modelling the incongruent dissolution of hydrated cement minerals, *Radiochim. Acta*, **44/45**, (1988), 387-393. Cited on pages: 170, 172.

[1988BRO/CAL] Brown, G. E., Calas, G., Waychunas, G. A., Petiau, J., X-ray absorption spectroscopy and its applications in mineralogy and geochemistry, *Spectroscopic methods in mineralogy and geology*, *Reviews in Mineralogy*, Mineralogical Society of America, (1988). Cited on pages: 146, 148, 149.

[1988BRU/GER] Brümmer, B. W., Gerth, J., Tiller, K. G., Reaction kinetics of the adsorption and desorption of nickel, zinc and cadmium by goethite. I. Adsorption and diffusion of metals, *J. Soil Sci.*, **39**, (1988), 37-52. Cited on page: 11.

[1988BRY/KLE] Bryndzia, T., Kleppa, O. J., Standard molar enthalpies of formation of realgar(α-AsS) and orpiment (As_2S_3) by high temperature direct synthesis calorimetry, *J. Chem. Thermodyn.*, **20**, (1988), 755. Cited on pages: 24, 153.

[1988HOC] Hochella, M. F., Auger electron and x-ray photoelectron spectroscopies, *Spectroscopic methods in mineralogy and geology*, *Reviews in Mineralogy*, Mineralogical Society of America, (1988). Cited on page: 151.

[1988KIR] Kirkpatrick, R. J., MAS NMR spectroscopy of minerals and glasses, *Spectroscopic methods in mineralogy and geology Reviews in mineralogy*, Hawthorne, F. C., Ed., vol. 18, pp.341-403, Rev. Mineral. Soc. Am., Michigan, (1988). Cited on page: 150.

[1988KLE3] Kleykamp, H., The chemical state of fission products in oxide fuels at different stages of the nuclear fuel cycle, *Nucl. Technol.*, **80**, (1988), 412-422. Cited on pages: 32, 195, 199, 202.

[1988MCM/HOF] McMillan, P. F., Hofmeister, A. M., Infrared and Raman spectroscopy, *Spectroscopic methods in mineralogy and geology*, Hawthorne, F. C., Ed., Mineralogical Society of America, (1988), Reviews in Mineralogy. Cited on page: 144.

[1988STE] Stebbins, J. F., NMR spectroscopy and dynamic processes in mineralogy and geochemistry, *Spectroscopic methods in mineralogy and geology Reviews in mineralogy*, Hawthorne, F. C., Ed., Rev. Mineral. Soc. Am., (1988). Cited on page: 150.

[1988TER/MAS] Terakado, Y., Masada, A., The coprecipitation of rare-earth elements with calcite and aragonite, *Chem. Geol.*, **69**, (1988), 103-110. Cited on pages: 185, 186.

[1988WAY] Waychunas, G. A., Luminescence, x-ray emission and new spectroscopies, *Spectroscopic methods in mineralogy and geology*, Hawthorne, F. C., Ed., Mineralogical Society of America, (1988), Reviews in Mineralogy. Cited on page: 149.

[1989BIS/POT] Bish, D. L., Post, J. E., *Modern powder diffraction*, vol. 20, *Reviews in Mineralogy*, p. 369, Mineralogical Society of America, (1989). Cited on page: 143.

[1989ERI/THO] Eriksson, G., Thompson, W. T., A procedure to estimate equilibrium concentrations in multicomponent systems and related applications, *CALPHAD: Comput. Coupling Phase Diagrams Thermochem.*, **13**, (1989), 389-400. Cited on pages: 60, 95.

[1989GAL/DAN] Galinier, C., Dandurand, J. L., Souissi, C., Schott, J., Sur le caractère non-idéal des solutions solides $(Ba,Sr)SO_4$: mise en évidence et détermination des paramètres thermodynamiques par essais de dissolution a 25°C, *C. R. Hebd. Acad. Sci.*, **308**, (1989), 1363-1368. Cited on pages: 155, 156.

[1989GRE/MOL] Greenberg, J. P., Møller, N., The prediction of mineral solubilities in natural waters: A chemical equilibrium model for the Na-K-Ca-Cl-SO_4-H_2O system to high concentration from 0 to 250°C, *Geochim. Cosmochim. Acta*, **53**, (1989), 2503-2518. Cited on page: 70.

[1989HEL/WOO] Helffrich, G., Wood, B. J., Subregular model for multicomponent solutions, *Am. Mineral.*, **74**, (1989), 1016-1022. Cited on page: 47.

[1989KLE] Kleykamp, H., Constitution and thermodynamics of the Mo-Ru, Mo-Pd, Ru-Pd and Mo-Ru-Pd systems, *J. Nucl. Mater.*, **167**, (1989), 49-63. Cited on page: 195.

[1989MAC/LUK] Macphee, D. E., Luke, K., Glasser, F. P., Lachowski, E. E., Solubility and aging of calcium silicate hydrates in alkaline solutions at 25C, *J. Am. Ceram. Soc.*, **72**, (1989), 646-654. Cited on page: 183.

[1989POL] Pöllmann, H., Solid solution of $3CaO.Al_2O_3.CaSO_4.12H_2O$ and $3CaO.Al_2O_3.Ca(OH)_2.12H_2O$ at 25C, 45C and 60C, *Neues Jahrb. Mineral. Abh.*, **161**, (1989), 27-40. Cited on page: 184.

[1989WER/CHA] Wersin, P., Charlet, L., Karthein, R., Stumm, W., From adsorption to precipitation: Sorption of Mn^{2+} on $FeCO_3$(s), *Geochim. Cosmochim. Acta*, **53**, (1989), 2787-2796. Cited on pages: 10, 23.

[1990BAL/PEL] Bale, C. W., Pelton, A. D., The unified interaction parameter formalism: Thermodynamic consistency and applications, *Metall. Mater. Trans. A*, **21**, (1990), 1997-2002. Cited on pages: 14, 50.

[1990BRO] Brown, P. W., The system Na_2O-CaO-SiO_2-H_2O, *J. Am. Ceram. Soc.*, **73**, (1990), 3457-3461. Cited on page: 183.

[1990DZO/MOR] Dzombak, D. A., Morel, F. M. M., *Surface complexation modeling. Hydrous ferric oxide*, Wiley Intersc. Publ., New York, (1990), 393 pp.. Cited on page: xxi.

[1990ERI/HAC] Eriksson, G., Hack, K., ChemSage - a computer program for the calculation of complex chemical equilibria, *Metall. Trans.*, **21B**, (1990), 1013-1023. Cited on pages: 37, 60, 95.

[1990FIL/RUM] Filippov, V., Rumyantsev, A., Application of Pitzer's equations to calculation of solubility diagrams in aqueous - salt systems with continuous solid solution series, *Dokl. Akad. Nauk SSSR*, **315**, (1990), 659-664. Cited on page: 106.

[1990GLY/REA] Glynn, P. D., Reardon, E. J., Solid-solution aqueous-solution equilibria: thermodynamic theory and representation, *Am. J. Sci.*, **290**, (1990), 164-201. Cited on pages: 16, 18, 19, 22, 72, 78, 83, 84, 94, 108, 114, 129, 136, 138, 140, 141.

[1990GLY/REA2] Glynn, P. D., Reardon, E. J., Plummer, L. N., Busenberg, E., Reaction paths and equilibrium end-points in solid-solution aqueous-solution systems, *Geochim. Cosmochim. Acta*, **54**, (1990), 267-282. Cited on pages: 18, 78.

[1990GLY] Glynn, P. D., Modeling solid-solution reactions in low-temperature aqueous systems, *Chemical modeling in aqueous systems II*, Bassett, R. L., Melchior, D. C., Eds., vol. 416, pp.74-86, American Chemical Society, (1990). Cited on pages: 32, 78, 129, 155, 157, 197.

[1990KON/GAM] Königsberger, E., Gamsjäger, H., Solid-solute phase equilibria in aqueous solution. III. A new application of an old chemical potentiometer, *Mar. Chem.*, **30**, (1990), 317-327. Cited on pages: 23, 80, 82, 122, 123, 124, 125, 126.

[1990KON/GAM2] Königsberger, E., Gamsjäger, H., Solid-solute phase equilibria in aqueous solution: IV. Calculation of phase diagrams, *Z. Anorg. Allg. Chem.*, **584**, (1990), 185-192. Cited on pages: 78, 79.

[1990MIL] Millero, F. J., Marine solution chemistry and ionic interactions, *Mar. Chem.*, **30**, (1990), 205-229. Cited on page: 68.

[1990NOR/PLU] Nordstrom, D. K., Plummer, L. N., Langmuir, D., Busenberg, E., May, H. M., Jones, B. F., Parkhurst, D. L., Revised chemical equilibrium data for major water-mineral reactions and their limitations, Chemical modeling of aqueous systems II, vol. 416, pp.398-413, American Chemical Society, Washington, D.C., USA, (1990). Cited on pages: 61, 67.

[1990PAQ/REE] Paquette, J., Reeder, R. J., New type of compositional zoning in calcite - Insights into crystal-growth mechanisms, *Geology*, **18**, (1990), 1244-1247. Cited on pages: 132, 145.

[1990PAR] Parkhurst, D. L., Ion-association models and mean activity coefficients of various salts, *Chemical modeling in aqueous systems II*, Bassett, R. L., Melchior, D. C., Eds., vol. 416, *American Chemical Society Symposium Series*, pp.31-43, American Chemical Society, (1990). Cited on page: 68.

[1990WIL] Wilson, C. N., Results from NNWSI series 2 bare fuel dissolution tests, Pacific Northwest Laboratory, Report PNL-7169, UC-802, (1990). Cited on page: 193.

[1991GLY] Glynn, P. D., MBSSAS: A computer code for the computation of Margules Parameters and equilibrium relations in binary solid-solution aqueous-solution systems, *Comput. Geosci.*, **17**, (1991), 907-966. Cited on pages: 18, 45, 78, 79, 80, 81, 82, 85, 94, 125, 126, 127, 128, 129.

[1991KON] Königsberger, E., Improvement of excess parameters from thermodynamic and phase diagram data by a sequentital Bayes algorithm, *CALPHAD: Comput. Coupling Phase Diagrams Thermochem.*, **15**, (1991), 69-78. Cited on page: 121.

[1991KOR/PRE] Kornicker, W. A., Presta, P. A., Paige, C. R., Johnson, D. M., Hileman, O. E., Snodgrass, W. J., The aqueous dissolution kinetics of the barium/lead sulphate solid solution series at 25 degrees Celsius and 60 degress Celsius, *Geochim. Cosmochim. Acta*, **55**, (1991), 3531-3541. Cited on page: 157.

[1991PIT] Pitzer, K. S., Ion interaction approach: theory and data correlation, *Activity coefficients in electrolyte solutions*, Pitzer, K. S., Ed., pp.75-153, CRC Press, Boca Raton, Florida, (1991). Cited on pages: 61, 69, 70.

[1991TAI/STR] Tait, J. C., Stroes-Gascoyne, S., Hocking, W. H., Duclos, A. M., Porth, R. J., Wilkin, D. L., Dissolution behaviour of used CANDU fuel under disposal conditions, *Sci. Basis Nucl. Waste Manage. XIV*, **212**, (1991), 189. Cited on page: 193.

[1992BER] Berner, U., Evolution of pore water chemistry during degradation of cement in a radioactive waste repository environment, *Waste Manage. (Oxford)*, **12**, (1992), 201-219. Cited on pages: 27, 169.

[1992BOE/CAL] Boerio-Goates, J., Callanan, J. E., Differential thermal methods, *Phys. Methods Chem. (2nd Ed.)*, (1992). Cited on pages: 24, 152.

[1992BOR/SHV] Borisov, M. V., Shvarov, Yu V., *Thermodynamics of geochemical processes*, Moscow State University Publishers, (1992), 254 pp.. Cited on pages: 60, 95.

[1992CAR/BRU] Carroll, S. A., Bruno, J., Petit, J. C., Dran, J. C., Interactions of U(VI) Nd and Th(IV) at the calcite - solution interface, *Radiochim. Acta*, **58**, (1992), 245-252. Cited on pages: 29, 185.

[1992FOU/REE] Fouke, B. W., Reeder, R. J., Surface structural controls on dolomite composition - Evidence from sectoral zoning, *Geochim. Cosmochim. Acta*, **56**, (1992), 4015-4024. Cited on pages: 132, 145.

[1992GLY/PAR] Glynn, P. D., Parkhurst, D. L., Modeling non-ideal solid-solution aqueous-solution reactions in mass-transfer computer codes, *Water-Rock Interaction*, Kharaka, Y. K., Maest, J., Eds., vol. 1, pp.175-179, Balkema, (1992). Cited on page: 60.

[1992GLY/REA] Glynn, P. D., Reardon, E. J., Plummer, L. N., Busenberg, E., Reply to Dr. Stoessells's comment on "Reaction paths and equilibrium end-points in solid-solution aqueous-solution systems", *Geochim. Cosmochim. Acta*, **56**, (1992), 2559-2572. Cited on pages: 72, 129.

[1992GLY/REA2] Glynn, P. D., Reardon, E. J., Reply, *Am. J. Sci.*, **292**, (1992), 215-225. Cited on page: 129.

[1992GRE/FUG] Grenthe, I., Fuger, J., Konings, R. J. M., Lemire, R. J., Muller, A. B., Nguyen-Trung, C., Wanner, H., *Chemical Thermodynamics of Uranium*, Wanner, H., Forest, I., Nuclear Energy Agency, Organisation for Economic Co-operation, Development, Eds., vol. 1, *Chemical Thermodynamics*, North Holland Elsevier Science Publishers B. V., Amsterdam, The Netherlands, (1992), 715 pp.. Cited on pages: 3, 60, 69.

[1992HOL/POW] Holland, T., Powell, R., Palgioclase feldspars: Activity-composition relations based upon Darken's quadratic formalism and Landau theory, *Am. Mineral.*, **77**, (1992), 53-61. Cited on page: 52.

[1992JAN/EWI] Janeczek, J., Ewing, R. C., Structural formula of uraninite, *J. Nucl. Mater.*, **190**, (1992), 128-132. Cited on page: 194.

[1992JOH/OEL] Johnson, J. W., Oelkers, E. H., Helgeson, H. C., SUPCRT92: a software package for calculating the standard molal thermodynamic properties of minerals, gases, aqueous species, and reactions from 1 to 5000 bar and 0 to 1000°C, *Comput. Geosci.*, **18**, (1992), 899-947. Cited on page: 69.

[1992KON/GAM] Königsberger, E., Gamsjäger, H., Comment on: Solid-Solution Aqueous-Solution Equilibria: Thermodynamic Theory and Representation by P. Glynn, *Am. J. Sci.*, **292**, (1992), 199-214. Cited on pages: 18, 72, 74, 75, 78, 114, 140.

[1992KON/GAM2] Königsberger, E., Gamsjäger, H., Solid-solute phase equilibria in aqueous solution: VII. A re-interpretation of magnesian calcite stabilities, *Geochim. Cosmochim. Acta*, **56**, (1992), 4095-4098. Cited on pages: 14, 50.

[1992OLL] Ollila, K., SIMFUEL dissolution studies in granitic groundwater, *J. Nucl. Mater.*, **190**, (1992), 70-77. Cited on page: 193.

[1992PUT/FER] Putnis, A., Fernández-Díaz, L., Prieto, M., Experimentally produced oscillatory zoning in the (Ba,Sr)SO_4 solid solution, *Nature (London)*, **358**, (1992), 743-745. Cited on pages: 132, 155.

[1992REA] Reardon, E. J., Problems and approaches to the prediction of the chemical composition in cement / water systems, *Waste Manage. (Oxford)*, **12**, (1992), 221-239. Cited on pages: 27, 169.

[1992STI/HOC] Stipp, S. L., Hochella, M. F., Parks, G. A., Leckie, J. O., Cd^{2+} uptake by calcite, solid-state diffusion and the formation of solid solution: Interface processes observed with near-surface sensitive techniques (XPS, LEED, and AES), *Geochim. Cosmochim. Acta*, **56**, (1992), 1941-1954. Cited on page: 10.

[1992STR] Stroes-Gascoyne, S., Trends in the short-term release of fission products and actinides to aqueous solution from used CANDU fuels at elevated temperatures, *J. Nucl. Mater.*, **190**, (1992), 87. Cited on page: 193.

[1992TAY] Taylor, H. F. W., Tobermorite, jennite, and cement gel, *Z. Kristallogr.*, **202**, (1992), 41-50. Cited on page: 169.

[1992WIL/POW] Holland, T., Powell, R., Plagioclase feldspars: Activity-composition relations based upon Darken's quadratic formalism and Landau theory, *Am. Mineral.*, **77**, (1992), 53-61. Cited on page: 52.

[1992YEH] Yeh, G. T., EQMOD: A chemical equilibrium model of complexation, adsorption, ion-exchange, precipitation/dissolution, oxidation-reduction and acid-base reactions, Department of Civil Engineering. The Pennsylvania State University, Report , (1992). Cited on pages: 26, 160.

[1993AND/CRE] Anderson, G. M., Crerar, D. A., *Thermodynamics in geochemistry: The equilibrium model*, Oxford Univ. Press, (1993). Cited on pages: 45, 62, 71, 87, 102.

[1993BOE/EMR] Boerjesson, K. S., Emren, A. T., SOLISOL - a program using PHREEQE to solve solid solution / aqueous equilibria, *Comput. Geosci.*, **19**, (1993), 1065-1070. Cited on page: 91.

[1993FEL/RAI2] Felmy, A. R., Rai, D., Moore D. A., The solubility of (Ba,Sr)SO_4 precipitates: Thermodynamic equilibrium and reaction path analysis, *Geochim. Cosmochim. Acta*, **57**, (1993), 4345-4363. Cited on page: 155.

[1993MOR/HER] Morel, F. M. M., Hering, J. G., *Principles and applications of aquatic chemistry*, John Wiley & Sons Inc., New York, (1993), 588 pp.. Cited on pages: 61, 66, 88.

[1993NIK/RAS] Nikolaisen, H., Rasmussen, P., Sørensen, J. M., Correlation and prediction of mineral solubilities in the reciprocal salt system (Na^+,K^+)(Cl^-,SO_4^{2-}) - H_2O at 0-100°C, *Chem. Eng. Sci.*, **48**, (1993), 3149-3158. Cited on page: 70.

[1993PRI/PUT] Prieto, M., Putnis, A., Fernández-Díaz, L., Crystallisation of solid solutions from aqueous solutions in a porous medium: Zoning in (Ba,Sr)SO_4, *Geol. Mag.*, **130**, (1993), 289-299. Cited on pages: 20, 132, 135, 155.

[1993TAY] Taylor, H. F. W., A discussion on the papers "Models for the composition and structure of calcium silicate hydrate (C-S-H) gel in hardened tricalcium silicate pastes" and "The incorporation of minor and trace elements into calcium silicate hydrate (C-S-H) gel in hardened cement pastes" by I.G.Richardson and G.W.Groves, *Cem. Concr. Res.*, **23**, (1993), 995-998. Cited on page: 170.

[1993VAN/HOL] Vance, D., Holland, T., A detailed isotopic and petrological study of a single garnet from the Gassetts Schist, Vermont, *Contrib. Mineral. Petrol.*, **114**, (1993), 101-118. Cited on page: 52.

[1994CAS/BRU] Casas, I., Bruno, J., Cera, E., Finch, R. J., Ewing, R. C., Kinetic and thermodynamic studies of uranium minerals. Assessment of the long-term evolution of spent nuclear fuel, Swedish Nucl. Fuel Waste Manag. Co., Report SKB-TR-94-16, (1994), 73 pp.. Cited on page: 194.

[1994CHR/PET] Christov, C., Petrenko, S., Balarew, C., Valyashko, V., Calculation of the Gibbs energy of mixing in crystals using Pitzer's model, *J. Solution Chem.*, **23**, (1994), 795-812. Cited on page: 106.

[1994DEL/ABA] Denlinger, D. W., Abarra, E. N., Allen, K., Rooney, P. W., Watson, S. K., Hellman, F., Thin film microcalorimeter for heat capacity measurements from 1.5 K to 800 K, *Rev. Sci. Instrum.*, **65**, (1994), 946. Cited on page: 152.

[1994GHI] Ghiorso, M. S., Algorithms for the estimation of phase stability in heterogeneous thermodynamic systems, *Geochim. Cosmochim. Acta*, **58**, (1994), 5489-5501. Cited on pages: 37, 60.

[1994NAV/RAP] Navrotsky, A., Rapp, R. P., Smelik, E., Burnley, P., Circone, S., Chai, L., Bose, K., Westrich, H. R., The behavior of H_2O and CO_2 in high-temperature lead borate solution calorimetry of volatile-bearing phases, *Am. Mineral.*, **79**, (1994), 1099-1109. Cited on page: 155.

[1994NAV] Navrotsky, A., *Physics and chemistry of earth materials*, London, New York, Cambridge University Press, (1994), 417 pp.. Cited on page: 37.

[1994NOR/MUN] Nordstrom, D. K., Muñoz, J. L., *Geochemical thermodynamics*, 2nd. Edition, Blackwell Sci. Publ., Boston, (1994), 483 pp.. Cited on pages: 45, 61, 71, 87.

[1994ROC/CAS] Rock, P. A., Casey, W. H., McBeath, M. K., Walling, E. M., A new method for determining Gibbs energies of formation of metal-carbonate solid solutions: I. The $Ca_xCd_{1-x}CO_3$(s) system at 298 K and 1 bar, *Geochim. Cosmochim. Acta*, **58**, (1994), 4281-4291. Cited on pages: 23, 122.

[1995FOR] Forsyth, R., Spent nuclear fuel. A review of properties of possible relevance to corrosion processes, SKB, Report TR 95-23, (1995). Cited on page: 202.

[1995GAS] Gaskell, D. R., *Introduction to the thermodynamics of materials*, Washington DC, Talor & Francis, Ed., (1995), 568 pp.. Cited on page: 37.

[1995JAN/EWI] Janeczek, J., Ewing, R. C., Mechanisms of lead release from uraninite in the natural fission reactors in Gabon, *Geochim. Cosmochim. Acta*, **59**, (1995), 1917-1931. Cited on page: 194.

[1995KON/ERI] Königsberger, E., Eriksson, G., A new optimization routine for Chemsage, *CALPHAD: Comput. Coupling Phase Diagrams Thermochem.*, **19**, (1995), 207-214. Cited on page: 121.

[1995PAQ/REE] Paquette, J., Reeder, R. J., Relationship between surface-structure, growth-mechanism, and trace-element incorporation in calcite, *Geochim. Cosmochim. Acta*, **59**, (1995), 735-749. Cited on pages: 132, 145.

[1995SIL/BID] Silva, R. J., Bidoglio, G., Rand, M. H., Robouch, P., Wanner, H., Puigdomènech, I., *Chemical Thermodynamics of Americium*, Nuclear Energy Agency, Organisation for Economic Co-operation, Development, Ed., vol. 2, *Chemical Thermodynamics*, North Holland Elsevier Science Publishers B. V., Amsterdam, The Netherlands, (1995), 374 pp.. Cited on pages: 3, 60.

[1995ZHO/MUC] Zhong, S., Mucci, A., Partitioning of rare earth elements (REEs) between calcite and seawater solutions at 25C and 1 atm, and at high dissolved REE concentrations, *Geochim. Cosmochim. Acta*, **59**, (1995), 443-453. Cited on pages: 30, 31, 185, 186, 188, 189.

[1996BET] Bethke, C. M., *Geochemical reaction modeling: Concepts and applications*, Oxford Univ. Press, (1996), 397 pp.. Cited on pages: 87, 88, 89.

[1996CHA/HOW] Chang, L. L. Y., Howie, R. A., Zussman, J., *Non-silicates: Sulfates, carbonates, phosphates, halides. Rock-forming minerals*, vol. 5B, (1996), 383 pp.. Cited on page: 156.

[1996CHA/NAV] Chai, L., Navrotsky, A., Synthesis, characterization, and energetics of solid solution along the dolomite-ankerite join, and implication for the stability of ordered $CaFe(CO_3)_2$, *Am. Mineral.*, **81**, (1996), 1141-1147. Cited on page: 60.

[1996CHR] Christov, C., A simplified model for calculation of the Gibbs energy of mixing in crystals: Thermodynamic theory, restrictions, and applicability, *Collect. Czech. Chem. Commun.*, **61**, (1996), 1585-1599. Cited on page: 106.

[1996GRA/LOI] Grambow, B., Loida, A., Dressler, P., Geckeis, H., Gago, J., Casas, I., de Pablo, J., Giménez, J., Torrero, M. E., Long term safety of radioactive waste disposal: Chemical reaction of fabricated and high burnup spent UO_2 fuel with saline brines, FZK, Report 5702, (1996). Cited on page: 193.

[1996GUI/POW] Guiraud, M., Powell, R., How well known are the thermodynamics of Fe-Mg-Ca garnet? Evidence from experimentally determined exchange equilibria, *J. Metamorph. Geol.*, **14**, (1996), 75-84. Cited on page: 52.

[1996HER/WES] Herbelin, A. L., Westall, J. C., *FITEQL: A computer program for determination of chemical equilibrium constants from experimental data*, vol. Report 96-01, Department of Chemistry, Oregon State University, Version 3.2, (1996), 150 pp.. Cited on pages: 105, 121.

[1996KIR] Kirfel, A., Cation distribution in olivines and orthopyroxenes. An interlaboratory study, *Phys. Chem. Miner.*, **25**, (1996), 503-519. Cited on page: 148.

[1996LAN/HIL] Lange, L. C., Hills, C. D., Poole, A. B., Preliminary investigation into the effects of carbonation on cement-solidified hazardous wastes, *Environ. Sci. Technol.*, **30**, (1996), 25-30. Cited on page: 178.

[1996PAY/MOO] Paytan, A., Moore, W. S., Kastner, M., Sedimentation rate as determined by Ra-226 activity in marine barite, *Geochim. Cosmochim. Acta*, **60**, (1996), 4313-4319. Cited on page: 160.

[1996RUT/DUD] Rutherford, P. M., Dudas, M. J., Arocena, J. M., Heterogeneous distribution of radionuclides, barium and strontium in phospogypsum by-product, *Sci. Total Environ.*, **180**, (1996), 201-209. Cited on page: 159.

[1996TES/PAN] Tesoriero, A. J., Pankow, J. F., Solid solution partitioning of Sr^{2+}, Ba^{2+}, and Cd^{2+} to calcite, *Geochim. Cosmochim. Acta*, **60**, (1996), 1053-1063. Cited on pages: 14, 15.

[1997BRU/CER2] Bruno, J., Cera, E., Duro, L., Eriksen, T., Sellin, P., Spahiu, K., Werme, L., A kinetic model for the stability of the spent fuel matrix under oxic conditions; Model development against experimental evidence, *Mater. Res. Soc. Symp. Proc.*, **465**, (1997), 491-502. Cited on page: 198.

[1997FOR] Forsyth, R., The SKB spent fuel corrosion programme. An evaluation of results from the experimental programme performed in the Studsvik hot cell laboratory, SKB, Report TR 97-25, (1997). Cited on pages: 193, 198, 199, 200, 202, 203.

[1997GLA] Glasser, F. P., Fundamental aspects of cement solidification and stabilization, *J. Hazard. Mater.*, **52**, (1997), 151-170. Cited on pages: 27, 169.

[1997GRE/PLY2] Grenthe, I., Plyasunov, A. V., Spahiu, K., Estimations of medium effects on thermodynamic data, *Modelling in Aquatic Chemistry*, Grenthe, I., Puigdomènech, I., Eds., pp.325-426, Nuclear Energy Agency, Organisation for Economic Co-operation and Development, Paris, France, (1997). Cited on pages: 61, 66, 68, 69, 70.

[1997JOH/TAI] Johnson, L. H., Tait, J. C., Release of segregated nuclides from spent fuel, SKB, Report TR-97-18, (1997). Cited on page: 199.

[1997KAR/CHU] Karpov, I. K., Chudnenko, K. V., Kulik, D. A., Modeling chemical mass-transfer in geochemical processes: Thermodynamic relations, conditions of equilibria and numerical algorithms, *Am. J. Sci.*, **297**, (1997), 767-806. Cited on pages: 60, 95, 96, 97, 103.

[1997KIP] Kipp, K. L., Guide to the revised heat and solute transport simulator, HST3D-version 2. U.S. Geological Survey Water Resources Investigations, Report 97-4157, (1997). Cited on page: 164.

[1997KRO/LUE] Kroll, H., Lueder, T., Schlenz, H., Kirfel, A., Vad, T., The Fe^{2+}-Mg distribution in orthopyroxene: a critical assesment of its potential as a geospeedometer, *Eur. J. Mineral.*, **9**, (1997), 705-733. Cited on page: 148.

[1997LAN] Langmuir, D., *Aqueous environmental geochemistry*, Prentice Hall, New Jersey, USA, (1997). Cited on pages: 61, 67, 68, 72, 74.

[1997MCN/WIL] McNaught, A. D., Wilkinson, A., *Compendium of chemical therminology. IUPAC recommendation*, 2nd. Edition, Blackwell Science, (1997). Cited on page: 62.

[1997NAV] Navrotsky, A., Progress and new directions in high temperature calorimetry revisited, *Phys. Chem. Miner.*, **24**, (1997), 222-241. Cited on pages: 24, 25, 153.

[1997OTT] Ottonello, G., *Principles of geochemistry*, New York Columbia University Press, (1997), 894 pp.. Cited on page: 37.

[1997PIR/FED] Piriou, B., Fedoroff, M., Jeanjean, J., Bercis, L., Characterization of the sorption of Europium(III) on Calcite by Site-Selective and Time-Resolved Luminescence Spectroscopy, *J. Colloid Interface Sci.*, **194**, (1997), 440-447. Cited on page: 190.

[1997PRI/FER] Prieto, M., Fernández-González, A., Putnis, A., Fernández-Díaz, L., Nucleation, growth, and zoning phenomena in cristallizing $(Ba,Sr)CO_3$, $Ba(SO_4,CrO_4)$, $(Ba,Sr)SO_4$, and $(Cd,Ca)CO_3$ solid solutions from aqueous solutions, *Geochim. Cosmochim. Acta*, **61**, (1997), 3383-3397. Cited on pages: 20, 132, 135, 155, 156, 157.

[1997PUI/RAR] Puigdomènech, I., Rard, J. A., Plyasunov, A. V., Grenthe, I., Temperature corrections to thermodynamic data and enthalpy calculations, *Modelling in Aquatic Chemistry*, Grenthe, I., Puigdomènech, I., Eds., pp.427-493, Nuclear Energy Agency, Organisation for Economic Co-operation and Development, Paris, France, (1997). Cited on page: 61.

[1997SIN/KUL] Sinitsyn, V. A., Kulik, D. A., Khodorivski, M. S., Karpov, I. K., Prediction of solid-aqueous equilibria in cementitious systems using Gibbs energy minimization: I. Multiphase aqueous - ideal solid solution models, MRS 1997 Fall meeting, pp.72-73, Davos, Switzerland, (1997). Cited on page: 174.

[1997THO] Thomsen, K., Aqueous electrolytes: model parameters and process simulation, Ph. D. Thesis, Technical University of Denmark, (1997). Cited on pages: 65, 69, 70, 107.

[1997WAL/BIN] Walton, J. C., Bin-Shafique, S., Smith, R. W., Gutierrez, N., Tarquin, A., Role of carbonation in transient leaching of cementitious wasteforms, *Environ. Sci. Technol.*, **21**, (1997), 2345-2349. Cited on page: 178.

[1998BOT/BRO] Bothe, J. V. J., Brown, P. W., Phase equilibria in the system CaO-Al_2O_3-B_2O_3-H_2O at 23±1 C, *Adv. Cem. Res.*, **10**, (1998), 121-127. Cited on page: 183.

[1998BRA/BAE] Bradbury, M. H., Baeyens, B., A physicochemical characterisation and geochemical modelling approach for determining porewater chemistries in argillaceous rocks, *Geochim. Cosmochim. Acta*, **62**, (1998), 783-795. Cited on pages: 29, 184.

[1998BRU/CER] Bruno, J., Cera, E., Duro, L., Pon, J., de Pablo, J., Eriksen, T., Development of a kinetic model for the dissolution of the UO2 spent nuclear fuel. Application of the model to the minor radionuclides, SKB, Report TR-98-22, (1998). Cited on pages: 193, 201, 202.

[1998BRU/DUR] Bruno, J., Duro, L., de Pablo, J., Casas, I., Ayora, C., Delgado, J., Gimeno, M. J., Peña, J., Linklater, C., Perez del Villar, L., Gomez, P., Estimation of the concentrations of trace metals in natural systems. The application of codissolution and coprecipitation approaches to El Berrocal (Spain) and Pocos de Caldas (Brazil), *Chem. Geol.*, **151**, (1998), 277-291. Cited on page: 160.

[1998FIS] Fisher, R. S., Geologic and geochemical controls on naturally occurring radioactive materials (NORM) in produced water from oil, gas and geothermal operations, *Environ. Geosci.*, **5**, (1998), 139-150. Cited on page: 158.

[1998HIL] Hillert, M., *Phase equilibria, phase diagrams and phase transformations: Their thermodynamic basis*, Cambridge Univ. Press, (1998). Cited on page: 47.

[1998MCB/ROC] McBeath, M. K., Rock, P. A., Casey, W. H., Mandell, G. K., Gibbs energies of formation of metal-carbonate solid solutions: Part 3. The $Ca_xMn_{1-x}CO_3$ system at 298 K and 1 bar, *Geochim. Cosmochim. Acta*, **62**, (1998), 2799-2808. Cited on pages: 23, 122.

[1998MCH/NAV] McHale, J. M., Navrotsky, A., Kirkpatrick, R. J., Nanocrystalline spinel from freeze dried nitrates: Synthesis, energetics of product formation, and cation distribution, *Chem. Mater.*, **10**, (1998), 1083-1090. Cited on page: 56.

[1998MIL/PIE] Millero, F. J., Pierrot, D., A chemical equilibrium model for natural waters, *Aquat. Geochem.*, **4**, (1998), 153-199. Cited on page: 70.

[1998NAV] Navrotsky, A., Thermochemistry of crystalline and amorphous phases related to radioactive waste, *Actinides and the environment*, pp.267-297, The Netherlands: Kluwer Academic Publishers, (1998). Cited on page: 37.

[1998PIA/TOU] Pialoux, A., Touzelin, B., Etude du système U-Ca-O par diffractométrie de rayons X à haute température, *J. Nucl. Mater.*, **255**, (1998), 14-25. Cited on page: 194.

[1998RIM/BAL] Rimstidt, J. D., Balog, A., Webb, J., Distribution of trace elements between carbonate minerals and aqueous solutions, *Geochim. Cosmochim. Acta*, **62**, (1998), 1851-1863. Cited on pages: 130, 131, 132, 184.

[1998WIL] Will, T., *Phase equilibria in metamorphic rocks. Thermodynamic background and petrological applications*, Springer, Berlin, (1998). Cited on pages: 52, 54, 55.

[1999ADL/MAD] Adler, M., Mäder, U., Waber, N., High-pH alteration of argilaveous rocks: An experimental study, *Schweiz. Mineral. Petrogr. Mitt.*, **79**, (1999), 445-454. Cited on page: 184.

[1999BRU/CER] Bruno, J., Cera, E., Grivé, M., Eklund, U. B., Eriksen, T., Experimental determination and chemical modelling of radiolytic processes at the spent fuel/water interface, SKB, Report TR-99-26, (1999). Cited on pages: 32, 193, 198, 200.

[1999CUR] Curti, E., Coprecipitation of radionuclides with calcite: estimation of partition coefficients based on a review of laboratory investigations and geochemical data, *Appl. Geochem.*, **14**, (1999), 433-445. Cited on pages: 14, 29, 130, 132, 184.

[1999FIN/MUR] Finch, R., Murakami, T., Systematics and paragenesis of uranium minerals, *Mineralogy, geochemistry and the environment*, Burns, P.C., Finch, R., Eds., (1999), Mineralogical Society of America and Geochemical Society, 38 (1999) 91-180. Cited on page: 195.

[1999GLA/HON] Glasser, F. P., Hong, S.-Y., Alkali binding in cement pastes. Part I. The C-S-H phase, *Cem. Concr. Res.*, **29**, (1999), 1893-1903. Cited on page: 183.

[1999GRU/KWA] Grutzeck, M., Kwan, S., Thompson, J. L., Benesi, A., Sorocilicate model for calcium silicate hydrate (C-S-H), *J. Mater. Sci. Lett.*, **18**, (1999), 217-220. Cited on page: 173.

[1999GRU] Grutzeck, M., A new model for the formation of calcium silicate hydrate (C-S-H), *Mater. Res. Innovations.*, **3**, (1999), 160-170. Cited on page: 172.

[1999HOC/MOO] Hochella, M. F., Moore, J. N., Golla, U., Putnis, A., A TEM study of samples from acid mine drainage systems: Metal-mineral association with implications for transport, *Geochim. Cosmochim. Acta*, **63**, (1999), 3395-3406. Cited on page: 145.

[1999JOH/KER] Johnson, C. A., Kersten, M., Solubility of Zn(II) in association with calcium silicate hydrates in alkaline solutions, *Environ. Sci. Technol.*, **33**, (1999), 2296-2298. Cited on pages: 29, 179, 181, 182.

[1999LIA/TOP] Liang, J.-J., Topor, L., Navrotsky, A., Mitomo, M., Silicon nitride: enthalpy of formation of the α- and β-polymorphs and the effect of C and O impurities, *J. Mater. Chem.*, **14**, (1999), 1959-1968. Cited on page: 155.

[1999MAR/AKB] Martin, P., Akber, R.A. , Radium isotopes as indicators of adsorption-desorption interactions and barite formation in groundwater, *J. Environ. Radioact.*, **46**, (1999), 271-286. Cited on pages: 25, 159.

[1999NAV/DOO] Navrotsky, A., Dooley, D., Reeder, R. J., Brady, P., Calorimetric studies of the energetics of order-disorder in the system $Mg_{1-x}Fe_xCa(CO_3)_2$, *Am. Mineral.*, **84**, (1999), 1622-1626. Cited on pages: 60, 155.

[1999NEA] TDB-0-TDB-6, TDB project guidelines, NEA Web site PDF documents, (1999). Cited on page: 22.

[1999NED/BUR] Neder, R. B, Burghammer, M., Grasl, T., Schulz, H., Bram, A., Fiedler, S., Refinement of the kaolinite structure from single-crystal synchrotron data, *Clays Clay Miner.*, **47**, (1999), 487-494. Cited on page: 143.

[1999PAR/APP] Parkhurst, D. L., Appelo, C. A. J., User's guide to PHREEQC (version 2) - A computer program for speciation, batch-reaction, one-dimensional transport, and inverse geochemical calculations, U.S.G.S. Water-Resources Investigations, Report 99-4259, (1999). Cited on pages: 26, 67, 87, 91, 160, 164.

[1999PER/PAL] Perkins, R. B., Palmer, C. D., Solubility of ettringite $(Ca_6[Al(OH)_6]_2(SO_4)_3 \cdot 26H_2O)$ at 5-75 C, *Geochim. Cosmochim. Acta*, **63**, (1999), 1969-1980. Cited on page: 183.

[1999PUI/RAR] Puigdomènech, I., Rard, J. A., Plyasunov, A. V., Grenthe, I., TDB-4: Temperature corrections to thermodynamic data and enthalpy calculations, Nuclear Energy Agency Data Bank, Organisation for Economic Co-operation and Development, Report , (1999), 96 pp.. Cited on page: 23.

[1999RAR/RAN] Rard, J. A., Rand, M. H., Anderegg, G., Wanner, H., *Chemical Thermodynamics of Technetium*, Sandino, M. C. A., Östhols, E., Nuclear Energy Agency Data Bank, Organisation for Economic Co-operation, Development, Eds., vol. 3, *Chemical Thermodynamics*, North Holland Elsevier Science Publishers B. V., Amsterdam, The Netherlands, (1999). Cited on pages: 3, 60.

[1999SKB] SKB97, Deep repository for spent nuclear fuel. SR 97 - Post-closure safety. Main report, Report TR-99-06, (1999). Cited on page: 2.

[2000BEC/CAR] Becerro, A. I., Carpenter, M. A., Ballaran, T. B., seifert, F., Hard mode infrared spectroscopy of $CaTiO_3$-$CaFeO_{2.5}$ perovskites, *Phase Transitions*, **71**, (2000), 161-172. Cited on page: 150.

[2000BEC/FER] Becker, U., Fernández-González, A., Prieto, M., Harrison, R. M., Putnis, A., Direct calculation of thermodynamic properties of the barite/celestite solid solution from molecular principles, *Phys. Chem. Miner.*, **27**, (2000), 291-300. Cited on pages: 112, 122.

[2000GAM/KON] Gamsjäger, H., Königsberger, E., Preis, W., Lippmann diagrams: Theory and application to carbonate systems, *Aquat. Geochem.*, **6**, (2000), 119-132. Cited on pages: 18, 19, 77, 78, 80, 82, 114.

[2000GLY] Glynn, P. D., Solid solution solubilities and thermodynamics: Sulfates, carbonates and halides, *Sulfate minerals: Crystallography, geochemistry and environmental significance*, Jambor, J. L., Nordstrom, D. K., Eds., vol. 40, *Reviews in Mineralogy and Geochemistry*, pp.481-511, Mineralogical Society of America and Geochemical Society, (2000). Cited on pages: 16, 19, 29, 45, 60, 112, 114, 125, 127, 128, 129, 130, 137, 138, 141, 142, 156, 185.

[2000GRA/LOI] Grambow, B., Loida, A., Martínez-Esparza, A., Díaz-Arocas, P., de Pablo, J., Paul, J.-L., Marx, G., Glatz, J.-P., Lemmens, K., Ollila, K., Christensen, H., Source term for performance assessment of spent fuel as a waste form, Report EUR 19140 EN, (2000). Cited on page: 193.

[2000HAN] Hanor, J. S., Barite-celestine geochemistry and environments of formation. In Reviews in Mineralogy, *Mineral. Soc. Am.*, **40**, (2000), 193-276. Cited on pages: 155, 156.

[2000HAW/KRI] Hawthorne, F. C., Krivovichev, S. V., Burns, P. C., *The crystal chemistry of sulphte minerals*, vol. 40, *Reviews in Mineralogy*, pp.1-112, Mineralogical Society of America, (2000). Cited on page: 156.

[2000JEN] Jennings, H. M., A model the microstructure of calcium silicate hydrate in cement paste, *Cem. Concr. Res.*, **30**, (2000), 101-116. Cited on page: 170.

[2000KUL/KER] Kulik, D. A., Kersten, M., Heiser, U., Neumann, T., Application of Gibbs energy minimization to model early-diagenetic solid-solution aqueous-solution equilibria involving authigenic rhodochrosites in anoxic Baltic sea sediments, *Aquat. Geochem.*, **6**, (2000), 147-199. Cited on page: 110.

[2000OTT/BOE] Ott, J. B., Boerio-Goates, J., Chemical thermodynamics: Advanced applications, , p. 438, San Diego CA. Academic Press, (2000). Cited on page: 37.

[2000OTT/BOE2] Ott, J. B., Boerio-Goates, J., Chemical thermodynamics: Principles and applications, , p. 664, San Diego CA. Academic Press, (2000). Cited on page: 37.

[2000PER/PAL] Perkins, R. B., Palmer, C. D., Solubility of $Ca_6[Al(OH)_6]_2(CrO_4)_3.26H_2O$, the chromate analog of ettringite, *Appl. Geochem.*, **15**, (2000), 1203-1218. Cited on page: 183.

[2000PRI/FER] Prieto, M., Fernández-González, A., Becker, U., Putnis, A., Computing Lippmann diagrams from direct calculation of mixing properties of solid solutions: Application to the barite-celestite system., *Aquat. Geochem.*, **6**, (2000), 133-146. Cited on pages: 18, 45, 78, 85, 155, 156.

[2000TRA/BRO] Trainor, T. P., Brown Jr., G. E., Parks, G. A., Adsorption and precipitation of aqueous Zn(II) on alumina powders, *J. Colloid Interface Sci.*, **231**, (2000), 359-372. Cited on page: 10.

[2000WOL/KON] Wolf, G., Königsberger, E., Schmidt, H. G., Königsberger, L. C., Gamsjäger, H., Thermodynamic aspects of the vaterite-calcite phase transition, *J. Therm. Anal. Calorim.*, **60**, (2000), 463-472. Cited on page: 133.

[2001AND] Dossier 2001 Argile, ANDRA, Report , (2001). Cited on pages: 29, 184.

[2001BAL/CAR] Ballaran, T. B., Carpenter, M. A., Domeneghetti, M. C., Phase transitions and mixing behaviour of the cummingtonite-grunerite solid solution, *Phys. Chem. Miner.*, **28**, (2001), 87-101. Cited on page: 150.

[2001BAL/CAR2] Ballaran, T. B., Carpenter, M. A., Ross, N. L., Infrared powder-absorption spectroscopy of Ca-free P2(1)/c clinopyroxenes, *Mineral. Mag.*, **65**, (2001), 339-350. Cited on page: 150.

[2001CAR/BOF] Carpenter, M. A., Boffa Ballaran, T., The influence of elastic strain heterogeneities in silicate solid solutions, *Solid solutions in silicate and oxide systems*, *Eötvös University Press, Budapest*, EMU Notes in Mineralogy, (2001). Cited on page: 150.

[2001CAR/YOD] Carbajo, J. J., Yoder, G. L., Popov, S. G., Ivanov, V. K., A review of thermophysical properties of MOX and UO_2 fuels, *J. Nucl. Mater.*, **299**, (2001), 181-198. Cited on page: 196.

[2001FIA/NAV] Fialips, C. I., Navrotsky, A., Petit, S., Crystal properties and energetics of synthetic kaolinite, *Am. Mineral.*, **86**, (2001), 304-311. Cited on page: 155.

[2001GAN] Ganguly, J., Thermodynamic modelling of solid solutions, *Solid solutions in silicate and oxide systems of geological importance*, vol. 3, *Eötvös University Press, Budapest*, pp.37-69, EMU Notes in Mineralogy, (2001). Cited on pages: 37, 52, 60.

[2001GEI] Geiger, C. A., Solid solutions in silicate and oxide systems of geological importance, *European mineralogical union notes in mineralogy*, Papp, G., Weiszburg, T. G., Eds., vol. 3, p. 458, Eötvös University Press, (2001). Cited on page: 37.

[2001GRA/MUL] Grambow, B., Müller, R., First order dissolution rate law and the role of surface layers in glass performance assessment, *J. Nucl. Mater.*, **2998**, (2001), 112-124. Cited on page: xxi.

[2001HAB/NIK] Habermann, D., Niklas, J.R., Meijer, J., Stephan, A., Gotte, T., Structural point defects in "Iceland spar" calcite, *Nucl. Instrum. Methods Phys. Res., Sect. B*, **181**, (2001), 563-569. Cited on page: 184.

[2001KAR/CHU] Karpov, I. K., Chudnenko, K. V., Kulik, D. A., Avchenko, O. V., Bychinskii, V. A., Minimization of Gibbs free energy in geochemical systems by convex programming, *Geochem. Int.*, **39**, (2001), 1108-1119. Cited on pages: 60, 95, 97, 103, 110.

[2001KUL/KER] Kulik, D. A., Kersten, M., Aqueous solubility diagrams for cementitious waste stabilization systems: II, End-member stoichiometries of ideal calcium silicate hydrate solid solutions, *J. Am. Ceram. Soc.*, **84**, (2001), 3017-3026. Cited on pages: 28, 169, 170, 172, 174, 176, 177.

[2001LEM/FUG] Lemire, R. J., Fuger, J., Nitsche, H., Potter, P. E., Rand, M. H., Rydberg, J., Spahiu, K., Sullivan, J. C., Ullman, W. J., Vitorge, P., Wanner, H., *Chemical Thermodynamics of Neptunium and Plutonium*, Nuclear Energy Agency Data Bank, Organisation for Economic Co-operation, Development, Ed., vol. 4, *Chemical Thermodynamics*, North Holland Elsevier Science Publishers B. V., Amsterdam, The Netherlands, (2001). Cited on pages: 3, 60.

[2001OBE] Oberti, R., The diffraction experiment in the study of solid solutions: Long-range properties, *Solid solutions in silicate and oxide systems, Eötvös University Press, Budapest*, EMU Notes in Mineralogy, (1998). Cited on page: 147.

[2001PAR/VAN] Paridaens, J., Vanmarcke, H., Radium contamination of the banks of the river Laak as a consequence of the phosphate industry in Belgium, *J. Environ. Radioact.*, **54**, (2001), 53-60. Cited on page: 160.

[2001PEL] Pelton, A. D., A general "geometric" thermodynamic model for multicomponent solutions, *CALPHAD: Comput. Coupling Phase Diagrams Thermochem.*, **25**, (2001), 319-328. Cited on page: 60.

[2001POI/TOU] Poinssot, C., Toulhoat, P., Grouiller, J. P., Pavageau, J., Piron, J. P., Pelletier, M., Dehaudt, P., Cappelaere, C., Limon, R., Desgranges, L., Jegou, C., Corbel, C., Maillard, S., Faure, M. H., Cicariello, J. C., Masson, M., Synthesis on the long term behaviour of the spent nuclear fuel, CEA, Report R-5958 (E), (2001). Cited on page: 196.

[2001ROY/FOR] De Roy, A., Forano, C., Besse, J. P., Layered Double Hydroxides: Synthesis and post-synthesis modification, *Layered Double Hydroxides: Present and Future*, V. Rives, Ed., pp.1-38, Nova Science Publishers, Inc., New York, (2001). Cited on page: 184.

[2001URU] Urusov, V. S., Solid solutions in silicate and oxide systems of geological, *The phenomenological theory of solid solutions*, Geiger, C. A., Ed., vol. 3, pp.121-153, Eötvös University Press, (2001). Cited on page: 147.

[2001WAN/XU] Wang, Y., Xu, H., Prediction of trace metal partitioning between minerals and aqueous solutions: A linear free energy correlation approach, *Geochim. Cosmochim. Acta*, **65**, (2001), 1529-1543. Cited on page: 132.

[2001YAM/AKI] Yamashita,T., Akie, H., Nakano, Y., Kuramoto, K., Nitani, N., Nakamura T., Current status of researches on the plutonium rock-like oxide fuel and its burning in light water reactors, *Prog. Nucl. Energy*, **38**, (2001), 327-330. Cited on page: 196.

[2001YAN/NAV] Yang, S., Navrotsky, A., Wilkin, R., Thermodynamics of ion-exchanged clinoptilolite, *Am. Mineral.*, **86**, (2001), 438-447. Cited on page: 155.

[2001ZIE/OTT] Zielinski, R. A., Otton, J. K., Budahn, J. R., Use of radium isotopes to determine the age and origin of radioactive barite at oilfield production sites, *Environ. Pollution*, **113**, (2001), 299-309. Cited on page: 159.

[2002BAL/CHA] Bale, C. W., Chartrand, P., Degterov, S. A., Eriksson, G., Hack, K., Ben Mahfoud, R., Melancon, J., Pelton, A. D., Petersen, S., FactSage thermochemical software and databases, *CALPHAD: Comput. Coupling Phase Diagrams Thermochem.*, **26**, (2002), 189-228. Cited on pages: 60, 95.

[2002BEC/POL] Becker, U., Pollok, K., Molecular simulations of interfacial and thermodynamic mixing properties of grossular- andradite garnets, *Phys. Chem. Miner.*, **29**, (2002), 52-64. Cited on page: 122.

[2002BER/CUR] Berner, U., Curti, E., Radium solubilities from SF/HLW wastes using solid solution and co-precipitation models, Paul Scherrer Institute, Villigen, Switzerland, Internal Report TM-44-02-04, (2002). Cited on pages: 26, 162, 163, 165.

[2002CHU/KAR] Chudnenko, K. V., Karpov, I. K., Kulik, D. A., A high-precision IPM-2 non-linear minimization module of GEM-Selektor v.2-PSI program code for geochemical thermodynamic modeling, Paul Scherrer Institute, Report TM-44-04-02, (2002). Cited on pages: 97, 99, 100.

[2002ELZ/REE] Elzinga, E. J., Reeder, R. J., Withers, S. H., Peale, R. E., Mason, R. A., Beck, K. M., Hess, W. P., EXAFS study of rare-earth element coordination in calcite, *Geochim. Cosmochim. Acta*, **66**, (2002), 2875-2885. Cited on pages: 30, 189, 190.

[2002FAN] Fanghänel, T., The use of thermodynamic databases in performance assessment, NEA TDB International Workshop, Barcelona, Spain, 29-30 May 2001, pp.45-60, (2002). Cited on pages: 69, 70.

[2002GLA/HON] Glasser, F. P., Hong, S.-Y., Alkali sorption by C-S-H and C-A-S-H gels Part II. Role of alumina, *Cem. Concr. Res.*, **32**, (2002), 1101-1111. Cited on page: 183.

[2002HEL/NAV] Helean, K. B., Navrotsky, A., Oxide melt solution calorimetry of rare earth oxides: Techniques, problems, cross-checks, successes, *J. Therm. Anal. Calorim.*, **69**, (2002), 751-771. Cited on page: 155.

[2002HEL/NAV2] Helean, K. B., Navrotsky, A., Vance, E. R., Carter, M. L., Ebbinghaus, B., Krikorian, O., Kian, J., Wang, L. M., Catalano, J. G., Enthalpies of formation of Ce-pyrochlore, $Ca_{0.93}Ce_{1.00}Ti_{2.035}O_{7.00}$, U-pyrochlore, $Ca_{1.46}U_{0.23}{}^{4+}U_{0.46}{}^{6+}Ti_{1.85}O_{7.00}$ and Gd-pyrochlore, $Gd_2Ti_2O_7$: Three materials relevant to the proposed waste form for excess weapons plutonium, *J. Nucl. Mater.*, **303**, (2002), 226-239. Cited on page: 155.

[2002HUM/BER] Hummel, W., Berner, U., Curti, E., Pearson, F. J., Thoenen, T., Nagra/PSI chemical thermodynamic data base 01/01, Nagra, Report NTB 02-16 and Universal Publishers/uPublish.com, Parkland, Florida, USA, (2002). Cited on pages: 61, 81, 97, 103, 116, 164, 177.

[2002ILI/THO] Iliuta, M. C., Thomsen, K., Rasmussen, P., Modeling of heavy metal salt solubility using the Extended UNIQUAC model, *Am. Inst. Chem. Eng. J.*, **48**, (2002), 2664-2689. Cited on page: 70.

[2002KON] Königsberger, E., Solubility equilibria. From data optimization to process simulation, *Pure Appl. Chem.*, **74**, (2002), 1831-1841. Cited on page: 70.

[2002KUL/KER] Kulik, D. A., Kersten, M., Aqueous solubility diagrams for cementitious waste stabilization systems. 4. A carbonation model for Zn-doped calcium silicate hydrate by Gibbs energy minimization, *Environ. Sci. Technol.*, **36**, (2002), 2926-2931. Cited on pages: 29, 110, 174, 177, 179, 180, 181, 182.

[2002LHE/JAM] L'Heureux, I., Jamtveit, B., A model of oscillatory zoning in solid solutions grown from aqueous solutions: Applications to the $(Ba,Sr)SO_4$ system, *Geochim. Cosmochim. Acta*, **66**, (2002), 417-429. Cited on pages: 132, 145, 155.

[2002MAN/MAR] Manceau, A., Marcus, M. A., Tamura, N., Quantitative speciation of heavy metals in soils and sediments by synchrotron X-ray techniques, *Applications of Synchrotron Radiation in Low-Temperature Geochemistry and Environmental Science*, P. Fenter, N. C. Sturchio, Ed., vol. 49, pp.341-428, Mineralogy and Geochemistry, Mineralogical Society of America, Washington, DC, (2002). Cited on pages: 8, 9, 11.

[2002PER/UME] Perales-Perez, O., Umetsu, Y., Ambient-temperature precipitation of Zn ion from aqueous solutions as ferrite-type compounds, *Hydrometallurgy*, **63**, (2002), 235-248. Cited on page: 11.

[2002SPA] Spahiu, K., The use of SIT in the NEA TDB project - advantages, drawbacks and comparison with the approaches used in some geochemical codes, The use of thermodynamic databases in performance assessment. NEA TDB International Workshop, Barcelona, Spain, 29-30 May 2001, pp.61-68, (2002). Cited on page: 69.

[2002STU/FAN2] Stumpf, T., Fanghänel, T., A time resolved laser fluorescence sprectoscopy (TRLFS) study of the interaction of trivalent actinides (Cm(III)) with calcite, *J. Colloid Interface Sci.*, **2**, (2002), 119-125. Cited on pages: 29, 149, 185, 190.

[2002TSU/KAG] Tsuno, H., Kagi, H., Akagi, T., High yield of vaterite precipitation induced by trace lanthanum ion from supersaturated solution of calcium carbonate at 50°C, *Chem. Lett.*, XX, (2002), 960-961. Cited on page: 185.

[2002WAN/LEE] Wang, H. R., Lee, J. S., Yu, S. C., Synthesis of zoning-free $BaSO_4$-$PbSO_4$ solid solutions and its structural characterizations., *Z. Kristallogr.*, **217**, (2002), 143-148. Cited on page: 157.

[2003BAU/JOH] Baur, I., Johnson, C. A., The solubility of selenate-AFt ($3CaOxAl_2O_3$ x $3CaSeO_4$ x $37.5H_2O$) and selenate-AFm ($3CaO$ x Al_2O_3 x $CaSeO_4$ x H_2O), *Cem. Concr. Res.*, **33**, (2003), 1741-1748. Cited on pages: 183, 184.

[2003BIS/VAN] Bish, D. L., Vaniman, D. T., Chipera, S. J., Carey, J. W., The distribution of zeolites and their effects on the performance of a nuclear waste repository at Yucca Mountain, Nevada, U.S.A., *Am. Mineral.*, **88**, (2003), 1889-1902. Cited on page: 43.

[2003BLA/AGU] Blanco-Varela, M. T., Aguilera, J., Martínez-Ramírez, S., Puertas, F., Palomo, A., Sabbioni, C., Zappia, G., Riontino, C., Van Balen, K., Toumbakari, E. E., Thaumasite formation due to atmospheric SO_2-hydraulic mortar interaction, *Cem. Concr. Res.*, **25**, (2003), 983-990. Cited on page: 12.

[2003BRU/CER] Bruno, J., Cera, E., Grivé, M., Duro, L., Eriksen, T., Experimental determination and chemical modelling of radiolytic processes at the spent fuel/water interface. Experiments carried out in carbonate solutions in absence and presence of chloride, SKB, Report TR-03-03, (2003). Cited on pages: 32, 193, 198, 199, 200, 201.

[2003FER/ALV] Fernández-Prini, R., Alvarez, J., Harvey, A. H., Henry's constants and vapor-liquid distribution constants for gaseous solutes in H_2O and D_2O at high temperatures, *J. Phys. Chem. Ref. Data*, **32**, (2003), 903-916. Cited on page: 72.

[2003GAM/KON] Gamsjäger, H., Königsberger, E., Solubility of sparingly soluble solids in liquids, *The experimental determination of solubilities*, Hefter, G. T, Tomkins, R. P. T., Eds., pp.315-358, John Wiley & Sons, Ltd, (2003). Cited on pages: 62, 72, 74, 76, 77, 94.

[2003GLY] Glynn, P. D., Modeling Np and Pu transport with a surface complexation model and spatially variant sorption capacities: implications for reactive transport modeling and performance assessments of nuclear waste disposal sites, *Comput. Geosci.*, **29**, (2003), 331-349. Cited on pages: 2, 9.

[2003GUI/FAN] Guillaumont, R., Fanghänel, T., Fuger, J., Grenthe, I., Neck, V., Palmer, D. A., Rand, M. H., *Update on the chemical thermodynamics of Uranium, Neptunium, Plutonium, Americium and Technetium*, Nuclear Energy Agency Data Bank, Organisation for Economic Co-operation, Development, Ed., vol. 5, *Chemical Thermodynamics*, North Holland Elsevier Science Publishers B. V., Amsterdam, The Netherlands, (2003). Cited on pages: 3, 60.

[2003HUG/HEL] Hughes Kubatko, K.-A., Helean, K. B., Navrotsky, A., Burns, P. C., Stability of peroxide-containing uranyl minerals, *Science*, **302**, (2003), 1191-1193. Cited on page: 155.

[2003JOH/GLA] Johnson, C. A., Glasser, F. P., Hydrotalcite-like minerals $M_2Al(OH)_6(CO_3)_{0.5}xH_2O$, where M = Mg, Zn, Co, Ni in the environment: Synthesis, characterization and thermodynamic stability, *Clays Clay Miner.*, **51**, (2003), 1-8. Cited on page: 184.

[2003KUL/DMY] Kulik, D. A., Dmytriyeva, S. V., Rysin, A.V., Chudnenko, K. V., Karpov, I. K., GEM-Selektor (GEMS): a research program package for interactive thermodynamic modelling of aquatic (geo)chemical systems, Waste Management Laboratory, Paul Scherrer Institute, Report , (2003-on). Cited on page: 95.

[2003LAS/HUN] Lashley, J. C., Hundley, M. F., Migliori, A., Sarrao, J. L., Pagliuso, P. G., Darling, T. W., Jaime, M., Cooley, J. C., Hults, W. L., Morales, L., Thoma, D. J., Smith, J. L., Boerio-Goates, J., Woodfield, B. F., Stewart, G. R., Fisher, R. A., Phillips, N. E., Critical examination of heat capacity measurements made on a Quantum Design physical property measurement system, *Cryogenics*, **43**, (2003), 369-378. Cited on page: 152.

[2003LOR/COH] Lorimer, J. W., Cohen-Adad, R., Thermodynamics of solubility, *The Experimental Determination of Solubilities*, Hefter, G. T., Tomkins, R. P. T., Eds., pp.19-76, John Wiley and Sons, Ltd, (2003). Cited on pages: 62, 63, 65, 71.

[2003LOR] Lorimer, J. W., Quantities, units and conversions, *The Experimental Determination of Solubilities*, Hefter, G. T., Tomkins, R. P. T., Eds., pp.1-15, John Wiley and Sons, Ltd, (2003). Cited on pages: 62, 72.

[2003MAR/CRU] Martin, A. J., Crusius, J., Jay McNee, J., Yanful, E. K., The mobility of radium-226 and trace metals in pre-oxidized subaqueous uranium mill tailings, *Appl. Geochem.*, **18**, (2003), 1095-1100. Cited on pages: 25, 159.

[2003PET/PUI] Pettit, L. D., Puigdomènech, I., Wanner, H., Ionic strength corrections using specific interaction theory, IUPAC, Version: 1.5, Report URL: http://www.iupac.org/projects/2000/2000-003-1-500.html, (2003). Cited on pages: 69, 81.

[2003TIT/STU] Tits, J., Stumpf, T., Rabung, T., Wieland, E., Fanghänel, T., Uptake of Cm(III) and Eu(III) by calcium silicate hydrates: A solution chemistry and time-resolved laser fluorescence spectroscopy study, *Environ. Sci. Technol.*, **37**, (2003), 3568-3576. Cited on page: 149.

[2003WER] Wersin, P., Geochemical modelling of bentonite pore water in high-level waste repository, *J. Contam. Hydrol.*, **61**, (2003), 405-422. Cited on page: 161.

[2003WHI/PEA] Withers, S. H., Peale, R. E., Schulte, A. F., Braunsrein, G., Beck, K. M., Hess, W. P., Reeder, R. J., Broad distribution of the crystal field environments for Nd^{3+} in calcite, *Phys. Chem. Miner.*, **30**, (2003), 440-448. Cited on pages: 30, 190, 191, 192.

[2003XU/SU] Xu, H., Su, Y., Balmer, M. L., Navrotsky, A., A new series of oxygen vacancy perovskites in the $NaTi_xNb_{1-x}O_{3-0.5x}$ system: synthesis, crystal chemistry and energetics, *Chem. Mater.*, **15**, (2003), 1872-1878. Cited on page: 155.

[2004BEC/REY] Van Beck, P., Reyes, J. L., Paterne, M., Gersonde, R., Van der Loeff, M. R., Kuhn, G., Ra-226 in barite: Absolute dating of Holocene Southern Ocean sediments and reconstruction of sea-surface reservoir ages, *Geology*, **30**, (2004), 731-734. Cited on page: 160.

[2004BOS/RAB] Bosbach, D., Rabung, T., Brandt, F., Fanghänel, T., Trivalent actinide coprecipitation with powellite ($CaMoO_4$): Secondary solid solution formation during HLW borosilicate-glass dissolution, *Radiochim. Acta*, **92**, (2004), 639-644. Cited on page: 149.

[2004CEC/BLA] Ceccarello, S., Black, S., Read, D., Hodson, M. E., Industrial radioactive barite scale: suppression of radium uptake by introduction of competing ion, *Miner. Eng.*, **17**, (2004), 323-330. Cited on page: 159.

[2004CHR/MOL] Christov, C., Møller, N., A chemical equilibrium model of solution behavior and solubility in the H-Na-K-Ca-OH-Cl-HSO_4-SO_4-H_2O system to high concentration and temperature, *Geochim. Cosmochim. Acta*, **67**, (2004), 3717-3739. Cited on pages: 69, 70.

[2004HEL/USH] Helean, K. B., Ushakov, S. V., Brown, C. E., Navrotsky, A., Lian, J., Ewing, R. C., Farmer, J. M., Boatner, L. A., Formation enthalpies of rare earth titanate pyrochlores, *J. Solid State Chem.*, **177**, (2004), 1858-1866. Cited on page: 155.

[2004KLE] Kleykamp, H., Post-irradiation studies on LWR-MOX fuel fabricated by the optimized co-milling process, *J. Nucl. Mater.*, **324**, (2004), 198-202. Cited on page: 196.

[2004KUL/BER2] Kulik, D. A., Berner, U., Curti, E., Modelling chemical equilibrium partitioning with the GEMS-PSI code, *PSI Scientific Report 2003 / Volume IV, Nuclear Energy and Safety*, Smith, B., Gschwend, B., Eds., pp.109-122, Paul Scherrer Institut, (2004). Cited on pages: 95, 97, 109, 164, 166.

[2004LAK/STI] Lakshtanov, L. Z., Stipp, S. L. S., Experimental study of europium(III) coprecipitation with calcite, *Geochim. Cosmochim. Acta*, **68**, (2004), 819-827. Cited on pages: 30, 31, 116, 188, 189, 192.

[2004MAC/BAR] Macphee, D. E., Barnett, S. J., Solution properties of solids in the ettringite-thaumasite solid solution series, *Cem. Concr. Res.*, **34**, (2004), 1591-1598. Cited on page: 183.

[2004PAR/KIP] Parkhurst, D. L., Kipp, K. L., Engesgaard, P., Charlton, S. R., PHAST - A program for simulating ground-water flow, solute transport, and multicomponent geochemical reactions, U.S. Geological Survey, Techniques and Methods, Report 6-A8, (2004). Cited on page: 164.

[2004RIC] Richardson, I. G., Tobermorite/jennite- and tobermorite/calcium hydroxide-based models for the structure of C-S-H: applicability to hardened pastes of tricalcium silicate, h-dicalcium silicate, Portland cement, and blends of Portland cement with blast-furnace slag, metakaolin, or silica fume, *Cem. Concr. Res.*, **34**, (2004), 1733-1777. Cited on pages: 169, 170, 171.

[2004ROD/CAR] Rodehurst, U., Carpenter, M. A., Ballaran, T. B., Geiger, C. A., Structural heterogeneity, mixing behaviour and saturation effects in the glossular-spessartine solid solution, *Phys. Chem. Miner.*, **31**, (2004), 387-404. Cited on page: 150.

[2004ROU/ELZ] Rouff, A. A., Elzinga, E. J., Reeder, R. J., Fisher, N. S., X-ray absorption spectroscopic evidence for the formation of Pb(II) inner sphere adsorption complexes and precipitates at the calcite-water interface, *Environ. Sci. Technol.*, **38**, (2004), 1700-1707. Cited on page: 10.

[2004SCH/HAR] Schindler, M., Hawthorne, F. C., Putnis, C. V., Putnis, A., Growth of uranyl-hydroxy-hydrate and uranyl-carbonate minerals on the (104) surface of calcite, *Can. Mining J.*, **42**, (2004), 1683-1697. Cited on page: 145.

[2004SCH/PUT] Schindler, M., Putnis, A., Cystal growth of schoepite on the (104) surface of calcite, *Can. Mining J.*, **42**, (2004), 1667-1681. Cited on page: 145.

[2004STU/TIT] Stumpf, T., Tits, J., Walther, C., Wieland, E., Fanghänel, T., Uptake of trivalent actinides (curium(III)) by hardened cement paste: a time-resolved laser fluorescence spectroscopy study, *J. Colloid Interface Sci.*, **276**, (2004), 118-124. Cited on page: 149.

[2004TAN/OHT] Tanaka, K., Ohta, A., Kawabe, I., Experimental REE partitioning between calcite and aqueous solution at 25^{o} and 1 atm: Constraints on the incorporation of seawater REE into seamount-type limestone, *Geochem. J.*, **38**, (2004), 19-32. Cited on pages: 184, 188, 189.

[2004ZHU] Zhu, C., Coprecipitation in the barite isostructural family:1. Binary mixing properties, *Geochim. Cosmochim. Acta*, **68**, (2004), 3327-3337. Cited on pages: 155, 157.

[2004ZHU2] Zhu, C., Coprecipitation in the barite isostructural family:1. Numerical simulations of reactions and mass transport, *Geochim. Cosmochim. Acta*, **68**, (2004), 3339-3349. Cited on pages: 26, 160, 161.

[2005ALL/NAV] Allada, R. K., Navrotsky, A., Boerio-Goates, J., Thermochemistry of hydrotalcite-like phases in the MgO-Al_2O_3-CO_2-H_2O system: A determination of enthalpy, entropy, and free energy, *Am. Mineral.*, **90**, (2005), 329-335. Cited on page: 184.

[2005BRO/CUR] Brown, P. L., Curti, E., Grambow, B., *Chemical thermodynamics of Zirconium*, Nuclear Energy Agency Data Bank, Organisation for Economic Co-operation, Development, Ed., vol. 8, *Chemical Thermodynamics*, North Holland Elsevier Science Publishers B. V., Amsterdam, The Netherlands, (2005). Cited on pages: 3, 60.

[2005CUR/KUL] Curti, E., Kulik, D. A., Tits, J., Solid solutions of trace Eu(III) in calcite: thermodynamic evaluation of experimental data over a wide range of pH and pCO_2, *Geochim. Cosmochim. Acta*, **69**, (2005), 1721-1737. Cited on pages: 31, 110, 116, 117, 118, 119, 120, 189, 192.

[2005EWI] Ewing, R. C., Plutonium and "minor" actinides: safe sequestration, *Earth Planet. Sci. Lett.*, **229**, (2005), 165-181. Cited on page: 196.

[2005GAM/BUG] Gamsjäger, H., Bugajski, J., Gajda, T., Lemire, R. J., Preis, W., *Chemical thermodynamics of Nickel*, Nuclear Energy Agency Data Bank, Organisation for Economic Co-operation, Development, Ed., vol. 6, *Chemical Thermodynamics*, North Holland Elsevier Science Publishers B. V., Amsterdam, The Netherlands, (2005). Cited on pages: 3, 60.

[2005GUI/NAV] Guillemet-Fritsch, S., Navrotsky, A., Tailhades, P., Coradin, H., Wang, M., Thermochemistry of iron manganese oxide spinels, *J. Solid State Chem.*, **178**, (2005), 106-113. Cited on page: 155.

[2005HOC/MOO] Hochella, M. F., Moore, J. N., Putnis, C. V., Putnis, A., Kasana, T., Eberl, D. D., Direct observation of heavy metal-mineral association from the Clark Fork River Superfund Complex: Implications for metal transport and bioavailability, *Geochim. Cosmochim. Acta*, **69**, (2005), 1651-1663. Cited on page: 145.

[2005HUM/AND] Hummel, W., Anderegg, G., Puigdomènech, I., Rao, L., Tochiyama, O., *Chemical thermodynamics of complexes and compounds of U, Np, Pu, Am, Tc, Zr, Ni and Se with selected organic ligands*, Nuclear Energy Agency Data Bank, Organisation for Economic Co-operation, Development, Ed., vol. 9, *Chemical Thermodynamics*, North Holland Elsevier Science Publishers B. V., Amsterdam, The Netherlands, (2005). Cited on pages: 3, 60.

[2005LEE/WAN] Lee, J. S., Wang, H. R., Izuka, Y., Yu, S. C., Crystal structure and Raman spectral studies of $BaSO_4$-$PbSO_4$ solid solution, *Z. Kristallogr.*, **220**, (2005), 1-9. Cited on page: 157.

[2005MAR/STU] Marques Fernandes, M., Stumpf, T., Rabung, T., Bosbach, D., Bauer, A., Fanghänel, T., Structural incorporation of trivalent actinides in calcite: A time resolved laser fluorescence spectroscopy (TRLFS) study. Part I., *Geochim. Cosmochim. Acta*, (2005), in preparation. Cited on pages: 29, 31, 185, 190, 191.

[2005MAZ/USH] Mazeina, L., Ushakov, S. V., Navrotsky, A., Boatner, L. A., Formation enthalpy of $ThSiO_4$ and enthalpy of the thorite -> huttonite phase transition, *Geochim. Cosmochim. Acta*, **69**, (2005), 4675-4683. Cited on pages: 153, 155.

[2005MOR/NAV] Moriya, Y., Navrotsky, A., High-temperature calorimetry of zirconia: heat capacity and thermodynamics of monoclinic-tetragonal phase transition, *J. Chem. Thermodyn.*, (2005), -, in press. Cited on pages: 24, 152.

[2005NAV/BEN] Navrotsky, A., Benoist, L., Lefebvre, H., Direct calorimetric measurement of enthalpies of phase transitions at 2000-2400°C in yttria and zirconia, *J. Am. Ceram. Soc.*, (2005), -, in press. Cited on pages: 24, 152.

[2005OLI/NOL] Olin, Å., Noläng, B., Öhman, L.-O., Osadchii, E. G., Rosén, E., *Chemical thermodynamics of Selenium*, Nuclear Energy Agency Data Bank, Organisation for Economic Co-operation, Development, Ed., vol. 7, *Chemical Thermodynamics*, North Holland Elsevier Science Publishers B. V., Amsterdam, The Netherlands, (2005). Cited on pages: 3, 60.

[2005PIT/USH] Pitcher, M. W., Ushakov, S. V., Navrotsky, A., Woodfield, B. F., Li, G., Boerio-Goates, J., Tissue, B. M., Energy crossovers in nanocrystalline zirconia, *J. Am. Ceram. Soc.*, **88**, (2005), 160-167. Cited on page: 155.

[2005THO] Thomsen, K., Modeling electrolyte solutions with the Extended UNIQUAC model, *Pure Appl. Chem.*, **77**, (2005), 531-542. Cited on pages: 69, 70, 107.

[2005VIL/THO] Villafafila Garcia, A., Thomsen, K., Stenby, E. H., Prediction of mineral scale formation in geothermal and oilfield operations using the Extended UNIQUAC Model. Part I: Sulphate scaling minerals, *Geothermics*, **34**, (2005), 61-97. Cited on page: 70.

[2005ZAV/ROB] Zavarin, M., Roberts, S. K., Hakem, N., Kersting, A. B., Eu(III), Sm(III), Np(V), Pu(V), and Pu(VI) sorption to calcite, *Radiochim. Acta*, **93**, (2005), 93-102. Cited on pages: 29, 185.

[2006AYO] Ayora, C., Personal communication, (2006). Cited on page: 19.

[2006KOH/HEI] Köhler, S., Heinz, D., Urbonas, L., Effect of ettringite on thaumasite formation, *Cem. Concr. Res.*, **36**, (2006), 697-706. Cited on page: 12.

[2006KUL] Kulik, D. A., Dual-thermodynamic estimation of stoichiometry and stability of solid solution end members in aqueous - solid solution systems, *Chem. Geol.*, **225**, (2006), 189-212. Cited on pages: 109, 115.

[2006LIC/CAR] Lichtner, P. C., Carey, J. W., Incorporating solid solutions in reactive transport equations using a kinetic discrete compostion approach, *Geochim. Cosmochim. Acta*, **70**, (2006), 1356-1378. Cited on page: 18.

[2006LOT/WIN] Lothenbach, B., Winnefeld, F., Thermodynamic modelling of the hydratation of Portland cement, *Cem. Concr. Res.*, **36**, (2006), 209-226. Cited on pages: 28, 174, 177.

[2006TIT/WIE] Tits, J., Wieland, E., Müller, C. J., Landesman, C., Bradbury, M. H., Strontium binding by calcium silicate hydrates, *J. Colloid Interface Sci.*, **300**, (2006), 78-87. Cited on page: 183.

[2006VIL/THO] Villafafila Garcia, A., Thomsen, K., Stenby, E. H., Prediction of mineral scale formation in geothermal and oilfield opera-tions using the Extended UNIQUAC Model. Part II: Carbonate scaling minerals, *Geothermics*, **35**, (2006), 239-284. Cited on page: 70.

List of cited authors

This chapter contains an alphabetical list of the authors of the references cited in this book. The reference codes given with each name correspond to the publications of which the person is the author or a co-author. Note that inconsistencies may occur due to a variation in spelling between different publications. No attempt was made to correct for such inconsistencies in this volume.

Author	Reference
Abarra, E. N.	[1994DEL/ABA]
Abrams, D. S.	[1975ABR/PRA]
Adler, M.	[1999ADL/MAD]
Aguilera, J.	[2003BLA/AGU]
Akagi, T.	[2002TSU/KAG]
Akber, R.A.	[1999MAR/AKB]
Akie, H.	[2001YAM/AKI]
Allada, R. K.	[2005ALL/NAV]
Allen, K.	[1994DEL/ABA]
Alvarez, J.	[2003FER/ALV]
Anderegg, G.	[1999RAR/RAN], [2005HUM/AND]
Anders, C.	[1986FED/WES]
Anderson, G. M.	[1993AND/CRE]
Anderson, W. B.	[1986FED/WES]
Appelo, C. A. J.	[1999PAR/APP]
Arocena, J. M.	[1996RUT/DUD]
Avchenko, O. V.	[2001KAR/CHU]
Ayora, C.	[1998BRU/DUR], [2006AYO]
Baeyens, B.	[1998BRA/BAE]
Balarew, C.	[1994CHR/PET]
Bale, C. W.	[1977PEL/BAL], [1990BAL/PEL], [2002BAL/CHA]
Ballaran, T. B.	[2000BEC/CAR], [2001BAL/CAR], [2001BAL/CAR2], [2004ROD/CAR]
Balmer, M. L.	[2003XU/SU]
Balog, A.	[1998RIM/BAL]

(Continued on next page)

Author	Reference
Barnett, S. J.	[2004MAC/BAR]
Bauer, A.	[2005MAR/STU]
Baur, I.	[2003BAU/JOH]
Bausch, W. M.	[1977PAR/MOL]
Becerro, A. I.	[2000BEC/CAR]
Beck, K. M.	[2002ELZ/REE], [2003WHI/PEA]
Becker, U.	[2000BEC/FER], [2000PRI/FER], [2002BEC/POL]
Ben Mahfoud, R.	[2002BAL/CHA]
Benesi, A.	[1999GRU/KWA]
Benoist, L.	[2005NAV/BEN]
Bercis, L.	[1997PIR/FED]
Berman, H.	[1951PAL/BER]
Berner, U.	[1988BER2], [1992BER], [2002BER/CUR], [2002HUM/BER], [2004KUL/BER2]
Besse, J. P.	[2001ROY/FOR]
Bethke, C. M.	[1996BET]
Bidoglio, G.	[1995SIL/BID]
Bin-Shafique, S.	[1997WAL/BIN]
Bish, D. L.	[1989BIS/POT], [2003BIS/VAN]
Black, S.	[2004CEC/BLA]
Blanco-Varela, M. T.	[2003BLA/AGU]
Blankenburg, J.	[1967BOS/FRA]
Blount, C. W.	[1977BLO]
Boatner, L. A.	[2004HEL/USH], [2005MAZ/USH]
Boerio-Goates, J.	[1992BOE/CAL], [2000OTT/BOE], [2000OTT/BOE2], [2003LAS/HUN], [2005ALL/NAV], [2005PIT/USH]
Boerjesson, K. S.	[1993BOE/EMR]
Boffa Ballaran, T.	[2001CAR/BOF]
Bolt, G. H.	[1964LAH/BOL]
Borisov, M. V.	[1992BOR/SHV]
Bosbach, D.	[2004BOS/RAB], [2005MAR/STU]
Bose, K.	[1994NAV/RAP]
Boström, K.	[1967BOS/FRA]
Bothe, J. V. J.	[1998BOT/BRO]
Box, G. E. P.	[1978BOX/HUN]
Brümmer, B. W.	[1988BRU/GER]
Bradbury, M. H.	[1998BRA/BAE], [2006TIT/WIE]
Brady, P.	[1999NAV/DOO]
Bram, A.	[1999NED/BUR]
Brandt, F.	[2004BOS/RAB]

(Continued on next page)

Author	Reference
Braunsrein, G.	[2003WHI/PEA]
Brower, E.	[1971BRO/REN]
Brown Jr., G. E.	[2000TRA/BRO]
Brown, C. E.	[2004HEL/USH]
Brown, G. E.	[1988BRO/CAL]
Brown, P. L.	[2005BRO/CUR]
Brown, P. W.	[1990BRO], [1998BOT/BRO]
Brown, T. H.	[1974BRO/SKI], [1987CAP/BRO]
Bruno, J.	[1992CAR/BRU], [1994CAS/BRU], [1997BRU/CER2], [1998BRU/CER], [1998BRU/DUR], [1999BRU/CER], [2003BRU/CER]
Bryndzia, T.	[1988BRY/KLE]
Budahn, J. R.	[2001ZIE/OTT]
Bugajski, J.	[2005GAM/BUG]
Burghammer, M.	[1999NED/BUR]
Burkhard, G.	[1944FLA/BUR]
Burnley, P.	[1994NAV/RAP]
Burns, P. C.	[2000HAW/KRI], [2003HUG/HEL]
Burton, B. P.	[1987BUR], [1987CAP/BUR]
Busenberg, E.	[1987PLU/BUS], [1990GLY/REA2], [1990NOR/PLU], [1992GLY/REA]
Bychinskii, V. A.	[2001KAR/CHU]
Calas, G.	[1988BRO/CAL]
Callanan, J. E.	[1992BOE/CAL]
Capobianco, C.	[1987CAP/BUR], [1987NAV/CAP]
Cappelaere, C.	[2001POI/TOU]
Carbajo, J. J.	[2001CAR/YOD]
Carey, J. W.	[2003BIS/VAN], [2006LIC/CAR]
Carmichael, I. S. E.	[1982STE/WEI]
Carpenter, M. A.	[1985CAR/MCC], [2000BEC/CAR], [2001BAL/CAR], [2001BAL/CAR2], [2001CAR/BOF], [2004ROD/CAR]
Carroll, S. A.	[1992CAR/BRU]
Carter, M. L.	[2002HEL/NAV2]
Casas, I.	[1994CAS/BRU], [1996GRA/LOI], [1998BRU/DUR]
Casey, W. H.	[1994ROC/CAS], [1998MCB/ROC]
Catalano, J. G.	[2002HEL/NAV2]
Ceccarello, S.	[2004CEC/BLA]
Cera, E.	[1994CAS/BRU], [1997BRU/CER2], [1998BRU/CER], [1999BRU/CER], [2003BRU/CER]
Chai, L.	[1994NAV/RAP], [1996CHA/NAV]

(Continued on next page)

Author	Reference
Chang, L. L. Y.	[1996CHA/HOW]
Chang, T. N.	[1965GRE/CHA]
Charlet, L.	[1989WER/CHA]
Charlton, S. R.	[2004PAR/KIP]
Chartrand, P.	[2002BAL/CHA]
Chernov, A. A.	[1984CHE]
Chipera, S. J.	[2003BIS/VAN]
Christensen, H.	[2000GRA/LOI]
Christov, C.	[1994CHR/PET], [1996CHR], [2004CHR/MOL]
Chudnenko, K. V.	[1997KAR/CHU], [2001KAR/CHU], [2002CHU/KAR], [2003KUL/DMY]
Church, T. M.	[1970CHU]
Cicariello, J. C.	[2001POI/TOU]
Circone, S.	[1994NAV/RAP]
Cohen-Adad, R.	[2003LOR/COH]
Cooley, J. C.	[2003LAS/HUN]
Coradin, H.	[2005GUI/NAV]
Corbel, C.	[2001POI/TOU]
Crerar, D. A.	[1993AND/CRE]
Crusius, J.	[2003MAR/CRU]
Curti, E.	[1999CUR], [2002BER/CUR], [2002HUM/BER], [2004KUL/BER2], [2005BRO/CUR], [2005CUR/KUL]
Díaz-Arocas, P.	[2000GRA/LOI]
Dandurand, J. L.	[1989GAL/DAN]
Darken, L. S.	[1967DAR], [1967DAR2]
Darling, T. W.	[2003LAS/HUN]
Davidson, P. M.	[1987CAP/BUR]
De Capitani, C.	[1987CAP/BRO]
De Pablo, J.	[1996GRA/LOI], [1998BRU/CER], [1998BRU/DUR], [2000GRA/LOI]
De Roy, A.	[2001ROY/FOR]
Degterov, S. A.	[2002BAL/CHA]
Dehaudt, P.	[2001POI/TOU]
Delgado, J.	[1998BRU/DUR]
Denis, J.	[1983DEN/MIC]
Denlinger, D. W.	[1994DEL/ABA]
Desgranges, L.	[2001POI/TOU]
Dmytriyeva, S. V.	[2003KUL/DMY]
Doerner, H.	[1925DOE/HOS]
Domeneghetti, M. C.	[2001BAL/CAR]

(Continued on next page)

Author	Reference
Dooley, D.	[1999NAV/DOO]
Dran, J. C.	[1992CAR/BRU]
Dressler, P.	[1996GRA/LOI]
Duclos, A. M.	[1991TAI/STR]
Dudas, M. J.	[1996RUT/DUD]
Dukski, P.	[1977PAR/MOL]
Duro, L.	[1997BRU/CER2], [1998BRU/CER], [1998BRU/DUR], [2003BRU/CER]
Dzombak, D. A.	[1990DZO/MOR]
Ebbinghaus, B.	[2002HEL/NAV2]
Eberl, D. D.	[2005HOC/MOO]
Eklund, U. B.	[1999BRU/CER]
Elzinga, E. J.	[2002ELZ/REE], [2004ROU/ELZ]
Emren, A. T.	[1993BOE/EMR]
Engesgaard, P.	[2004PAR/KIP]
Eriksen, T.	[1997BRU/CER2], [1998BRU/CER], [1999BRU/CER], [2003BRU/CER]
Eriksson, G.	[1973ERI/ROS], [1989ERI/THO], [1990ERI/HAC], [1995KON/ERI], [2002BAL/CHA]
Ewing, R. C.	[1992JAN/EWI], [1994CAS/BRU], [1995JAN/EWI], [2004HEL/USH], [2005EWI]
Fanghänel, T.	[2002FAN], [2002STU/FAN2], [2003GUI/FAN], [2003TIT/STU], [2004BOS/RAB], [2004STU/TIT], [2005MAR/STU]
Farmer, J. M.	[2004HEL/USH]
Faure, M. H.	[2001POI/TOU]
Fedorak, P. M.	[1986FED/WES]
Fedoroff, M.	[1997PIR/FED]
Felmy, A. R.	[1993FEL/RAI2]
Fernández-Díaz, L.	[1992PUT/FER], [1993PRI/PUT], [1997PRI/FER]
Fernández-González, A.	[1997PRI/FER], [2000BEC/FER], [2000PRI/FER]
Fernández-Prini, R.	[2003FER/ALV]
Fialips, C. I.	[2001FIA/NAV]
Fiedler, S.	[1999NED/BUR]
Filippov, V.	[1990FIL/RUM]
Finch, R.	[1999FIN/MUR]
Finch, R. J.	[1994CAS/BRU]
Fisher, N. S.	[2004ROU/ELZ]
Fisher, R. A.	[2003LAS/HUN]
Fisher, R. S.	[1998FIS]

(Continued on next page)

Author	Reference
Flatt, R.	[1944FLA/BUR]
Flowers, G. C.	[1981HEL/KIR]
Forano, C.	[2001ROY/FOR]
Forsyth, R.	[1995FOR], [1997FOR]
Fouke, B. W.	[1992FOU/REE]
Frazer, J.	[1967BOS/FRA]
Frondell, C	[1951PAL/BER]
Fuger, J.	[1992GRE/FUG], [2001LEM/FUG], [2003GUI/FAN]
Fujii, K.	[1981FUJ/KON], [1983FUJ/KON]
Gago, J.	[1996GRA/LOI]
Gajda, T.	[2005GAM/BUG]
Galinier, C.	[1989GAL/DAN]
Gamsjäger, H.	[1985GAM], [1990KON/GAM], [1990KON/GAM2], [1992KON/GAM], [1992KON/GAM2], [2000GAM/KON], [2000WOL/KON], [2003GAM/KON], [2005GAM/BUG]
Ganguly, J.	[2001GAN]
Garrels, R.	[1978GAR/WOL]
Gartner, E. M.	[1987GAR/JEN]
Gaskell, D. R.	[1995GAS]
Geckeis, H.	[1996GRA/LOI]
Geiger, C. A.	[2001GEI], [2004ROD/CAR]
Gersonde, R.	[2004BEC/REY]
Gerth, J.	[1988BRU/GER]
Ghiorso, M. S.	[1994GHI]
Giménez, J.	[1996GRA/LOI]
Gimeno, M. J.	[1998BRU/DUR]
Glasser, F. P.	[1989MAC/LUK], [1997GLA], [1999GLA/HON], [2002GLA/HON], [2003JOH/GLA]
Glatz, J.-P.	[2000GRA/LOI]
Glynn, P. D.	[1990GLY/REA], [1990GLY/REA2], [1990GLY], [1991GLY], [1992GLY/PAR], [1992GLY/REA], [1992GLY/REA2], [2000GLY], [2003GLY]
Goldschmidt, B.	[1938GOL]
Goldsmith, J. R.	[1961GOL/HEA], [1972GOL]
Golla, U.	[1999HOC/MOO]
Gomez, P.	[1998BRU/DUR]
Gotte, T.	[2001HAB/NIK]
Grambow, B.	[1996GRA/LOI], [2000GRA/LOI], [2001GRA/MUL], [2005BRO/CUR]
Grasl, T.	[1999NED/BUR]

(Continued on next page)

Author	Reference
Gray, W. J.	[1987GRA]
Green, E. J.	[1970GRE]
Greenberg, J. P.	[1987HAR/GRE], [1989GRE/MOL]
Greenberg, S. A.	[1965GRE/CHA]
Grenthe, I.	[1992GRE/FUG], [1997GRE/PLY2], [1997PUI/RAR], [1999PUI/RAR], [2003GUI/FAN]
Grivé, M.	[1999BRU/CER], [2003BRU/CER]
Grouiller, J. P.	[2001POI/TOU]
Grutzeck, M.	[1999GRU/KWA], [1999GRU]
Gu, Q.	[1981XU/WAN]
Guggenheim, E. A.	[1952GUG], [1967GUG], [1986GUG]
Guillaumont, R.	[2003GUI/FAN]
Guillemet-Fritsch, S.	[2005GUI/NAV]
Guiraud, M.	[1996GUI/POW]
Gutierrez, N.	[1997WAL/BIN]
Habermann, D.	[2001HAB/NIK]
Hack, K.	[1990ERI/HAC], [2002BAL/CHA]
Hakem, N.	[2005ZAV/ROB]
Hanor, J. S.	[1968HAN], [2000HAN]
Harned, H. S.	[1958HAR/OWE]
Harrison, R. M.	[2000BEC/FER]
Harvey, A. H.	[2003FER/ALV]
Harvie, C. E.	[1984HAR/MOL], [1987HAR/GRE]
Hawthorne, F. C.	[1983HAW], [2000HAW/KRI], [2004SCH/HAR]
Heard, H. C.	[1961GOL/HEA]
Heinz, D.	[2006KOH/HEI]
Heiser, U.	[2000KUL/KER]
Helean, K. B.	[2002HEL/NAV], [2002HEL/NAV2], [2003HUG/HEL], [2004HEL/USH]
Helffrich, G.	[1989HEL/WOO]
Helgeson, H. C.	[1981HEL/KIR], [1992JOH/OEL]
Hellman, F.	[1994DEL/ABA]
Hemingway, B. S.	[1972ROB/HEM2]
Henry, D. J.	[1981HON/HEN], [1982HEN/NAV]
Herbelin, A. L.	[1996HER/WES]
Hering, J. G.	[1993MOR/HER]
Hess, W. P.	[2002ELZ/REE], [2003WHI/PEA]
Hileman, O. E.	[1985SNO/HIL], [1991KOR/PRE]
Hillert, M.	[1998HIL]
Hills, C. D.	[1996LAN/HIL]

(Continued on next page)

Author	Reference
Hochella, M. F.	[1988HOC], [1992STI/HOC], [1999HOC/MOO], [2005HOC/MOO]
Hocking, W. H.	[1991TAI/STR]
Hodson, M. E.	[2004CEC/BLA]
Hofmeister, A. M.	[1988MCM/HOF]
Holland, T.	[1992HOL/POW], [1992WIL/POW], [1993VAN/HOL]
Hon, R.	[1980WEI/HON], [1981HON/HEN]
Hong, S.-Y.	[1999GLA/HON], [2002GLA/HON]
Hoskins, W. M.	[1925DOE/HOS]
Hovis, G. L.	[1977HOV/WAL]
Howie, R. A.	[1996CHA/HOW]
Huang, Y.	[1981XU/WAN]
Huck, P. M.	[1986FED/WES]
Hughes Kubatko, K.-A.	[2003HUG/HEL]
Hults, W. L.	[2003LAS/HUN]
Hummel, W.	[2002HUM/BER], [2005HUM/AND]
Hundley, M. F.	[2003LAS/HUN]
Hunter, W. G.	[1978BOX/HUN]
Iliuta, M. C.	[2002ILI/THO]
Ivanov, V. K.	[2001CAR/YOD]
Izuka, Y.	[2005LEE/WAN]
Jaime, M.	[2003LAS/HUN]
Jamtveit, B.	[2002LHE/JAM]
Janeczek, J.	[1992JAN/EWI], [1995JAN/EWI]
Jay McNee, J.	[2003MAR/CRU]
Jeanjean, J.	[1997PIR/FED]
Jegou, C.	[2001POI/TOU]
Jennings, H. M.	[1986JEN], [1987GAR/JEN], [2000JEN]
Johnson, C. A.	[1999JOH/KER], [2003BAU/JOH], [2003JOH/GLA]
Johnson, D. M.	[1991KOR/PRE]
Johnson, J. W.	[1992JOH/OEL]
Johnson, L. H.	[1997JOH/TAI]
Jones, B. F.	[1974TRU/JON], [1990NOR/PLU]
Köhler, S.	[2006KOH/HEI]
Königsberger, E.	[1990KON/GAM], [1990KON/GAM2], [1991KON], [1992KON/GAM], [1992KON/GAM2], [1995KON/ERI], [2000GAM/KON], [2000WOL/KON], [2002KON], [2003GAM/KON]
Königsberger, L. C.	[2000WOL/KON]
Kagi, H.	[2002TSU/KAG]

(Continued on next page)

Author	Reference
Karpov, I. K.	[1981KAR], [1997KAR/CHU], [1997SIN/KUL], [2001KAR/CHU], [2002CHU/KAR], [2003KUL/DMY]
Karthein, R.	[1989WER/CHA]
Kasana, T.	[2005HOC/MOO]
Kastner, M.	[1996PAY/MOO]
Kawabe, I.	[2004TAN/OHT]
Kersten, M.	[1999JOH/KER], [2000KUL/KER], [2001KUL/KER], [2002KUL/KER]
Kersting, A. B.	[2005ZAV/ROB]
Khodorivski, M. S.	[1997SIN/KUL]
Kian, J.	[2002HEL/NAV2]
Kielland, J.	[1937KIE]
Kipp, K. L.	[1997KIP], [2004PAR/KIP]
Kirfel, A.	[1996KIR], [1997KRO/LUE]
Kirkham, D. H.	[1981HEL/KIR]
Kirkpatrick, R. J.	[1988KIR], [1998MCH/NAV]
Kleppa, O. J.	[1988BRY/KLE]
Kleykamp, H.	[1985KLE/PAS], [1988KLE3], [1989KLE], [2004KLE]
Kondo, W.	[1981FUJ/KON], [1983FUJ/KON]
Konings, R. J. M.	[1992GRE/FUG]
Kornicker, W. A.	[1991KOR/PRE]
Kratochvil, B.	[1986FED/WES]
Krikorian, O.	[2002HEL/NAV2]
Krivovichev, S. V.	[2000HAW/KRI]
Kroll, H.	[1997KRO/LUE]
Kuhn, G.	[2004BEC/REY]
Kulik, D. A.	[1997KAR/CHU], [1997SIN/KUL], [2000KUL/KER], [2001KAR/CHU], [2001KUL/KER], [2002CHU/KAR], [2002KUL/KER], [2003KUL/DMY], [2004KUL/BER2], [2005CUR/KUL], [2006KUL]
Kuramoto, K.	[2001YAM/AKI]
Kwan, S.	[1999GRU/KWA]
L'Heureux, I.	[2002LHE/JAM]
Lachowski, E. E.	[1989MAC/LUK]
Lahav, N.	[1964LAH/BOL]
Lakshtanov, L. Z.	[2004LAK/STI]
Landa, E. R.	[1986LAN/MIL]
Landesman, C.	[2006TIT/WIE]
Lange, L. C.	[1996LAN/HIL]

(Continued on next page)

Author	Reference
Langmuir, D.	[1985LAN/MEL], [1985LAN/RIE], [1990NOR/PLU], [1997LAN]
Lashley, J. C.	[2003LAS/HUN]
Leckie, J. O.	[1992STI/HOC]
Lee, J. S.	[2002WAN/LEE], [2005LEE/WAN]
Lefebvre, H.	[2005NAV/BEN]
Lemire, R. J.	[1992GRE/FUG], [2001LEM/FUG], [2005GAM/BUG]
Lemmens, K.	[2000GRA/LOI]
Li, G.	[2005PIT/USH]
Lian, J.	[2004HEL/USH]
Liang, J.-J.	[1999LIA/TOP]
Lichtner, P. C.	[2006LIC/CAR]
Limon, R.	[2001POI/TOU]
Lin, P. L.	[1983PEL/LIN]
Linklater, C.	[1998BRU/DUR]
Lippmann, F.	[1977LIP], [1980LIP], [1982LIP]
Loida, A.	[1996GRA/LOI], [2000GRA/LOI]
Lorens, R. B.	[1981LOR]
Lorimer, J. W.	[2003LOR/COH], [2003LOR]
Lothenbach, B.	[2006LOT/WIN]
Lueder, T.	[1997KRO/LUE]
Luke, K.	[1989MAC/LUK]
Mäder, U.	[1999ADL/MAD]
Möller, P.	[1977PAR/MOL]
Müller, C. J.	[2006TIT/WIE]
Müller, R.	[2001GRA/MUL]
Macphee, D. E.	[1989MAC/LUK], [2004MAC/BAR]
Maillard, S.	[2001POI/TOU]
Manceau, A.	[2002MAN/MAR]
Mandell, G. K.	[1998MCB/ROC]
Marcus, M. A.	[2002MAN/MAR]
Marques Fernandes, M.	[2005MAR/STU]
Martínez-Esparza, A.	[2000GRA/LOI]
Martínez-Ramírez, S.	[2003BLA/AGU]
Martin, A. J.	[2003MAR/CRU]
Martin, P.	[1999MAR/AKB]
Marx, G.	[2000GRA/LOI]
Masada, A.	[1988TER/MAS]
Mason, R. A.	[2002ELZ/REE]
Masson, M.	[2001POI/TOU]

(Continued on next page)

Author	Reference
May, H. M.	[1990NOR/PLU]
Mazeina, L.	[2005MAZ/USH]
McBeath, M. K.	[1994ROC/CAS], [1998MCB/ROC]
McBride, M. B.	[1982MCB]
McConnell, J. D. C.	[1985CAR/MCC]
McCoy, W. H.	[1956MCC/WAL]
McHale, J. M.	[1998MCH/NAV]
McMillan, P. F.	[1988MCM/HOF]
McNaught, A. D.	[1997MCN/WIL]
Meijer, J.	[2001HAB/NIK]
Melancon, J.	[2002BAL/CHA]
Melchior, D.	[1985LAN/MEL]
Michard, G.	[1983DEN/MIC]
Migliori, A.	[2003LAS/HUN]
Miller, C. L.	[1986LAN/MIL]
Millero, F. J.	[1990MIL], [1998MIL/PIE]
Mitomo, M.	[1999LIA/TOP]
Moore D. A.	[1993FEL/RAI2]
Moore, J. N.	[1999HOC/MOO], [2005HOC/MOO]
Moore, W. S.	[1996PAY/MOO]
Morales, L.	[2003LAS/HUN]
Morel, F. M. M.	[1986WES/ZAC], [1990DZO/MOR], [1993MOR/HER]
Moriya, Y.	[2005MOR/NAV]
Morse, J. W.	[1982SHA/MOR]
Motkosky, N.	[1986FED/WES]
Muñoz, J. L.	[1994NOR/MUN]
Mucci, A.	[1995ZHO/MUC]
Muller, A. B.	[1992GRE/FUG]
Murakami, T.	[1999FIN/MUR]
Møller, N.	[1984HAR/MOL], [1989GRE/MOL], [2004CHR/MOL]
Nakamura T.	[2001YAM/AKI]
Nakano, Y.	[2001YAM/AKI]

(Continued next page)

Author	Reference
Navrotsky, A.	[1977NAV], [1980WEI/HON], [1981HON/HEN], [1982HEN/NAV], [1984ONE/NAV], [1985CAR/MCC], [1987CAP/BUR], [1987NAV/CAP], [1987NAV], [1994NAV/RAP], [1994NAV], [1996CHA/NAV], [1997NAV], [1998MCH/NAV], [1998NAV], [1999LIA/TOP], [1999NAV/DOO], [2001FIA/NAV], [2001YAN/NAV], [2002HEL/NAV], [2002HEL/NAV2], [2003HUG/HEL], [2003XU/SU], [2004HEL/USH], [2005ALL/NAV], [2005GUI/NAV], [2005MAZ/USH], [2005MOR/NAV], [2005NAV/BEN], [2005PIT/USH]
Neck, V.	[2003GUI/FAN]
Neder, R. B	[1999NED/BUR]
Neumann, T.	[2000KUL/KER]
Nguyen-Trung, C.	[1992GRE/FUG]
Nicholls, J.	[1978WOO/NIC]
Niklas, J.R.	[2001HAB/NIK]
Nikolaisen, H.	[1993NIK/RAS]
Nirdosh, I.	[1987NIR]
Nitani, N.	[2001YAM/AKI]
Nitsche, H.	[2001LEM/FUG]
Noläng, B.	[2005OLI/NOL]
Nordstrom, D. K.	[1990NOR/PLU], [1994NOR/MUN]
O'Neill, H. St. C.	[1984ONE/NAV]
Oates, W. A.	[1969OAT]
Oberti, R.	[2001OBE]
Oelkers, E. H.	[1992JOH/OEL]
Ohta, A.	[2004TAN/OHT]
Olin, Å.	[2005OLI/NOL]
Ollila, K.	[1992OLL], [2000GRA/LOI]
Osadchii, E. G.	[2005OLI/NOL]
Ott, J. B.	[2000OTT/BOE], [2000OTT/BOE2]
Otton, J. K.	[2001ZIE/OTT]
Ottonello, G.	[1997OTT]
Owen, B. B.	[1958HAR/OWE]
Pöllmann, H.	[1989POL]
Pagel, M.	[1985PAG/PIN]
Pagliuso, P. G.	[2003LAS/HUN]
Paige, C. R.	[1991KOR/PRE]
Palache, C.	[1951PAL/BER]
Palmer, C. D.	[1999PER/PAL], [2000PER/PAL]

(Continue on next page)

Author	Reference
Palmer, D. A.	[2003GUI/FAN]
Palomo, A.	[2003BLA/AGU]
Pankow, J. F.	[1996TES/PAN]
Paquette, J.	[1990PAQ/REE], [1995PAQ/REE]
Parekh, P. P.	[1977PAR/MOL]
Paridaens, J.	[2001PAR/VAN]
Parkhurst, D. L.	[1990NOR/PLU], [1990PAR], [1992GLY/PAR], [1999PAR/APP], [2004PAR/KIP]
Parks, G. A.	[1992STI/HOC], [2000TRA/BRO]
Paschoal, J. O.	[1985KLE/PAS]
Paterne, M.	[2004BEC/REY]
Paul, J.-L.	[2000GRA/LOI]
Pavageau, J.	[2001POI/TOU]
Paytan, A.	[1996PAY/MOO]
Peña, J.	[1998BRU/DUR]
Peale, R. E.	[2002ELZ/REE], [2003WHI/PEA]
Pearson, F. J.	[2002HUM/BER]
Pejsa, R.	[1985KLE/PAS]
Pelletier, M.	[2001POI/TOU]
Pelton, A. D.	[1977PEL/BAL], [1983PEL/LIN], [1990BAL/PEL], [2001PEL], [2002BAL/CHA]
Perales-Perez, O.	[2002PER/UME]
Perez del Villar, L.	[1998BRU/DUR]
Perkins, R. B.	[1999PER/PAL], [2000PER/PAL]
Petersen, S.	[2002BAL/CHA]
Petiau, J.	[1988BRO/CAL]
Petit, J. C.	[1992CAR/BRU]
Petit, S.	[2001FIA/NAV]
Petrenko, S.	[1994CHR/PET]
Pettit, L. D.	[2003PET/PUI]
Phillips, N. E.	[2003LAS/HUN]
Pialoux, A.	[1998PIA/TOU]
Pierrot, D.	[1998MIL/PIE]
Pinte, G.	[1985PAG/PIN]
Piriou, B.	[1997PIR/FED]
Piron, J. P.	[2001POI/TOU]
Pitcher, M. W.	[2005PIT/USH]
Pitzer, K. S.	[1991PIT]
Plummer, L. N.	[1977THO/PLU], [1987PLU/BUS], [1990GLY/REA2], [1990NOR/PLU], [1992GLY/REA]

(Continued on next page)

Author	Reference
Plyasunov, A. V.	[1997GRE/PLY2], [1997PUI/RAR], [1999PUI/RAR]
Poinssot, C.	[2001POI/TOU]
Pollok, K.	[2002BEC/POL]
Pon, J.	[1998BRU/CER]
Poole, A. B.	[1996LAN/HIL]
Popov, S. G.	[2001CAR/YOD]
Porth, R. J.	[1991TAI/STR]
Post, J. E.	[1989BIS/POT]
Potter, P. E.	[2001LEM/FUG]
Powell, R.	[1987POW], [1992HOL/POW], [1992WIL/POW], [1996GUI/POW]
Prausnitz, J. M.	[1975ABR/PRA]
Preis, W.	[2000GAM/KON], [2005GAM/BUG]
Presta, P. A.	[1991KOR/PRE]
Prieto, M.	[1992PUT/FER], [1993PRI/PUT], [1997PRI/FER], [2000BEC/FER], [2000PRI/FER]
Puertas, F.	[2003BLA/AGU]
Puigdomènech, I.	[1995SIL/BID], [1997PUI/RAR], [1999PUI/RAR], [2003PET/PUI], [2005HUM/AND]
Putnis, A.	[1992PUT/FER], [1993PRI/PUT], [1997PRI/FER], [1999HOC/MOO], [2000BEC/FER], [2000PRI/FER], [2004SCH/HAR], [2004SCH/PUT], [2005HOC/MOO]
Putnis, C. V.	[2004SCH/HAR], [2005HOC/MOO]
Rabung, T.	[2003TIT/STU], [2004BOS/RAB], [2005MAR/STU]
Rai, D.	[1983RYA/RAI], [1993FEL/RAI2]
Rand, M. H.	[1995SIL/BID], [1999RAR/RAN], [2001LEM/FUG], [2003GUI/FAN]
Rao, L.	[2005HUM/AND]
Rapp, R. P.	[1994NAV/RAP]
Rard, J. A.	[1997PUI/RAR], [1999PUI/RAR], [1999RAR/RAN]
Rasmussen, P.	[1993NIK/RAS], [2002ILI/THO]
Read, D.	[2004CEC/BLA]
Reardon, E. J.	[1990GLY/REA], [1990GLY/REA2], [1992GLY/REA], [1992GLY/REA2], [1992REA]
Reed, M. H.	[1982REE2]
Reeder, R. J.	[1984REE], [1990PAQ/REE], [1992FOU/REE], [1995PAQ/REE], [1999NAV/DOO], [2002ELZ/REE], [2003WHI/PEA], [2004ROU/ELZ]
Renault, J.	[1971BRO/REN]
Reyes, J. L.	[2004BEC/REY]

(Continued on next page

Author	Reference
Richardson, I. G.	[2004RIC]
Riese, A. C.	[1985LAN/RIE]
Rimstidt, J. D.	[1998RIM/BAL]
Riontino, C.	[2003BLA/AGU]
Roberts, S. K.	[2005ZAV/ROB]
Robie, R. A.	[1972ROB/HEM2]
Robinson, R. A.	[1970ROB/STO]
Robouch, P.	[1995SIL/BID]
Rock, P. A.	[1994ROC/CAS], [1998MCB/ROC]
Rodehurst, U.	[2004ROD/CAR]
Rooney, P. W.	[1994DEL/ABA]
Rosén, E.	[1973ERI/ROS], [2005OLI/NOL]
Ross, N. L.	[2001BAL/CAR2]
Rotach-Toulhoat, N.	[1985PAG/PIN]
Rouff, A. A.	[2004ROU/ELZ]
Rumyantsev, A.	[1990FIL/RUM]
Rutherford, P. M.	[1996RUT/DUD]
Ryan, J. L.	[1983RYA/RAI]
Rydberg, J.	[2001LEM/FUG]
Rysin, A.V.	[2003KUL/DMY]
SKB97	[1999SKB]
Sabbioni, C.	[2003BLA/AGU]
Sarrao, J. L.	[2003LAS/HUN]
Schindler, M.	[2004SCH/HAR], [2004SCH/PUT]
Schlenz, H.	[1997KRO/LUE]
Schmidt, H. G.	[2000WOL/KON]
Schott, J.	[1989GAL/DAN]
Schulte, A. F.	[2003WHI/PEA]
Schulz, H.	[1999NED/BUR]
Sellin, P.	[1997BRU/CER2]
Shanbhag, P. M.	[1982SHA/MOR]
Shannon, R. D.	[1976SHA2]
Shaw, H. F.	[1987WIL/SHA]
Shvarov, Yu V.	[1992BOR/SHV]
Silva, R. J.	[1995SIL/BID]
Sinitsyn, V. A.	[1997SIN/KUL]
Skinner, B. J.	[1974BRO/SKI]
Smelik, E.	[1994NAV/RAP]
Smith, J. L.	[2003LAS/HUN]
Smith, R. W.	[1997WAL/BIN]

(Continued on next page)

Author	Reference
Snodgrass, W. J.	[1985SNO/HIL], [1991KOR/PRE]
Souissi, C.	[1989GAL/DAN]
Spahiu, K.	[1997BRU/CER2], [1997GRE/PLY2], [2001LEM/FUG], [2002SPA]
Sposito, G.	[1986SPO]
Starke, R.	[1964STA]
Stebbins, J. F.	[1982STE/WEI], [1988STE]
Stenby, E. H.	[2005VIL/THO], [2006VIL/THO]
Stephan, A.	[2001HAB/NIK]
Stewart, G. R.	[2003LAS/HUN]
Stipp, S. L.	[1992STI/HOC]
Stipp, S. L. S.	[2004LAK/STI]
Stokes, R. H.	[1970ROB/STO]
Storey, S. H.	[1970VAN/STO]
Stroes-Gascoyne, S.	[1991TAI/STR], [1992STR]
Stumm, W.	[1989WER/CHA]
Stumpf, T.	[2002STU/FAN2], [2003TIT/STU], [2004STU/TIT], [2005MAR/STU]
Su, Y.	[2003XU/SU]
Sullivan, J. C.	[2001LEM/FUG]
Sverjensky, D. A.	[1984SVE]
Sørensen, J. M.	[1993NIK/RAS]
Tailhades, P.	[2005GUI/NAV]
Tait, J. C.	[1991TAI/STR], [1997JOH/TAI]
Takano, B.	[1969TAK/YAN]
Tamura, N.	[2002MAN/MAR]
Tanaka, K.	[2004TAN/OHT]
Tarquin, A.	[1997WAL/BIN]
Taylor, H. F. W.	[1986TAY], [1992TAY], [1993TAY]
Terakado, Y.	[1988TER/MAS]
Tesoriero, A. J.	[1996TES/PAN]
Thümmler, F.	[1985KLE/PAS]
Thoenen, T.	[2002HUM/BER]
Thoma, D. J.	[2003LAS/HUN]
Thompson, J. L.	[1999GRU/KWA]
Thompson, W. T.	[1989ERI/THO]
Thomsen, K.	[1997THO], [2002ILI/THO], [2005THO], [2005VIL/THO], [2006VIL/THO]
Thomson, J. B.	[1967THO], [1969THO]
Thorstenson, D. C.	[1977THO/PLU]

(Continued on next page)

Author	Reference
Tiller, K. G.	[1988BRU/GER]
Tissue, B. M.	[2005PIT/USH]
Tits, J.	[2003TIT/STU], [2004STU/TIT], [2005CUR/KUL], [2006TIT/WIE]
Tochiyama, O.	[2005HUM/AND]
Topor, L.	[1999LIA/TOP]
Torrero, M. E.	[1996GRA/LOI]
Toulhoat, P.	[2001POI/TOU]
Toumbakari, E. E.	[2003BLA/AGU]
Touzelin, B.	[1998PIA/TOU]
Trainor, T. P.	[2000TRA/BRO]
Truesdell, A. H.	[1974TRU/JON]
Tsuno, H.	[2002TSU/KAG]
Ullman, W. J.	[2001LEM/FUG]
Umetsu, Y.	[2002PER/UME]
Updegraff, D. M.	[1986LAN/MIL]
Urbonas, L.	[2006KOH/HEI]
Urusov, V. S.	[1975URU], [2001URU]
Ushakov, S. V.	[2004HEL/USH], [2005MAZ/USH], [2005PIT/USH]
Vad, T.	[1997KRO/LUE]
Valyashko, V.	[1994CHR/PET]
Van Balen, K.	[2003BLA/AGU]
Van Beck, P.	[2004BEC/REY]
Van Zeggren, F.	[1970VAN/STO]
Van der Loeff, M. R.	[2004BEC/REY]
Vance, D.	[1993VAN/HOL]
Vance, E. R.	[2002HEL/NAV2]
Vaniman, D. T.	[2003BIS/VAN]
Vanmarcke, H.	[2001PAR/VAN]
Villafafila Garcia, A.	[2005VIL/THO], [2006VIL/THO]
Vitorge, P.	[2001LEM/FUG]
Waber, N.	[1999ADL/MAD]
Waldbaum, D. R.	[1977HOV/WAL]
Wallace, W. E.	[1956MCC/WAL]
Walling, E. M.	[1994ROC/CAS]
Walther, C.	[2004STU/TIT]
Walton, J. C.	[1997WAL/BIN]
Wang, A.	[1981XU/WAN]
Wang, H. R.	[2002WAN/LEE], [2005LEE/WAN]
Wang, L. M.	[2002HEL/NAV2]

(Continued on next page)

Author	Reference
Wang, M.	[2005GUI/NAV]
Wang, Y.	[2001WAN/XU]
Wanner, H.	[1992GRE/FUG], [1995SIL/BID], [1999RAR/RAN], [2001LEM/FUG], [2003PET/PUI]
Watanuki, K.	[1969TAK/YAN]
Watson, S. K.	[1994DEL/ABA]
Waychunas, G. A.	[1988BRO/CAL], [1988WAY]
Weare, J. H.	[1984HAR/MOL], [1987HAR/GRE]
Webb, J.	[1998RIM/BAL]
Weill, D. F.	[1980WEI/HON], [1981HON/HEN], [1982STE/WEI]
Werme, L.	[1997BRU/CER2]
Wersin, P.	[1989WER/CHA], [2003WER]
Westall, J. C.	[1986WES/ZAC], [1996HER/WES]
Westlake, D. W. S.	[1986FED/WES]
Westrich, H. R.	[1994NAV/RAP]
Wieland, E.	[2003TIT/STU], [2004STU/TIT], [2006TIT/WIE]
Wilkin, D. L.	[1991TAI/STR]
Wilkin, R.	[2001YAN/NAV]
Wilkinson, A.	[1997MCN/WIL]
Will, T.	[1998WIL]
Wilson, C. N.	[1987WIL/SHA], [1990WIL]
Winnefeld, F.	[2006LOT/WIN]
Withers, S. H.	[2002ELZ/REE], [2003WHI/PEA]
Wolf, G.	[2000WOL/KON]
Wollast, R.	[1978GAR/WOL]
Wood, B. J.	[1978WOO/NIC], [1987WOO], [1989HEL/WOO]
Woodfield, B. F.	[2003LAS/HUN], [2005PIT/USH]
Xu, G.	[1981XU/WAN]
Xu, H.	[2001WAN/XU], [2003XU/SU]
Yamashita,T.	[2001YAM/AKI]
Yanagisawa, M.	[1969TAK/YAN]
Yanful, E. K.	[2003MAR/CRU]
Yang, S.	[2001YAN/NAV]
Yeh, G. T.	[1992YEH]
Yoder, G. L.	[2001CAR/YOD]
Yu, S. C.	[2002WAN/LEE], [2005LEE/WAN]
Zachary, J. L.	[1986WES/ZAC]
Zappia, G.	[2003BLA/AGU]
Zavarin, M.	[2005ZAV/ROB]
Zhang, J.	[1981XU/WAN]
Zhang, Z.	[1981XU/WAN]

This volume provides a state-of-the-art report on the modelling of aqueous-solid solution systems by the combined use of chemical thermodynamics and experimental and computational techniques. These systems are ubiquitous in nature and therefore intrinsic to the understanding and quantification of radionuclide containment and retardation processes present in geological repositories of radioactive waste. Representative cases for study have been chosen from the radioactive waste literature to illustrate the application of the various approaches. This report has been prepared by a team of four leading experts in the field under the auspices of the OECD/NEA Thermochemical Database (TDB) Project.

(66 2007 04 1 P) € 80
ISBN 978-92-64-02655-1

www.oecd.org